Local Exchange Potentials in Density Functional Theory

HOLLINS, THOMAS,WILLIAM

Local Exchange Potentials in Density Functional Theory

Thomas William Hollins

A thesis submitted in partial fulfilment
of the requirements for the degree of
Doctor of Philosophy

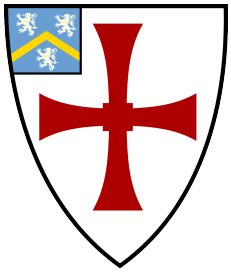

Department of Physics
University of Durham
2014

Local Exchange Potentials in Density Functional Theory

Thomas William Hollins

Abstract

DFT is a method that deals efficiently with the ground state many-electron problem. It replaces the solution of the many-electron Schrödinger's equation with an equation to determine the electronic density alone. In the Kohn-Sham (KS) scheme, this density is obtained as the ground state density of a fictitious system of non-interacting electrons. The aim is to determine the local potential for these electrons so that their density equals the interacting density of the physical system. This potential is the sum of the electron-nuclear attraction, the Hartree repulsion from the density and finally the exchange and correlation potential. The central approximation in DFT is the functional form of the exchange-correlation potential. The most basic approximate functionals are explicit functions of the electron density. More sophisticated approximations are orbital dependent functionals or hybrids of density and orbital dependent functionals. In this work we present the implementation of some accurate local exchange potentials, the exact exchange (EXX) potential, the local Fock exchange (LFX) potential and an approximation to EXX, the common energy denominator approximation (CEDA) potential. The EXX potential minimises the Hartree-Fock (HF) total energy and is calculated using perturbation theory and the Hylleraas variational method, improving upon previous implementations. Optimising a local potential that adopts the HF density as its own ground state density, gives the LFX potential, which is simple to calculate and physically equivalent to the EXX potential. Both the EXX and LFX methods are extended to be applicable to metallic systems. The implemented potentials are used to calculate the electronic band structures for semiconductors, insulators, antiferromagnetic insulators and metals. For the semiconducting, insulating and metallic systems studied, the LFX method gives very similar results to EXX. In the systems characterised by stronger correlations, we observe a small disparity between the two exchange methods. When compared to experiment, the results are surprisingly accurate, given the complete neglect of correlation in these calculations. This is remarkable for the strongly correlated systems and also for the simple metals, given the well-known qualitative failure of Hartree-Fock for metals. The fundamental gap of a system is the sum of the KS eigenvalue gap and a correction known as the derivative discontinuity. The exact derivative discontinuity for a system is derived from ensemble density functional theory, thus allowing the full calculation of fundamental band gaps. Approximate forms of the discontinuity for the local density approximation (LDA), generalised gradient approximations (GGA), EXX and LFX are also derived and implemented. Contrary to the accepted wisdom, that the derivative discontinuity for local approximations (LDA/GGA) vanishes, calculated LDA and GGA fundamental band gaps give a much improved result over the corresponding Kohn-Sham band gaps, with accuracy comparable to EXX and LFX KS band gaps. Finally the derivative discontinuity using exact exchange and an orbital dependent correlation functional was also derived but not implemented.

Declaration

The work presented here was undertaken within the Department of Physics of the University of Durham between October 2010 and May 2014. I confirm that no part of this work has been submitted for a degree at this or any other institution and, unless otherwise stated is the original work of the author.

Thomas W. Hollins
June 2014

Contents

List of Figures

List of Tables

Acknowledgements

My thanks go to Stewart for his supervision and single malt whisky. Nikitas for his ideas and encouragement. Paul and Dominik for the advice, mainly programming related. Keith for correcting my spelling, grammar and yet more programming help and Peter for putting up with me for four years.

My thanks also go to my fellow students Robyn, Lara, Ewan and Tom. To my house mates; DC, Will, Adam and David. To my friends (in no particular order); Hugh, Ben, Donald, BJ, Kate, Dave, Olivia, Andy, Ian, Cally and to the chaps at Van Mildert College Darts Club, Van Mildert College Rugby Football Club and Durham City Rugby Football Club.

And finally to my parents, to my brother James and to Lucy for all their love, support, encouragement and patience.

An education was a bit like a communicable sexual disease. It made you unsuitable for a lot of jobs and then you had the urge to pass it on.

Sir Terry Pratchett, *Hogfather*.

Chapter 1

Introduction

1.1 Introduction

The large advances in computational power in the last decades increasingly allow the investigation of the physics of materials via numerical simulations. These can complement the interpretation of experimental results or to make predictions that can be tested by experiment. Simulations can also be used to investigate material properties that would be extremely labourious to reproduce, prohibitively expensive to attempt or inaccessible to experiment.

This thesis demonstrates new methods and theories for the accurate calculation of the electronic structure of condensed matter systems. We adopt a first principles approach, starting from the basic building blocks of materials, namely the positively charged nuclei and the negatively charged electrons and, by modelling their interactions without knowledge derived from experimental results, calculate the electronic structure of a material.[1]

While the interactions between a set of electrons and nuclei is basic quantum mechanics, the large number of particles in a material and the consequent interactions between these particles create an almost intractable many-body problem. To this end we employ density functional theory (DFT), a popular method for calculating electronic structure that can be applied to any condensed matter system of interest. DFT finds applications for example in the simulation of: semiconductors, magnetic materials and organic, inorganic and biological chemistry.[2, 3]

DFT is an exact method but relies on approximating the interactions between the electrons to make the many-body problem tractable. The success and popularity of DFT lies largely in its simplicity, even simple approximations to the electronic interactions can give remarkably accurate results. Since its inception considerable work as gone into developing improved approximations to the electronic interactions, however typically in DFT there is a trade off between the computational simplicity of an approximation and its accuracy. Early approximations greatly simplified the interactions, but allowed the simulation of large systems with relative ease. Later approximations accurately simulate the interactions but are restricted to the study of small systems due to the increased

computational expense of implementing them.[4]

This thesis concerns the development and implementation of approximations in DFT that give accurate electronic structures and are computationally efficient to use.

1.2 Outline of Thesis

This thesis presents the application of local exact exchange potentials to crystalline semiconducting, antiferromagnetic and metallic systems. The first part of this work discusses the theoretical techniques employed, whilst the second part presents calculated results. The work described in this thesis is organised as follows:

Chapter 2

The quantum mechanical many-body problem is introduced, approximations to the many-body wave function are discussed resulting in the Hartree and Hartree-Fock approximations. The Hohenberg-Kohn theorems are shown and proved, and the Kohn-Sham formalism is introduced. Common approximations to the exchange-correlation term are described. Application of density functional theory to crystalline systems and the choice of a plane wave basis set is explained and the use of pseudopotentials discussed. Schemes for solving the Kohn-Sham equations are reviewed.

Chapter 3

The motivations for using accurate local exchange-correlation potentials are detailed. A variational method for calculating the exact exchange potential (EXX) using the Hylleraas variational method is derived using the Sternheimer equation. Approximations to EXX are reviewed and the method for calculating the common energy denominator approximation (CEDA) potential outlined. A local exchange potential with the same density as Hartree-Fock is derived and called the local Fock exchange (LFX) potential. Extension of these potentials to partially occupied systems is derived allowing the application of these potentials to metallic systems. Theoretical arguments for the physical equivalence of EXX and LFX are also explained.

Chapter 4

The implementation of the local potentials into the plane wave pseudopotential code CASTEP are discussed. The algorithms to optimise the local potentials are outlined. The methodology to solve the Sternheimer equation is described. The steepest descents, conjugate gradients and quasi-Newton's methods are introduced and discussed to optimise the potentials. The performance of the minimisers is calculated, as well as convergence of the potentials with respect to the calculation parameters is calculated and the parallelisation and scaling of the methods is considered and calculated.

Chapter 5

The application of EXX, CEDA and LFX to calculate the electronic structure of group IV, group III-V, group II-VI semiconductors, insulators, transition metal monoxides and metals are presented and compared to experimental results.

Chapter 6

The derivative discontinuity to find the fundamental band gap is derived using ensemble density functional theory. The discontinuity for LDA/GGA functionals is found, as well as the exchange-only discontinuity for EXX/LFX and an approximate correlation energy derivative discontinuity is also derived. Results for the calculated discontinuities for LDA, PBE, EXX and LFX are presented and discussed.

Chapter 7

A summary of the conclusions of the previous chapters and suggestions for further investigation are outlined.

Chapter 2

The Many Body Problem and Density Functional Theory

2.1 The Many-Body Problem

A condensed matter system is by its very nature an interacting system involving many particles. In almost all cases these particles are the positively charged nuclei of the atoms in our system and the negatively charged electrons. The energetics of their interaction can be described through the many-body Schrödinger equation;

$$\hat{H}\Phi = E\Phi, \tag{2.1}$$

where $\hat{H}$ is the Hamiltonian operator, Φ is the many-body wave function of the system of N electrons and M nuclei and E is the total energy of the system.[1] The wave function contains the probability amplitude for all possible configurations of the electrons and nuclei and is dependent on the coordinates of all the particles in the system;

$$\Phi = \Phi(\mathbf{r}_1, \mathbf{r}_2, ..., \mathbf{r}_N, \mathbf{R}_1, \mathbf{R}_2, ..., \mathbf{R}_M), \tag{2.2}$$

where $\mathbf{r}_i$ and $\mathbf{R}_I$ are the coordinates of the electrons and nuclei respectively.[1]

An initial simplification to separate to the nuclear and electronic wave functions can be accomplished by noting that the mass of a typical nucleus is several thousand times ($10^3 \sim 10^5$) that of an electron. Hence the time scales for any nuclear motion will be much longer than the time scales of the electron motion and the nuclear motion can be considered classical. If we assume the electrons adopt the ground state configuration as the nuclei move and that the Born-Oppenheimer approximation is valid, the nuclei can be considered as static classical point charges.[5] The wave function can then be written

[1] Currently we consider only spinless systems, spin polarisation is described in section 2.3.5. Hence $\mathbf{r}_i$ and $\mathbf{R}_I$ depend only on spatial coordinates.

as an adiabatic product of an electronic wave function and a nuclear wave function;

$$\Phi = \Psi(\mathbf{r}_1, \mathbf{r}_2, ..., \mathbf{r}_N) \times \chi(\mathbf{R}_1, \mathbf{R}_2, ..., \mathbf{R}_M). \tag{2.3}$$

It is worth noting that the electronic wave function, Ψ remains dependent on the nuclear positions, as the parameters; $\mathbf{R}_1, \mathbf{R}_2, ..., \mathbf{R}_M$ appear in the electronic Hamiltonian.

The electronic Hamiltonian describes the interactions of the electrons with each other and the electrostatic field created by the nuclei. The electronic Schrödinger equation (in atomic units)[2] is then given by;

$$\hat{H}\Psi = \left(-\frac{1}{2}\sum_{i=1}^{N} \nabla^2_{\mathbf{r}_i} + \frac{1}{2}\sum_{i=1}^{N}\sum_{j=1, j\neq i}^{N} \frac{1}{|\mathbf{r}_i - \mathbf{r}_j|} - \sum_{i=1}^{N}\sum_{I=1}^{M} \frac{Z_I}{|\mathbf{r}_i - \mathbf{R}_I|} \right) \Psi = E\Psi, \tag{2.4}$$

with $\nabla^2_{\mathbf{r}_i}$ operating on spatial coordinates of the i-th electron, Z_I is the charge of the I-th nuclei, the first term is the kinetic energy of the system, the second term is the Coulomb electron-electron interaction and the third term is the Coulomb electron-nuclei interaction. The total energy of the system is not completely described by the energy of the electrons in the Schrödinger equation. The total energy is;

$$E_{\text{total}} = E + E_{\text{ion}}, \tag{2.5}$$

where E_{ion} is the potential energy due to the Coulomb interaction of the nuclei, given by the classical Coulomb energy of the repulsion between the nuclei;

$$E_{\text{ion}} = \frac{1}{2}\sum_{I=1}^{M}\sum_{J=1, J\neq I}^{M} \frac{Z_I Z_J}{|\mathbf{R}_I - \mathbf{R}_J|}. \tag{2.6}$$

The wave function that is a solution to the many-electron Schrödinger equation must obey two constraints; it must be normalised, such that the total probability is 1;

$$\int d\mathbf{r}_1 \int d\mathbf{r}_2 ... \int d\mathbf{r}_N \Psi^\dagger(\mathbf{r}_1, \mathbf{r}_2, ..., \mathbf{r}_N)\Psi(\mathbf{r}_1, \mathbf{r}_2, ..., \mathbf{r}_N) = 1, \tag{2.7}$$

and that it is anti-symmetric under exchange of any two electrons coordinates;

$$\Psi(\mathbf{r}_1, \mathbf{r}_2, ..., \mathbf{r}_N) = -\Psi(\mathbf{r}_2, \mathbf{r}_1, ..., \mathbf{r}_N). \tag{2.8}$$

This arises from the electrons being Fermions and indistinguishable from one another. Anti-symmetry gives rise to the Pauli exclusion principle. The probability density of finding an electron at spatial position $\mathbf{r}$ is given by;

$$n(\mathbf{r}) = \int d\mathbf{r}_2 ... \int d\mathbf{r}_N \Psi^\dagger(\mathbf{r}, \mathbf{r}_2, ..., \mathbf{r}_N)\Psi(\mathbf{r}, \mathbf{r}_2, ..., \mathbf{r}_N), \tag{2.9}$$

[2] All equations in this work will be in atomic units.

and the charge density of the system by;

$$\rho(\mathbf{r}) = N \int d\mathbf{r}_2 ... \int d\mathbf{r}_N \Psi^\dagger(\mathbf{r}, \mathbf{r}_2, ..., \mathbf{r}_N)\Psi(\mathbf{r}, \mathbf{r}_2, ..., \mathbf{r}_N). \tag{2.10}$$

While the Schrödinger equation is exact, the equation is nearly impossible to solve (except for some very simple cases) as the many-electron wave function has $3N$ degrees of freedom and due to the Coulomb interaction any calculation scales exponentially with the number of degrees of freedom, making any realistic problem beyond 3 to 4 electrons impractical. Hence to create a tractable problem the many-body system must be approximated.

2.2 Approximations to the Wave Function

2.2.1 The Hartree Approximation

The Hartree approximation is the most basic approximation that can be made to the wave function.[6, 7, 8] The many-body wave function is assumed to be written as a product of single particle orbitals;

$$\Psi(\mathbf{r}_1, \mathbf{r}_2, ..., \mathbf{r}_N) = \psi_1(\mathbf{r}_1)\psi_2(\mathbf{r}_2)...\psi_N(\mathbf{r}_N). \tag{2.11}$$

Substitution of the approximate wave function into the many-body Hamiltonian leads to;

$$\begin{aligned}
&\langle\Psi|\hat{H}|\Psi\rangle = E \qquad (2.12)\\
&= -\frac{1}{2}\sum_{i=1}^{N}\langle\psi_i|\nabla^2|\psi_i\rangle - \sum_{i=1}^{N}\sum_{I=1}^{M}\langle\psi_i|\frac{Z_I}{|\mathbf{r}_i - \mathbf{R}_I|}|\psi_i\rangle + \frac{1}{2}\sum_{i=1}^{N}\sum_{j=1,j\neq i}^{N}\langle\psi_i\psi_j|\frac{1}{|\mathbf{r}_i - \mathbf{r}_j|}|\psi_i\psi_j\rangle\\
&= -\frac{1}{2}\sum_{i=1}^{N}\int d\mathbf{r}\psi_i(\mathbf{r})\nabla^2\psi_i(\mathbf{r}) - \sum_{I=1}^{M}\int d\mathbf{r}\frac{Z_I}{|\mathbf{r} - \mathbf{R}_I|}\rho(\mathbf{r}) + \frac{1}{2}\iint d\mathbf{r}d\mathbf{r}'\frac{\rho(\mathbf{r})\rho(\mathbf{r}')}{|\mathbf{r} - \mathbf{r}'|}\\
&- \frac{1}{2}\sum_{i=1}^{N}\iint d\mathbf{r}d\mathbf{r}'\frac{|\psi_i(\mathbf{r})|^2|\psi_i(\mathbf{r}')|^2}{|\mathbf{r} - \mathbf{r}'|}.
\end{aligned}$$

This form of the wave function allows the N-body Hamiltonian to be written as N coupled one-electron Schrödinger equations as the wave function is now separable. The one-electron Schrödinger equations take the form;

$$\left(-\frac{1}{2}\nabla^2 - \sum_{I=1}^{M}\frac{Z_I}{|\mathbf{r} - \mathbf{R}_I|} + \sum_{j=1,j\neq i}^{N}\int d\mathbf{r}'\frac{|\psi_j(\mathbf{r}')|^2}{|\mathbf{r} - \mathbf{r}'|}\right)\psi_i(\mathbf{r}) = \varepsilon_i\psi_i(\mathbf{r}), \tag{2.13}$$

the last term on the left hand side is known as the Hartree potential and is a classical mean field interaction arising from all N electrons minus the i-th orbital and ε_i is the eigenvalue of the i-th orbital. The density couples the one-electron Schrödinger equations

and is defined as;

$$\rho(\mathbf{r}) = \sum_{i=1}^{N} \psi_i^\dagger(\mathbf{r})\psi_i(\mathbf{r}). \tag{2.14}$$

The Hartree approximation to the wave function fails to enforce the anti-symmetry required by Pauli's exclusion principle. Hence the orthogonality of the orbitals must be artificially imposed on the problem.

2.2.2 The Hartree-Fock Approximation

The anti-symmetry of the wave function can be enforced by forming the set of N single particle orbitals as a Slater determinant;

$$\Psi(\mathbf{r}_1, \mathbf{r}_2, ..., \mathbf{r}_N) = \frac{1}{\sqrt{N!}} \begin{vmatrix} \psi_1(\mathbf{r}_1) & \psi_1(\mathbf{r}_2) & \cdots & \psi_1(\mathbf{r}_N) \\ \psi_2(\mathbf{r}_1) & \psi_2(\mathbf{r}_2) & \cdots & \psi_2(\mathbf{r}_N) \\ \vdots & \vdots & \ddots & \vdots \\ \psi_N(\mathbf{r}_1) & \psi_N(\mathbf{r}_2) & \cdots & \psi_N(\mathbf{r}_N) \end{vmatrix}, \tag{2.15}$$

which due to the properties of a determinant will cause the wave function to switch sign under any swapping of rows or columns.[9] The Slater determinant can be explicitly written as the product of N orbitals acted on by the anti-symmetrising operator;

$$\Psi(\mathbf{r}_1, \mathbf{r}_2, ..., \mathbf{r}_N) = \hat{A}|\psi_1(\mathbf{r}_1)\psi_2(\mathbf{r}_2)\cdots\psi_N(\mathbf{r}_N)|. \tag{2.16}$$

The anti-symmetrising operator acting on the orbital product yields a sum of orbital products spanning all possible combinations of orbital index and position index. Following the Slater-Condon rules[10, 11] the kinetic energy operator is a single particle operator, and hence can be written as;

$$\hat{T} = -\frac{1}{2}\sum_{i=1}^{N} \nabla_{\mathbf{r}_i}^2. \tag{2.17}$$

Applying the kinetic energy operator to the Slater determinant gives;

$$T = \langle\Psi|\hat{T}|\Psi\rangle = -\frac{1}{2}\sum_{i=1}^{N} \int d\mathbf{r}\psi_i^\dagger(\mathbf{r})\nabla^2\psi_i(\mathbf{r}). \tag{2.18}$$

By the same considerations the electron-ion energy simplifies to;

$$E_{\text{ext}} = -\int d\mathbf{r} \sum_{I=1}^{M} \frac{Z_I}{|\mathbf{r} - \mathbf{R}_I|}\rho(\mathbf{r}), \tag{2.19}$$

with $\rho(\mathbf{r})$ retaining the definition given in equation 2.14. The electron-electron repulsion operator is a two body operator, given by;

$$\hat{V}_{\text{ee}} = \frac{1}{2}\sum_{i=1}^{N}\sum_{j=1,j\neq i}^{N}\frac{1}{|\mathbf{r}_i - \mathbf{r}_j|}. \tag{2.20}$$

The electron-electron repulsion operator couples pairs of orbitals, hence the electron-electron repulsion energy is given by;

$$\begin{aligned} E_{\text{ee}} =& \frac{1}{2}\sum_{i=1}^{N}\sum_{j=1}^{N}\iint d\mathbf{r}d\mathbf{r}'\left[\frac{\psi_i^\dagger(\mathbf{r})\psi_j^\dagger(\mathbf{r}')\psi_i(\mathbf{r})\psi_j(\mathbf{r}')}{|\mathbf{r}-\mathbf{r}'|} - \frac{\psi_i^\dagger(\mathbf{r})\psi_j^\dagger(\mathbf{r}')\psi_j(\mathbf{r})\psi_i(\mathbf{r}')}{|\mathbf{r}-\mathbf{r}'|}\right] \\ =& \frac{1}{2}\iint d\mathbf{r}d\mathbf{r}'\left[\frac{\rho(\mathbf{r})\rho(\mathbf{r}')}{|\mathbf{r}-\mathbf{r}'|} - \sum_{i=1}^{N}\sum_{j=1}^{N}\frac{\psi_i^\dagger(\mathbf{r})\psi_j^\dagger(\mathbf{r}')\psi_j(\mathbf{r})\psi_i(\mathbf{r}')}{|\mathbf{r}-\mathbf{r}'|}\right]. \end{aligned} \tag{2.21}$$

The second from last term is the Hartree energy, E_{H} and the last term is the Fock exchange energy, E_{x}.

Using the form of the wave function given in equation 2.15 gives rise to N single particle equations with form very similar to those of the Hartree approximation;

$$\left(-\frac{1}{2}\nabla^2 - \sum_{I=1}^{M}\frac{Z_I}{|\mathbf{r}-\mathbf{R}_I|} + \int d\mathbf{r}'\frac{\rho(\mathbf{r}')}{|\mathbf{r}-\mathbf{r}'|}\right)\psi_i(\mathbf{r}) - \sum_{j=1}^{N}\int d\mathbf{r}'\frac{\psi_j^\dagger(\mathbf{r}')\psi_j(\mathbf{r})}{|\mathbf{r}-\mathbf{r}'|}\psi_i(\mathbf{r}') = \varepsilon_i\psi_i(\mathbf{r}), \tag{2.22}$$

where the last term is the exchange or Fock operator, $\hat{V}_{\text{x}}$ applied to an orbital $\psi_i(\mathbf{r})$ and the set of N single particle equations are known as the Hartree-Fock (HF) equations.[12] The exchange term is an energetic manifestation of the anti-symmetry of the wave function under exchange of particle position and can also be interpreted as enforcing Pauli's exclusion principle by spatially separating the electrons.[3]

The Fock term can also be written in terms of the one-body reduced density matrix of the electrons, given by;

$$\rho(\mathbf{r},\mathbf{r}') = \sum_{i=1}^{N}\psi_i^\dagger(\mathbf{r})\psi_i(\mathbf{r}'). \tag{2.23}$$

With the Fock term written as;

$$\hat{V}_{\text{x}}\psi_i(\mathbf{r}) = -\int d\mathbf{r}'\frac{\rho(\mathbf{r},\mathbf{r}')}{|\mathbf{r}-\mathbf{r}'|}\psi_i(\mathbf{r}'), \tag{2.24}$$

and the exchange energy as;

$$E_{\text{x}} = -\frac{1}{2}\iint d\mathbf{r}d\mathbf{r}'\frac{|\rho(\mathbf{r},\mathbf{r}')|^2}{|\mathbf{r}-\mathbf{r}'|}.$$

[3] In a spin polarised system, the exclusion principle applies only to electrons of the same spin

The Hartree-Fock total energy is then given by;

$$E_{\mathrm{HF}} = -\frac{1}{2}\sum_{i}^{N}\int d\mathbf{r}\psi_i(\mathbf{r})\nabla^2\psi_i(\mathbf{r}) - \int d\mathbf{r}\sum_{j=1}^{M}\frac{Z_i}{|\mathbf{r}-\mathbf{R_j}|}\rho(\mathbf{r}) \\ +\frac{1}{2}\iint d\mathbf{r}d\mathbf{r}'\frac{\rho(\mathbf{r})\rho(\mathbf{r}')}{|\mathbf{r}-\mathbf{r}'|} - \frac{1}{2}\iint d\mathbf{r}d\mathbf{r}'\frac{|\rho(\mathbf{r},\mathbf{r}')|^2}{|\mathbf{r}-\mathbf{r}'|}, \tag{2.25}$$

alternatively the total energy can be written in a shorthand form;

$$E_{\mathrm{HF}} = T + E_{\mathrm{ext}} + E_{\mathrm{H}} + E_{\mathrm{x}}, \tag{2.26}$$

with T being the kinetic energy, E_{H} being the Hartree potential energy, E_{x} being the exchange energy and E_{ext} being the electron-ion potential energy. The electron-ion energy will be referred to as the external potential energy, E_{ext} as the external potential can encompass the energetics of the electrons interacting with items external to the interacting electron system, for instance applied fields as well as the potential energy due to the ions.

Similarly the Hartree-Fock equations can be written as;

$$\left(\hat{T}(\mathbf{r}) + \hat{V}_{\mathrm{ext}}(\mathbf{r}) + \hat{V}_{\mathrm{H}}(\mathbf{r}) + \hat{V}_{\mathrm{x}}\right)\psi_i(\mathbf{r}) = \varepsilon_i\psi_i(\mathbf{r}), \tag{2.27}$$

with $\hat{T}(\mathbf{r})$ being the kinetic energy operator, $\hat{V}_{\mathrm{ext}}(\mathbf{r})$ is the external potential operator, $\hat{V}_{\mathrm{H}}(\mathbf{r})$ is the Hartree potential operator and $\hat{V}_{\mathrm{x}}$ is the Fock operator.

The Hartree-Fock equations are considerably more difficult to solve than the Hartree equations due to the Fock term; the non-locality in the definition of the exchange term substantially increases the difficulty of the problem. The Hartree approximation scales cubicly with electron number, Hartree-Fock scales with the number of electrons to the fourth power, as calculating the Fock exchange integral requires a double sum over orbital indexes, i and j.

The Hartree-Fock approximation improves upon the Hartree approximation, as by construction the wave function is fully antisymmetric.[3] The Hartree-Fock equations treat exchange exactly, but the approximation is not without its drawbacks. Most notably the approximation is only definitely self-interaction free for orbitals that are occupied and hence an electron is repelled by $N-1$ electrons. In HF, any virtual orbital (which would represent an excited state) is repelled by N rather than $N-1$ electrons, leading to very large excitation energies.[13] The complexity of the Hartree-Fock equations leads to a search for a more computationally practical method. This search leads us to consider the simplicity of density functional theory.

2.3 Density Functional Theory

At its core density functional theory proves that the central variable of the many-electron problem can be the electron density (equation 2.10) rather than the many-electron wave function. This replaces a large, mathematically complex object with a very simple object.[14]

2.3.1 The Hohenberg-Kohn Theorems

Density functional theory is underpinned by the Hohenberg-Kohn theorems. The first of their theorems states that ground state (gs) energy is a unique functional of the ground state electron density. This means there is one and only one electron density that describes the ground state of a system and further to this the external potential $\hat{V}_{\text{ext}}(\mathbf{r})$ uniquely defines the ground state electron density, hence;

$$E_{\text{gs}} = E[\rho_{\text{gs}}(\mathbf{r})] = E\left[\rho[\hat{V}_{\text{ext}}(\mathbf{r})]\right]. \tag{2.28}$$

The inverse also holds; the external potential is uniquely determined by the ground state density. In addition implicitly the many-electron Hamiltonian is a functional of the electron density.[15]

This can be proved firstly by taking two external potentials, $\hat{V}_1(\mathbf{r})$ and $\hat{V}_2(\mathbf{r})$ that are different by more than a constant. We then assume that the two Hamiltonians, $\hat{H}_1$ and $\hat{H}_2$ containing respectively the external potentials $\hat{V}_1(\mathbf{r})$ and $\hat{V}_2(\mathbf{r})$, both generate the same ground state wave function, Ψ. The Schrödinger equations of the two systems are then;

$$E_1\Psi(\mathbf{r}_1, \mathbf{r}_2, \cdots, \mathbf{r}_N) = \left[\hat{T} + \hat{V}_{\text{ee}} + \sum_i^N \hat{V}_1(\mathbf{r}_i)\right]\Psi(\mathbf{r}_1, \mathbf{r}_2, \cdots, \mathbf{r}_N), \tag{2.29}$$

and;

$$E_2\Psi(\mathbf{r}_1, \mathbf{r}_2, \cdots, \mathbf{r}_N) = \left[\hat{T} + \hat{V}_{\text{ee}} + \sum_i^N \hat{V}_2(\mathbf{r}_i)\right]\Psi(\mathbf{r}_1, \mathbf{r}_2, \cdots, \mathbf{r}_N). \tag{2.30}$$

For regions where $\Psi(\mathbf{r}_1, \mathbf{r}_2, \cdots, \mathbf{r}_N) \neq 0$, the difference in the two equations (after dividing by Ψ) is;

$$E_1 - E_2 = \left[\sum_{i=1}^N \hat{V}_1(\mathbf{r}_i) - \hat{V}_2(\mathbf{r}_i)\right], \tag{2.31}$$

which contradicts our definition of the difference in the two external potentials as the two potentials are different by only a constant. This implies the each external potential will generate a different ground state wave function.

The uniqueness of the mapping between potentials and densities can then be proved by taking the two external potentials, $\hat{V}_1(\mathbf{r})$ and $\hat{V}_2(\mathbf{r})$, the respective Hamiltonians $\hat{H}_1$ and $\hat{H}_2$ generate different ground state wave functions (Ψ_1 and Ψ_2 respectively) but the

same ground state density. The energies of the two systems are;

$$E_1[\rho(\mathbf{r})] = \langle\Psi_1|\hat{H}_1|\Psi_1\rangle = \int d\mathbf{r}\hat{V}_1(\mathbf{r})\rho(\mathbf{r}) + \langle\Psi_1|\hat{T} + \hat{V}_{ee}|\Psi_1\rangle, \tag{2.32}$$

and;

$$E_2[\rho(\mathbf{r})] = \langle\Psi_2|\hat{H}_2|\Psi_2\rangle = \int d\mathbf{r}\hat{V}_2(\mathbf{r})\rho(\mathbf{r}) + \langle\Psi_2|\hat{T} + \hat{V}_{ee}|\Psi_2\rangle. \tag{2.33}$$

Using the variational principle;

$$\begin{aligned} E_1 < \langle\Psi_2|\hat{H}_1|\Psi_2\rangle =& \langle\Psi_2|\hat{H}_2|\Psi_2\rangle + \langle\Psi_2|\hat{H}_1 - \hat{H}_2|\Psi_2\rangle \\ =& E_2 + \int d\mathbf{r}\rho(\mathbf{r})[\hat{V}_1(\mathbf{r}) - \hat{V}_2(\mathbf{r})], \end{aligned} \tag{2.34}$$

and by interchanging potentials 1 and 2;

$$\begin{aligned} E_2 < \langle\Psi_1|\hat{H}_2|\Psi_1\rangle =& \langle\Psi_1|\hat{H}_1|\Psi_1\rangle + \langle\Psi_1|\hat{H}_2 - \hat{H}_1|\Psi_1\rangle \\ =& E_1 + \int d\mathbf{r}\rho(\mathbf{r})[\hat{V}_2(\mathbf{r}) - \hat{V}_1(\mathbf{r})] \end{aligned} \tag{2.35}$$

adding the two inequalities leads to;

$$E_1 + E_2 < E_1 + E_2, \tag{2.36}$$

which is contradictory. Therefore different external potentials $\hat{V}_1(\mathbf{r})$ and $\hat{V}_2(\mathbf{r})$ always have different ground state densities, $\rho_1(\mathbf{r})$ and $\rho_2(\mathbf{r})$ respectively. This means the density uniquely determines the external potential (to within a constant). Then in principle, the wave function of any state (ground or excited) is determined by solving the Schrödinger equation with the ground state Hamiltonian. While this theory proves that the density can be used as a central variable, we are still required to deal with the many-body Schrödinger equation and hence are no closer to simplifying the problem at hand.

The second theorem states that the ground state energy can be found variationally by optimising an energy functional and the density at the minimum of the energy functional is the ground state density. This theorem is restricted to densities that are ground state densities of some external potential, such densities are "V-representable". These densities are the densities for which a functional can be constructed. Hence each term in the Hamiltonian can be written as a functional of the density, so the total energy can be written as;

$$E_{\text{Total}}[\rho(\mathbf{r})] = T[\rho(\mathbf{r})] + E_{\text{ee}}[\rho(\mathbf{r})] + \int d\mathbf{r}\hat{V}_{\text{ext}}(\mathbf{r})\rho(\mathbf{r}) + V_{\text{ion}}, \tag{2.37}$$

where $E_{\text{ee}}[\rho(\mathbf{r})]$ is the electron-electron interaction energy and V_{ion} is the electrostatic repulsion of the ions in the system, as defined in equation 2.6. For the ground state density, $\rho_0(\mathbf{r})$ corresponding to the external potential, $\hat{V}_0(\mathbf{r})$, the density functional energy

is the same as the expectation of the Hamiltonian, $\hat{H}_0$ which has the many-body wave function, Ψ_0 as its ground state wave function;

$$E[\rho_0(\mathbf{r})] = \langle \Psi_0 | \hat{H}_0 | \Psi_0 \rangle. \tag{2.38}$$

Considering another density, $\rho_1(\mathbf{r})$ corresponding to the wave function, Ψ_1, the energy for this state is given by;

$$E[\rho_1(\mathbf{r})] = \langle \Psi_1 | \hat{H}_0 | \Psi_1 \rangle > E[\rho_0(\mathbf{r})], \tag{2.39}$$

thus the energy given by the density functional energy is minimised by the ground state density, $\rho_0(\mathbf{r})$. Hence the energy can be minimised variationally. However while this theorem provides a method for finding the ground state, it provides no insight as to how to solve the many-electron Schrödinger equation.

2.3.2 The Kohn-Sham Method

A highly successful method for finding solutions to the many-electron problem, is the Kohn-Sham method.[16] This method replaces the interacting system of electrons described by the many-electron wave function, with an auxiliary system of non-interacting independent particles. The central ansatz of the Kohn-Sham method is that the ground state density of the auxiliary system is the same as the ground state electronic many-electron density. As the particles are non-interacting and hence separable, the independent N-particle Hamiltonian of the auxiliary system can be written as the sum of N single-particle Hamiltonians, as was done for the Hartree and Hartree-Fock approximations;

$$\left[\hat{T}_\mathrm{s}(\mathbf{r}) + \hat{V}_\mathrm{ext}(\mathbf{r}) + \hat{V}(\mathbf{r})\right] \phi_i(\mathbf{r}) = \varepsilon_i \phi_i(\mathbf{r}), \tag{2.40}$$

where the single-particle wave functions are known as the Kohn-Sham orbitals. The density of the Kohn-Sham system is given by;

$$\rho(\mathbf{r}) = \sum_{i=1}^{N} \phi_i^\dagger(\mathbf{r}) \phi_i(\mathbf{r}). \tag{2.41}$$

The kinetic energy is given by;

$$T_\mathrm{s}[\rho(\mathbf{r})] = -\frac{1}{2} \sum_{i=1}^{N} \int d\mathbf{r} \phi_i^\dagger(\mathbf{r}) \nabla^2 \phi_i(\mathbf{r}), \tag{2.42}$$

and the kinetic energy operator is;

$$\hat{T}_\mathrm{s}(\mathbf{r}) \phi_i(\mathbf{r}) = -\frac{1}{2} \nabla^2 \phi_i(\mathbf{r}), \tag{2.43}$$

the kinetic energy given by the non-interacting system is not equal to the kinetic energy of the physical many-body system, as one is an interacting system and the other is non-interacting. The potential $\hat{V}(\mathbf{r})$ is a non-interacting effective potential, representing the electron-electron interaction. It is usually partitioned into two terms;

$$\hat{V}(\mathbf{r}) = \hat{V}_{\mathrm{H}}(\mathbf{r}) + \hat{V}_{\mathrm{xc}}(\mathbf{r}), \tag{2.44}$$

the first term is the Hartree potential as previously defined as the third term in equation 2.22;

$$\hat{V}_{\mathrm{H}}(\mathbf{r}) = \frac{\delta E_{\mathrm{H}}}{\delta \rho(\mathbf{r})} = \int d\mathbf{r}' \frac{\rho(\mathbf{r}')}{|\mathbf{r} - \mathbf{r}'|}, \tag{2.45}$$

and the Hartree energy as defined in equation 2.25;

$$E_{\mathrm{H}} = \frac{1}{2} \iint d\mathbf{r} d\mathbf{r}' \frac{\rho(\mathbf{r})\rho(\mathbf{r}')}{|\mathbf{r} - \mathbf{r}'|}. \tag{2.46}$$

The second term is the exchange-correlation potential;

$$\hat{V}_{\mathrm{xc}}(\mathbf{r}) = \frac{\delta E_{\mathrm{xc}}}{\delta \rho(\mathbf{r})}, \tag{2.47}$$

the properties and functional form of this term will be discussed later, but the exchange-correlation potential ensures the Kohn-Sham auxiliary system has the same density as the interacting system.

The Kohn-Sham method allows the N-electron problem to be written as a set of coupled N single particle Schrödinger equations, by the use of an auxiliary system of non-interacting particles, which are coupled by the density. The main issue is then the exchange-correlation potential, as the form and functional dependence on the density is unknown.

2.3.3 The Exchange and Correlation Potential

The exchange-correlation potential has no definitive rigorous universal functional form, however the exchange-correlation energy can be formally defined as;

$$E_{\mathrm{xc}}[\rho(\mathbf{r})] = \langle \Psi | \hat{T} | \Psi \rangle - T_{\mathrm{s}}[\rho(\mathbf{r})] + \frac{1}{2} \sum_{i \neq j} \langle \Psi | \frac{1}{|\mathbf{r}_i - \mathbf{r}_j|} | \Psi \rangle - E_{\mathrm{H}}[\rho(\mathbf{r})], \tag{2.48}$$

where the density of the Kohn-Sham system is required to be the exact density.[1] Physically, this can be interpreted as containing all the energetic contributions that are neglected by the Kohn-Sham kinetic energy and Hartree energy with respect to the exact many-body kinetic energy and electron-electron interaction. This includes the exchange energy which can be found exactly from the Fock exchange integral and the correlation energy which accounts for all other missing many-body energy contributions. The Fock

exchange integral is given by;

$$E_{\mathrm{x}} = -\frac{1}{2}\sum_{i,j}\iint d\mathbf{r}d\mathbf{r}'\frac{\phi_i^{\dagger}(\mathbf{r})\phi_j(\mathbf{r})\phi_j^{\dagger}(\mathbf{r}')\phi_i(\mathbf{r}')}{|\mathbf{r}-\mathbf{r}'|}, \tag{2.49}$$

where the orbitals satisfy the Kohn-Sham equations. While the exchange energy can be exactly calculated, the correlation energy is only defined as the difference in the total energies of the many-body and Kohn-Sham systems;

$$E_{\mathrm{c}}[\rho(\mathbf{r})] = \langle\Psi|\hat{T}|\Psi\rangle - T_{\mathrm{s}}[\rho(\mathbf{r})] + \frac{1}{2}\sum_{i\neq j}\langle\Psi|\frac{1}{|\mathbf{r}_i-\mathbf{r}_j|}|\Psi\rangle - E_{\mathrm{H}}[\rho(\mathbf{r})] - E_{\mathrm{x}}[\rho(\mathbf{r})]. \tag{2.50}$$

As the exact correlation energy can only be found by solving the many-electron problem, it is always approximated in any practical calculation. In fact although the exchange energy can be found exactly, it too is frequently approximated as a functional of the density.

2.3.4 Exchange-Correlation Functionals

The simplest, earliest and hence most commonly used exchange-correlation functional is the local density approximation (LDA).[14, 16] The LDA assumes that the exchange-correlation energy per electron at point $\mathbf{r}$, $\epsilon_{\mathrm{xc}}(\mathbf{r})$ with density, $\rho(\mathbf{r})$ is the same as the exchange-correlation energy of the homogeneous electron gas (HEG) with that density. The exchange-correlation energy is given by;

$$E_{\mathrm{xc}}^{\mathrm{LDA}}[\rho(\mathbf{r})] = \int d\mathbf{r}\rho(\mathbf{r})\epsilon_{\mathrm{xc}}^{\mathrm{HEG}}(\rho(\mathbf{r})), \tag{2.51}$$

and the potential is given by;

$$V_{\mathrm{xc}}^{\mathrm{LDA}}(\mathbf{r}) = \frac{\delta E_{\mathrm{xc}}^{\mathrm{LDA}}}{\delta\rho(\mathbf{r})}. \tag{2.52}$$

The exchange-correlation energy per electron is parameterised from quantum Monte Carlo calculations of the homogeneous electron gas at various densities. Hence the LDA is only exact for the homogeneous electron gas. The LDA gives system geometries, binding and vibrational energies within approximately 10% of the experimental value but grossly underestimates the excitation energies of a system and has a tendency to over-bind the system.[4, 17, 18]

An extension to the LDA is to include some knowledge of inhomogeneities in the density by including the local density gradient, $|\nabla\rho(\mathbf{r})|$. This type of approximation is known as generalised gradient approximation (GGA). The GGA exchange correlation energy is defined as;

$$E_{\mathrm{xc}}^{\mathrm{GGA}}[\rho(\mathbf{r})] = \int d\mathbf{r}\rho(\mathbf{r})F(\rho(\mathbf{r}),|\nabla\rho(\mathbf{r})|)\epsilon_{\mathrm{xc}}^{\mathrm{HEG}}(\rho(\mathbf{r})), \tag{2.53}$$

the $F(\rho(\mathbf{r}), |\nabla\rho(\mathbf{r})|)$ is the enhancement factor parameterised from a set of homogeneous electron gas calculations using different densities and is chosen to satisfy select exact properties while maintaining the correct behaviour that the LDA satisfies. [19, 20, 21, 22, 23, 24]. The most commonly used GGA is the PBE form.[23] The GGA improves upon the LDA with regard to geometries, binding energies, still underestimates excitation energies but to a lesser degree than LDA.[4]

Further extension in the next logical direction is to include second, third and fourth derivatives of the density $\nabla^2\rho(\mathbf{r}), \nabla^3\rho(\mathbf{r}), \nabla^4\rho(\mathbf{r})$, known as the meta-GGAs.[4][25] This series of parameterisations based on increasing knowledge of the nature of the density has become known as the 'Jacobs Ladder' in a biblical analogy on the assumption that at the top of the ladder lies the universal (and heavenly) all encompassing functional, and the LDA, GGA and meta-GGAs lie at the bottom on successively higher rungs.[26, 27] Despite promising increasing accuracy with more information about the inhomogeneities in the density, the extensions beyond the GGAs depend on empirical parameters. Hence the functionals give very accurate results for the systems to which they are fitted and worse results compared to the GGAs for systems to which they are not fitted. For more detailed discussion please see [4] and references therein.

Another direction to approximate the exchange-correlation functional that is especially popular with the computational chemistry community is hybrid functionals. These mix in a fraction of the Fock exchange integral into the local LDA or GGA exchange-correlation energy. These typically take the following form;

$$E_{\mathrm{xc}}^{\mathrm{Hybrid}}[\rho(\mathbf{r})] = bE_{\mathrm{x}}^{\mathrm{Fock}} + (1-b)E_{\mathrm{x}}^{Local} + E_{\mathrm{c}}[\rho(\mathbf{r})], \tag{2.54}$$

where b is a fitting parameter that can range between 0 and 1. The most popular hybrid functional is the Becke three-parameter functional with the Lee-Yang-Parr correlation functional (B3LYP), which takes the form;

$$\begin{aligned} E_{\mathrm{xc}}^{\mathrm{B3LYP}}[\rho(\mathbf{r})] =& E_{\mathrm{xc}}^{\mathrm{LDA}}[\rho(\mathbf{r})] + a_0(E_{\mathrm{x}}^{\mathrm{Fock}} - E_{\mathrm{x}}^{\mathrm{LDA}}[\rho(\mathbf{r})]) + a_{\mathrm{x}}\Delta E_{\mathrm{x}}^{\mathrm{GGA}}[\rho(\mathbf{r})] \\ &+ a_{\mathrm{c}}E_{\mathrm{c}}^{\mathrm{LYP}}[\rho(\mathbf{r})] + (1-a_{\mathrm{c}})E_{\mathrm{c}}^{\mathrm{LDA}}[\rho(\mathbf{r})], \end{aligned} \tag{2.55}$$

with $a_0 = 0.2$, $a_{\mathrm{x}} = 0.72$ and $a_{\mathrm{c}} = 0.81$ and $\Delta E_{\mathrm{x}}^{\mathrm{GGA}}[\rho(\mathbf{r})]$ is the GGA correction to the LDA exchange functional.[28, 29, 30] These Becke 3-parameter functionals typically give accurate system geometries for molecular systems and improved excitation energies relative to the LDA/GGA's, however the parameters are fitted to give accurate results for a representative set of molecules.

Another popular hybrid is the screened exchange functional (sX), this functional takes the Fock exchange integral and includes some correlation in the form of long range screening of the exchange term, with the addition of local LDA correlation. The sX

[4]However typically the kinetic energy density, $\tau(\mathbf{r})$, is used instead of the second derivative of the density.

exchange-correlation energy takes the form;

$$E_{\mathrm{xc}}^{\mathrm{sX}}[\rho(\mathbf{r})] = -\frac{1}{2}\sum_{i=1}^{N}\sum_{j=1}^{N}\iint d\mathbf{r}d\mathbf{r}'\frac{\phi_i^{\dagger}(\mathbf{r})\phi_i(\mathbf{r}')\phi_j^{\dagger}(\mathbf{r}')\phi_j(\mathbf{r})}{|\mathbf{r}-\mathbf{r}'|}e^{-k_{\mathrm{s}}|\mathbf{r}-\mathbf{r}'|} + E_{\mathrm{c}}^{\mathrm{LDA}}[\rho(\mathbf{r})], \quad (2.56)$$

the term k_{s} is a density dependent screening wave-vector. The screened exchange functional gives accurate system geometries for solids and accurate excitation energies when compared to the LDA/GGA's.[31, 32, 33, 34]

A significant theoretical deficiency is introduced by the use of the approximate local functionals, the exchange-correlation potential does not fully correct the self-interaction present in the Hartree potential.[18, 35] The Fock exchange and hybrid exchange-correlation potentials also do not satisfy the requirement of the Kohn-Sham system that the potentials are local in form, depending on $\mathbf{r}$ and $\mathbf{r}'$ explicitly. Addressing these issues with the exchange-correlation potential will be discussed in later chapters.

2.3.5 Spin Polarised Density Functional Theory

So far the discussion of the many-electron problem and density functional theory has been limited to spin neutral systems, where for the N electrons in the system there are $\frac{N}{2}$ electrons with spin up and $\frac{N}{2}$ electrons with spin down. This spin symmetry allows us to consider only one spin channel and assume the result applies to both spins.

However many real world materials are not spin neutral and so a spin polarised Hamiltonian needs to be considered. Each electron can be spin-up or spin-down, so an electron orbital needs to be written with a spin index, σ;

$$\phi_i(\mathbf{r}) \rightarrow \phi_i^{\sigma}(\mathbf{r}), \quad (2.57)$$

the total number of electrons in the system will be $N = N^{\uparrow} + N^{\downarrow} = \sum_{\sigma} N^{\sigma}$, the charge density is then given by;

$$\rho(\mathbf{r}) = \sum_{\sigma}\sum_{i=1}^{N^{\sigma}}\phi_i^{\sigma\dagger}(\mathbf{r})\phi_i^{\sigma}(\mathbf{r}), \quad (2.58)$$

the spin densities ($\rho^{\uparrow}(\mathbf{r})$ and $\rho^{\downarrow}(\mathbf{r})$) have the same form but drop the sum over spins.[36, 37] The Kohn-Sham Hamiltonian is given by;

$$\left[-\frac{1}{2}\nabla^2 + \hat{V}_{\mathrm{ext}}(\mathbf{r}) + \int d\mathbf{r}'\frac{\rho(\mathbf{r}')}{|\mathbf{r}-\mathbf{r}'|} + \hat{V}_{\mathrm{xc}}^{\sigma}[\rho^{\uparrow}(\mathbf{r}),\rho^{\downarrow}(\mathbf{r})](\mathbf{r})\right]\phi_i^{\sigma}(\mathbf{r}) = \varepsilon_i^{\sigma}\phi_i^{\sigma}(\mathbf{r}), \quad (2.59)$$

with $\hat{V}_{\mathrm{xc}}(\mathbf{r})$ depending on the spin densities. The Fock exchange integral has the form;

$$\hat{V}_{\mathrm{x}}^{\sigma}\phi_i^{\sigma}(\mathbf{r}) = -\int d\mathbf{r}'\frac{\rho^{\sigma}(\mathbf{r},\mathbf{r}')}{|\mathbf{r}-\mathbf{r}'|}\phi_i^{\sigma}(\mathbf{r}'), \quad (2.60)$$

the spin polarised reduced density matrix is given by;

$$\rho^{\sigma}(\mathbf{r},\mathbf{r}') = \sum_{i=1}^{N^{\sigma}} \phi_i^{\sigma\dagger}(\mathbf{r})\phi_i^{\sigma}(\mathbf{r}'). \tag{2.61}$$

This form of spin polarisation assumes the spins of the electrons are collinear, i.e. they all lie in the same direction throughout the material, which we define as the z-axis. In a physical sense all the Kohn-Sham orbitals must be eigenfunctions of the z-axis spin operator;

$$\hat{S}_z\phi_i^{\sigma}(\mathbf{r}) = \pm\frac{1}{2}\phi_i^{\sigma}(\mathbf{r}), \tag{2.62}$$

this only allows the spins to be in one direction with two values.[2]

More generally the spins do not have to be collinear, this requires a more generalised and sophisticated way of dealing with the spins, as they can potentially point in any direction.[3, 38] These non-collinear systems typically result from the relativistic effects of spin-orbit interaction, which tilts the magnetic moments resulting in the weak ferromagnetism seen in some antiferromagnets.[39] The application of density functional theory to non-collinear systems can be accomplished but is beyond the scope of this thesis.[40]

2.4 The Crystalline System

2.4.1 Periodic Boundary Conditions

While we have discussed a solvable method for finding the electronic structure of a system, the nature of the system we wish to investigate has not yet been discussed. The systems of interest are crystalline solids, which can contain upwards of N^{23} atoms, this still poses an intractably large problem. Paradoxically by expanding the solid so it is infinite in all directions allows us to exploit the periodic unit cells that form the crystal by imposing periodic boundary conditions. This condition constrains the potentials and density to be periodic in space;

$$\hat{V}(\mathbf{r}+\mathbf{R}) = \hat{V}(\mathbf{r}), \tag{2.63}$$

and;

$$\rho(\mathbf{r}+\mathbf{R}) = \rho(\mathbf{r}), \tag{2.64}$$

the vector $\mathbf{R}$ is any lattice vector, formed by;

$$\mathbf{R} = i\mathbf{a} + j\mathbf{b} + k\mathbf{c}, \tag{2.65}$$

i, j and k are integers and $\mathbf{a}$, $\mathbf{b}$ and $\mathbf{c}$ are the lattice vectors that define the unit cell of the crystal. The unit cell is a parallelepiped containing an arrangement of atoms that the entire crystal can be built from. The unit cell is defined in terms of 6 parameters,

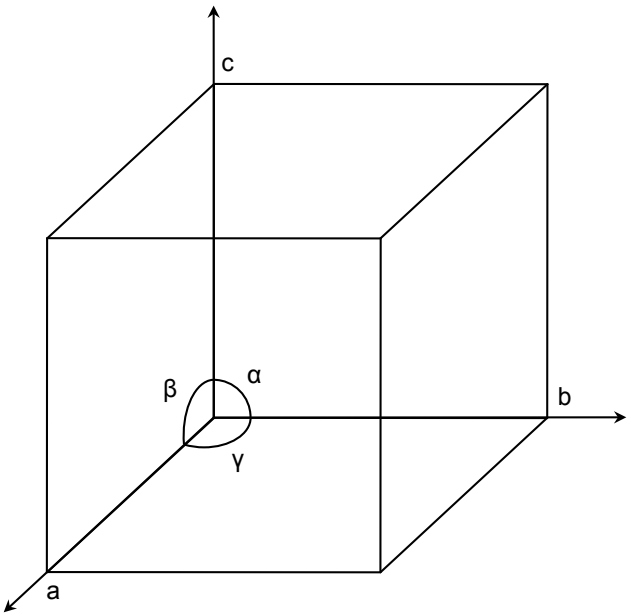

Figure 2.1: Unit cell with defining parameters labelled.

the lengths of the three vectors (a, b, c) and the angles between them (α, β, γ), as shown in figure 2.1.

2.4.2 Bloch's Theorem

Even if the density is periodic there is no guarantee that the individual orbitals that form the density are periodic. To represent the orbitals in a periodic system we employ Bloch's theorem.[41] The orbitals then take the form;

$$\phi^{\sigma}_{j,\mathbf{k}}(\mathbf{r}) = u^{\sigma}_{j,\mathbf{k}}(\mathbf{r})e^{i\mathbf{k}.\mathbf{r}}, \tag{2.66}$$

where $u^{\sigma}_{j,\mathbf{k}}(\mathbf{r})$ is a periodic function; $u_{j,\mathbf{k}}(\mathbf{r}) = u_{j,\mathbf{k}}(\mathbf{r}+\mathbf{R})$ and $\mathbf{k}$ is a wave vector that lies within the first Brillouin zone of the reciprocal lattice, such that; $-\frac{1}{2} \leq k_{\mathrm{x}}, k_{\mathrm{y}}, k_{\mathrm{z}} \leq \frac{1}{2}$ where;

$$\mathbf{k} = k_{\mathrm{x}}\mathbf{a}^* + k_{\mathrm{y}}\mathbf{b}^* + k_{\mathrm{z}}\mathbf{c}^*, \tag{2.67}$$

the reciprocal lattice vectors $\mathbf{a}^*$, $\mathbf{b}^*$ and $\mathbf{c}^*$ are related to $\mathbf{a}$, $\mathbf{b}$ and $\mathbf{c}$ by;

$$\mathbf{a}^* = 2\pi\frac{\mathbf{b}\times\mathbf{c}}{\Omega}, \tag{2.68}$$

$$\mathbf{b}^* = 2\pi\frac{\mathbf{c}\times\mathbf{a}}{\Omega}, \tag{2.69}$$

$$\mathbf{c}^* = 2\pi\frac{\mathbf{a}\times\mathbf{b}}{\Omega}, \tag{2.70}$$

and the volume of the unit cell is;

$$\Omega = |\mathbf{a}.(\mathbf{b} \times \mathbf{c})|. \tag{2.71}$$

Using $\mathbf{a}^*$, $\mathbf{b}^*$ and $\mathbf{c}^*$ we can define reciprocal lattice vectors by;

$$\mathbf{G} = i\mathbf{a}^* + j\mathbf{b}^* + k\mathbf{c}^*, \tag{2.72}$$

and are related to the real lattice vectors, $\mathbf{R}$ by; $\mathbf{R}.\mathbf{G} = 2\pi n$, where n is an integer.

2.4.3 Choice of Basis Sets

The function $u^{\sigma}_{j,\mathbf{k}}(\mathbf{r})$ is undetermined but can be expanded as a linear combination of known functions. The set of functions are known as a basis set; such basis sets can be plane waves, Gaussians, atomic orbitals among others. For atomic and molecular calculations, atom centred basis sets are good choices as they allow accurate representation of the electrons with a small set of basis functions without having to resort to pseudopotentials. The two most popular choices are linear combinations of atomic orbitals (LCAO) and Gaussians. The atom centred basis sets are particularly powerful in isolated systems as the functions used only have values near atoms which is where the electrons are localised and treat the vacuum around systems coarsely. For a linear combination of atomic orbitals centred on an atomic site, each orbital is formed of a series of atomic orbitals, which are themselves solutions to the hydrogen-like atom problem;

$$\varphi_i(r,\theta,\phi) = \sum_{nlm} c_{i,n,l,m}\chi_{nlm}(r,\theta,\phi) = \sum_{nlm} c_{i,n,l,m}R_{nl}(r)Y_{lm}(\theta,\phi). \tag{2.73}$$

These functions have the advantage of being orthogonal and the series does not have to be expanded to very high order, allowing a small basis set, but has the disadvantage of being an incomplete basis set and being difficult to achieve well-behaved convergence with the addition of extra atomic orbitals.[5][42, 43]

Another atom centred basis-set is to use an expansion of Gaussians, like the linear combination of atomic orbitals. An orbital can be expanded in terms of n, l and m;

$$\chi_{nlm}(r,\theta,\phi) = \frac{2(2\alpha_{n,l})^{\frac{3}{4}}}{\pi^{\frac{1}{4}}}\sqrt{\frac{2^l}{(2l+1)!}}\left(\sqrt{2\alpha_{nl}}r\right)^l e^{-\alpha_{nl}r^2}Y_{l,m}(\theta,\phi), \tag{2.74}$$

the primary advantages of Gaussians is that all integrals can be performed analytically, this allows very quick calculations even for integrals that require integration across many co-ordinates.[44] However the disadvantage remains the difficulty of achieving convergence with the addition of further Gaussians and the poor description of continuum states.

[5] Even a large orbital basis will neglect continuum states.

Plane waves are the wave functions the orbitals would adopt in the homogeneous electron gas and can be used the expand $u^{\sigma}_{j,\mathbf{k}}(\mathbf{r})$ as a Fourier series;

$$u^{\sigma}_{j,\mathbf{k}}(\mathbf{r}) = \frac{1}{\sqrt{\Omega}} \sum_{\mathbf{G}} c^{\sigma}_{j,\mathbf{k}}(\mathbf{G}) e^{i\mathbf{G}.\mathbf{r}}, \tag{2.75}$$

hence the orbitals can be written as;

$$\phi^{\sigma}_{j,\mathbf{k}}(\mathbf{r}) = \frac{1}{\sqrt{\Omega}} \sum_{\mathbf{G}} c^{\sigma}_{j,\mathbf{k}}(\mathbf{G}) e^{i(\mathbf{k}+\mathbf{G}).\mathbf{r}}, \tag{2.76}$$

the wave vector $\mathbf{k}$ can adopt any value within the Brillouin zone, hence there are an infinite number of $\mathbf{k}$'s to consider. The plane wave basis is complete, the plane waves are orthogonal and quantities can be easily represented and evaluated in real or reciprocal space depending on which is least computationally intensive. For these reasons plane waves are the choice of basis set to be used in this work.

The localised basis sets work well for isolated systems, as the assumption that the electronic orbitals remain atomic-like remains valid. In a solid this assumption becomes less valid as the electrons can de-localise. However the advantages of a localised basis set (small basis set, no need for a pseudopotential) and the advantages of plane-waves (accurate description of bonding regions and delocalised electrons) can be combined by using the augmented plane wave (APW) method. This method assumes that the solid is composed of spherically symmetric potentials centred on the lattice sites, surrounded by an interstitial region. Inside the spheres the wave functions are the solutions to the spherically harmonic Schrödinger equation like the linear combination of atomic orbitals method. Outside the spheres the wave-functions are plane waves, at the interface between the spheres and the interstitial region the wave functions must be continuous and the derivatives must be matched. Augmenting the plane waves with a spherically symmetric set of atomic orbitals allows an accurate all-electron treatment of a condensed matter system without prohibitive computational cost.[45, 46] The use of augmented plane waves has been extended to linearised augmented plane waves (LAPW) [47, 48] and projector augmented plane waves (PAW),[49, 50] the latter having a very similar methodology to standard plane waves using ultrasoft pseudopotentials.[6] However the augmented plane wave methods are basis set incomplete and non-orthogonal and computationally intensive due to the complicated mixing of basis sets.

2.4.4 Monkhorst-Pack Grids and Plane Wave Cut Off Energies

With the choice of plane waves the issue of having an infinite number of k-points must be addressed. This issue can be avoided without significant loss of accuracy by discretising the Brillouin zone and using a finite number of k-points, which are chosen using a Monkhorst-Pack grid.[51] The Monkhorst-Pack grid is a regular array of k-points, the

[6] See section 2.5.4 for discussion of ultrasoft pseudopotentials

dimensions of which are chosen such that the total energy of the system does not change (to within a chosen uncertainty) with increasing sampling.

Much like the k-points the reciprocal lattice vectors $\mathbf{G}$ form an infinite set. The orbitals and density are assumed to be smoothly varying at small scales so that the plane wave components (with large $|\mathbf{G}|$) that describe this scale are negligible. This allows us to assume that the $c^{\sigma}_{j,\mathbf{k}}(\mathbf{G})$ for large $\mathbf{G}$ are nearly zero and for some value $\mathbf{G}$ we can truncate the infinite sum. The $\mathbf{G}$ that truncates the sum is defined by the associated kinetic energy of the plane wave it describes, hence we introduce a kinetic energy cut off that determines the largest reciprocal lattice vector, $\mathbf{G}_{\max}$;

$$E_{\text{cutoff}} = \frac{1}{2}|\mathbf{k} + \mathbf{G}_{\max}|^2, \tag{2.77}$$

the orbitals are then written as;

$$\phi^{\sigma}_{j,\mathbf{k}}(\mathbf{r}) = \frac{1}{\sqrt{\Omega}} \sum_{|\mathbf{G}|=\mathbf{0}}^{|\mathbf{G}_{\max}|} c^{\sigma}_{j,\mathbf{k}}(\mathbf{G}) e^{i(\mathbf{k}+\mathbf{G}).\mathbf{r}}, \tag{2.78}$$

and the reverse procedure to find the reciprocal space coefficients as;

$$c^{\sigma}_{j,\mathbf{k}}(\mathbf{G}) = \frac{1}{\sqrt{\Omega}} \int d\mathbf{r} \phi^{\sigma}_{j,\mathbf{k}}(\mathbf{r}) e^{-i(\mathbf{k}+\mathbf{G}).\mathbf{r}}. \tag{2.79}$$

Employing Bloch's theorem allows an infinite electron problem to be considered as a problem involving only the number of electrons in the unit cell (usually 10s-1000s)[7] with a finite set of k-points and $\mathbf{G}$'s.

It is also worth mentioning that the plane wave method can be trivially modified to allow calculations on extended systems such as defects, surfaces and isolated molecules. In the instance of the defect, a crystal super cell of many unit cells can be built with one unit cell having a defect, this results in an infinite array of defects due to the periodic boundary conditions. As long as the super cell is large enough to minimise any electrostatic interaction between the defects, then the results will be those for effectively a single defect in a crystal. Similarly we can surround an isolated molecule or surface slab with a larger volume of vacuum to minimise the interactions between the periodic mirrors of the system to consider them in isolation.[52]

[7] Typical ranges accessible to current computational methods.

2.4.5 The Kohn-Sham Equations and Other Quantities in Reciprocal Space

All quantities that can be considered in real space can also be considered in reciprocal space e.g. the density can be written as a Fourier transform;

$$\begin{aligned}\rho(\mathbf{G}) &= \int d\mathbf{r}\rho(\mathbf{r})e^{-i\mathbf{G}.\mathbf{r}} = \sum_{\sigma}\int d\mathbf{r}\sum_{i,\mathbf{k}}\frac{1}{N_{\mathbf{k}}}\phi^{\sigma}_{i,\mathbf{k}}(\mathbf{r})\phi^{\sigma\dagger}_{i,\mathbf{k}}(\mathbf{r})e^{-i\mathbf{G}.\mathbf{r}},\\ &= \sum_{\sigma}\sum_{i,\mathbf{k}}\frac{1}{N_{\mathbf{k}}}\sum_{\mathbf{G}'}c^{\sigma\dagger}_{i,\mathbf{k}}(\mathbf{G}')\int d\mathbf{r}\frac{1}{\sqrt{\Omega}}\phi^{\sigma}_{i,\mathbf{k}}(\mathbf{r})e^{-i(\mathbf{k}+\mathbf{G}+\mathbf{G}').\mathbf{r}},\\ &= \sum_{\sigma}\sum_{i,\mathbf{k}}\frac{1}{N_{\mathbf{k}}}\sum_{\mathbf{G}'}c^{\sigma\dagger}_{i,\mathbf{k}}(\mathbf{G}')c^{\sigma}_{i,\mathbf{k}}(\mathbf{G}+\mathbf{G}'),\end{aligned} \tag{2.80}$$

where $N_{\mathbf{k}}$ is the total number of k-points and the division by $N_{\mathbf{k}}$ is due to the sum over k-points as well as electrons. It is worth noting that $\rho(\mathbf{G})$ has a plane wave cut off that is twice as large as the plane wave cut off of the set of $c^{\sigma}_{i,\mathbf{k}}(\mathbf{G})$'s, as the maximum size that $|\mathbf{G}+\mathbf{G}'|$ can take is $2|\mathbf{G}_{\max}|$.

Any real space quantity can be found in reciprocal space or vice versa by Fourier transformation, a generic local potential for example;

$$\hat{V}(\mathbf{r}) = \frac{1}{\Omega}\sum_{\mathbf{G}}\hat{V}(\mathbf{G})e^{i\mathbf{G}.\mathbf{r}}, \tag{2.81}$$

becomes;

$$\hat{V}(\mathbf{G}) = \int d\mathbf{r}\hat{V}(\mathbf{r})e^{-i\mathbf{G}.\mathbf{r}}. \tag{2.82}$$

For potentials the plane wave cut off is also twice as large as the plane wave cut off for the orbitals. The kinetic and Hartree potentials have particularly simple forms. The kinetic energy operator has the form;

$$\begin{aligned}\hat{T}_{\mathrm{s}}\phi^{\sigma}_{i,\mathbf{k}}(\mathbf{r}) &= -\frac{1}{2}\nabla^2\phi^{\sigma}_{i,\mathbf{k}}(\mathbf{r}) = -\frac{1}{2\sqrt{\Omega}}\sum_{\mathbf{G}}c^{\sigma}_{i,\mathbf{k}}(\mathbf{G})\nabla^2 e^{i(\mathbf{k}+\mathbf{G}).\mathbf{r}}\\ &= -\frac{1}{2\sqrt{\Omega}}\sum_{\mathbf{G}}|\mathbf{k}+\mathbf{G}|^2 c^{\sigma}_{i,\mathbf{k}}(\mathbf{G})e^{i(\mathbf{k}+\mathbf{G}).\mathbf{r}}.\end{aligned} \tag{2.83}$$

Implying the kinetic energy operator in reciprocal space is;

$$\hat{T}_{\mathrm{s},\mathbf{k}}(\mathbf{G}) = -\frac{1}{2}|\mathbf{k}+\mathbf{G}|^2, \tag{2.84}$$

with the kinetic energy being given by;

$$T_{\mathrm{s}} = \sum_{\sigma}\frac{1}{N_{\mathbf{k}}}\sum_{i,\mathbf{k}}\int d\mathbf{r}\phi^{\sigma\dagger}_{i,\mathbf{k}}(\mathbf{r})\hat{T}_{\mathrm{s}}\phi^{\sigma}_{i,\mathbf{k}}(\mathbf{r})$$

$$= -\frac{1}{2\sqrt{\Omega}N_{\mathbf{k}}} \sum_{\sigma} \sum_{i,\mathbf{k}} \sum_{\mathbf{G}} |\mathbf{k}+\mathbf{G}|^2 c^{\sigma}_{i,\mathbf{k}}(\mathbf{G}) \int d\mathbf{r} \phi^{\sigma\dagger}_{i,\mathbf{k}}(\mathbf{r}) e^{i(\mathbf{k}+\mathbf{G}).\mathbf{r}} \tag{2.85}$$
$$= -\frac{1}{2N_{\mathbf{k}}} \sum_{\sigma} \sum_{i,\mathbf{k}} \sum_{\mathbf{G}} |\mathbf{k}+\mathbf{G}|^2 c^{\sigma}_{i,\mathbf{k}}(\mathbf{G}) c^{\sigma\dagger}_{i,\mathbf{k}}(\mathbf{G}).$$

The Hartree potential can be found directly from the real space representation of the potential;

$$\begin{aligned}
\hat{V}_{\mathrm{H}}(\mathbf{G}) = \int d\mathbf{r} \hat{V}_{\mathrm{H}}(\mathbf{r}) e^{-i\mathbf{G}.\mathbf{r}} &= \iint d\mathbf{r} d\mathbf{r}' \frac{\rho(\mathbf{r}')}{|\mathbf{r}-\mathbf{r}'|} e^{-i\mathbf{G}.\mathbf{r}} \\
&= \frac{1}{\Omega} \int d\mathbf{r} \sum_{\mathbf{G}'} \rho(\mathbf{G}') e^{-i\mathbf{G}.\mathbf{r}} \int d\mathbf{r}' e^{i\mathbf{G}'.\mathbf{r}'} \frac{1}{|\mathbf{r}-\mathbf{r}'|} \\
&= \frac{4\pi}{\Omega} \sum_{\mathbf{G}'} \frac{\rho(\mathbf{G}')}{|\mathbf{G}'|^2} \int d\mathbf{r} e^{i(\mathbf{G}'-\mathbf{G}).\mathbf{r}} \\
&= \frac{4\pi}{\Omega} \frac{\rho(\mathbf{G})}{|\mathbf{G}|^2},
\end{aligned} \tag{2.86}$$

where the identity;

$$\int d\mathbf{r} \frac{e^{i\alpha.\mathbf{r}}}{|\mathbf{r}|} = \frac{4\pi}{\alpha^2}, \tag{2.87}$$

is used and the Hartree energy is given by;

$$E_{\mathrm{H}} = \frac{2\pi}{\Omega} \sum_{\mathbf{G}} \frac{|\rho(\mathbf{G})|^2}{|\mathbf{G}|^2}. \tag{2.88}$$

The Fock exchange potential in reciprocal space can similarly be derived, however as the operator is orbital dependent it will have a wave-vector and spin dependence;

$$\begin{aligned}
\hat{V}^{\sigma}_{\mathrm{x},\mathbf{k}}(\mathbf{G},\mathbf{G}') &= \frac{1}{\Omega} \int d\mathbf{r} e^{-i(\mathbf{k}+\mathbf{G}).\mathbf{r}} \int d\mathbf{r}' \hat{V}^{\sigma}_{\mathrm{x}} e^{i(\mathbf{k}+\mathbf{G}').\mathbf{r}'} \\
&= -\frac{1}{\Omega} \frac{1}{N_{\mathbf{q}}} \sum_{j,\mathbf{q}} \iint d\mathbf{r} d\mathbf{r}' \frac{\phi^{\sigma\dagger}_{j\mathbf{q}}(\mathbf{r}') \phi^{\sigma}_{j\mathbf{q}}(\mathbf{r})}{|\mathbf{r}-\mathbf{r}'|} e^{i(\mathbf{k}+\mathbf{G}').\mathbf{r}' - i(\mathbf{k}+\mathbf{G}).\mathbf{r}} \\
&= -\frac{1}{\Omega^{3/2}} \frac{1}{N_{\mathbf{q}}} \sum_{j,\mathbf{q}} \iint d\mathbf{r} d\mathbf{r}' \frac{\phi^{\sigma}_{j\mathbf{q}}(\mathbf{r})}{|\mathbf{r}-\mathbf{r}'|} \sum_{\mathbf{G}''} c^{\sigma\dagger}_{j\mathbf{q}}(\mathbf{G}'') e^{i(\mathbf{k}+\mathbf{G}'-\mathbf{q}-\mathbf{G}'').\mathbf{r}' - i(\mathbf{k}+\mathbf{G}).\mathbf{r}} \\
&= -\frac{4\pi}{\Omega^{3/2}} \frac{1}{N_{\mathbf{q}}} \sum_{j,\mathbf{q}} \int d\mathbf{r} \frac{\phi^{\sigma}_{j\mathbf{q}}(\mathbf{r})}{|\mathbf{k}+\mathbf{G}'-\mathbf{q}-\mathbf{G}''|^2} \sum_{\mathbf{G}''} c^{\sigma\dagger}_{j\mathbf{q}}(\mathbf{G}'') e^{i(\mathbf{k}+\mathbf{G}'-\mathbf{q}-\mathbf{G}'').\mathbf{r} - i(\mathbf{k}+\mathbf{G}).\mathbf{r}} \\
&= -\frac{4\pi}{\Omega^{3/2}} \frac{1}{N_{\mathbf{q}}} \sum_{j,\mathbf{q}} \int d\mathbf{r} \sum_{\mathbf{G}''} \frac{\phi^{\sigma}_{j\mathbf{q}}(\mathbf{r})}{|\mathbf{k}+\mathbf{G}'-\mathbf{q}-\mathbf{G}''|^2} c^{\sigma\dagger}_{j\mathbf{q}}(\mathbf{G}'') e^{-i(\mathbf{q}+\mathbf{G}-\mathbf{G}'+\mathbf{G}'').\mathbf{r}} \\
&= -\frac{4\pi}{\Omega} \frac{1}{N_{\mathbf{q}}} \sum_{\mathbf{G}''} \sum_{j,\mathbf{q}} \frac{c^{\sigma\dagger}_{j\mathbf{q}}(\mathbf{G}'') c^{\sigma}_{j\mathbf{q}}(\mathbf{G}-\mathbf{G}'+\mathbf{G}'')}{|\mathbf{k}+\mathbf{G}'-\mathbf{q}-\mathbf{G}''|^2}.
\end{aligned} \tag{2.89}$$

The exchange energy is then;

$$E_{\mathrm{x}} = \frac{1}{2}\frac{1}{N_{\mathbf{k}}}\sum_{\sigma}\sum_{i,\mathbf{k}}\sum_{\mathbf{G}}\sum_{\mathbf{G}'} c_{i\mathbf{k}}^{\sigma\dagger}(\mathbf{G})\hat{V}_{\mathrm{x},\mathbf{k}}^{\sigma}(\mathbf{G},\mathbf{G}')c_{i\mathbf{k}}^{\sigma\dagger}(\mathbf{G}') \tag{2.90}$$

$$= \frac{2\pi}{\Omega}\frac{1}{N_{\mathbf{q}}N_{\mathbf{k}}}\sum_{\sigma}\sum_{i,\mathbf{k}}\sum_{j,\mathbf{q}}\sum_{\mathbf{G}}\sum_{\mathbf{G}'}\sum_{\mathbf{G}''} c_{i\mathbf{k}}^{\sigma\dagger}(\mathbf{G})\frac{c_{j\mathbf{q}}^{\sigma\dagger}(\mathbf{G}'+\mathbf{G}'')c_{j\mathbf{q}}^{\sigma}(\mathbf{G}+\mathbf{G}'')}{|\mathbf{q}-\mathbf{k}+\mathbf{G}''|^2}c_{i\mathbf{k}}^{\sigma\dagger}(\mathbf{G}'),$$

the multiple sums over reciprocal lattice vectors and double sum over wave-vectors mean that the calculation of the exchange energy is of substantially greater difficulty than any of the other operators in the Hamiltonian.

The Kohn-Sham equations have a convenient matrix form when Fourier transformed into reciprocal space;

$$\sum_{\mathbf{G}'}\Big(\frac{1}{2}|\mathbf{k}+\mathbf{G}|^2\delta_{\mathbf{G},\mathbf{G}'} + \hat{V}_{\mathrm{ext}}(\mathbf{G}-\mathbf{G}') + \hat{V}_{\mathrm{H}}(\mathbf{G}-\mathbf{G}') + \hat{V}_{\mathrm{xc}}^{\sigma}(\mathbf{G}-\mathbf{G}')\Big)c_{i,\mathbf{k}}^{\sigma}(\mathbf{G}')$$

$$= \varepsilon_i^{\sigma}c_{i,\mathbf{k}}^{\sigma}(\mathbf{G}), \tag{2.91}$$

the kinetic energy forms the diagonal of this matrix and the off diagonal terms are formed by the potentials. This equation can be solved by using several different techniques which will be discussed in section 2.6.1.

2.4.6 The Electrostatic Potential Energy

As well as having the Kohn-Sham equations that give the orbitals within one unit cell, we also need the total energy within one unit cell. This energy per unit cell is;

$$E = \frac{1}{N_{\mathrm{cell}}}\left[T_{\mathrm{s}}[\rho] + E_{\mathrm{H}}[\rho] + E_{\mathrm{ext}}[\rho] + E_{\mathrm{xc}}[\rho] + E_{\mathrm{ion}}\right], \tag{2.92}$$

for an infinite periodic system the total energy will diverge to infinity, however the total energy per unit cell is a non-divergent quantity. By construction the exchange-correlation energy per unit cell for local potentials like the LDA or GGA can be defined wholly within one unit cell and trivially the kinetic energy per unit cell also can be defined within just one unit cell. However the Hartree, Fock exchange integral, external and ion-ion energies are not defined within one unit cell. The individual energies per unit cell diverge in an infinite system, however the total energy per unit cell of the four remains finite.

For the Hartree energy and Fock exchange energy this is due to the total energy quantifying the interaction of the electron density (or reduced density matrix in the case of the Fock exchange energy) within one unit cell, with an infinite electron density. Similarly for the external potential the electron density interacts with an infinite array of ions and for the ion-ion energy the interactions of an infinite array of positively charged ions must be taken into account. This is due to all four representing four separate interactions, all of which are non-charge neutral, yet over all the system is neutral.[2]

To make the four energy sums non-divergent, each one must be made charge neutral. To accomplish this we include an additive factor onto the electron density; for the Hartree energy this density is uniform and positive, $\rho'(\mathbf{r}) = \rho(\mathbf{r}) + \rho^+$, giving a density that is overall charge neutral, the Hartree energy is then;

$$E_{\mathrm{H}}[\rho'] = \iint d\mathbf{r}d\mathbf{r}' \frac{(\rho(\mathbf{r}) + \rho^+)(\rho(\mathbf{r}') + \rho^+)}{|\mathbf{r} - \mathbf{r}'|} = \frac{2\pi}{\Omega} \sum_{\mathbf{G}\neq\mathbf{0}} \frac{|\rho(\mathbf{G})|^2}{|\mathbf{G}|^2}, \tag{2.93}$$

where we no longer have to consider the divergent $|\mathbf{G}| = 0$ term as the system of interest is charge neutral. In a similar way the external potential energy can be found by adding a uniform negative charge to the potential formed by the ions, $\hat{V}'_{\mathrm{ext}}(\mathbf{r}) = \hat{V}_{\mathrm{ext}}(\mathbf{r}) + \rho^-$, this amounts to removing the $|\mathbf{G}| = 0$ term for the external potential energy.[1] Using similar considerations the Fock exchange energy is non-divergent if the term in equation 2.90 when $\mathbf{G}'' = 0$ and $\mathbf{k} = \mathbf{q}$ is not evaluated (The procedure to make the Fock exchange energy non-divergent is detailed in ref. [53]).

The ion-ion interaction energy is somewhat more mathematically tricky, involving an Ewald transformation of the energy expression,[54] which exploits that any sum in a periodic system can be split into a real space (short ranged) and reciprocal space (long ranged) components;

$$\begin{aligned} E_{\mathrm{ion}} &= \frac{1}{2} \sum_{m,n} \sum_{\mathbf{R}} \frac{Z_n Z_m}{|\mathbf{R}_n + \mathbf{R}_m + \mathbf{R}|} \\ &= \frac{1}{2} \sum_{m,n} \sum_{\mathbf{R}} Z_n Z_m \frac{\mathrm{erfc}(|\mathbf{R}_n + \mathbf{R}_m + \mathbf{R}|\eta)}{|\mathbf{R}_n + \mathbf{R}_m + \mathbf{R}|} \\ &+ \frac{1}{2\Omega} \sum_{|\mathbf{G}|\neq 0} \frac{4\pi}{|\mathbf{G}|^2} e^{-|\mathbf{G}|^2/8\eta^2} \left[\sum_{n=1} Z_n e^{i\mathbf{G}.\mathbf{R}_n} \right]^2 - \frac{\eta}{\sqrt{\pi}} \sum_{n=1} Z_n^2 - \frac{1}{2} \left(\sum_n Z_n \right)^2 \frac{\pi}{\eta^2 \Omega}, \end{aligned} \tag{2.94}$$

where $\mathbf{R}_n$ and $\mathbf{R}_m$ ionic positions in the unit cell, $\mathbf{R}$ is a lattice vector of the periodic system and multiples thereof extending from $-\infty$ to $+\infty$ although in practice only the nearest neighbours of unit cells need to be summed over to converge the sum.[55] Note that for $|\mathbf{R}| = 0$ the term $\mathbf{R}_n = \mathbf{R}_m$ must be ignored to remove the unphysical self-interaction of the ion cores. The second term in the last line in equation 2.94, cancels the self interaction in the first term. The last term is the analytic limit of $\mathbf{G} \to 0$ for the uniform additive negative charge density, ρ^- that is added to the lattice of positive point charges. $\mathrm{erfc}(r)$ is the complementary error function given by;

$$\mathrm{erfc}(r) = 1 - \frac{2}{\sqrt{\pi}} \int_0^r dr e^{-r^2}, \tag{2.95}$$

and η determines how the sum is split between real space and reciprocal space.

The addition of the uniform charges does not change any of the physics or energies of the problem. As the system remains charge neutral they are purely mathematical artefacts to allow the non-divergent computation of each electrostatic term separately in

the total energy.[1, 2]

2.4.7 Symmetry

Using Bloch's theorem we have already managed to reduce the problem we need to solve to that of one of the electrons and ions in one unit cell of an infinite crystal. However, we can further exploit the crystal's symmetry to reduce the complexity of the calculation. The symmetry of a crystal is defined by the number and type of symmetry operations that can be performed on the crystal. A symmetry operation relates two points in the unit cell through; a reflection in a plane, a rotation about an axis, an inversion through a point or a translation in an direction, this operation is applied to all elements of the unit cell.

Any crystal can be classified with one of 32 point group symmetries. Point groups comprise a set of reflections, rotations, inversions and improper rotations (a combination of a rotation followed by an inversion). The crystal also has a space group, of which there are 230, that comprise the translational symmetries of the crystal and contain translations, screw axis (a rotation about an axis then a translation along the axis) and a glide plane (a reflection in the plane then a translation along the plane). The combination of the space and point groups allows any crystal system to be reduced to a periodic unit cell and for that cell to be classified with one of 14 unique Bravais lattice types.[41]

The symmetry operations allow two simplifications to be made to calculations, the first is in real space. Exploiting the symmetry of the crystal allows a unit cell to be reorientated into its smallest repeating unit. As shown in figure 2.2 the conventional face centred cubic Bravais lattice of silicon containing eight atoms can be reduced to a primitive unit cell containing only two. This reduces the volume we need to consider and the number of electrons under consideration within a calculation.

The second simplification is in reciprocal space, using the symmetry of the reciprocal lattice we can map the k-points in the Monkhorst-Pack grid into symmetry matched sets. This allows us to calculate the coefficients of an orbital at a particular k-point and know that the orbital also has that set of values at all other k-points that are symmetry related to the initial k-point. The initial Monkhorst-Pack grid can then be reduced to a set of points that are not symmetry related. The only additional complication is that every k-point is no longer equally weighted, when integrating quantities across the Brillouin zone each k-point has its own weighting factor, $f_{\mathbf{k}}$;

$$f_{\mathbf{k}} = \frac{n_{\mathbf{k}}}{N_{\mathbf{k}}}, \tag{2.96}$$

with $n_{\mathbf{k}}$ being the number k-points in the initial Monkhorst-Pack grid that are related to the k-point in the reduced k-point set and $N_{\mathbf{k}}$ being the total number of k-points in the initial Monkhorst-Pack grid.[1] Any quantity that requires integration across reciprocal

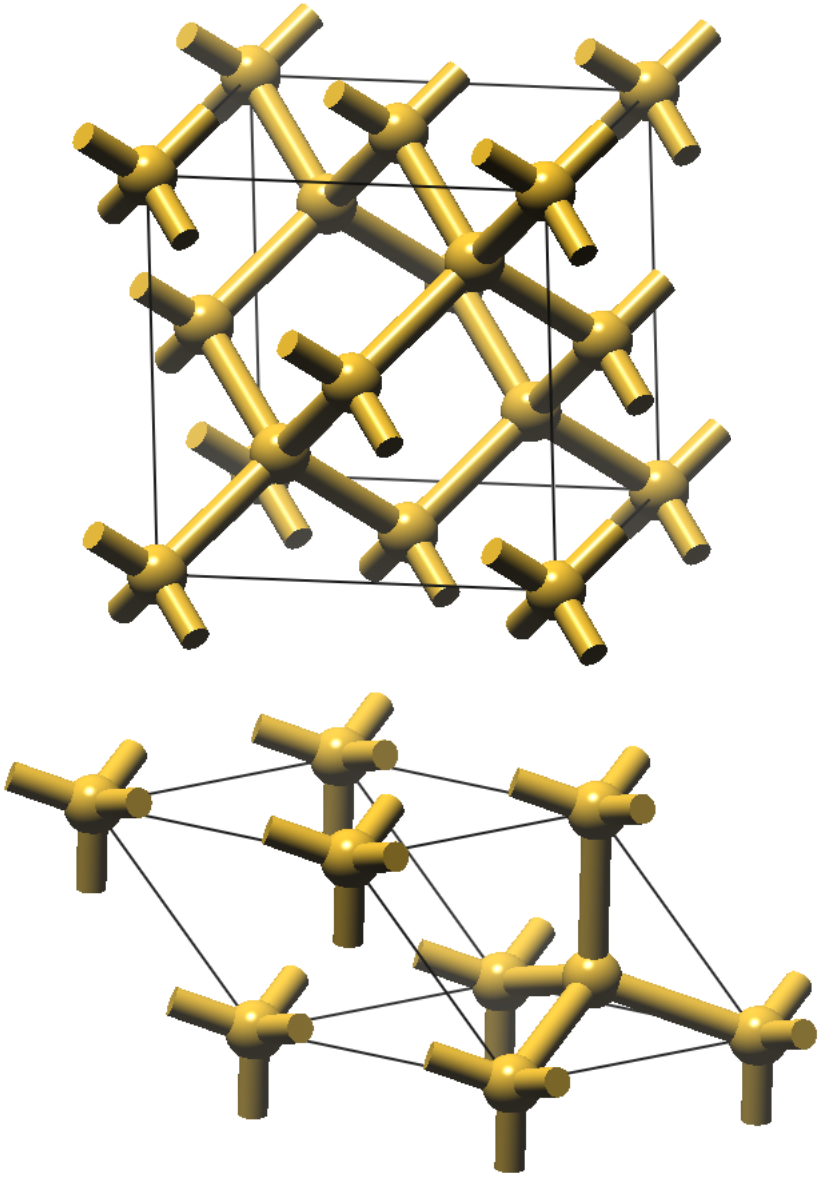

Figure 2.2: Conventional (top) and primitive (bottom) unit cells of silicon.

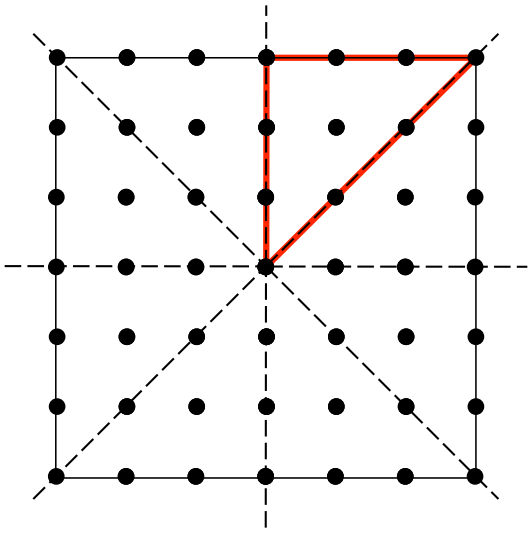

Figure 2.3: Two dimensional square Brillouin zone with a 7×7 Monkhorst-Pack grid, dashed lines indicate symmetry planes. Using the 4 fold symmetry of the square the zone can be reduced to a single symmetry element denoted by the red triangle using only the 10 k-points that border or are enclosed by the triangle. Note the k-points will have differing weights.

space (in this case the density) then has the form;

$$\rho(\mathbf{r}) = \sum_{\sigma} \sum_{i}^{N^{\sigma}} \sum_{\mathbf{k}} f_{\mathbf{k}} \phi_{i,\mathbf{k}}^{\sigma\dagger}(\mathbf{r}) \phi_{i,\mathbf{k}}^{\sigma}(\mathbf{r}), \tag{2.97}$$

with the additional requirement that the quantity conforms to the symmetry of the lattice.

The use of symmetry in reciprocal space allows the Monkhorst-Pack grid to be greatly reduced, but this is highly dependent on the degree of symmetry in the material under investigation. For diamond; an $8 \times 8 \times 8$ grid reduces from 512 points to 80 points, a smaller $6 \times 6 \times 6$ grid reduces from 216 points to 28 points and a $5 \times 5 \times 5$ grid reduces from 125 points to 10 points. A two dimensional example that reduces 49 points in a 7×7 grid to 10 is shown in figure 2.3. The reduced grid of points will have differing weights, the point in the centre of the square zone (also known as the gamma point, Γ) borders 8 symmetry elements and hence has a weight of $\frac{1}{36}$, the point on the corner of the square zone also borders 8 symmetry elements and has weight of $\frac{1}{36}$, the point at the right angle corner of the element borders 4 elements and has weight $\frac{1}{18}$, the 6 points along the edges border 2 elements and have weight $\frac{1}{9}$ and the point in the centre of the element has weight $\frac{2}{9}$. Summing all the weights gives 1.

2.5 Pseudopotentials

In the simplest form of the external potential in the Kohn-Sham equations the external potential consists of Coulombic potentials centred at each lattice site in the material. The Kohn-Sham equations then include the interactions of all the electrons in the material, this results in a prohibitively high cut off energy for the Bloch orbitals (almost 100,000eV for diamond) as the plane wave expansion must describe tightly bound core electron states and the valence electron wave functions must contain many nodes to ensure orthogonality between all the electrons.[52]

The solution to making tractable calculations is to reduce the cut off energy of the orbitals, but this is only possible if the Coulombic potential and core electrons can be replaced with another potential, which does not require such a high cut off.[56, 57, 58] Using this replacement potential or pseudopotential requires the electrons in the material to be partitioned into core and valence types. Core electrons are taken to be the electrons that are tightly bound and localised on the lattice sites. Hence the energy states of the core electrons are assumed not to change when the atomic chemical environment is changed (i.e. changing from an isolated atom in vacuum to an atom in a solid). The valence electrons are the electrons with higher energy states that typically form the bonding orbitals in a solid, as such for the valence electrons the energy states of the orbitals associated with them will be greatly changed by a change in chemical environment.

The pseudopotential must satisfy several conditions; the first is that outside a core radius (r_c) the valence electron orbitals and pseudopotential should exactly match the valence all-electron orbitals and the Coulomb potential respectively. Secondly the pseudopotential should also have the same scattering properties as the all-electron calculation. Thirdly the pseudopotential should be spherically symmetric and the valence orbitals should have no nodes inside the core region.

The scattering properties are determined by the angular momentum of the electron, so the pseudopotential must be angular momentum state dependent, but as it has to be spherically symmetric, the angular momentum states are fully separable. The pseudopotential can be written in a semi-local form that projects the valence orbitals onto the angular momentum dependent potential;

$$\hat{V}_{\text{ext}}^{\text{SL}}(\mathbf{r}) = \sum_{l,m} |Y_{l,m}\rangle V_l(\mathbf{r}) \langle Y_{l,m}|, \tag{2.98}$$

with $Y_{l,m}(\theta, \phi) = P_l(\cos(\theta))e^{im\phi}$ where $P_l(\cos(\theta))$ are Legrendre polynomials.[52] The potential is semi-local as it is local in position, but non-local in angular momentum.

2.5.1 Norm-Conserving Pseudopotentials

The properties the pseudopotential must satisfy provide a starting place to find a pseudopotential. However there exist a near infinite number of possible potentials that could satisfy those conditions. To allow accurate transferable pseudopotentials to be made using *ab-initio* methods the pseudopotential should also satisfy the "norm-conservation" conditions.[8][1, 59] The norm-conservation conditions are:

1. The integrated charge, Q inside r_{c} for each valence electron state must agree for the pseudo and all-electron orbitals (norm-conservation), such that; $Q = \int_0^{r_{\mathrm{c}}} d\mathbf{r}|\phi^{\sigma}(\mathbf{r})|^2 = \int_0^{r_{\mathrm{c}}} d\mathbf{r}|\phi^{\sigma,\mathrm{PS}}(\mathbf{r})|^2$.
2. All-electron and pseudo eigenvalues agree (for a given reference electron configuration, usually the neutral atom), such that; $(\hat{H}^{\sigma}_{\mathrm{KS}} - \varepsilon^{\sigma}_i)\phi^{\sigma}_i(\mathbf{r}) = (\hat{H}^{\sigma,\mathrm{PS}}_{\mathrm{KS}} - \varepsilon^{\sigma}_i)\phi^{\sigma,\mathrm{PS}}_i(\mathbf{r}) = 0$.
3. All-electron and pseudo valence orbitals agree outside of r_{c}.
4. The logarithmic derivative of the all-electron and pseudo valence orbitals agree at r_{c}.
5. The first energy derivative of the logarithmic derivative of the all-electron and pseudo valence orbitals agree at r_{c} and beyond.

These conditions rely on the pseudo-orbitals satisfying the orthonormality conditions that the all electron orbitals must obey;

$$\langle \phi^{\sigma,\mathrm{PS}}_i | \phi^{\sigma',\mathrm{PS}}_j \rangle = \delta_{i,j}\delta_{\sigma,\sigma'}. \tag{2.99}$$

2.5.2 Pseudopotential Generation

Pseudopotential generation consists of several distinct steps, the first involves solving the radial Schrödinger equation for the reference configuration;

$$\left(-\frac{1}{2}\frac{\delta^2}{\delta r^2} + \frac{l(l+1)}{2r^2} - \frac{Z}{r} + \int \frac{\rho(r')}{|r-r'|}dr' + V_{\mathrm{xc}}(r)[\rho] \right) rR^{nl}(r) = \varepsilon_{nl} rR^{nl}(r), \tag{2.100}$$

where the density is given by;

$$\rho(r) = \sum_n \sum_{l=0}^{l_{\max}} \sum_{m=-l}^{l} |rR^{nl}(r)|^2. \tag{2.101}$$

The pseudo-orbitals are then generated from equation 2.100 according to the previously mentioned conditions. The screened pseudopotential can be obtained by inversion of the

[8] A "good" transferable pseudopotential is one that provides accurate results for a material in a variety of chemical conditions, from isolated atoms to ionic compounds to covalently bonded materials. Transferability is usually increased by reducing the core radius of the pseudopotential.

radial Schrödinger equation using the pseudo-orbitals;

$$V_{\mathrm{PS}}^{\mathrm{sc},l}(r) = \varepsilon_l - \frac{l(l+1)}{2r^2} + \frac{1}{2rR_{\mathrm{PS}}^l(r)}\frac{\delta^2}{\delta r^2} rR_{\mathrm{PS}}^l(r), \tag{2.102}$$

note the index n has been dropped as the potential is generated using the lowest lying valence state for each angular momentum value.[2] The pseudopotential is finally obtained by unscreening the electronic contributions to the potential from the valence electrons, this amounts to subtracting the valence Hartree and exchange-correlation terms from the screened potential;

$$V_{\mathrm{PS}}^{l}(r) = V_{\mathrm{PS}}^{\mathrm{sc},l}(r) - \int \frac{\rho_{\mathrm{v}}(r')}{|r-r'|}dr' - V_{\mathrm{xc}}(r)[\rho_{\mathrm{v}}], \tag{2.103}$$

where $\rho_{\mathrm{v}}(\mathbf{r})$ is the density of the valence electrons.

The possible forms of the pseudo-orbitals are the main deterministic factor in the pseudopotential as the form of the orbitals determine the "smoothness" of the potential. A potential would be described as "smoother" than another potential if the plane wave energy cut off required for a calculation is lower than the other potential otherwise it would be described as "harder". The chosen approximate forms of the pseudo-orbitals are numerous but in this work the work of Rappe *et al* was used,[60] other potential forms are laid out in refs [61, 62, 63, 64, 65]. The pseudo-orbitals inside r_{c} are expanded as a series of spherical Bessel functions, with the coefficients of the expansion optimised to minimise the residual of the kinetic energy under the constraint that the Bessel functions have continuity of first and second derivatives in the core region as well as satisfying the norm-conservation conditions. (Further details in refs [60] and [66]) An example pseudopotential and pseudo-orbital for oxygen are shown in figure 2.4.

A further complication is that to ensure identical treatment of core and valence electrons the same exchange-correlation functional should be used in the core and the valence. This raises a problem when considering non-local exchange-correlation potentials as when unscreening the potential the non-local nature of the potentials can prevent a pseudopotential being generated that maintains the condition that the pseudo-orbitals are identical to the original all-electron reference orbitals outside the core region. This is an acute problem as the use of Hartree-Fock and other exchange-only calculations require HF pseudopotentials.[67]

However by enforcing a localisation constraint on the non-local unscreened pseudopotential a tractable local Hartree-Fock norm-conserving potential can be found. The potential is unscreened as in equation 2.103 with a non-local exchange term replacing the local exchange-correlation potential;

$$V_{\mathrm{PS}}^{l}(r) = V_{\mathrm{PS}}^{\mathrm{sc},l}(r) - \int \frac{\rho_{\mathrm{v}}(r')}{|r-r'|}dr' - V_{\mathrm{x}}[\{R_l\}_{\mathrm{v}}], \tag{2.104}$$

the pseudopotential form however is not guaranteed to decay as $1/r$. To ensure this

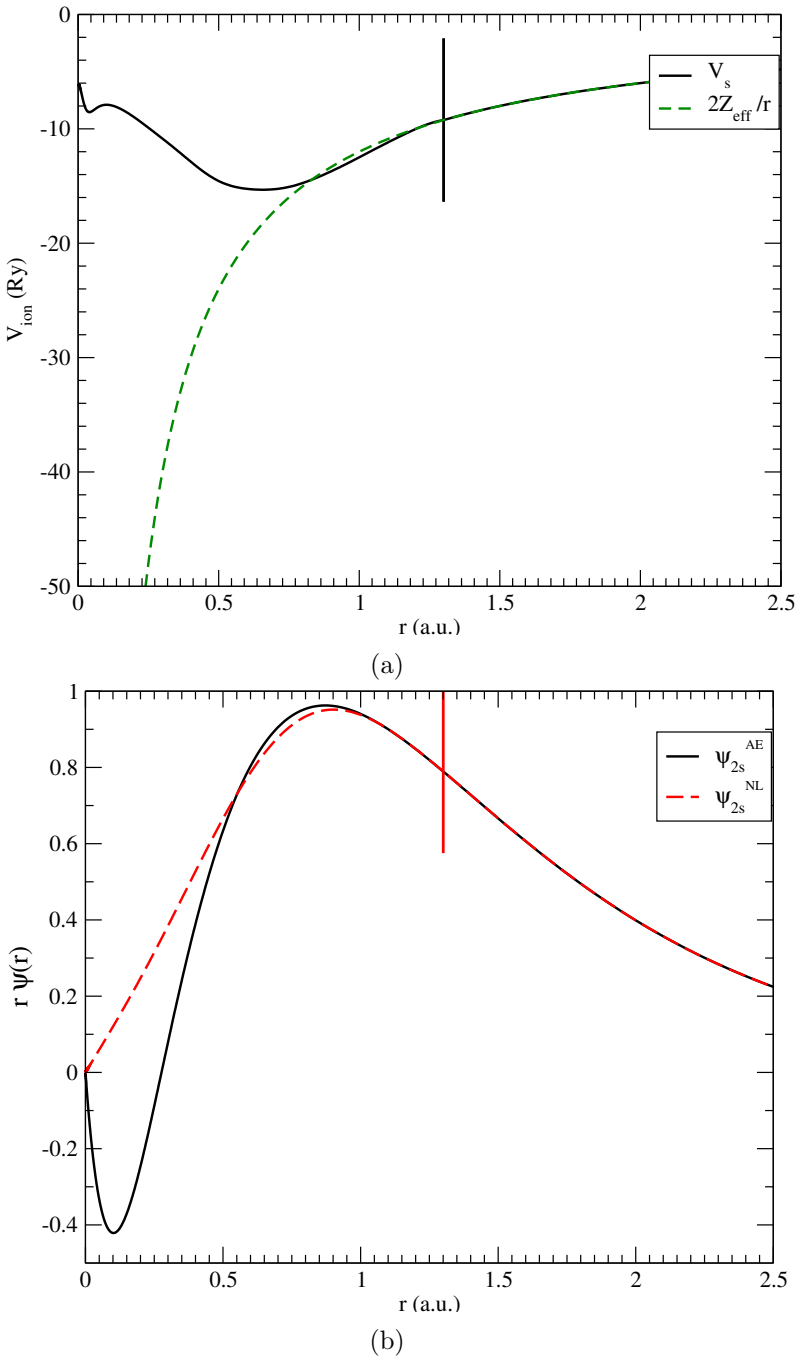

Figure 2.4: Comparison of pseudopotential and pseudo-orbital for the 2s electron in oxygen generated using PBE as the exchange-correlation functional, a) pseudopotential for the $l = 0$ channel in oxygen (black) and the correct Coulomb potential (dashed green), b) pseudo-orbital for the 2s state in oxygen (dashed red) and all-electron 2s orbital (black). Vertical lines indicate core radius.

the potential must be localised and have the correct behaviour outside the core region, this can be accomplished in a self consistent manner. Full details and the form of the localised potential can be found in refs [66] and [67].

2.5.3 The Kleinman-Bylander Separable Pseudopotential

The previously discussed form of the pseudopotential requires an inseparable double sum over the reciprocal lattice vectors to find the electron-ion energy, as the calculation of the energy requires the matrix elements; $\langle\phi_i|\hat{V}_{\mathrm{SL}}|\phi_j\rangle$ to be calculated and these depend on $\mathbf{G}$ and $\mathbf{G}'$. This forces the calculation of this energy to scale as N_{pw}^2 which severely limits the size of a calculation if the number of reciprocal lattice vectors required is large.

If the Kleinman-Bylander form [68] of the pseudopotential is employed, the double sum can be split into two products, the potential is written as the sum of a local potential (independent of l and m) and a non-local potential (dependent on l and m);

$$\hat{V}_{\mathrm{ext}}(\mathbf{r}) = \hat{V}_{\mathrm{local}}(\mathbf{r}) + \delta\hat{V}_{\mathrm{NL}}(\mathbf{r},\mathbf{r}') = \hat{V}_{\mathrm{local}}(\mathbf{r}) + \sum_{l,m}\frac{|\phi_{l,m}^{\mathrm{PS}}\delta V_l\rangle\langle\delta V_l\phi_{l,m}^{\mathrm{PS}}|}{\langle\phi_{l,m}^{\mathrm{PS}}|\delta V_l|\phi_{l,m}^{\mathrm{PS}}\rangle}, \tag{2.105}$$

δV_l is fully non-local and $\phi_{l,m}^{\mathrm{PS}}$ are the pseudo-orbitals. The matrix elements are then separable as each of the three matrix elements is local;

$$\langle\phi_i|\delta V_{\mathrm{NL}}|\phi_j\rangle = \sum_{l,m}\langle\phi_i|\phi_{l,m}^{\mathrm{PS}}\delta V_l\rangle\frac{1}{\langle\phi_{l,m}^{\mathrm{PS}}|\delta V_l|\phi_{l,m}^{\mathrm{PS}}\rangle}\langle\delta V_l\phi_{l,m}^{\mathrm{PS}}|\phi_j\rangle, \tag{2.106}$$

this form then scales as N_{pw}. The Kleinman-Bylander form of the pseudopotential however may suffer from unphysical "ghost-states" which must to identified to ensure a good physical potential, see ref [69] for a detailed discussion of the causes of identification of ghost-states.[9]

2.5.4 Ultrasoft Pseudopotentials

While norm-conserving pseudopotentials are the ones used in this work, the quality of the pseudopotential is always a compromise between transferability and smoothness. The harder the pseudopotential (typically by employing a very small core radius) the more transferable it is, but this requires a very large energy cut-off to be employed. If the pseudopotential is very smooth (large core radius) it may not be very transferable.

A pseudopotential that is both smooth and highly transferable can be constructed by relaxing the norm-conservation requirement when constructing the potential. The transferability can be increased further by employing multiple reference configurations.[70] The degree of which the pseudopotential is norm-conserving for each state in the pseu-

[9] "Ghost states" are states of the potential with unphysically low eigenvalues.

dopotential can be measured by using;

$$\Delta Q_{i,j}(r) = \int_0^{r_c} \phi_i^{\dagger}(r)\phi_j(r) - \phi_i^{\mathrm{PS}\dagger}(r)\phi_j^{\mathrm{PS}}(r)dr, \tag{2.107}$$

where here i and j are composite indexes over reference state ε_i and angular momentum, l,m, such that $i = \{\varepsilon_i, l, m\}$, if $\Delta Q_{i,j} = 0$ then the potential is norm-conserving. If the Kleinman-Bylander form the $\delta\hat{V}_{NL}$ term is redefined as;

$$\delta\hat{V}_{\mathrm{NL}} = \sum_{i,j}(B_{i,j} + \varepsilon_i \Delta Q_{i,j})|\beta_i\rangle\langle\beta_j|, \tag{2.108}$$

with $B_{i,j} = \langle\phi_i|\chi_j\rangle$ and $\beta_i = \sum_j B^{-}_{i,j}1\chi_j$. With a local orbital χ_i given by;

$$\chi_i = \left(\varepsilon_i - \frac{1}{2}\nabla^2 + V_{\mathrm{local}}(r)\right)\phi_i^{\mathrm{PS}}(r), \tag{2.109}$$

where $V_{\mathrm{local}}(r)$ is the local potential in the Kleinman-Bylander form of the potential. The pseudo-orbitals then are the solutions to the generalised eigenvalue problem;

$$\left(\frac{1}{2}\nabla^2 + V_{\mathrm{local}}(r) + \delta V_{\mathrm{NL}} - \varepsilon_i\hat{S}\right)\phi_i^{\mathrm{PS}}(r), \tag{2.110}$$

where $\hat{S}$ is the overlap operator;

$$\hat{S} = \hat{1} + \sum_{i,j}\Delta Q_{i,j}|\beta_i\rangle\langle\beta_j|, \tag{2.111}$$

which only differs from 1 inside the core region. The pseudo-orbitals are then orthonormalised under the condition;

$$\langle\phi_i|\hat{S}|\phi_j\rangle = \delta_{i,j}. \tag{2.112}$$

As the norm-conservation constraint is relaxed the pseudo-orbitals can be made much smoother and the cut-off energy required for a calculation becomes much smaller.[70] However use of a pseudopotential in this form in a real calculation would lead to a deficit of charge in the density in the core region, hence the density must be corrected to ensure the correct amount of charge;

$$\rho_{\Gamma}(\mathbf{r}) = \sum_{n,\mathbf{k}}\phi^{\dagger}_{n,\mathbf{k}}(\mathbf{r})\phi_{n,\mathbf{k}}(\mathbf{r}) + \sum_{i,j}\sum_{n,\mathbf{k}}\langle\beta_i|\phi_{n,\mathbf{k}}(\mathbf{r})\rangle\langle\phi_{n,\mathbf{k}}(\mathbf{r})|\beta_j\rangle\Delta Q_{i,j}(\mathbf{r}). \tag{2.113}$$

The use of norm-conserving pseudopotentials rather than the more transferable and smoother ultrasoft pseudopotentials is due to technical reasons which will be discussed later.

2.6 Finding the Ground State

2.6.1 Energy Minimisation

The Hohenberg-Kohn theorems guarantee that the total energy is variational, hence the minimising Kohn-Sham orbitals and density can be found by iterative minimisation. The total energy can be directly minimised by varying the orbitals, using a steepest descent method. Starting from a trial set of Kohn-Sham orbitals, the steepest descent algorithm proceeds iteratively by calculating the search direction, ζ_i^p for a single orbital, i, at iteration p, which is given by;

$$\zeta_i^p = -(\hat{H} - \langle\phi_i^p|\hat{H}|\phi_i^p\rangle)\phi_i^p. \tag{2.114}$$

The minimisation of the total energy must also proceed under the constraint that the orbitals remain orthogonal. This is achieved by orthogonalising the search direction against all the other orbitals in the calculation, using the Gram-Schmidt scheme;

$$\zeta_i'^p = \zeta_i^p - \sum_{j\neq i}\langle\phi_j^p|\zeta_i^p\rangle\phi_j^p. \tag{2.115}$$

By adding this search direction to the orbital under consideration and sampling the total energy, a function can be fitted to find the minima in that search direction. Typically three sampling points are used (allowing a parabola to be fitted); more points can be used to build a higher order polynomial but typically this is unnecessary. The density and potentials are then updated and the total energy calculated. This scheme proceeds iteratively, band by band until the change in the total energy is within a convergence tolerance. The full procedure for the three point minimisation is shown in figure 2.5.

2.6.2 Conjugate Gradients

While the steepest descent method is simple it does not guarantee convergence in a finite number of steps.[52] A slight modification to the algorithm that ensures convergence in n-steps is the conjugate gradient method, where each search direction is conjugate to all the previous search directions. For a general minimisation problem with a gradient, $\mathbf{g}^p$ the conjugate gradient search direction, $\mathbf{d}^p$ is given by;

$$\mathbf{d}^p = \mathbf{g}^p + \gamma^p\mathbf{d}^{p-1}, \tag{2.116}$$

with γ^p typically given by the Fletcher-Reeves form for conjugate gradients;[71]

$$\gamma^p = \frac{\mathbf{g}^p.\mathbf{g}^p}{\mathbf{g}^{p-1}.\mathbf{g}^{p-1}}. \tag{2.117}$$

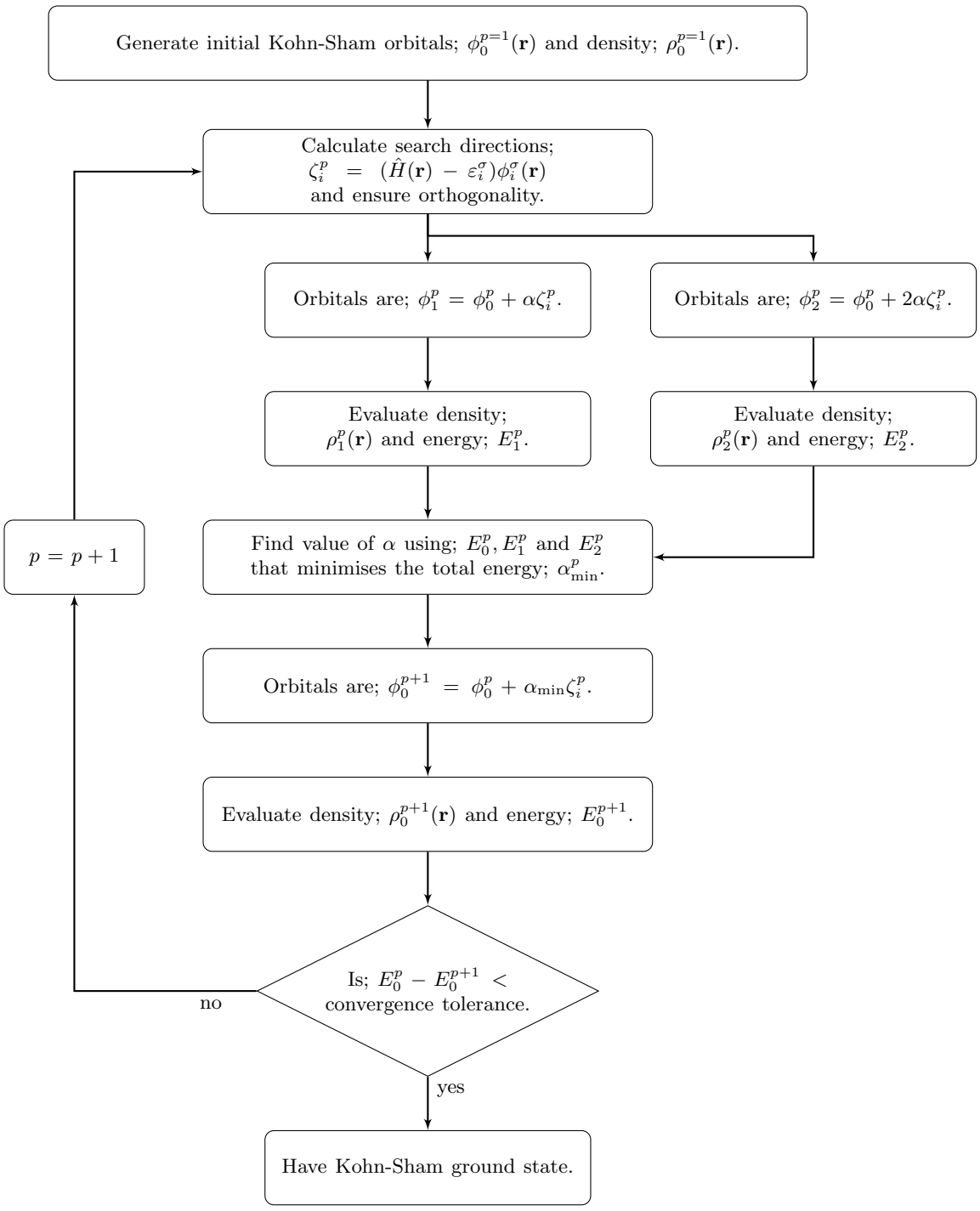

Figure 2.5: The procedure for the calculation of total energy of a Kohn-Sham system, using a steepest descent method and a parabolic line search.

2.6.3 Preconditioning

While conjugate gradients decrease the number of iterations needed to obtain convergence over steepest descent, the number of iterations can be further reduced by preconditioning the search direction. The Kohn-Sham Hamiltonian is considered an ill-conditioned problem due to the wide range of values the eigenvalues can take. By applying a transformation to reduce the range of the eigenvalue spectrum the problem can converge in tens of iterations.[72]

If a calculation was exactly at the energy minimum then the steepest descent's search direction would have zero magnitude, this implies that the search direction can be used to measure the error in the current orbitals.[52] The error in an orbital, $\delta\phi_i$ can be written as an expansion in the eigenstates of the Kohn-Sham Hamiltonian;

$$\delta\phi_i = \sum_\alpha c_{i,\alpha}\xi_\alpha, \tag{2.118}$$

this is related to the search direction by;

$$\zeta_i = -\sum_\alpha (\varepsilon_\alpha - \langle\phi_i|\hat{H}|\phi_i\rangle)c_{i,\alpha}\xi_\alpha, \tag{2.119}$$

with ε_α is the eigenvalue associated with the eigenstate, ξ_α. If the eigenvalues were made degenerate then the search direction would be a multiple of the error in the orbital.

From equation 2.91 the diagonal kinetic energy term dominates the total energy relative to the other energy contributions for the higher energy states (large $\mathbf{G}$). If the Hamiltonian is multiplied by a matrix that is the inverse of the kinetic energy operator, the higher order states become effectively degenerate and the search direction a multiple of the error in the orbital. The preconditioning matrix, $K_{\mathbf{G},\mathbf{G}'}$ approximates this inverse operator. The most commonly used form is the Teter, Allen and Payne (TPA) form;[72]

$$K_{\mathbf{G},\mathbf{G}'} = \delta_{\mathbf{G},\mathbf{G}'}\frac{27+18x+12x^2+8x^3}{27+18x+12x^2+8x^3+16x^4}, \tag{2.120}$$

where x is a function of the kinetic energy;

$$x = \frac{|\mathbf{k}+\mathbf{G}|^2}{\langle\phi_i|\nabla^2|\phi_i\rangle}. \tag{2.121}$$

This form is attractive for use as a preconditioner for the orbitals as it is well behaved (and has well behaved derivatives) as $x \to 0$ and it has minimal effect on the search direction for small wave vectors ($x < 1$).

2.6.4 Density Mixing

A less computationally expensive method for minimising the total energy is density mixing; the method as shown in figure 2.6, starts with an initial guess of the Kohn-Sham

orbitals. The orbitals generate a density, Hartree and exchange-correlation potentials and the single-particle Kohn-Sham Hamiltonian. The eigenfunctions (orbitals) of this Kohn-Sham Hamiltonian are then found by iterative diagonalisation of the Hamiltonian matrix. Iterative diagonalisation variationally minimises the eigenvalue of an individual orbital by varying the plane wave coefficients, while maintaining the orthogonality of the orbitals.

The eigenfunctions and eigenvalues of the Hamiltonian matrix can also be found using conventional matrix diagonalisation of the Hamiltonian.[10] It is however computationally expensive scaling as N_{pw}^3 and wasteful as the method calculates all the eigenvalues and states of the matrix (which can number in the thousands) when we are only interested in the lowest occupied states (which usually number in the 10s).[52]

If the density that results from these new orbitals is sufficiently similar to the input density, such that the density is "self consistent" (the Hamiltonian constructed from the density generates a set of orbitals that give the input density) and the difference in total energy between iterations is small, then the Kohn-Sham ground state is found. If the densities are different (the change in energy will also be large), then a new density is chosen based on a density mixing formula that mixes densities from the current and previous iterations and the procedure repeated. See refs; [74, 75, 76, 77] for further details on density mixing, mixing schemes and its implementation. The Hohenberg-Kohn theorems guarantee that the self-consistent density is also the ground state density.[52]

While density mixing is computationally simple and usually quick to converge to the ground state, it can suffer from discontinuous changes in the Hamiltonian; this can result in the total energy increasing and instabilities in the minimisation, especially when using the Fock integral for the exchange interaction as it is not explicitly density dependent.[11]

2.6.5 Ground State Geometry

The methods described above allow the electronic ground state energy to be found for an arbitrary arrangement of atoms. One of the many uses for density functional theory is to find optimal arrangements of ions by minimising the total energy of the system. The force acting on an ion is given by the Hellman-Feynman theorem as;

$$\begin{aligned} F_I = \frac{\delta E}{\delta \mathbf{R}_I} &= \sum_i \langle \phi_i | \frac{\delta \hat{H}}{\delta \mathbf{R}_I} | \phi_i \rangle + \langle \frac{\delta \phi_i}{\delta \mathbf{R}_I} | \hat{H} | \phi_i \rangle + \langle \phi_i | \hat{H} | \frac{\delta \phi_i}{\delta \mathbf{R}_I} \rangle \\ &= \sum_i \langle \phi_i | \frac{\delta \hat{H}}{\delta \mathbf{R}_I} | \phi_i \rangle, \end{aligned} \tag{2.122}$$

[10] Conventional matrix diagonalisation was used in early electronic structure calculations using empirical pseudopotentials.[73]

[11] The discontinuous changes are usually due to "charge sloshing" where density is moved between two near degenerate states, resulting in minimal changes in the energy but relatively large changes in the electronic structure.

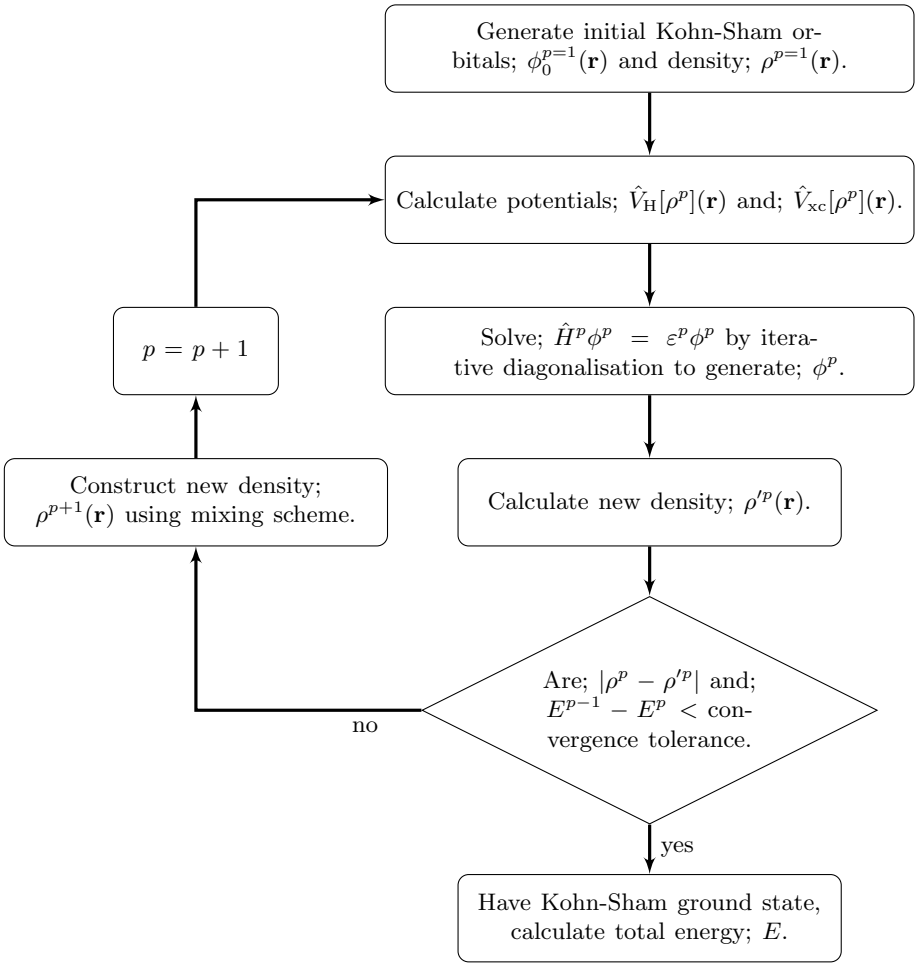

Figure 2.6: The procedure for the calculation of total energy of a Kohn-Sham system, using density mixing.

as the last two terms equal zero as long as the orbitals are eigenfunctions of $\hat{H}$. $\mathbf{R}_I$ is the position of an ion.[78] The stress on the unit cell can similarly be calculated.[1, 53]

The geometry of the system can be optimised by relaxing the forces and stress on the unit cell and its constituent ions to minimise the total energy. Using the calculated forces and stresses a minimisation of the total energy can be performed using a similar methodology as that shown in figure 2.5, except instead of varying the orbitals the ionic positions and unit cell dimensions are varied. The total energy, magnitude of the forces and stresses can all be used to determine whether the calculation of the geometry has reached a minimum.[52] Finding the actual global ground state structure of a system is the subject of considerable research.[79]

2.7 The CASTEP Code

The calculations described within this thesis (unless otherwise stated) were carried out using the CASTEP electronic structure code.[80, 81] This code uses the techniques described in the previous sections to solve the Kohn-Sham equations. The theory and functionality that is described in subsequent chapters has been implemented into the code.

The code is written in FORTRAN 90 and supports efficient fast-Fourier transforms (FFTs) to transform quantities between real and reciprocal space. The code is also parallelised to increase the speed of the calculation by distributing the information and work required across multiple processors. Parallelisation can be implemented by dividing the calculation up by k-point or **G**-vector, both methods can be used simultaneously. The limiting factor on parallelisation is the requirement for the individual processors to share information, for large scale parallelisation the time required to pass around the information can come to dominate the total time required for the calculation. Due to this the preference for parallelisation is to divide the calculation into k-point groups first and then to subdivide the k-point groups into **G**-vector groups.

To reduce the memory overheads, especially for memory intensive non-local functionals calculations, CASTEP also supports shared memory processes; this allows a subgroup of processors in the same **G**-vector group to share the memory for the storage of orbitals and other quantities. For a non-local calculation (as a large number of calculations presented here will be) this gives a large speed up to the calculation and reduces the amount of memory required by reducing duplicate information, as in a non-local calculation each process requires a copy of all the orbitals in a calculation.

Chapter 3

Theory of Local Exchange Potentials

3.1 Properties of the Exchange-Correlation Potential

3.1.1 The Exchange-Correlation Hole

As discussed in the previous chapter there are many varieties of approximate exchange-correlation functionals. Many depend on the density (or derivatives of the density). The success of the LDA and successor functionals is attributed to the satisfaction of "the exchange-correlation sum rule" (as well as various scaling relations; for further details on sum rules and scaling relations see ref. [82]). The pair density of an interacting system is defined as;

$$\Gamma(\mathbf{r},\mathbf{r}') = N(N-1)\int d\mathbf{r}_3 ... \int d\mathbf{r}_N |\Psi^{\dagger}(\mathbf{r},\mathbf{r}',\mathbf{r}_3,...,\mathbf{r}_N)|^2, \tag{3.1}$$

which is the probability of finding one electron at $\mathbf{r}$ and another electron at $\mathbf{r}'$. The integrals of the pair density and density are;

$$\iint d\mathbf{r} d\mathbf{r}' \Gamma(\mathbf{r},\mathbf{r}') = N(N-1), \tag{3.2}$$

$$\int d\mathbf{r} \rho(\mathbf{r}) = N. \tag{3.3}$$

However in a fully non-interacting system the probability of finding a classical particle at $\mathbf{r}$ and another particle at $\mathbf{r}'$ is the classical pair density, as given by; $\rho(\mathbf{r})\rho(\mathbf{r}')$, which when integrated over $\mathbf{r}$ and $\mathbf{r}'$ will not yield the correct value for the pair density. The effect of the exchange potential on the non-interacting electrons represents the effect of the electrons being identical and satisfying Fermi-Dirac statistics. The effect of the correlation potential on the non-interacting electrons represents interactions beyond the mean field. The effect of exchange and correlation is to reduce the classical value of the electron density at $\mathbf{r}$ due to the instantaneous position of the second electron at $\mathbf{r}'$.

Therefore each electron depletes the electron density around itself as a direct consequence of exchange-correlation effects. This depletion or hole is the exchange-correlation hole, $\Delta\rho_{xc}(\mathbf{r},\mathbf{r}')$. Equating the pair density, the non-interacting pair density and the exchange-correlation hole gives;

$$\rho(\mathbf{r},\mathbf{r}') = \rho(\mathbf{r})\rho(\mathbf{r}') + \rho(\mathbf{r})\Delta\rho_{\mathrm{xc}}(\mathbf{r},\mathbf{r}'), \tag{3.4}$$

and integrating over $\mathbf{r}'$;

$$(N-1)\rho(\mathbf{r}) = N\rho(\mathbf{r}) + \rho(\mathbf{r})\int d\mathbf{r}'\Delta\rho_{\mathrm{xc}}(\mathbf{r},\mathbf{r}'), \tag{3.5}$$

which rearranges to give for every $\mathbf{r}$;

$$\int d\mathbf{r}'\Delta\rho_{\mathrm{xc}}(\mathbf{r},\mathbf{r}') = -1. \tag{3.6}$$

This implies that due to the exchange correlation interaction an electron at $\mathbf{r}$ displaces an equal and opposite amount of charge around itself. The combined charge of the electron and the change in density (or 'hole') are in total charge neutral.[1] The LDA, GGA and HF satisfy this property of the exchange correlation potential.

3.1.2 Self Interaction

The Hartree potential represents a classical charge interaction and when applied to an electron, that electron interacts with all N electrons in the density. Interaction with the density includes the interaction of the electron with itself, which is an unphysical interaction known as 'self interaction'. In equation 2.4 the Coulomb interaction explicitly excludes all self interaction terms (the sum includes all terms, except when $i = j$). Self interaction is introduced by the use of the Hartree potential and the exchange-correlation potential must fully correct the spurious self interaction.

To demonstrate the correct behaviour of the exchange-correlation potential we use the simplest case of a hydrogen atom, where there is only one electron. The Kohn-Sham total energy is then;

$$E_{\mathrm{total}} = -\frac{1}{2}\int d\mathbf{r}\phi(\mathbf{r})\nabla^2\phi(\mathbf{r}) - \int d\mathbf{r}\frac{\rho(\mathbf{r})}{r} + \frac{1}{2}\iint d\mathbf{r}d\mathbf{r}'\frac{\rho(\mathbf{r})\rho(\mathbf{r}')}{|\mathbf{r}-\mathbf{r}'|} + E_{\mathrm{xc}}[\rho(\mathbf{r})], \tag{3.7}$$

the Hartree energy is purely composed of self-interaction energy and hence the exchange-correlation energy must correct this spurious contribution. Indeed for any single orbital (with single orbital density, $\rho_i(\mathbf{r})$) the sum of the Hartree and exchange-correlation energies is zero. Using the exact exchange energy (from Hartree-Fock theory) the sum of

[1] It should be noted that the charge of the hole is actually +1, but we follow the convention that the charge of an electron is 1, despite the electron being negatively charged.

the energies is given by;

$$\frac{1}{2}\iint d\mathbf{r}d\mathbf{r}'\frac{\rho_i(\mathbf{r})\rho_i(\mathbf{r}')}{|\mathbf{r}-\mathbf{r}'|}-\frac{1}{2}\iint d\mathbf{r}d\mathbf{r}'\frac{\phi_i^\dagger(\mathbf{r})\phi_i(\mathbf{r}')\phi_i^\dagger(\mathbf{r}')\phi_i(\mathbf{r})}{|\mathbf{r}-\mathbf{r}'|}+E_{\mathrm{c}}[\rho_i(\mathbf{r})]=0, \tag{3.8}$$

it is easy to see that the Hartree and Fock energies cancel exactly, leaving the single orbital correlation energy to be zero. For Hartree-Fock the self-interaction is cancelled, however for the LDA and its derivatives the self-interaction is not fully cancelled.[3] This also implies that an electron interacts only with the $N-1$ other electrons in the material.

The interaction of an electron with only the other $N-1$ electrons leads to a third property. Considering an electron in an atomic N electron system that is at $r\to\infty$, at this distance the external potential is;

$$\hat{V}_{\mathrm{ext}}(\mathbf{r})\to-\frac{N}{r}, \tag{3.9}$$

and the Hartree potential as;

$$\hat{V}_{\mathrm{H}}(\mathbf{r})\to\frac{N}{r}. \tag{3.10}$$

However the electron at $r\to\infty$ should interact with the positive ion (the atomic core has charge $+N$) and the remaining electrons (with charge $-(N-1)$) but instead sees a neutral atom due to self interaction. Therefore in an exact system the exchange-correlation potential must decay as;

$$\hat{V}_{\mathrm{xc}}(\mathbf{r})\to-\frac{1}{r}, \tag{3.11}$$

to fully cancel the self interaction at long range. This property is satisfied by the Hartree-Fock approximation by virtue of it cancelling self interaction but not the LDA or its derivatives.

Due to satisfying the above conditions, Hartree-Fock seems like a natural choice to produce accurate electronic structures. However Hartree-Fock suffers from other issues due to the non-local orbital dependent nature of the exchange potential. The exchange potential was previously defined as;

$$\hat{V}_{\mathrm{x}}^\sigma\psi_i^\sigma(\mathbf{r})=\sum_{j=1}^{N^\sigma}\iint d\mathbf{r}d\mathbf{r}'\frac{\phi_j^\sigma(\mathbf{r})\phi_j^{\dagger\sigma}(\mathbf{r}')}{|\mathbf{r}-\mathbf{r}'|}\phi_i^\sigma(\mathbf{r}'). \tag{3.12}$$

In Hartree-Fock the excitation energies are very large, due to a difference in treatment of the occupied and unoccupied orbitals. The occupied orbitals interact with $N-1$ electrons, whereas the unoccupied orbitals interact with N electrons.[13] This amounts to adding an electron to the system, assuming no response of the system and no correlation, resulting in a very large energy. Whereas for a local exchange-correlation potential the occupied and unoccupied orbitals interact with the same potential.[1] This leads to smaller excitation energies than those found for HF. Due to the self-interaction error

in the LDA and GGAs the excitation energies are very small relative to experiment, as the self interaction in the occupied orbitals shifts the eigenvalues for these states by a positive amount.

These issues lead naturally to the proposition of finding an exchange-correlation functional that satisfies the exact properties that HF satisfies, that is orbital rather than density dependent (like HF), while retaining the local nature of the Kohn-Sham scheme, such that;

$$\hat{V}^{\sigma}_{\mathrm{xc}}(\mathbf{r}) = \frac{\delta E_{\mathrm{xc}}[\phi^{\sigma}_{i}]}{\delta \rho^{\sigma}(\mathbf{r})}. \tag{3.13}$$

However the functional form of this potential is not known explicitly in a closed form.

In analogy to the second Hohenberg-Kohn theorem, there must exist a local exchange-correlation potential that minimises the total energy functional for a given system. This also implies that the total energy is a functional of the exchange-correlation potential;

$$E[\hat{V}^{\sigma}_{\mathrm{xc}}(\mathbf{r})] = E[\{\phi_i[\hat{V}^{\sigma}_{\mathrm{xc}}(\mathbf{r})]\}]. \tag{3.14}$$

Additionally as the exchange-correlation potential will determine the orbitals through the Kohn-Sham equations, the orbitals are then functionals of the potential. The total energy for a given exchange-correlation potential can then be found from the orbitals, allowing an orbital dependent total energy functional to be used which is implicitly dependent on the potential.[1, 83]

Finding the potential that optimises the total energy using a local potential for the exchange-correlation potential while having an orbital dependent functional for the exchange-correlation energy is known as the "Optimised Effective Potential Method".[3, 4, 35, 84]

3.2 Exact Exchange by the Optimised Effective Potential Method

3.2.1 Exact Exchange by Chain Rule Expansion

The local exchange-only potential that minimises the Hartree-Fock total energy is known as the exact exchange (EXX) potential. The EXX potential for an insulating Kohn-Sham system can be found exactly using the optimised effective potential method.[2] Correlation between the electrons is neglected. Using approximate correlation functionals for the missing interactions such as the correlation part of the LDA (LDAc) or GGAs (PBEc) are an option but the exchange-correlation potential may no longer benefit from a cancellation of errors between exchange and correlation.[3] The exchange-only potential

[2] The generalisation of the exact exchange potential to include metallic systems is addressed in section 3.6.

[3] This cancellation of errors is part of the success of the LDA and GGA.

is given by;

$$\hat{V}_{\mathrm{x}}^{\sigma}(\mathbf{r}) = \frac{\delta E_{\mathrm{x}}[\phi_i^{\sigma}]}{\delta \rho^{\sigma}(\mathbf{r})}. \tag{3.15}$$

The orbitals are the solutions to the Kohn-Sham equations;

$$\left[-\frac{\nabla^2}{2} + \hat{V}_{\mathrm{ext}}(\mathbf{r}) + \int d\mathbf{r}' \frac{\rho(\mathbf{r}')}{|\mathbf{r}-\mathbf{r}'|} + \hat{V}_{\mathrm{x}}^{\sigma}(\mathbf{r})\right] \phi_i^{\sigma}(\mathbf{r}) = \varepsilon_i^{\sigma} \phi_i^{\sigma}(\mathbf{r}). \tag{3.16}$$

The total energy is given by the Hartree-Fock energy functional;

$$\begin{aligned}\sum_{\sigma}\sum_{i=1}^{N^{\sigma}} -\frac{1}{2}\int d\mathbf{r}\phi_i^{\sigma\dagger}(\mathbf{r})\nabla^2\phi_i^{\sigma}(\mathbf{r}) + \int d\mathbf{r}\hat{V}_{\mathrm{ext}}(\mathbf{r})\rho(\mathbf{r}) + \frac{1}{2}\iint d\mathbf{r}d\mathbf{r}'\frac{\rho(\mathbf{r}')\rho(\mathbf{r})}{|\mathbf{r}-\mathbf{r}'|} \\ - \sum_{\sigma}\sum_{i=1}^{N^{\sigma}}\sum_{j=1}^{N^{\sigma}}\frac{1}{2}\iint d\mathbf{r}d\mathbf{r}'\frac{\phi_i^{\sigma\dagger}(\mathbf{r})\phi_i^{\sigma}(\mathbf{r}')\phi_j^{\sigma}(\mathbf{r})\phi_j^{\sigma\dagger}(\mathbf{r}')}{|\mathbf{r}-\mathbf{r}'|} = E[\phi_i^{\sigma}],\end{aligned} \tag{3.17}$$

with the orbitals and densities generated from the Kohn-Sham equations.

Expanding the local exchange potential using the chain rule gives;

$$\hat{V}_{\mathrm{x}}^{\sigma}(\mathbf{r}) = \frac{\delta E_{\mathrm{x}}[\phi_i^{\sigma}]}{\delta \rho^{\sigma}(\mathbf{r})} = \sum_{\sigma'}\sum_{i=1}^{N^{\sigma}}\int d\mathbf{r}'\frac{\delta E_{\mathrm{x}}[\phi_i^{\sigma}]}{\delta \phi_i^{\sigma'}(\mathbf{r}')}\frac{\delta \phi_i^{\sigma'}(\mathbf{r}')}{\delta \rho^{\sigma}(\mathbf{r})} + \mathrm{h.c.} \tag{3.18}$$

expanding the potential using the chain rule again gives;

$$\hat{V}_{\mathrm{x}}^{\sigma}(\mathbf{r}) = \sum_{\sigma',\sigma''}\sum_{i=1}^{N^{\sigma}}\iint d\mathbf{r}'d\mathbf{r}''\left(\frac{\delta E_{\mathrm{x}}[\phi_i^{\sigma}]}{\delta \phi_i^{\sigma'}(\mathbf{r}')}\frac{\delta \phi_i^{\sigma'}(\mathbf{r}')}{\delta \hat{V}_{\mathrm{S}}^{\sigma''}(\mathbf{r}'')} + \mathrm{h.c.}\right)\frac{\delta \hat{V}_{\mathrm{S}}^{\sigma''}(\mathbf{r}'')}{\delta \rho^{\sigma}(\mathbf{r})}, \tag{3.19}$$

where $\hat{V}_{\mathrm{S}}^{\sigma}(\mathbf{r})$ is the full Kohn-Sham potential (all non-kinetic energy components of the Kohn-Sham equations, equation 3.16).

The last partial derivative on the right hand side is the inverse static density-density response function of a non-interacting system;

$$\hat{\chi}_{\mathrm{S}}^{\sigma,\sigma''}(\mathbf{r},\mathbf{r}'') = \frac{\delta \rho^{\sigma}(\mathbf{r})}{\delta \hat{V}_{\mathrm{S}}^{\sigma''}(\mathbf{r}'')}, \tag{3.20}$$

The integral equation is only non-zero when $\sigma = \sigma''$, which reduces the response function to a single spin variable;

$$\hat{V}_{\mathrm{x}}^{\sigma}(\mathbf{r}) = \sum_{\sigma'}\sum_{i=1}^{N^{\sigma}}\iint d\mathbf{r}'d\mathbf{r}''\left(\frac{\delta E_{\mathrm{x}}[\phi_i^{\sigma}]}{\delta \phi_i^{\sigma'}(\mathbf{r}')}\frac{\delta \phi_i^{\sigma'}(\mathbf{r}')}{\delta \hat{V}_{\mathrm{S}}^{\sigma}(\mathbf{r}'')} + \mathrm{h.c.}\right)(\hat{\chi}_{\mathrm{S}}^{\sigma}(\mathbf{r},\mathbf{r}''))^{-1}. \tag{3.21}$$

Acting with the response function on both sides leads to;

$$\int d\mathbf{r}'\hat{V}_{\mathrm{x}}^{\sigma}(\mathbf{r}')\hat{\chi}_{\mathrm{S}}^{\sigma}(\mathbf{r},\mathbf{r}') = \sum_{\sigma'}\sum_{i=1}^{N^{\sigma}}\int d\mathbf{r}'\frac{\delta E_{\mathrm{x}}[\phi_i^{\sigma}]}{\delta \phi_i^{\sigma'}(\mathbf{r}')}\frac{\delta \phi_i^{\sigma'}(\mathbf{r}')}{\delta \hat{V}_{\mathrm{S}}^{\sigma}(\mathbf{r})} + \mathrm{h.c.} \tag{3.22}$$

The rational for expanding the local exchange potential using the chain rule is that while the functional derivative cannot be explicitly evaluated, the components under expansion can be directly calculated. The derivative of an orbital with respect to the potential is given by;

$$\frac{\delta\phi_i^{\sigma'}(\mathbf{r}')}{\delta\hat{V}_{\mathrm{S}}^{\sigma}(\mathbf{r})} = \delta_{\sigma,\sigma'}\sum_{k=1,k\neq i}^{\infty}\frac{\phi_k^{\sigma}(\mathbf{r}')\phi_k^{\sigma\dagger}(\mathbf{r})}{\varepsilon_i^{\sigma}-\varepsilon_k^{\sigma}}\phi_i^{\sigma}(\mathbf{r}). \tag{3.23}$$

Expansion of the density in the response function and substitution of the above, leads to;

$$\begin{aligned}\hat{\chi}_{\mathrm{S}}^{\sigma}(\mathbf{r},\mathbf{r}') &= \sum_{i=1}^{N^{\sigma}}\frac{\delta}{\delta\hat{V}_{\mathrm{S}}^{\sigma}(\mathbf{r}')}\left(\phi_i^{\sigma\dagger}(\mathbf{r}')\phi_i^{\sigma}(\mathbf{r})\right),\\ &= \sum_{i=1}^{N^{\sigma}}\sum_{k=1,k\neq i}^{\infty}\frac{\phi_i^{\sigma\dagger}(\mathbf{r})\phi_k^{\sigma}(\mathbf{r})\phi_k^{\sigma\dagger}(\mathbf{r}')\phi_i^{\sigma}(\mathbf{r}')}{\varepsilon_i^{\sigma}-\varepsilon_k^{\sigma}} + \text{h.c.}\end{aligned} \tag{3.24}$$

The density-density response function as shown above was defined by Grabo *et al.*[84] However the density-density response function is more commonly written;

$$\hat{\chi}_{\mathrm{S}}^{\sigma}(\mathbf{r},\mathbf{r}') = -\sum_{i=1}^{N^{\sigma}}\sum_{a=N^{\sigma}+1}^{\infty}\frac{\phi_i^{\sigma\dagger}(\mathbf{r})\phi_a^{\sigma}(\mathbf{r})\phi_a^{\sigma\dagger}(\mathbf{r}')\phi_i^{\sigma}(\mathbf{r}')}{\varepsilon_a^{\sigma}-\varepsilon_i^{\sigma}} + \text{h.c.}, \tag{3.25}$$

as the portions of the response function indexed by k that involve occupied states ($k \leq N^{\sigma}$) have zero effect on the density, leaving only unoccupied states in the sum over k.[4] The density-density response function, $\hat{\chi}_{\mathrm{S}}^{\sigma}(\mathbf{r},\mathbf{r}')$ is a negative definite function as all its eigenvalues are negative, except for one. In the case of the change in the potential being a constant, the density-density response function has zero eigenvalue, as changing the potential by a constant does not affect the orbitals or the density.

Substitution of equations 3.23 and 3.24 into equation 3.22 gives;

$$\begin{aligned}&\sum_{i=1}^{N^{\sigma}}\int d\mathbf{r}'\phi_i^{\sigma\dagger}(\mathbf{r}')\left(\hat{V}_{\mathrm{x}}^{\sigma}(\mathbf{r}') - \frac{1}{\phi_i^{\sigma\dagger}(\mathbf{r}')}\frac{\delta E_{\mathrm{x}}[\phi_i^{\sigma}]}{\delta\phi_i^{\sigma}(\mathbf{r}')}\right)\sum_{k=1,k\neq i}^{\infty}\frac{\phi_k^{\sigma}(\mathbf{r})\phi_k^{\sigma\dagger}(\mathbf{r}')}{\varepsilon_i^{\sigma}-\varepsilon_k^{\sigma}}\phi_i^{\sigma}(\mathbf{r}) + \text{h.c.}\\ &\sum_{i=1}^{N^{\sigma}}\int d\mathbf{r}'\phi_i^{\sigma\dagger}(\mathbf{r}')\left(\hat{V}_{\mathrm{x}}^{\sigma}(\mathbf{r}') - \hat{u}_{\mathrm{x},i}^{\sigma}(\mathbf{r})\right)\hat{G}_{\mathrm{S},i}^{\sigma}(\mathbf{r},\mathbf{r}')\phi_i^{\sigma}(\mathbf{r}) + \text{h.c.} = 0,\end{aligned} \tag{3.26}$$

where;

$$\hat{u}_{\mathrm{x},i}^{\sigma}(\mathbf{r}) = \frac{1}{\phi_i^{\sigma\dagger}(\mathbf{r})}\frac{\delta E_{\mathrm{x}}[\phi_i^{\sigma}]}{\delta\phi_i^{\sigma}(\mathbf{r})}, \tag{3.27}$$

[4]Sums over occupied states are typically indexed by i, sums over unoccupied states are indexed by a.

and we define a Green's function as;

$$\hat{G}^{\sigma}_{\mathrm{S},i}(\mathbf{r},\mathbf{r}') = \sum_{k=1,k\neq i}^{\infty} \frac{\phi_k^{\sigma\dagger}(\mathbf{r})\phi_k^{\sigma}(\mathbf{r}')}{\varepsilon_i^{\sigma} - \varepsilon_k^{\sigma}}, \tag{3.28}$$

this results in the standard form of the OEP integral equation, in this case for the exchange only potential but this equation is fully general.[84, 85, 86, 87]

3.2.2 Exact Exchange by Minimisation

The optimised effective potential integral equation can also be obtained from having a local potential that minimises the total energy functional, in our case equation 3.17. Minimisation leads to the condition of;

$$\left.\frac{\delta E[\hat{V}^{\sigma}_{\mathrm{x}}]}{\delta \hat{V}^{\sigma}_{\mathrm{S}}(\mathbf{r})}\right|_{\hat{V}^{\sigma}_{\mathrm{S}}(\mathbf{r})=\hat{V}_{\mathrm{ext}}(\mathbf{r})+\hat{V}_{\mathrm{H}}(\mathbf{r})+\hat{V}^{\sigma}_{\mathrm{x}}(\mathbf{r})} = 0, \tag{3.29}$$

this is equivalent to the second Hohenberg-Kohn theorem but with the density replaced with the potential.[88] Expansion of the above condition using the chain rule gives;

$$\frac{\delta E[\hat{V}^{\sigma}_{x}]}{\delta \hat{V}^{\sigma}_{S}(\mathbf{r})} = \sum_{\sigma'}\sum_{i=1}^{N^{\sigma}} \int d\mathbf{r}' \frac{\delta E[\hat{V}^{\sigma}_{x}]}{\delta \phi_i^{\sigma'}(\mathbf{r}')} \frac{\delta \phi_i^{\sigma'}(\mathbf{r}')}{\delta \hat{V}^{\sigma}_{S}(\mathbf{r})} + \mathrm{h.c.} = 0. \tag{3.30}$$

Using our previous definition of the Green's function and equation 3.23 gives;

$$\frac{\delta \phi_i^{\sigma'}(\mathbf{r}')}{\delta \hat{V}^{\sigma}_{\mathrm{S}}(\mathbf{r})} = \delta_{\sigma,\sigma'} \hat{G}^{\sigma}_{\mathrm{S},i}(\mathbf{r},\mathbf{r}')\phi_i^{\sigma}(\mathbf{r}). \tag{3.31}$$

The derivative of the total energy is;

$$\begin{aligned}
\frac{\delta E[\hat{V}^{\sigma}_{\mathrm{x}}]}{\delta \phi_i^{\sigma}(\mathbf{r})} &= \phi_i^{\sigma\dagger}(\mathbf{r}) \left[-\frac{\nabla^2}{2} + \hat{V}_{\mathrm{ext}}(\mathbf{r}) + \int d\mathbf{r}' \frac{\rho(\mathbf{r}')}{|\mathbf{r}-\mathbf{r}'|} \right] \\
&\quad - \sum_{j=1}^{N^{\sigma}} \int d\mathbf{r}' \phi_i^{\sigma\dagger}(\mathbf{r}') \frac{\phi_j^{\sigma}(\mathbf{r})\phi_j^{\sigma\dagger}(\mathbf{r}')}{|\mathbf{r}-\mathbf{r}'|}, \\
&= \phi_i^{\sigma\dagger}(\mathbf{r}) \left[-\frac{\nabla^2}{2} + \hat{V}_{\mathrm{ext}}(\mathbf{r}) + \int d\mathbf{r}' \frac{\rho(\mathbf{r}')}{|\mathbf{r}-\mathbf{r}'|} + \frac{1}{\phi_i^{\sigma\dagger}(\mathbf{r})} \frac{\delta E_{\mathrm{x}}[\phi_i^{\sigma}]}{\delta \phi_i^{\sigma}(\mathbf{r})} \right],
\end{aligned} \tag{3.32}$$

substitution of the Kohn-Sham equation (equation 3.16) into the above then gives;

$$\frac{\delta E[\hat{V}^{\sigma}_{\mathrm{x}}]}{\delta \phi_i^{\sigma}(\mathbf{r})} = \phi_i^{\sigma\dagger}(\mathbf{r}) \left[\varepsilon_i^{\sigma} - \hat{V}^{\sigma}_{\mathrm{x}}(\mathbf{r}) + \frac{1}{\phi_i^{\sigma\dagger}(\mathbf{r})} \frac{\delta E_{\mathrm{x}}[\phi_i^{\sigma}]}{\delta \phi_i^{\sigma}(\mathbf{r})} \right]. \tag{3.33}$$

Putting both of the above expressions back into equation 3.30;

$$\sum_{i=1}^{N^\sigma} \int d\mathbf{r}' \phi_i^{\sigma\dagger}(\mathbf{r}') \left[\varepsilon_i^\sigma - \hat{V}_{\mathrm{x}}^\sigma(\mathbf{r}') + \frac{1}{\phi_i^{\sigma\dagger}(\mathbf{r}')} \frac{\delta E_{\mathrm{x}}[\phi_i^\sigma]}{\delta \phi_i^\sigma(\mathbf{r}')} \right] \hat{G}_{\mathrm{S},i}^\sigma(\mathbf{r}, \mathbf{r}') \phi_i^\sigma(\mathbf{r}) + \mathrm{h.c.} = 0. \quad (3.34)$$

Using;

$$\int d\mathbf{r}' \phi_i^{\sigma\dagger}(\mathbf{r}') \hat{G}_{\mathrm{S},i}^\sigma(\mathbf{r}, \mathbf{r}') = 0, \quad (3.35)$$

and our previous definition of $\hat{u}_{\mathrm{x},i}^\sigma(\mathbf{r})$, equation 3.27, then gives the standard integral equation;

$$\sum_{i=1}^{N^\sigma} \int d\mathbf{r}' \phi_i^{\sigma\dagger}(\mathbf{r}') \left[\hat{V}_{\mathrm{x}}^\sigma(\mathbf{r}') - \hat{u}_{\mathrm{x},i}^\sigma(\mathbf{r}') \right] \hat{G}_{\mathrm{S,i}}^\sigma(\mathbf{r}, \mathbf{r}') \phi_i^\sigma(\mathbf{r}) + \mathrm{h.c.} = 0, \quad (3.36)$$

having multiplied through by -1.[89, 90, 91]

Unfortunately, there is no analytic solution to the integral equation and hence it must solved numerically. Doing so is rather computationally demanding, largely due to the infinite sum over all states present in the Green's function, $\hat{G}_{\mathrm{S},i}^\sigma(\mathbf{r}, \mathbf{r}')$. As an infinite sum in any practical calculation is truncated to finite order, such truncation yields a slowly converging series in which many excited states must be considered. Truncation of the sum also introduces an error in the potential which can reduce the accuracy of the resulting potential.[92] The relatively large computational expense is the reason that exact exchange (EXX) calculated via the optimised effective potential (OEP) is not as widely used as the LDA, GGAs or hybrid functional methods. Despite these problems calculations have been done for solids using the augmented plane-wave (APW), the full potential linearised augmented plane-wave (FPLAPW) methods[93, 94, 95, 96] and the plane-wave pseudopotential method.[97, 98, 99, 100, 101, 102, 103]

3.3 Exact Exchange by the Hylleraas Variational Method

3.3.1 Exact Exchange by Perturbation Theory

We now demonstrate that the EXX potential can also be calculated without summing over all unoccupied states of the Hamiltonian. As the EXX potential satisfies a Hohenberg-Kohn like term, equation (3.29), the potential can be found by direct variation. Varying the potential;

$$\hat{V}_{\mathrm{x}}^\sigma(\mathbf{r}) \to \hat{V}_{\mathrm{x}}^\sigma(\mathbf{r}) + \delta \hat{V}_{\mathrm{x}}^\sigma(\mathbf{r}), \quad (3.37)$$

causes the orbitals to change by;

$$\phi_i^\sigma(\mathbf{r}) \to \phi_i^\sigma(\mathbf{r}) + \tilde{\phi}_i^\sigma(\mathbf{r}) = \phi_i^\sigma(\mathbf{r}) + \int d\mathbf{r}' \delta \hat{V}_{\mathrm{x}}^\sigma(\mathbf{r}') \frac{\delta \phi_i^\sigma(\mathbf{r})}{\delta \hat{V}_{\mathrm{x}}^\sigma(\mathbf{r}')}, \quad (3.38)$$

if expanded to first order where $\tilde{\phi}_i^\sigma(\mathbf{r})$ is the first order response of an orbital to the perturbation.[104, 105, 106] The first order orbital can be written;

$$\tilde{\phi}_i^\sigma(\mathbf{r}) = -\sum_{k=1,k\neq i}^{\infty} \int d\mathbf{r}' \frac{\phi_k^\sigma(\mathbf{r})\phi_k^{\sigma\dagger}(\mathbf{r}')}{\varepsilon_k^\sigma - \varepsilon_i^\sigma} \left[\hat{u}_{\mathrm{x},i}^{\sigma\dagger}(\mathbf{r}') - \hat{V}_\mathrm{x}^\sigma(\mathbf{r}')\right] \phi_i^\sigma(\mathbf{r}'). \tag{3.39}$$

The change in the total energy is then;

$$\Delta E = \int d\mathbf{r} \delta\hat{V}_\mathrm{x}^\sigma(\mathbf{r}) \frac{\delta E[\hat{V}_\mathrm{x}^\sigma]}{\delta\hat{V}_\mathrm{x}^\sigma(\mathbf{r})}. \tag{3.40}$$

Using the expanded minimisation condition of the optimised effective potential (equation 3.29) gives;

$$\begin{aligned}\frac{\delta E[\hat{V}_\mathrm{x}^\sigma]}{\delta\hat{V}_\mathrm{x}^\sigma(\mathbf{r})} &= \sum_{\sigma'}\sum_{i=1}^{N^\sigma} \int d\mathbf{r}' \frac{\delta E[\hat{V}_\mathrm{x}^\sigma]}{\delta\phi_i^{\sigma'}(\mathbf{r}')} \frac{\delta\phi_i^{\sigma'}(\mathbf{r}')}{\delta\hat{V}_\mathrm{x}^\sigma(\mathbf{r})} + \mathrm{h.c.}, \\ = -\sum_{i=1}^{N^\sigma}\sum_{k=1,k\neq i}^{\infty} &\int d\mathbf{r}' \frac{\phi_k^{\sigma\dagger}(\mathbf{r})\phi_i^\sigma(\mathbf{r})\phi_k^\sigma(\mathbf{r}')}{\varepsilon_k^\sigma - \varepsilon_i^\sigma} \left[\hat{u}_{\mathrm{x},i}^\sigma(\mathbf{r}') - \hat{V}_\mathrm{x}^\sigma(\mathbf{r}')\right] \phi_i^{\sigma\dagger}(\mathbf{r}') + \mathrm{h.c},\end{aligned} \tag{3.41}$$

where we have used the forms given in equations 3.23 and 3.33. It can be readily seen that contributions to the functional derivative of the energy between products of occupied states and their hermitian conjugates cancel (if $k \leq N^\sigma$) as the response of a system due to a perturbation depends only on the component of the perturbation that couples occupied states to unoccupied states, giving;

$$\begin{aligned}\frac{\delta E[\hat{V}_\mathrm{x}^\sigma]}{\delta\hat{V}_\mathrm{x}^\sigma(\mathbf{r})} = -\sum_{i=1}^{N^\sigma}\sum_{a=N^\sigma+1}^{\infty} &\int d\mathbf{r}' \frac{\phi_a^{\sigma\dagger}(\mathbf{r})\phi_i^\sigma(\mathbf{r})\phi_a^\sigma(\mathbf{r}')}{\varepsilon_a^\sigma - \varepsilon_i^\sigma} \\ &\times \left[\hat{u}_{\mathrm{x},i}^\sigma(\mathbf{r}') - \hat{V}_\mathrm{x}^\sigma(\mathbf{r}')\right] \phi_i^{\sigma\dagger}(\mathbf{r}') + \mathrm{h.c.}\end{aligned} \tag{3.42}$$

This implies the first order orbital can be written;

$$\tilde{\phi}_i^\sigma(\mathbf{r}) = -\sum_{a=N^\sigma+1}^{\infty} \int d\mathbf{r}' \frac{\phi_a^\sigma(\mathbf{r})\phi_a^{\sigma\dagger}(\mathbf{r}')}{\varepsilon_a^\sigma - \varepsilon_i^\sigma} \left[\hat{u}_{\mathrm{x},i}^{\sigma\dagger}(\mathbf{r}') - \hat{V}_\mathrm{x}^\sigma(\mathbf{r}')\right] \phi_i^\sigma(\mathbf{r}'), \tag{3.43}$$

and the functional derivative of the energy with respect to the potential is given by;

$$\frac{\delta E[\hat{V}_\mathrm{x}^\sigma]}{\delta\hat{V}_\mathrm{x}^\sigma(\mathbf{r})} = \sum_{i=1}^{N^\sigma} \phi_i^\sigma(\mathbf{r})\tilde{\phi}_i^{\sigma\dagger}(\mathbf{r}) + \mathrm{h.c}, \tag{3.44}$$

writing the functional derivative of the energy in this form was first shown in refs [107] and [108], where the first order response of the orbitals are referred to as "orbital shifts".

This functional derivative can be used to vary the potential such that;

$$\hat{V}_{\mathrm{x}}^{\sigma}(\mathbf{r}) \rightarrow \hat{V}_{\mathrm{x}}^{\sigma}(\mathbf{r}) + \delta\hat{V}_{\mathrm{x}}^{\sigma}(\mathbf{r}) = \hat{V}_{\mathrm{x}}^{\sigma}(\mathbf{r}) - \lambda \int d\mathbf{r}' \frac{1}{|\mathbf{r}-\mathbf{r}'|} \frac{\delta E[\hat{V}_{\mathrm{x}}^{\sigma}]}{\delta \hat{V}_{\mathrm{x}}^{\sigma}(\mathbf{r}')}. \tag{3.45}$$

With $\lambda > 0$, the resulting change in energy is then always negative;

$$\Delta E = -\lambda \iint d\mathbf{r} d\mathbf{r}' \frac{1}{|\mathbf{r}-\mathbf{r}'|} \frac{\delta E[\hat{V}_{\mathrm{x}}^{\sigma}]}{\delta \hat{V}_{\mathrm{x}}^{\sigma}(\mathbf{r})} \frac{\delta E[\hat{V}_{\mathrm{x}}^{\sigma}]}{\delta \hat{V}_{\mathrm{x}}^{\sigma}(\mathbf{r}')}. \tag{3.46}$$

Hence by varying the potential as shown in equation 3.45 the total energy can be minimised and the exchange potential optimised using the functional derivative in equation 3.44.

3.3.2 The Hylleraas Variational Method

A method for finding $\tilde{\phi}_i^{\sigma}(\mathbf{r})$ without having to explicitly include any unoccupied states is to use the Hylleraas variational principle.[109] We start by defining the second order functional;

$$\begin{aligned} G_i^{\sigma}[\tilde{\phi}_i^{\sigma}] =& \langle \tilde{\phi}_i^{\sigma} | \hat{T} + \hat{V}_{\mathrm{ext}} + \hat{V}_{\mathrm{H}} + \hat{V}_{\mathrm{x}}^{\sigma} - \varepsilon_i^{\sigma} | \tilde{\phi}_i^{\sigma} \rangle + \langle \tilde{\phi}_i^{\sigma} | \hat{u}_{\mathrm{x},i}^{\sigma\dagger} - \hat{V}_{\mathrm{x}}^{\sigma} - \tilde{\varepsilon}_i^{\sigma} | \phi_i^{\sigma} \rangle \\ &+ \langle \phi_i^{\sigma} | \hat{u}_{\mathrm{x},i}^{\sigma\dagger} - \hat{V}_{\mathrm{x}}^{\sigma} - \tilde{\varepsilon}_i^{\sigma} | \tilde{\phi}_i^{\sigma} \rangle, \end{aligned} \tag{3.47}$$

where $\tilde{\varepsilon}_i^{\sigma}$ is the first order correction to the eigenvalues. Under the constraint;

$$\langle \phi_i^{\sigma} | \tilde{\phi}_i^{\sigma} \rangle + \langle \tilde{\phi}_i^{\sigma} | \phi_i^{\sigma} \rangle = 0, \tag{3.48}$$

G_i^{σ} is variational with respect to $\tilde{\phi}_i^{\sigma}$. This constraint is known as the "parallel transport gauge". The second order variational functional when minimised and summed over all occupied states and spins equals the second order energy due to the perturbation and the $\tilde{\phi}_i^{\sigma}$ that minimises G_i^{σ} is the first order orbital given by equation 3.43.

As previously stated the response of a system due to a perturbation depends only on the component of the perturbation that couples occupied states to unoccupied states. Hence we only need to consider parts of the perturbation that project the occupied orbitals onto the unoccupied orbitals. This can be accomplished by projecting the perturbation onto the unoccupied orbitals, such that the last two terms in equation 3.47 can be rewritten;

$$\langle \tilde{\phi}_i^{\sigma} | \hat{u}_{\mathrm{x},i}^{\sigma\dagger} - \hat{V}_{\mathrm{x}}^{\sigma} - \tilde{\varepsilon}_i^{\sigma} | \phi_i^{\sigma} \rangle \rightarrow \langle \tilde{\phi}_i^{\sigma} | \hat{P}_{\mathrm{c}} (\hat{u}_{\mathrm{x},i}^{\sigma\dagger} - \hat{V}_{\mathrm{x}}^{\sigma}) | \phi_i^{\sigma} \rangle, \tag{3.49}$$

where $\hat{P}_{\mathrm{c}}$ is the projection operator onto the unoccupied states (conduction band) defined as;

$$\hat{P}_{\mathrm{c}} = \hat{I} - \sum_{j=1}^{N^{\sigma}} |\phi_j^{\sigma}\rangle\langle\phi_j^{\sigma}| = \sum_{a=N^{\sigma}+1}^{\infty} |\phi_a^{\sigma}\rangle\langle\phi_a^{\sigma}|, \tag{3.50}$$

$\hat{I}$ is the identity operator. The second order variational functional is then;

$$\begin{aligned} G_i^\sigma[\tilde{\phi}_i^\sigma] =& \langle\tilde{\phi}_i^\sigma|\hat{T}+\hat{V}_{\text{ext}}+\hat{V}_{\text{H}}+\hat{V}_{\text{x}}^\sigma-\varepsilon_i^\sigma|\tilde{\phi}_i^\sigma\rangle+\langle\tilde{\phi}_i^\sigma|\hat{P}_{\text{c}}(\hat{u}_{\text{x},i}^{\sigma\dagger}-\hat{V}_{\text{x}}^\sigma)|\phi_i^\sigma\rangle \\ &+\langle\phi_i^\sigma|(\hat{u}_{\text{x},i}^{\sigma\dagger}-\hat{V}_{\text{x}}^\sigma)\hat{P}_{\text{c}}|\tilde{\phi}_i^\sigma\rangle, \end{aligned} \tag{3.51}$$

Taking the derivative of G_i^σ with respect to $\tilde{\phi}_i^{\sigma\dagger}$ gives a Sternheimer equation[110] that can also be used to find $\tilde{\phi}_i^\sigma$;

$$(\hat{T}+\hat{V}_{\text{ext}}+\hat{V}_{\text{H}}+\hat{V}_{\text{x}}^\sigma-\varepsilon_i^\sigma)|\tilde{\phi}_i^\sigma\rangle+\hat{P}_{\text{c}}(\hat{u}_{\text{x},i}^\sigma-\hat{V}_{\text{x}}^\sigma)|\phi_i^\sigma\rangle=0. \tag{3.52}$$

The Sternheimer equation can also be variationally solved to find $\tilde{\phi}_i^\sigma$ and is preferable to using the second order variational functional, G_i^σ as it is trivial to verify that the Sternheimer equation is satisfied when calculating $\tilde{\phi}_i^\sigma$. Using the Sternheimer equation to find $\tilde{\phi}_i^\sigma$ and using the form of the functional derivative that depends only on ϕ_i^σ and $\tilde{\phi}_i^\sigma$ (equation 3.44) avoids having to perform the infinite sum over states required by the conventional EXX method.

Using equations 3.44 and 3.52 to calculate the EXX functional derivative that minimises the Hartree-Fock total energy, allows the EXX potential to be found using only the N lowest eigenvalues of the Kohn-Sham equation. This improves on previous implementations that calculate the functional derivative by truncating the infinite sum to arbitrary order. The EXX potential can be found using an iterative scheme, full details of which will be presented in the next chapter.[111]

3.3.3 The Form of the Functional Derivative

In equation 3.45 the change in the EXX potential was chosen to be the convolution of the EXX functional derivative and $\frac{1}{|r-r'|}$;

$$\delta\hat{V}_{\text{x}}^\sigma(\mathbf{r})=-\lambda\int d\mathbf{r}'\frac{1}{|\mathbf{r}-\mathbf{r}'|}\frac{\delta E[\hat{V}_{\text{x}}^\sigma]}{\delta\hat{V}_{\text{x}}^\sigma(\mathbf{r}')}. \tag{3.53}$$

We could also choose the change in the potential to be along the EXX functional derivative;

$$\delta\hat{V}_{\text{x}}^\sigma(\mathbf{r})=-\lambda\frac{\delta E[\hat{V}_{\text{x}}^\sigma]}{\delta\hat{V}_{\text{x}}^\sigma(\mathbf{r})}, \tag{3.54}$$

which would be the most obvious choice for the change in the potential. This is the choice of the change in the potential that we first implemented, in ref [111]. The simplicity of the latter algorithm is appealing, and until recently all results (for EXX, CEDA and LFX) were calculated using this method. However, we discovered that if this algorithm is iterated for a large number of cycles, past the satisfaction of our convergence criteria, then numerical instabilities in the potential develop.

These instabilities were documented and explained in ref [92] and can be avoided by use of (3.53) instead of (3.54). The former algorithm is an improvement over the method

based on (3.54), as can be seen by the following arguments: The functional derivative has units of charge density. A density is related to its corresponding potential by the Laplacian of the potential. For the Hartree potential;

$$\nabla^2 \hat{V}_{\mathrm{H}}(\mathbf{r}) = -4\pi\rho(\mathbf{r}), \tag{3.55}$$

which rearranges to give;

$$\hat{V}_{\mathrm{H}}(\mathbf{r}) = \int d\mathbf{r}' \frac{\rho(\mathbf{r}')}{|\mathbf{r} - \mathbf{r}'|}. \tag{3.56}$$

For the Hartree potential plus the EXX exchange potential;

$$\hat{V}_{\mathrm{H}}(\mathbf{r}) + \hat{V}_{\mathrm{x}}(\mathbf{r}) = \int d\mathbf{r}' \frac{\rho_{\mathrm{Hx}}(\mathbf{r})}{|\mathbf{r} - \mathbf{r}'|} \tag{3.57}$$

the Hartree exchange density, $\rho_{\mathrm{Hx}}(\mathbf{r})$ integrates to;

$$\int d\mathbf{r} \rho_{\mathrm{Hx}}(\mathbf{r}) = N - 1, \tag{3.58}$$

as the Hartree plus exchange potential is self interaction free. As the EXX functional derivative has units of the density it describes the change in the Hartree exchange density due to the perturbation, rather than the change in the potential. Hence the change in the potential is expressed as the electrostatic potential of a change in a density, with the change in the density given by the EXX functional derivative, leading to the form of the change in the potential as shown in equation 3.53.

3.3.4 Iterative Procedure to Calculate The EXX Potential

The Hohenberg-Kohn theorems guarantee that the total energy of a system is variational, hence the exchange potential that minimises the Hartree-Fock total energy can be found by iterative variational minimisation. At iteration p, the EXX potential can be optimised by calculating the functional derivative of the energy with respect to the potential and using that to optimise the potential for use in the next iteration $p + 1$;

$$\hat{V}_{\mathrm{x}}^{\sigma,p+1}(\mathbf{r}) = \hat{V}_{\mathrm{x}}^{\sigma,p}(\mathbf{r}) - \lambda \int d\mathbf{r}' \frac{1}{|\mathbf{r} - \mathbf{r}'|} \frac{\delta E[\hat{V}_{\mathrm{x}}^{\sigma,p}]}{\delta \hat{V}_{\mathrm{x}}^{\sigma,p}(\mathbf{r}')}, \qquad \lambda > 0, \tag{3.59}$$

the value of λ is determined by a line search.[5] The above requires the calculation of the first order orbitals from the Sternheimer equation (equation 3.52) to evaluate the functional derivative (equation 3.44). The Sternheimer equation itself can be determined iteratively, leading to a double loop iterative procedure to find the EXX potential;

1. For potential, $\hat{V}_{\mathrm{x}}^{\sigma,p}(\mathbf{r})$, determine the ground state orbitals $\phi_i^{\sigma,p}(\mathbf{r})$ from the Kohn-Sham equations and total energy from the Hartree-Fock total energy expression.

[5] The procedure for conducting a line search is outlined in section 4.1.5.

2. Iteratively solve the Sternheimer equation to get the first order orbitals; $\tilde{\phi}_i^{\sigma,p}(\mathbf{r})$.
3. Evaluate the functional derivative of the energy with respect to the potential and convolute with $\frac{1}{|\mathbf{r}-\mathbf{r}'|}$; $\int d\mathbf{r}' \frac{1}{|\mathbf{r}-\mathbf{r}'|} \frac{\delta E[\hat{V}_{\mathrm{x}}^{\sigma,p}]}{\delta \hat{V}_{\mathrm{x}}^{\sigma,p}(\mathbf{r}')}$.
4. Determine optimal value of λ.
5. Construct new potential by adding $\int d\mathbf{r}' \frac{1}{|\mathbf{r}-\mathbf{r}'|} \frac{\delta E[\hat{V}_{\mathrm{x}}^{\sigma,p}]}{\delta \hat{V}_{\mathrm{x}}^{\sigma,p}(\mathbf{r}')}$ multiplied by λ.

This procedure continues until the ground state is reached, which is when the difference of the total energy between iterations tends to zero.[111] The full computational details and implementation of this algorithm are detailed in the next chapter.

3.3.5 An Alternative Exact Exchange Objective Functional

The method outlined in sections 3.3.1-3.3.2 finds the EXX potential by minimising the Hartree-Fock total energy. The EXX potential also can also be derived by considering the energy difference T_Ψ;

$$T_\Psi[\hat{V}] = \langle \Psi | \hat{H}_{\mathrm{v}} | \Psi \rangle - E_{\mathrm{v}} > 0, \tag{3.60}$$

where Ψ is the ground state many-body wave function of a system of N interacting electrons. The interacting Hamiltonian that generates Ψ is;

$$\hat{H} = \sum_i -\frac{\nabla_{\mathbf{r}_i}^2}{2} + \sum_i \hat{V}_{\mathrm{ext}}(\mathbf{r}_i) + \frac{1}{2} \sum_{i \neq j} \frac{1}{|\mathbf{r}_i - \mathbf{r}_j|}. \tag{3.61}$$

The Hamiltonian $\hat{H}_v$ is the sum of the N non-interacting Kohn-Sham single particle Hamiltonians;

$$\hat{H}_{\mathrm{v}} = \sum_\sigma \sum_{i=1}^{N} \hat{h}_{\mathrm{v}}(\mathbf{r}_i) = \sum_\sigma \sum_{i=1}^{N} \left[-\frac{\nabla_{\mathbf{r}_i}^2}{2} + \hat{V}(\mathbf{r}_i) \right], \tag{3.62}$$

E_{v} is the sum of the eigenvalues of the Kohn-Sham system, $\hat{V}$ is an effective local potential and the ground state Slater determinant of this non-interacting system is, Φ_{v}.[6]

In the Hartree and Hartree-Fock approximations, the central idea is to approximate the interacting wave function. The approximate ground state is then found by minimising the interacting Hamiltonian, $\hat{H}$, using the approximate wave function. Instead, the inequality given by equation 3.60 suggests we try to optimise the effective non-interacting Hamiltonian, $\hat{H}_{\mathrm{v}}$ for which the interacting ground state, is a good approximate ground state, rather than approximating the wave function and minimising the interacting Hamiltonian. Using the Rayleigh-Ritz variational principle equation 3.60 results.[112]

Direct minimisation of $\hat{T}_\Psi[\hat{V}]$ by variation of $\hat{V}$, will find the optimising potential to be the Kohm-Sham potential, with the same density as Ψ. This follows easily, since the

[6] The set of N Kohn-Sham orbitals can be represented as a Slater determinant.

functional derivative of $\hat{T}_\Psi[\hat{V}]$ is;

$$\begin{aligned}\frac{\delta T_\Psi[\hat{V}]}{\delta \hat{V}(\mathbf{r})} =&\langle \frac{\delta \Psi}{\delta \hat{V}(\mathbf{r})}|\hat{H}_v|\Psi\rangle + \langle\Psi|\frac{\delta \hat{H}_v}{\delta \hat{V}(\mathbf{r})}|\Psi\rangle + \langle\Psi|\hat{H}_v|\frac{\delta \Psi}{\delta \hat{V}(\mathbf{r})}\rangle - \frac{\delta E_v}{\delta \hat{V}(\mathbf{r})}\\ =&\langle\Psi|\frac{\delta \hat{V}}{\delta \hat{V}(\mathbf{r})}|\Psi\rangle - \sum_{i=1}^{N^\sigma}\langle\phi_i^\sigma|\frac{\delta \hat{V}}{\delta \hat{V}(\mathbf{r})}|\phi_i^\sigma\rangle \\ =&\rho_\Psi(\mathbf{r}) - \rho_v(\mathbf{r}).\end{aligned} \tag{3.63}$$

At the minimum, the functional derivative of $\hat{T}_\Psi[\hat{V}]$ vanishes.

The interacting wave function, Ψ is not known. Still, following reference [112] it can be expanded in a perturbative expansion. We start with a non-interacting Hamiltonian as our zeroth-order approximation, with a local potential $\hat{V}_{\text{ext}}(\mathbf{r}) + \hat{U}(\mathbf{r})$, where $\hat{U}(\mathbf{r})$ is an undetermined potential that mimics the electron interaction potential. The non-interacting zeroth-order Hamiltonian is;

$$\hat{H}_{\hat{V}_{\text{ext}}+\hat{U}} = \hat{T} + \hat{V}_{\text{ext}} + \hat{U}, \qquad \hat{U} = \sum_i \hat{U}(\mathbf{r}_i), \tag{3.64}$$

the eigenstates and eigenvalues of which are $\Phi_{\text{u},n}$ and $E_{\text{u},n}$ respectively. It is worth noting that $\Phi_{\text{u},n}$ is an excited Slater determinant of the zeroth-order Hamiltonian, the index n sums all possible excited Slater determinants. The ground state Slater determinant is Φ_{u}.

If we consider the interaction as a perturbation to the non-interacting zeroth order Hamiltonian, we can define a tunable Hamiltonian that switches on interactions as a perturbation;

$$\hat{H}(\alpha) = \hat{H}_{\hat{V}_{\text{ext}}+\hat{U}} + \alpha(V_{\text{ee}} - \sum_{i=1}^{N}\hat{U}(\mathbf{r}_i)), \qquad 0 \leq \alpha \leq 1. \tag{3.65}$$

The interaction is linear in α and for $\alpha = 1$ the Hamiltonian is fully interacting and for $\alpha = 0$ the Hamiltonian is fully non-interacting. For small α the interacting ground state wave function of $\hat{H}(\alpha)$, $\Psi(\alpha)$ is to first order;

$$\Psi(\alpha) = \Phi_{\text{u}} + \alpha\Phi'_{\text{u}}. \tag{3.66}$$

To ensure $\Psi(\alpha)$ is properly normalised;

$$\langle\Psi(\alpha)|\Psi(\alpha)\rangle = 1 + \alpha^2\langle\Phi'_{\text{u}}|\Phi'_{\text{u}}\rangle, \tag{3.67}$$

hence $\Psi(\alpha)$ is written as;

$$\Psi(\alpha) = \Phi_u + \alpha\Phi'_{\text{u}} - \frac{\alpha^2}{2}\Phi_{\text{u}}\langle\Phi'_{\text{u}}|\Phi'_{\text{u}}\rangle, \tag{3.68}$$

up to order α^2.[7] The first order correction $\Phi'_{\rm u}$ is then given by;

$$\Phi'_{\rm u} = -\sum_n \frac{\langle \Phi_{{\rm u},n}|\hat{V}_{\rm ee} - \hat{U}|\Phi_{\rm u}\rangle}{E_{{\rm u},n} - E_{\rm u}}\Phi_{{\rm u},n}. \tag{3.69}$$

Turning to the effective non-interacting Hamiltonian, $\hat{H}_{\rm v}$ with the interacting wave function $\Psi(\alpha)$ as its approximate ground state, the effective potential $\hat{V}$ will be close to $\hat{V}_{\rm ext} + \hat{U}$ since at $\alpha = 0$, $\hat{V} = \hat{V}_{\rm ext} + \hat{U}$. Hence for small α, $\hat{V} = \hat{V}_{\rm ext} + \hat{U} + \alpha\hat{V}'$ where $\hat{V}'$ is a perturbing potential. We then consider the perturbed non-interacting Hamiltonian;

$$\hat{H}_{\rm v} = \hat{H}_{\hat{V}_{\rm ext}+\hat{U}} + \alpha\sum_{i=1}^{N}\hat{V}'(\mathbf{r}_i), \tag{3.70}$$

with a ground state Slater determinant given by, $\Phi_{\hat{\rm u}+\alpha\hat{\rm v}'}$. This ground state too can be expanded up to order α;

$$\Phi_{\hat{\rm u}+\hat{\rm v}'} = \Phi_{\rm u} + \alpha\tilde{\Phi}'_{\rm u} - \frac{\alpha^2}{2}\Phi_{\rm u}\langle\tilde{\Phi}'_{\rm u}|\tilde{\Phi}'_{\rm u}\rangle. \tag{3.71}$$

The first order correction $\tilde{\Phi}'_{\rm u}$ is then given by;

$$\tilde{\Phi}'_{\rm u} = -\sum_n \frac{\langle \Phi_{{\rm u},n}|\hat{V}'|\Phi_{\rm u}\rangle}{E_{{\rm u},n} - E_{\rm u}}\Phi_{{\rm u},n}. \tag{3.72}$$

In appendix B we show that if we substitute $\Psi(\alpha)$ in place of Ψ in the energy difference $\hat{T}_\Psi[\hat{V}]$ and expand in powers of α, the lowest order non-zero term is the second order energy difference, $T''_{\rm u}[\hat{V}]$;

$$T''_{\rm u} = \sum_\sigma\sum_{i=1}^{N^\sigma}\sum_{a=N^\sigma+1}^{\infty}\frac{|\langle\phi^\sigma_{{\rm u},i}|\hat{V}_{{\rm H,u}}(\mathbf{r}) + \hat{u}^\sigma_{{\rm x,u},i}(\mathbf{r}) - \hat{V}^\sigma(\mathbf{r})|\phi^\sigma_{{\rm u},a}\rangle|^2}{\varepsilon^\sigma_{{\rm u},a} - \varepsilon^\sigma_{{\rm u},i}} > 0. \tag{3.73}$$

If $\hat{V}^\sigma$ is changed by a small variation, $\delta\hat{V}^\sigma$ the change in the energy of $T''_{\rm u}$ is;

$$\begin{aligned}\Delta T''_{\rm u} &= T''_{\rm u}[\hat{V}^\sigma + \delta\hat{V}^\sigma] - T''_{\rm u}[\hat{V}^\sigma] \\ &= \int\delta\hat{V}^\sigma(\mathbf{r})\frac{\delta T''_{\rm u}[\hat{V}^\sigma]}{\delta\hat{V}^\sigma(\mathbf{r})} + \iint\delta\hat{V}^\sigma(\mathbf{r})\delta\hat{V}^\sigma(\mathbf{r}')\frac{\delta^2 T''_{\rm u}[\hat{V}^\sigma]}{\delta\hat{V}^\sigma(\mathbf{r})\delta\hat{V}^\sigma(\mathbf{r}')}\end{aligned} \tag{3.74}$$

where;

$$\frac{\delta T''_{\rm u}[\hat{V}^\sigma]}{\delta\hat{V}^\sigma(\mathbf{r})} = \sum_{i=1}^{N^\sigma}\sum_{a=N^\sigma+1}^{\infty}\frac{\langle\phi^\sigma_{{\rm u},i}|\hat{V}_{{\rm H,u}}(\mathbf{r}) + \hat{u}^\sigma_{{\rm x,u},i}(\mathbf{r}) - \hat{V}^\sigma(\mathbf{r})|\phi^\sigma_{{\rm u},a}\rangle}{\varepsilon^\sigma_{{\rm u},a} - \varepsilon^\sigma_{{\rm u},i}}\phi^{\sigma\dagger}_{{\rm u},a}(\mathbf{r})\phi^\sigma_{{\rm u},i}(\mathbf{r}), \tag{3.75}$$

[7] We obtain equation 3.68 by dividing the right hand side of equation 3.66 by the square root of the right hand side of equation 3.67 and Taylor expanding up to α^2.

and;

$$\frac{\delta T_{\mathrm{u}}''[\hat{V}^{\sigma}]}{\delta \hat{V}^{\sigma}(\mathbf{r})\delta \hat{V}^{\sigma}(\mathbf{r}')} = -\frac{1}{2}\hat{\chi}_{\mathrm{u}}(\mathbf{r},\mathbf{r}'). \tag{3.76}$$

As $\chi_{\mathrm{u}}^{\sigma}(\mathbf{r},\mathbf{r}')$ is a negative definite function, for fixed $\hat{U}$, $T_{\mathrm{u}}''[\hat{V}^{\sigma}]$ is a convex function of $\hat{V}^{\sigma}$. When the functional derivative in equation 3.75 is equal to zero, $T_{\mathrm{u}}[\hat{V}^{\sigma}]$ is minimised and $\hat{V}^{\sigma}$ is the minimising potential.

If we choose the local potential, $\hat{V}^{\sigma}(\mathbf{r})$ to be the minimising potential of $T_{\mathrm{u}}''[\hat{V}^{\sigma}]$ and the zeroth order potential $\hat{U}$ to be equal to $\hat{V}^{\sigma}$, then equation 3.75 is the EXX functional derivative (equation 3.42). $\hat{V}^{\sigma}(\mathbf{r})$ is then the sum of the Hartree potential and EXX potential; $\hat{V}^{\sigma}(\mathbf{r}) = \hat{V}_{\mathrm{H}}(\mathbf{r}) + \hat{V}_{\mathrm{x}}^{\sigma}(\mathbf{r})$. This implies $T_{\mathrm{u}}''[\hat{V}^{\sigma}]$ could be used as the objective function that is minimised to optimise the EXX potential.

In this work the optimisation of the EXX potential is accomplished by minimising the Hartree-Fock total energy rather than optimising $T_{\mathrm{u}}''[\hat{V}^{\sigma}]$. $T_{\mathrm{u}}''[\hat{V}^{\sigma}]$ is however useful for formulating approximations to the EXX potential.

3.4 Approximations to EXX

3.4.1 The Approximation of Krieger, Li and Iafrate

Due to the demanding numerical cost required to solve the full integral equation to the find the EXX potential, considerable work has gone into finding approximations to the potential that are less computationally expensive and retain some of the formal properties of the EXX potential. We now derive and discuss some approximations to the EXX potential.

The approximate exchange potential of Krieger, Li and Iafrate is a simple approximation that allows easy calculation of an approximate local exchange potential.[89] The starting point is the expansion of the functional derivative of the energy equation 3.41 and writing the first order orbital as;

$$\tilde{\phi}_i^{\sigma}(\mathbf{r}) = -\sum_{k=1,k\neq i}^{\infty}\int d\mathbf{r}'\frac{\phi_k^{\sigma}(\mathbf{r})\phi_k^{\sigma\dagger}(\mathbf{r}')}{\varepsilon_k^{\sigma}-\varepsilon_i^{\sigma}}\left[\hat{u}_{\mathrm{x},i}^{\sigma\dagger}(\mathbf{r}') - \hat{V}_{\mathrm{x}}^{\sigma}(\mathbf{r}')\right]\phi_i^{\sigma}(\mathbf{r}'). \tag{3.77}$$

If we then employ the Unsöld approximation [113] and set the eigenvalue difference; $\varepsilon_k^{\sigma} - \varepsilon_i^{\sigma} = \Delta\varepsilon$ to be constant; then the first order orbital can be approximated;

$$\tilde{\phi}_i^{\mathrm{KLI},\sigma}(\mathbf{r}) = -\sum_{k=1,k\neq i}^{\infty}\int d\mathbf{r}'\frac{\phi_k^{\sigma}(\mathbf{r})\phi_k^{\sigma\dagger}(\mathbf{r}')}{\Delta\varepsilon}\left[\hat{u}_{\mathrm{x},i}^{\sigma\dagger}(\mathbf{r}') - \hat{V}_{\mathrm{x}}^{\mathrm{KLI},\sigma}(\mathbf{r}')\right]\phi_i^{\sigma}(\mathbf{r}'), \tag{3.78}$$

we can then employ the closure relationship;

$$\sum_{k=1,k\neq i}^{\infty}\phi_k^{\sigma}(\mathbf{r})\phi_k^{\sigma\dagger}(\mathbf{r}') = \delta(\mathbf{r}-\mathbf{r}') - \phi_i^{\sigma}(\mathbf{r})\phi_i^{\sigma\dagger}(\mathbf{r}'), \tag{3.79}$$

and substitute to get;

$$\begin{aligned}\tilde{\phi}_i^{\mathrm{KLI},\sigma}(\mathbf{r}) =& -\frac{1}{\Delta\varepsilon}\left[\hat{u}_{\mathrm{x},i}^{\sigma\dagger}(\mathbf{r}) - \hat{V}_{\mathrm{x}}^{\mathrm{KLI},\sigma}(\mathbf{r})\right]\phi_i^{\sigma}(\mathbf{r}) \\ &+ \frac{1}{\Delta\varepsilon}\phi_i^{\sigma}(\mathbf{r})\int d\mathbf{r}'\phi_i^{\sigma\dagger}(\mathbf{r}')\left[\hat{u}_{\mathrm{x},i}^{\sigma\dagger}(\mathbf{r}') - \hat{V}_{\mathrm{x}}^{\mathrm{KLI},\sigma}(\mathbf{r}')\right]\phi_i^{\sigma}(\mathbf{r}'), \\ =& -\frac{1}{\Delta\varepsilon}\left[\hat{u}_{\mathrm{x},i}^{\sigma\dagger}(\mathbf{r}) - \hat{V}_{\mathrm{x}}^{\mathrm{KLI},\sigma}(\mathbf{r}) - \bar{u}_{\mathrm{x},i}^{\sigma} + \bar{V}_{\mathrm{x}}^{\mathrm{KLI},\sigma}\right]\phi_i^{\sigma}(\mathbf{r}),\end{aligned} \tag{3.80}$$

where;

$$\bar{u}_{\mathrm{x},i}^{\sigma} = \int d\mathbf{r}\phi_i^{\sigma\dagger}(\mathbf{r})\hat{u}_{\mathrm{x},i}^{\sigma\dagger}(\mathbf{r})\phi_i^{\sigma}(\mathbf{r}), \tag{3.81}$$

and;

$$\bar{V}_{\mathrm{x}}^{\mathrm{KLI},\sigma} = \int d\mathbf{r}\phi_i^{\sigma\dagger}(\mathbf{r})\hat{V}_{\mathrm{x}}^{\mathrm{KLI},\sigma}(\mathbf{r})\phi_i^{\sigma}(\mathbf{r}), \tag{3.82}$$

are the orbital dependent constants of the non-local Fock exchange term and the local KLI potential respectively. Substitution into equation 3.44 and rearrangement gives the KLI potential equation;

$$\hat{V}_{\mathrm{x}}^{\mathrm{KLI},\sigma}(\mathbf{r}) = \frac{1}{2\rho^{\sigma}(\mathbf{r})}\sum_{i=1}^{N^{\sigma}}|\phi_i^{\sigma}(\mathbf{r})|^2\left[\hat{u}_{\mathrm{x},i}^{\sigma}(\mathbf{r}) - \bar{u}_{\mathrm{x},i}^{\sigma} + \bar{V}_{\mathrm{x}}^{\mathrm{KLI},\sigma}\right] + \mathrm{h.c.} \tag{3.83}$$

A further approximation can be made if $\bar{u}_{\mathrm{x},i}^{\sigma}$ and $\bar{V}_{\mathrm{x}}^{\mathrm{KLI},\sigma}$ are assumed to be equal, resulting in the Slater approximation;[3]

$$\hat{V}_{\mathrm{x}}^{\mathrm{Slater},\sigma}(\mathbf{r}) = \frac{1}{2\rho^{\sigma}(\mathbf{r})}\sum_{i=1}^{N^{\sigma}}|\phi_i^{\sigma}(\mathbf{r})|^2\left[\hat{u}_{\mathrm{x},i}^{\sigma}(\mathbf{r}) + \hat{u}_{\mathrm{x},i}^{\sigma\dagger}(\mathbf{r})\right]. \tag{3.84}$$

Both the KLI and Slater potentials are mean field approximations to the EXX potential.

3.4.2 The Common Energy Denominator Approximation

A slightly improved approximation is the "common energy denominator approximation" (CEDA),[114] which is also equivalent [115] to the "effective local potential" (ELP)[116] and "localised Hartree Fock" (LHF) potential.[117] Starting from the first order orbital defined in equation 3.43 and again using the Unsöld approximation to set the eigenvalue difference to be constant then the first order orbital can be written;

$$\tilde{\phi}_i^{\mathrm{CEDA},\sigma}(\mathbf{r}) = -\sum_{a=N^{\sigma}+1}^{\infty}\int d\mathbf{r}'\frac{\phi_a^{\sigma}(\mathbf{r})\phi_a^{\sigma\dagger}(\mathbf{r}')}{\Delta\varepsilon}\left[\hat{u}_{\mathrm{x},i}^{\sigma\dagger}(\mathbf{r}') - \hat{V}_{\mathrm{x}}^{\mathrm{CEDA},\sigma}(\mathbf{r}')\right]\phi_i^{\sigma}(\mathbf{r}'), \tag{3.85}$$

we can then employ the closure relationship;

$$\sum_{a=N^{\sigma}+1,}^{\infty}\phi_a^{\sigma}(\mathbf{r})\phi_a^{\sigma\dagger}(\mathbf{r}') = \delta(\mathbf{r}-\mathbf{r}') - \sum_{j=1}^{N^{\sigma}}\phi_j^{\sigma}(\mathbf{r})\phi_j^{\sigma\dagger}(\mathbf{r}'), \tag{3.86}$$

which when substituted gives;

$$\tilde{\phi}_i^{\mathrm{CEDA},\sigma}(\mathbf{r}) = -\frac{1}{\Delta\varepsilon}\left[\hat{u}_{\mathrm{x},i}^{\sigma\dagger}(\mathbf{r}) - \hat{V}_{\mathrm{x}}^{\mathrm{CEDA},\sigma}(\mathbf{r})\right]\phi_i^{\sigma}(\mathbf{r}) + \frac{1}{\Delta\varepsilon}\sum_{j=1}^{N^\sigma}\int d\mathbf{r}'\phi_j^{\sigma}(\mathbf{r})\phi_j^{\sigma\dagger}(\mathbf{r}')\left[\hat{u}_{\mathrm{x},i}^{\sigma\dagger}(\mathbf{r}') - \hat{V}_{\mathrm{x}}^{\mathrm{CEDA},\sigma}(\mathbf{r}')\right]\phi_i^{\sigma}(\mathbf{r}'). \tag{3.87}$$

Substitution into the functional derivative of the energy gives;

$$\frac{\delta E[\hat{V}_{\mathrm{x}}^{\mathrm{CEDA},\sigma}]}{\delta\hat{V}_{\mathrm{x}}^{\mathrm{CEDA},\sigma}(\mathbf{r})} = -\frac{1}{\Delta\varepsilon}\sum_{i=1}^{N^\sigma}\phi_i^{\sigma\dagger}(\mathbf{r})\left[\hat{V}_{\mathrm{x}}^{\mathrm{CEDA},\sigma}(\mathbf{r}) - \hat{u}_{\mathrm{x},i}^{\sigma}(\mathbf{r})\right]\phi_i^{\sigma}(\mathbf{r}) + \frac{1}{\Delta\varepsilon}\sum_{i=1}^{N^\sigma}\sum_{j=1}^{N^\sigma}\phi_j^{\sigma\dagger}(\mathbf{r})\phi_i^{\sigma}(\mathbf{r})\int d\mathbf{r}'\phi_i^{\sigma\dagger}(\mathbf{r}')\left[\hat{u}_{\mathrm{x},i}^{\sigma}(\mathbf{r}') - \hat{V}_{\mathrm{x}}^{\mathrm{CEDA},\sigma}(\mathbf{r}')\right]\phi_j^{\sigma}(\mathbf{r}'). \tag{3.88}$$

The CEDA functional derivative will not fully minimise the Hartree-Fock total energy as the EXX potential will. However we can construct a minimising function for CEDA by returning to the second-order energy difference T_{u}'' and setting the energy denominator to a constant $\Delta\varepsilon = \varepsilon_a^\sigma - \varepsilon_i^\sigma$;

$$T_{\mathrm{u}}''^{\mathrm{CEDA}} = \sum_\sigma\sum_{i=1}^{N^\sigma}\sum_{a=N^\sigma+1}^{\infty}\frac{1}{\Delta\varepsilon}|\langle\phi_i^\sigma|\hat{u}_{\mathrm{x},i}^\sigma - \hat{V}_{\mathrm{x}}^\sigma|\phi_a^\sigma\rangle|^2 > 0. \tag{3.89}$$

Then applying the Unsöld approximation using the same closure relation as applied to the functional derivative (equation 3.86) to get;

$$S^{\mathrm{CEDA}} = \sum_\sigma\left[\sum_{i=1}^{N^\sigma}\langle\phi_i^\sigma|(\hat{u}_{\mathrm{x},i}^\sigma - \hat{V}_{\mathrm{x}}^\sigma)^2|\phi_i^\sigma\rangle - \sum_{i=1}^{N^\sigma}\sum_{j=1}^{N^\sigma}|\langle\phi_i^\sigma|\hat{u}_{\mathrm{x},i}^\sigma - \hat{V}_{\mathrm{x}}^\sigma|\phi_j^\sigma\rangle|^2\right], \tag{3.90}$$

where the objective function has the symbol S^{CEDA} as it is identical to the quantity used to optimise the ELP and we retain their symbol to give them credit.[116] The ELP minimising function is derived as the sum of the magnitude of the residual vector of the difference between the ELP and Fock integrals applied to the KS orbitals for the ELP KS equations. This choice of function is valid as the CEDA, ELP and LHF potentials are equivalent approximations.

While the KLI and CEDA approximate potentials exploit the same Unsöld approximation the CEDA potential should provide a better approximation to the exact exchange potential. The KLI potential is derived without removing the sum over states, k that are occupied in the ground state but which do not contribute to the first order orbital. These occupied states for $k < i$ will give $\varepsilon_k^\sigma - \varepsilon_i^\sigma < 0$ and for other states, $\varepsilon_k^\sigma - \varepsilon_i^\sigma > 0$ hence approximating the eigenvalue difference as a positive constant results in the first order orbital having the wrong sign for states where $k < i$. In the CEDA functional derivative all the eigenvalue differences have the same sign and so setting the eigenvalue

difference to a positive constant preserves the correct sign for each state in the first order orbital.

3.4.3 Iterative Procedure to Calculate the CEDA Potential

The objective function for the CEDA potential, S^{CEDA} has a functional form that is variational and hence can be used in iterative procedure similar to the one used for the EXX potential.

1. For potential, $\hat{V}_{\mathrm{x}}^{\sigma,p}(\mathbf{r})$, determine the ground state orbitals $\phi_i^{\sigma,p}(\mathbf{r})$ from the Kohn-Sham equations and value of S^{CEDA}.
2. Evaluate the CEDA functional derivative with respect to the potential, equation 3.88. Convolute the functional derivative with $\frac{1}{|\mathbf{r}-\mathbf{r}'|}$.
3. Determine optimal value of λ, via a line search.
4. Construct new potential by adding $\int d\mathbf{r}' \frac{1}{|\mathbf{r}-\mathbf{r}'|} \frac{\delta E[\hat{V}_{\mathrm{x}}^{\sigma,p}]}{\delta \hat{V}_{\mathrm{x}}^{\mathrm{CEDA},\sigma,p}(\mathbf{r}')}$ to the potential multiplied by λ.

This procedure continues until the ground state is reached, which is when the difference in S^{CEDA} between iterations tends to zero.

3.5 Exchange Potential by Optimisation of the Density

3.5.1 The LFX Potential

So far the local exchange potentials have been potentials that optimise the total energy of the system, or an approximate form of the total energy. However from the Hohenberg-Kohn theorems, the total energy is uniquely determined by the density of the system.[15] Hence by optimising the density rather than the energy we can also find the ground state of a system. We now consider a method for determining a local exchange potential that optimises the density of a reference system.

Returning to $T_\Psi[\hat{V}]$ (equation 3.60) for an interacting system with ground state Ψ and density $\rho_\Psi(\mathbf{r})$ there will be a Kohn-Sham system with an exchange-correlation potential $\hat{V}_{\mathrm{xc}}(\mathbf{r})$ and orbitals $\phi_i^\sigma(\mathbf{r})$ that also adopts $\rho_\Psi(\mathbf{r})$ as the ground state density.[112] Neglecting correlation the interacting system is Hartree-Fock, with its ground state wave function in the role of the Slater determinant Ψ_{HF} and density $\rho_{\mathrm{HF}}(\mathbf{r})$. The Kohn-Sham system only has an exchange potential $\hat{V}_{\mathrm{x}}(\mathbf{r})$ as its exchange-correlation potential. Using equation 3.60 the energy difference between the Hartree-Fock and Kohn-Sham systems is:

$$T_{\mathrm{HF}}[\hat{V}_{\mathrm{x}}^\sigma] = \langle \Psi_{\mathrm{HF}} | \hat{H}_{\mathrm{v}} | \Psi_{\mathrm{HF}} \rangle - E_{\mathrm{v}} \geq 0, \tag{3.91}$$

with $\hat{H}_{\mathrm{v}}$ the sum of the N Kohn-Sham single particle Hamiltonians, $\hat{h}_{\mathrm{v}} = -\frac{\nabla^2}{2} + \hat{V}^\sigma(\mathbf{r})$ and E_{v} is the sum of the eigenvalues of the KS system. The single particle orbitals, $\phi_i^\sigma(\mathbf{r})$ satisfy $\hat{h}_{\mathrm{v}}$ and generate a density $\rho_{\mathrm{v}}(\mathbf{r})$. The functional derivative of this energy,

$T_{\mathrm{HF}}[\hat{V}^{\sigma}]$ with respect to the exchange potential is given by;

$$\begin{aligned}\frac{\delta T_{\mathrm{HF}}[\hat{V}_{\mathrm{x}}^{\sigma}]}{\delta \hat{V}_{\mathrm{x}}^{\sigma}(\mathbf{r})} =&\langle \frac{\delta \Psi_{\mathrm{HF}}}{\delta \hat{V}_{\mathrm{x}}^{\sigma}(\mathbf{r})}|\hat{H}_{\mathrm{v}}|\Psi_{\mathrm{HF}}\rangle + \langle \Psi_{\mathrm{HF}}|\frac{\delta \hat{H}_{\mathrm{v}}}{\delta \hat{V}_{\mathrm{x}}^{\sigma}(\mathbf{r})}|\Psi_{\mathrm{HF}}\rangle + \langle \Psi_{\mathrm{HF}}|\hat{H}_{\mathrm{v}}|\frac{\delta \Psi_{\mathrm{HF}}}{\delta \hat{V}_{\mathrm{x}}^{\sigma}(\mathbf{r})}\rangle \\ &- \frac{\delta E_{\mathrm{v}}}{\delta \hat{V}_{\mathrm{x}}^{\sigma}(\mathbf{r})} \\ \\ =&\langle \Psi_{\mathrm{HF}}|\frac{\delta \hat{V}_{\mathrm{x}}^{\sigma}}{\delta \hat{V}_{\mathrm{x}}^{\sigma}(\mathbf{r})}|\Psi_{\mathrm{HF}}\rangle - \sum_{i=1}^{N^{\sigma}}\langle \phi_i^{\sigma}|\frac{\delta \hat{V}_{\mathrm{x}}^{\sigma}}{\delta \hat{V}_{\mathrm{x}}^{\sigma}(\mathbf{r})}|\phi_i^{\sigma}\rangle \\ =&\rho_{\mathrm{HF}}^{\sigma}(\mathbf{r}) - \rho_{\mathrm{v}}^{\sigma}(\mathbf{r}).\end{aligned} \tag{3.92}$$

Addition of this functional derivative to the potential can be used to minimise the energy difference in an iterative scheme and at the minimum of T_{HF} the two densities should be equal.[112]

To prove that T_{HF} can be used to optimise the potential $\hat{V}_{\mathrm{x}}^{\sigma}(\mathbf{r})$, we consider the change in T_{HF} for a change in the potential $\hat{V}_{\mathrm{x}}^{\sigma}(\mathbf{r}) \rightarrow \hat{V}_{\mathrm{x}}^{\sigma}(\mathbf{r}) + \lambda\delta\hat{V}_{\mathrm{x}}^{\sigma}(\mathbf{r})$ is written;

$$T_{\mathrm{HF}}[\hat{V}_{\mathrm{x}}^{\sigma} + \delta\hat{V}_{\mathrm{x}}^{\sigma}] = T_{\mathrm{HF}}[\hat{V}_{\mathrm{x}}^{\sigma}] + \lambda\sum_{\sigma}\int d\mathbf{r}\delta V_{\mathrm{x}}^{\sigma}(\mathbf{r})\frac{\delta T_{\mathrm{HF}}[\hat{V}_{\mathrm{x}}^{\sigma}]}{\delta \hat{V}_{\mathrm{x}}^{\sigma}(\mathbf{r})}, \tag{3.93}$$

for $\lambda > 0$ and choosing;

$$\delta\hat{V}_{\mathrm{x}}^{\sigma}(\mathbf{r}) = -\int d\mathbf{r}'\frac{\rho_{\mathrm{HF}}^{\sigma}(\mathbf{r}') - \rho_{\mathrm{v}}^{\sigma}(\mathbf{r}')}{|\mathbf{r} - \mathbf{r}'|}, \tag{3.94}$$

using the rational for the choice of the form $\delta\hat{V}_{\mathrm{x}}^{\sigma}$ as explained in 3.3.3.

$\Delta T_{\mathrm{HF}}[\hat{V}_{\mathrm{x}}^{\sigma} + \delta\hat{V}_{\mathrm{x}}^{\sigma}]$ can be written;

$$\begin{aligned}\Delta T_{\mathrm{HF}}[\hat{V}_{\mathrm{x}}^{\sigma} + \delta\hat{V}_{\mathrm{x}}^{\sigma}] &= T_{\mathrm{HF}}[\hat{V}_{\mathrm{x}}^{\sigma} + \delta\hat{V}_{\mathrm{x}}^{\sigma}] - T_{\mathrm{HF}}[\hat{V}_{\mathrm{x}}^{\sigma}] \\ &= \lambda\sum_{\sigma}\int d\mathbf{r}\delta V_{\mathrm{x}}^{\sigma}(\mathbf{r})\frac{\delta T_{\mathrm{HF}}[\hat{V}_{\mathrm{x}}^{\sigma}]}{\delta \hat{V}_{\mathrm{x}}^{\sigma}(\mathbf{r})} \\ &= -\lambda\sum_{\sigma}\iint d\mathbf{r}d\mathbf{r}'\frac{(\rho_{\mathrm{HF}}^{\sigma}(\mathbf{r}) - \rho_{\mathrm{v}}^{\sigma}(\mathbf{r}))(\rho_{\mathrm{HF}}^{\sigma}(\mathbf{r}') - \rho_{\mathrm{v}}^{\sigma}(\mathbf{r}'))}{|\mathbf{r} - \mathbf{r}'|},\end{aligned} \tag{3.95}$$

by substitution of the two definitions of $\delta V_{\mathrm{x}}^{\sigma}(\mathbf{r})$ and $\frac{\delta T_{\mathrm{HF}}[\hat{V}_{\mathrm{x}}^{\sigma}]}{\delta \hat{V}_{\mathrm{x}}^{\sigma}(\mathbf{r})}$. Defining the Hartree energy of the difference in the two densities;[8]

$$U[\hat{V}_{\mathrm{x}}^{\sigma}] = \sum_{\sigma}\iint d\mathbf{r}d\mathbf{r}'\frac{(\rho_{\mathrm{HF}}^{\sigma}(\mathbf{r}) - \rho_{\mathrm{v}}^{\sigma}(\mathbf{r}))(\rho_{\mathrm{HF}}^{\sigma}(\mathbf{r}') - \rho_{\mathrm{v}}^{\sigma}(\mathbf{r}'))}{|\mathbf{r} - \mathbf{r}'|}. \tag{3.96}$$

As $U[\hat{V}_{\mathrm{x}}^{\sigma}]$ is always positive this implies that $\Delta T_{\mathrm{HF}}[\hat{V}_{\mathrm{x}}^{\sigma}]$ is negative. Hence addition of $-\lambda\int d\mathbf{r}'\frac{1}{|\mathbf{r}-\mathbf{r}'|}\frac{\delta T_{\mathrm{HF}}[\hat{V}_{\mathrm{x}}^{\sigma}]}{\delta \hat{V}_{\mathrm{x}}^{\sigma}(\mathbf{r}')}$ to the potential $\hat{V}_{\mathrm{x}}^{\sigma}(\mathbf{r})$ will decrease the value of $T_{HF}[\hat{V}_{\mathrm{x}}^{\sigma}]$.

[8]Strictly twice the Hartree energy of the density difference

Furthermore adding $-\lambda \int d\mathbf{r}' \frac{1}{|\mathbf{r}-\mathbf{r}'|} \frac{\delta T_{\mathrm{HF}}[\hat{V}_{\mathrm{x}}^{\sigma}]}{\delta \hat{V}_{\mathrm{x}}^{\sigma}(\mathbf{r}')}$ to the potential will also decrease $U[\hat{V}_{\mathrm{x}}^{\sigma}]$ as a change in the potential induces the following change in the density, $\delta\rho^{\sigma}(\mathbf{r})$ of the Kohn-Sham system;

$$\delta\rho^{\sigma}(\mathbf{r}) = \int d\mathbf{r}' \hat{\chi}^{\sigma}(\mathbf{r},\mathbf{r}')\delta\hat{V}_{\mathrm{x}}^{\sigma}(\mathbf{r}') = -\lambda \int d\mathbf{r}' \hat{\chi}^{\sigma}(\mathbf{r},\mathbf{r}') \int d\mathbf{r}'' \frac{\rho_{\mathrm{HF}}^{\sigma}(\mathbf{r}'') - \rho_{\mathrm{v}}^{\sigma}(\mathbf{r}'')}{|\mathbf{r}' - \mathbf{r}''|}, \quad (3.97)$$

where $\hat{\chi}^{\sigma}(\mathbf{r},\mathbf{r}')$ is defined in equation 3.25. The change in $U[\hat{V}_{\mathrm{x}}^{\sigma}]$ due to the addition of $\lambda\delta\hat{V}_{\mathrm{x}}^{\sigma}(\mathbf{r})$ is given by;

$$\begin{aligned} U[\hat{V}_{\mathrm{x}}^{\sigma} + \lambda\delta\hat{V}_{\mathrm{x}}^{\sigma}] - U[\hat{V}_{\mathrm{x}}^{\sigma}] &= -2\lambda \sum_{\sigma} \iint d\mathbf{r} d\mathbf{r}' \frac{\delta\rho^{\sigma}(\mathbf{r})(\rho_{\mathrm{HF}}^{\sigma}(\mathbf{r}') - \rho_{\mathrm{v}}^{\sigma}(\mathbf{r}'))}{|\mathbf{r} - \mathbf{r}'|} \quad (3.98) \\ &= 2\lambda \sum_{\sigma} \iint d\mathbf{r} d\mathbf{r}' \frac{\rho_{\mathrm{HF}}^{\sigma}(\mathbf{r}') - \rho_{\mathrm{v}}^{\sigma}(\mathbf{r}')}{|\mathbf{r} - \mathbf{r}'|} \int d\mathbf{r}'' \hat{\chi}^{\sigma}(\mathbf{r},\mathbf{r}'') \int d\mathbf{r}''' \frac{\rho_{\mathrm{HF}}^{\sigma}(\mathbf{r}''') - \rho_{\mathrm{v}}^{\sigma}(\mathbf{r}''')}{|\mathbf{r}'' - \mathbf{r}'''|}, \end{aligned}$$

for $\delta\rho^{\sigma}(\mathbf{r})^2 \to 0$. As $\hat{\chi}^{\sigma}(\mathbf{r},\mathbf{r}')$ is a negative definite operator[9] the change in $U[\hat{V}_{\mathrm{x}}^{\sigma}]$ is always negative. E.g. Assuming $\hat{\chi}^{\sigma}(\mathbf{r},\mathbf{r}'') \approx -\delta(\mathbf{r} - \mathbf{r}'')$ gives;

$$U[\hat{V}_{\mathrm{x}}^{\sigma} + \lambda\delta\hat{V}_{\mathrm{x}}^{\sigma}] - U[\hat{V}_{\mathrm{x}}^{\sigma}] \approx -2\lambda \sum_{\sigma} \int d\mathbf{r} \left(\int d\mathbf{r}' \frac{\rho_{\mathrm{HF}}^{\sigma}(\mathbf{r}') - \rho_{\mathrm{v}}^{\sigma}(\mathbf{r}')}{|\mathbf{r} - \mathbf{r}'|} \right)^2, \quad (3.99)$$

which is always negative and hence $U[\hat{V}_{\mathrm{x}}^{\sigma}]$ can also be used to optimise the local potential that adopts the Hartree-Fock density. We choose to call the potential that reproduces the HF density the "Local Fock Exchange" (LFX) potential and can construct it by adding the LFX functional derivative (equation 3.92) to the potential in an iterative procedure.[118]

Relative to the procedure to construct the EXX potential, the LFX potential is much simpler to calculate as the functional derivative is just the difference between two densities rather than having to calculate the first order orbitals via a Sternheimer equation.

The optimising function $U[\hat{V}_{\mathrm{x}}^{\sigma}]$ can also be used to very efficiently invert any target density, and obtain the effective local potential that reproduces the target density. Inverting densities is a very active area of interest in the field of frozen density embedding schemes.[119, 120]

3.5.2 Iterative Procedure to Calculate the LFX Potential

In the previous section it was shown that the optimising function $U[\hat{V}_{\mathrm{x}}^{\sigma}]$ is variational and hence can use an iterative procedure similar to the one used for EXX to find the LFX potential.

1. Initially solve the HF equations to get the HF density.

[9] All its eigenvalues are negative

2. Evaluate the LFX functional derivative with respect to the potential, equation 3.94 and value of $U[\hat{V}_{\mathrm{x}}^{\sigma}]$ for the current potential.
3. Determine optimal value of λ, via a line search.
4. Construct new potential by adding the LFX functional derivative to the potential multiplied by λ.

This procedure continues until the ground state is reached, which is when $U[\hat{V}_{\mathrm{x}}^{\sigma}]$ tends to zero.

3.6 Extension to Metals

3.6.1 Fractional Occupancies

So far while we have not specified the type of system the theory applies to, there has been an implicit assumption that the eigenvalues of the Kohn-Sham system are divided into two kinds, occupied by an electron up to the N^{σ}-th band and unoccupied thereafter.[10] This restricts the application of a Kohn-Sham system to an insulating system. To extend the application of KS theory to metals and degenerate systems, each orbital must also have an occupancy assigned to it, n_i^{σ} with values; $0 \leq n_i^{\sigma} \leq 1$.[11]

Whenever there is a sum over the orbitals each term must be weighted by its occupancy. The density is then given by;

$$\rho(\mathbf{r}) = \sum_{\sigma} \sum_{i=1}^{\infty} n_i^{\sigma} \phi_i^{\sigma\dagger}(\mathbf{r}) \phi_i^{\sigma}(\mathbf{r}), \tag{3.100}$$

and quantities such as the kinetic energy are written as;

$$T = -\frac{1}{2} \sum_{\sigma} \sum_{i=1}^{\infty} n_i^{\sigma} \int d\mathbf{r} \phi_i^{\sigma\dagger}(\mathbf{r}) \nabla^2 \phi_i^{\sigma}(\mathbf{r}), \tag{3.101}$$

and the Fock exchange integral;

$$V_{\mathrm{x}} = -\frac{1}{2} \sum_{\sigma} \sum_{i=1}^{\infty} \sum_{j=1}^{\infty} \iint d\mathbf{r} d\mathbf{r}' n_i^{\sigma} n_j^{\sigma} \frac{\phi_i^{\sigma\dagger}(\mathbf{r}) \phi_i^{\sigma}(\mathbf{r}') \phi_j^{\sigma}(\mathbf{r}) \phi_j^{\sigma\dagger}(\mathbf{r}')}{|\mathbf{r} - \mathbf{r}'|}. \tag{3.102}$$

To consider a system with fractional occupancies while retaining numerical stability the occupancies must smoothly vary from $1 \to 0$. In an insulating system the eigenvalues are Dirac δ functions; in a partially occupied system the eigenvalues are broadened by using a smearing function, δ_{θ};

$$\varepsilon_i^{\sigma} \to \delta_{\theta}(\varepsilon_i^{\sigma}) = \frac{1}{\theta} \tilde{\delta} \left(\frac{\varepsilon_i^{\sigma}}{\theta} \right), \tag{3.103}$$

[10] Indexed by i and a respectively

[11] The occupancy also depends on the k-point of the orbital; $n_{i,\mathbf{k}}^{\sigma}$.

where $\delta_\theta(x)$ is a function that integrates to 1 and in the limit $\theta \to 0$, tends to the Dirac δ function. The smearing functions, $\tilde{\delta}(x)$ that can be used are: Fermi-Dirac broadening, Lorentzians, Gaussians, Gaussians combined with polynomials or cold smearing.[104] In this work by preference Gaussian broadening will be used, however the theory presented here remains fully general. The occupancy of a band is calculated from;

$$n_i^\sigma = \tilde{\Theta}\left(\frac{\varepsilon_\mathrm{F} - \varepsilon_i^\sigma}{\theta}\right) = \int_{-\infty}^{\frac{\varepsilon_\mathrm{F}-\varepsilon_i^\sigma}{\theta}} \tilde{\delta}(x)dx, \tag{3.104}$$

where $\tilde{\Theta}$ is a smooth approximation to the Heaviside step function and ε_F is the Fermi energy defined from the normalisation to the total number of electrons;[121]

$$N = \sum_\sigma \sum_{i=1}^{\infty} \tilde{\Theta}\left(\frac{\varepsilon_\mathrm{F} - \varepsilon_i^\sigma}{\theta}\right). \tag{3.105}$$

3.6.2 EXX Extended to Partial Occupancies

The extension of EXX to metals and other degenerate systems uses the same form as described in section 3.3. In a system with fractional occupancies the derivative of the orbital with respect to the potential can be partitioned;

$$\begin{aligned}\frac{\delta\phi_i^\sigma(\mathbf{r})}{\delta\hat{V}_\mathrm{x}^\sigma(\mathbf{r}')} &= -\sum_{j=1,j\neq i}^{\infty} \frac{\phi_j^\sigma(\mathbf{r})\phi_j^{\sigma\dagger}(\mathbf{r}')}{\varepsilon_j^\sigma - \varepsilon_i^\sigma}\phi_i^\sigma(\mathbf{r}'), \\ &= -\sum_{k=1,k\neq i}^{\infty} n_k^\sigma \frac{\phi_k^\sigma(\mathbf{r})\phi_k^{\sigma\dagger}(\mathbf{r}')}{\varepsilon_k^\sigma - \varepsilon_i^\sigma}\phi_i^\sigma(\mathbf{r}') - \sum_{a=1,a\neq i}^{\infty}(1-n_a^\sigma)\frac{\phi_a^\sigma(\mathbf{r})\phi_a^{\sigma\dagger}(\mathbf{r}')}{\varepsilon_a^\sigma - \varepsilon_i^\sigma}\phi_i^\sigma(\mathbf{r}'),\end{aligned} \tag{3.106}$$

as $1 = n_j^\sigma + (1 - n_j^\sigma)$. Substitution into the minimisation condition of the optimised effective potential (equation 3.29) gives;

$$\begin{aligned}\frac{\delta E[\hat{V}_\mathrm{x}^\sigma]}{\delta\hat{V}_\mathrm{x}^\sigma(\mathbf{r})} = &-\sum_{i=1}^{\infty}\sum_{k=1,k\neq i}^{\infty} n_i^\sigma n_k^\sigma \left[\int d\mathbf{r}' \frac{\phi_k^{\sigma\dagger}(\mathbf{r})\phi_i^\sigma(\mathbf{r})\phi_k^\sigma(\mathbf{r}')}{\varepsilon_k^\sigma - \varepsilon_i^\sigma}\left[\hat{u}_{\mathrm{x},i}^\sigma(\mathbf{r}') - \hat{V}_\mathrm{x}^\sigma(\mathbf{r}')\right]\phi_i^{\sigma\dagger}(\mathbf{r}') + \mathrm{h.c.}\right] \\ &-\sum_{i=1}^{\infty}\sum_{a=1,a\neq i}^{\infty} n_i^\sigma(1-n_a^\sigma)\left[\int d\mathbf{r}' \frac{\phi_a^{\sigma\dagger}(\mathbf{r})\phi_i^\sigma(\mathbf{r})\phi_a^\sigma(\mathbf{r}')}{\varepsilon_a^\sigma - \varepsilon_i^\sigma}\left[\hat{u}_{\mathrm{x},i}^\sigma(\mathbf{r}') - \hat{V}_\mathrm{x}^\sigma(\mathbf{r}')\right]\phi_i^{\sigma\dagger}(\mathbf{r}') + \mathrm{h.c.}\right] \\ &+\sum_{i=1}^{\infty}\Delta n_i^\sigma(\Delta\varepsilon_\mathrm{F} - \Delta\varepsilon_i^\sigma)|\phi_i^\sigma(\mathbf{r})|^2,\end{aligned} \tag{3.107}$$

where $\Delta n_i^\sigma(\Delta\varepsilon_\mathrm{F} - \Delta\varepsilon_i^\sigma)$ is a term that accounts for the changes in the occupancies and Fermi level induced by shifts in the single-particle energies due to the perturbation. The first order change in the eigenvalues is; $\Delta\varepsilon_i^\sigma = \langle\phi_i^\sigma|\delta\hat{V}_\mathrm{x}^\sigma|\phi_i^\sigma\rangle$.[104, 121]

The first term on the right hand side of equation 3.107 and its hermitian conjugate cancel upon interchange of the indices i and k. Additionally the second term can be rewritten by expanding the hermitian conjugate and interchanging the indexes i and a

for the hermitian conjugate. The functional derivative of the energy with respect to the potential can then be simplified to;

$$\frac{\delta E[\hat{V}_{\mathrm{x}}^{\sigma}]}{\delta \hat{V}_{\mathrm{x}}^{\sigma}(\mathbf{r})} = -2 \sum_{i=1}^{n_i^{\sigma}\to 0} \sum_{a=1}^{\infty} \frac{(n_i^{\sigma} - n_a^{\sigma})}{\varepsilon_a^{\sigma} - \varepsilon_i^{\sigma}} \tilde{\Theta}\left(\frac{\varepsilon_a^{\sigma} - \varepsilon_i^{\sigma}}{\theta}\right) \Bigg[\int d\mathbf{r}' \phi_a^{\sigma\dagger}(\mathbf{r}) \phi_i^{\sigma}(\mathbf{r}) \times \phi_a^{\sigma}(\mathbf{r}') \left[\hat{u}_{\mathrm{x},i}^{\sigma}(\mathbf{r}') - \hat{V}_{\mathrm{x}}^{\sigma}(\mathbf{r}')\right] \phi_i^{\sigma\dagger}(\mathbf{r}') \Bigg] + \sum_{i=1}^{\infty} \Delta\varepsilon_{\mathrm{F}} \Delta n_i^{\sigma} |\phi_i^{\sigma}(\mathbf{r})|^2, \tag{3.108}$$

where $\tilde{\Theta}$ was introduced in equation 3.104 and allows one sum to be truncated once the occupancy of the i-th state becomes negligible, due to the symmetry of i and a and $\tilde{\Theta}(-x) + \tilde{\Theta}(x) = 1$. The $a = i$ term can be evaluated as long as $(n_i^{\sigma} - n_a^{\sigma})/(\varepsilon_a^{\sigma} - \varepsilon_i^{\sigma})$ is replaced by the limit $-1/\theta\tilde{\delta}((\varepsilon_{\mathrm{F}}^{\sigma} - \varepsilon_i^{\sigma})/\theta)$ whenever $\varepsilon_a^{\sigma} - \varepsilon_i^{\sigma} \to 0$ which accounts for the changes in the occupancy due to $\Delta\varepsilon_i^{\sigma}$, and the last term then accounts for the change in the Fermi level with $\Delta\varepsilon_{\mathrm{F}}$ given by;

$$\Delta\varepsilon_{\mathrm{F}}(\Delta n_i^{\sigma}, \Delta\varepsilon_i^{\sigma}) = \frac{\sum_{i=1}^{\infty} \Delta n_i^{\sigma} \Delta\varepsilon_i^{\sigma}}{\sum_{i=1}^{\infty} \Delta n_i^{\sigma}}, \tag{3.109}$$

and the change in the occupancy, Δn_i^{σ} is given by;

$$\Delta n_i^{\sigma} = \frac{1}{\theta} \tilde{\delta}\left(\frac{\varepsilon_{\mathrm{F}} - \varepsilon_i^{\sigma}}{\theta}\right). \tag{3.110}$$

The first order orbital is then given by;

$$\tilde{\phi}_i^{\sigma}(\mathbf{r}) = -\sum_{a=1}^{\infty} \frac{(n_i^{\sigma} - n_a^{\sigma})}{n_i^{\sigma}} \tilde{\Theta}\left(\frac{\varepsilon_a^{\sigma} - \varepsilon_i^{\sigma}}{\theta}\right) \left[\int d\mathbf{r}' \frac{\phi_a^{\sigma}(\mathbf{r}) \phi_a^{\sigma\dagger}(\mathbf{r}')}{\varepsilon_a^{\sigma} - \varepsilon_i^{\sigma}} \left[\hat{u}_{\mathrm{x},i}^{\sigma\dagger}(\mathbf{r}') - \hat{V}_{\mathrm{x}}^{\sigma}(\mathbf{r}')\right] \phi_i^{\sigma}(\mathbf{r}') \right], \tag{3.111}$$

and the functional derivative of the energy with respect to the potential is;

$$\begin{aligned} \frac{\delta E[\hat{V}_{\mathrm{x}}^{\sigma}]}{\delta \hat{V}_{\mathrm{x}}^{\sigma}(\mathbf{r})} =& 2 \sum_{i=1}^{n_i^{\sigma}\to 0} \sum_{a=1}^{\infty} n_i^{\sigma} \tilde{\phi}_i^{\sigma\dagger}(\mathbf{r}) \phi_i^{\sigma}(\mathbf{r}) \\ &+ \sum_{i=1}^{\infty} \Delta\varepsilon_{\mathrm{F}} \Delta n_i^{\sigma} |\phi_i^{\sigma}(\mathbf{r})|^2. \end{aligned} \tag{3.112}$$

An unmodified Sternheimer equation can be found if the first order orbital is parti-

tioned;[12]

$$\tilde{\phi}_i^\sigma(\mathbf{r}) = -\sum_{k=1}^{n_k^\sigma \to 0} \frac{(n_i^\sigma - n_k^\sigma)}{n_i^\sigma} \tilde{\Theta}\left(\frac{\varepsilon_k^\sigma - \varepsilon_i^\sigma}{\theta}\right) \left[\int d\mathbf{r}' \frac{\phi_k^\sigma(\mathbf{r})\phi_k^{\sigma\dagger}(\mathbf{r}')}{\varepsilon_k^\sigma - \varepsilon_i^\sigma} \left[\hat{u}_{\mathrm{x},i}^{\sigma\dagger}(\mathbf{r}') - \hat{V}_\mathrm{x}^\sigma(\mathbf{r}')\right] \phi_i^\sigma(\mathbf{r}')\right]$$
$$- \sum_{a=n_a^\sigma \to 0}^{\infty} \left[\int d\mathbf{r}' \frac{\phi_a^\sigma(\mathbf{r})\phi_a^{\sigma\dagger}(\mathbf{r}')}{\varepsilon_a^\sigma - \varepsilon_i^\sigma} \left[\hat{u}_{\mathrm{x},i}^{\sigma\dagger}(\mathbf{r}') - \hat{V}_\mathrm{x}^\sigma(\mathbf{r}')\right] \phi_i^\sigma(\mathbf{r}')\right], \tag{3.113}$$

the index k is summed over all states with non-zero occupancy (hence the maximum value of the sum is the state with $n_k^\sigma \to 0$) and index a over all states with occupancy zero. $\tilde{\Theta}$ is always 1 for the states indexed by a as $\varepsilon_a^\sigma - \varepsilon_i^\sigma \gg 0$.

A Sternheimer equation is then tractable with a first order orbital contribution from all states with zero occupation provided the projector in equation 3.52 is defined;

$$\hat{P}_\mathrm{c} = \hat{I} - \sum_{j=1}^{n_j^\sigma \to 0} |\phi_j^\sigma\rangle\langle\phi_j^\sigma| = \sum_{a=n_a^\sigma \to 0}^{\infty} |\phi_a^\sigma\rangle\langle\phi_a^\sigma|, \tag{3.114}$$

the first term in equation 3.113 is then calculated directly, the second term from the Sternheimer equation and the two terms summed together to get the full first order orbital. It is trivial to show that for a system with non-partial occupancy the definitions of the first order orbital and function derivative of the energy revert to their insulating forms (equations 3.43 and 3.44).

3.6.3 LFX Extended to Fractional Occupancies

The extension of LFX to metals and other degenerate systems is again much simpler than EXX due to the much simpler form of the functional derivative. In a partially occupied system the LFX functional derivative can be written;

$$\int d\mathbf{r}' \frac{1}{|\mathbf{r} - \mathbf{r}'|} \frac{\delta T_\mathrm{HF}[\hat{V}_\mathrm{x}^\sigma]}{\delta \hat{V}_\mathrm{x}^\sigma(\mathbf{r}')} = \int d\mathbf{r}' \frac{\rho_\mathrm{HF}^\sigma(\mathbf{r}') - \rho_\mathrm{v}^\sigma(\mathbf{r}')}{|\mathbf{r} - \mathbf{r}'|} \tag{3.115}$$
$$= \sum_\sigma \int d\mathbf{r}' \frac{1}{|\mathbf{r} - \mathbf{r}'|} \left(\sum_{i=1}^{n_{\mathrm{HF},i}^\sigma \to 0} n_{\mathrm{HF},i}^\sigma \psi_i^{\sigma\dagger}(\mathbf{r}')\psi_i^\sigma(\mathbf{r}') - \sum_{i=1}^{n_i^\sigma \to 0} n_i^\sigma \phi_i^{\sigma\dagger}(\mathbf{r}')\phi_i^\sigma(\mathbf{r}') \right),$$

using the definition of the density from equation 3.100, $n_{\mathrm{HF},i}^\sigma$ are the HF occupancies and $\psi_i^{\sigma\dagger}(\mathbf{r})$ are the HF orbitals that comprise the HF Slater determinant. Similar considerations apply to the minimising function $U[\hat{V}_\mathrm{x}^\sigma]$.

[12] Modified Sternheimer equations that account for the entire first order orbital in a partially occupied system exist and are shown in reference [104].

3.7 The Physical Equivalence of EXX and LFX

The EXX potential is the local potential that minimises the Hartree-Fock (HF) total energy;

$$\langle \Phi_{\mathrm{v}} | \hat{H}_{\mathrm{HF}} | \Phi_{\mathrm{v}} \rangle = E_{\mathrm{EXX}}, \tag{3.116}$$

where Φ_{v} is the Slater determinant composed of the N Kohn-Sham orbitals, generated from the exchange-only Kohn-Sham equations containing the EXX potential as the exchange potential. The LFX potential optimally finds the HF density as its own ground state density. The two methods optimise two closely related quantities, as the ground state density uniquely determines the ground state energy and vice versa, hence there is a degree of physical equivalence between the two potentials.

This can be further illustrated by considering the energy difference the two methods minimise. The EXX potential will minimise the energy difference;

$$\langle \Phi_{\mathrm{v}} | \hat{H}_{\mathrm{HF}} | \Phi_{\mathrm{v}} \rangle - E_{\mathrm{HF}} \geq 0, \tag{3.117}$$

where E_{HF} is the HF total energy. The LFX potential minimises a similar energy difference, $T_{\mathrm{HF}}[\hat{V}_{\mathrm{x}}^{\sigma}]$ (equation 3.91);

$$\langle \Psi_{\mathrm{HF}} | \hat{H}_{\mathrm{v}} | \Psi_{\mathrm{HF}} \rangle - E_{\mathrm{v}} \geq 0, \tag{3.118}$$

where Ψ_{HF} is the HF Slater determinant, $\hat{H}_{\mathrm{v}}$ is the effective Hamiltonian with a local potential and E_{v} is the total energy of the effective Kohn-Sham system. At the minimum the local potential is the Hartree potential plus the LFX exchange potential.

If the constraint of having a local potential for either the EXX or LFX potentials is dropped (allowing a non-local exchange potential) the ground state Hamiltonian and ground state Slater determinant are optimally the HF ones.[118] It follows that the EXX and LFX potentials both simulate optimally the non-local exchange potential in the HF equations, even though they are determined differently (by satisfying different equations).

Additionally consider the perturbative expansion of the zeroth order non-interacting Kohn-Sham Hamiltonian, equation 3.64;

$$\hat{H}_{\hat{V}_{\mathrm{ext}}+\hat{U}} = \hat{T} + \hat{V}_{\mathrm{ext}} + \hat{U}, \qquad \hat{U} = \sum_i \hat{U}(\mathbf{r}_i), \tag{3.119}$$

with a perturbing potential, $\hat{V}'$ switching on interactions between the electrons; $\hat{V}' = \hat{V}_{\mathrm{ee}} - \sum_i \hat{U}(\mathbf{r}_i)$. According to reference [122] the density will not change to first order if the local potential, $\hat{U}$ is the sum of the Hartree and EXX potentials.

By similar considerations in the Moller-Plesset expansion, the zeroth order Hamiltonian is the HF Hamiltonian. Turning on interactions, the Moller-Plesset first order correction to the HF ground state Slater determinant contains only doubly excited Slater determinants, as from Brillouin's theorem singly excited determinants do not couple with

the HF ground state. Hence the density of the Moller-Plesset scheme is also unchanged to first order, because the density is a one-body operator and any matrix element of the double excitations with the ground state will be zero due to orthogonality. As the LFX density is the HF density this implies the LFX potential has no first order corrections, if interactions were switched on.[118, 112]

Hence, both the EXX and LFX potentials form the zeroth order terms of two similar perturbative power series expansions of the Kohn-Sham potential, where for both the first order term vanishes. These similarities do not however guarantee that the EXX and LFX potentials must always give the same results and only in materials where the exchange-correlation energy is dominated by the exchange term would it be reasonable to expect the two potentials to agree. For a system with significant correlation energy the second and higher order terms will be significant and the two methods cannot be expected to agree.

3.8 Summary

We have reviewed the optimised effective potential equations in the context of the exact exchange potential. A variational method for calculating the EXX potential without having to sum over all infinite unoccupied states by using the Hylleraas variational method is constructed. A two loop minimisation scheme was proposed, using equations 3.44 and 3.52. Two common approximations to EXX, the KLI and CEDA approximations were reviewed, derived and an algorithm to calculate the CEDA potential proposed. A potential similar to the EXX potential but that optimises the density of the reference HF system rather than the energy, called the LFX potential was proposed. A minimising function for the LFX potential, equation 3.96 and a functional derivative, equation 3.92 were derived. The EXX and LFX potentials were generalised to include metallic systems. And lastly some arguments for the physical equivalence of the EXX and LFX potentials were proposed.

Chapter 4

Implementation of Local Potentials

4.1 Plane Wave Implementation of Local Potentials

The use of plane waves as implemented in CASTEP has many advantages, as was outlined in section 2.4.

The orbitals, density and potentials are represented by regular grids in both real and reciprocal space.[123] The Kohn-Sham orbitals described in reciprocal space within a sphere of cut-off wave vector, $G_{\max}$, and the density and potentials are non-zero within a sphere of radius $2G_{\max}$. Therefore the grids used to represent the density and potentials have twice the dimensions of the orbital grid, in both real and reciprocal space. Strictly derivatives of potentials and densities should be represented within a sphere of radius $4G_{\max}$ however using a sphere of radius beyond $2G_{\max}$ for these quantities was found to make no difference on calculated total energies and band structures

Orbitals are stored in reciprocal space as arrays of plane wave coefficients, $c^{\sigma}_{i,\mathbf{k}}(\mathbf{G})$ and the density and potentials are stored in real space. The combination of plane waves with the use of fast Fourier transforms (FFTs) allows the easy transformation of the orbitals, density and potentials from real space to reciprocal space, in order to carry out the parts of the calculation in the space where least computational effort is required. For instance the exchange and Hartree potentials are most easily calculated in reciprocal space (equations 2.86 and 2.89 in section 2.4.5) while the external potential is easiest to deal with in real space.

4.1.1 Choice of Pseudopotentials

As previously mentioned in section 2.5 there are two forms of pseudopotential to choose from. In this work we will be using norm-conserving Hartree-Fock pseudopotentials using the OPIUM pseudopotential generation code,[60, 124] with the localisation and optimisation scheme of ref [66].

The choice of norm-conserving pseudopotentials is taken despite a norm-conserving potential requiring a higher cut off energy for the plane wave basis set than an equivalent ultrasoft potential. However the use of ultrasofts also increases the complexity of the expressions that need to be calculated, for instance the exchange energy when using ultrasoft pseudopotentials is given by;

$$\begin{aligned} E_{\mathrm{x}} =& \frac{1}{2}\sum_{\sigma}\sum_{i,\mathbf{k}}^{N^{\sigma}}\sum_{j,\mathbf{q}}^{N^{\sigma}}\iint d\mathbf{r}d\mathbf{r}'\frac{\phi^{\sigma\dagger}_{i,\mathbf{k}}(\mathbf{r})(1-\sum_{l,m}|\beta_{l,\mathbf{k}}\rangle\langle\beta_{m,\mathbf{q}}|)\phi^{\sigma}_{j,\mathbf{q}}(\mathbf{r})}{|\mathbf{r}-\mathbf{r}'|} \\ & \times \phi^{\sigma\dagger}_{j,\mathbf{q}}(\mathbf{r}')(1-\sum_{l,m}|\beta_{m,\mathbf{q}}\rangle\langle\beta_{l,\mathbf{k}}|)\phi^{\sigma}_{i,\mathbf{k}}(\mathbf{r}'), \end{aligned} \tag{4.1}$$

where $|\beta_l\rangle\langle\beta_m|$ are projectors defined in section 2.5 and the sums over l and m are combined indices over the angular momentum quantum numbers and reference state.[125, 126, 127] This form has rather unfavourable scaling properties scaling as; $N_{\mathrm{k}}^2 N_{\mathrm{b}}^2 N_{\mathrm{pjs}}^2 N_{\mathrm{pw}}^{\mathrm{usp2}}$ where N_{pjs} is the number of projectors required to form the full set of $|\beta_l\rangle$ and $N_{\mathrm{pw}}^{\mathrm{usp}}$ is the number of plane waves that converge the total energy for the chosen ultrasoft pseudopotentials. By contrast the norm-conserving form scales as; $N_{\mathrm{k}}^2 N_{\mathrm{b}}^2 N_{\mathrm{pw}}^{\mathrm{ncp2}}$ and $N_{\mathrm{pw}}^{\mathrm{ncp}}$ is the number of plane waves for the chosen norm-conserving pseudopotentials.

The number of plane waves required for a norm-conserving calculation is typically; $N_{\mathrm{pw}}^{\mathrm{ncp}} \approx$ 2-4$N_{\mathrm{pw}}^{\mathrm{usp}}$, of an equivalent ultrasoft calculation and typically N_{pjs} has a value of order 2-4. This leads to any saving made in lowering the required cut off energy by use of ultrasoft pseudopotentials being offset by the increased number of summations to actually calculate the exchange energy. Furthermore the functional derivatives required to calculate the local exchange potentials also need to be modified to include the contributions due to the overlap operators and the projector in the Sternheimer equation is required to be generalised to;

$$P_{\mathrm{c}}^{+} = 1 - \sum_{n=1}^{N^{\sigma}}(1+\sum_{l}|\beta_l\rangle\langle\beta_l|)|\phi_i^{\sigma}\rangle\langle\phi_i^{\sigma}|. \tag{4.2}$$

Due to the additional complexity of using ultrasofts the use of the norm-conserving pseudopotentials is no major disadvantage.

4.1.2 Evaluating the Fock Exchange Operator

The form of the non-local exchange operator used in the EXX formalism is given by;

$$\hat{u}^{\sigma}_{\mathrm{x},i,\mathbf{k}}(\mathbf{r}) = \frac{1}{\phi^{\sigma\dagger}_{i,\mathbf{k}}(\mathbf{r})}\frac{\partial E_{\mathrm{x}}[\phi^{\sigma}_{i,\mathbf{k}}]}{\partial\phi^{\sigma}_{i,\mathbf{k}}(\mathbf{r})}, \tag{4.3}$$

however this quantity is not itself evaluated directly. In any calculation the operator is always applied to an orbital and never calculated directly hence the following quantity

is evaluated;

$$\hat{u}^{\sigma\dagger}_{\mathrm{x},i,\mathbf{k}}(\mathbf{r})\phi^{\sigma}_{i,\mathbf{k}}(\mathbf{r}) = \frac{\phi^{\sigma}_{i,\mathbf{k}}(\mathbf{r})}{\phi^{\sigma}_{i,\mathbf{k}}(\mathbf{r})}\frac{\partial E_{\mathrm{x}}[\phi^{\sigma}_{i,\mathbf{k}}]}{\partial \phi^{\sigma\dagger}_{i,\mathbf{k}}(\mathbf{r})}, = \sum_{j,\mathbf{q}}^{N^{\sigma}} \int d\mathbf{r}' \frac{\phi^{\sigma}_{j,\mathbf{q}}(\mathbf{r})\phi^{\sigma\dagger}_{j,\mathbf{q}}(\mathbf{r}')}{|\mathbf{r}-\mathbf{r}'|}\phi^{\sigma}_{i,\mathbf{k}}(\mathbf{r}'), \tag{4.4}$$

which exchanges the indices of the applied $\phi^{\sigma}_{i,\mathbf{k}}(\mathbf{r})$ from $\mathbf{r}$ to $\mathbf{r}'$. Hence for each instance of $\hat{u}^{\sigma}_{\mathrm{x},i,\mathbf{k}}(\mathbf{r})$ applied to an orbital, the right hand side of equation 4.4 is the term we actually consider.

4.1.3 Iterative Procedure for the Calculation of the EXX Potential

The procedure for calculating the EXX potential is outlined in figure 4.1. The EXX potential is found by an iterative double nested loop minimisation. Before the minimisation there must be an initial trial potential to start the optimisation. By performing an initial calculation using the local density approximation (LDA) exchange correlation potential we obtain an initial set of orbitals, $\phi^{\sigma}_{i}(\mathbf{r})$ from which the density can be calculated; $\rho^{\sigma}_{\mathrm{LDA}}(\mathbf{r})$. This density then allows the initial potential representing electron repulsion (Hartree and exchange potentials) to be;

$$\hat{V}^{\sigma,p=1}_{\mathrm{Hx,EXX}}(\mathbf{r}) = \hat{V}_{\mathrm{H}}[\rho^{\sigma}_{\mathrm{LDA}}](\mathbf{r}) + \hat{V}^{\mathrm{LDA}}_{\mathrm{xc}}[\rho^{\sigma}_{\mathrm{LDA}}](\mathbf{r}), \tag{4.5}$$

where p is the iteration number. We combine the Hartree and exchange terms into one potential for computational convenience, of having one local potential that represents the effective electron-electron interaction, and to allow addition and substitution of other approximate exchange-correlation potentials, if required in the future. The Kohn-Sham Hamiltonian at iteration p is then given by;

$$\hat{H}^{\sigma,p} = -\frac{\nabla^2}{2} + \hat{V}_{\mathrm{ext}}(\mathbf{r}) + V^{\sigma,p}_{\mathrm{Hx}}(\mathbf{r}), \tag{4.6}$$

and the EXX total energy at iteration p;

$$\begin{aligned} E^{p}_{\mathrm{EXX}}[\hat{V}^{\sigma,p}_{\mathrm{Hx}}] = \Bigg[&- \sum_{\sigma}\sum_{i,\mathbf{k}} \int d\mathbf{r}\phi^{\sigma,p\dagger}_{i,\mathbf{k}}(\mathbf{r})\frac{\nabla^2}{2}\phi^{\sigma,p}_{i,\mathbf{k}}(\mathbf{r}) + \int d\mathbf{r}\hat{V}_{\mathrm{ext}}(\mathbf{r})\rho^{p}(\mathbf{r}) \\ &+ \frac{1}{2}\iint d\mathbf{r}d\mathbf{r}'\frac{\rho^{p}(\mathbf{r})\rho^{p}(\mathbf{r}')}{|\mathbf{r}-\mathbf{r}'|} \\ &- \frac{1}{2}\sum_{\sigma}\sum_{i,\mathbf{k}}\sum_{j,\mathbf{q}}\iint d\mathbf{r}d\mathbf{r}'\frac{\phi^{\sigma,p\dagger}_{i,\mathbf{k}}(\mathbf{r})\phi^{\sigma,p}_{j,\mathbf{q}}(\mathbf{r})\phi^{\sigma,p\dagger}_{j,\mathbf{q}}(\mathbf{r}')\phi^{\sigma,p}_{i,\mathbf{k}}(\mathbf{r}')}{|\mathbf{r}-\mathbf{r}'|}\Bigg], \end{aligned} \tag{4.7}$$

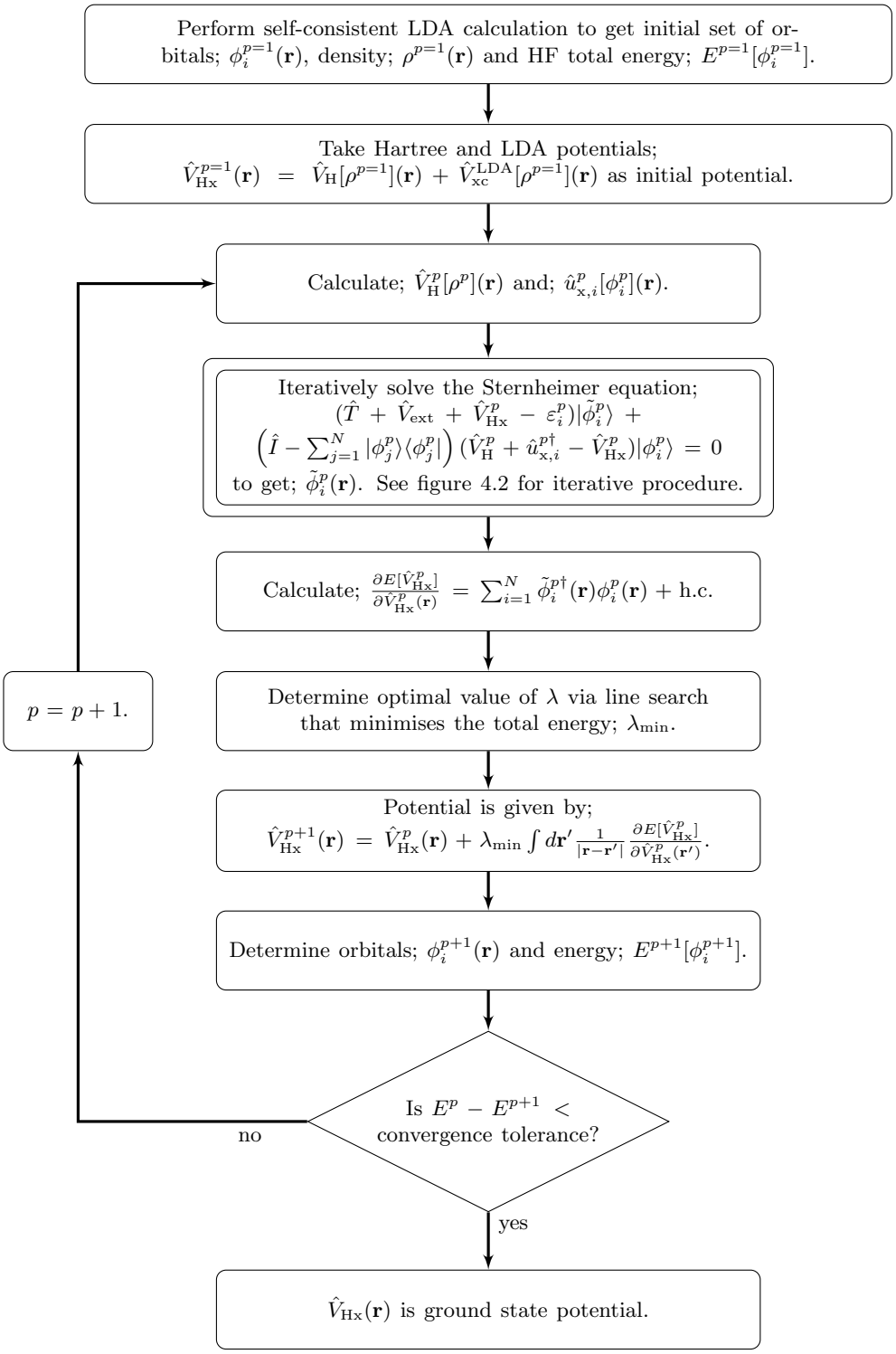

Figure 4.1: The procedure for the calculation of the EXX potential. Spin and k-point indexes are omitted for clarity.

using the orbitals generated by the Kohn-Sham Hamiltonian. The functional derivative at iteration p is given by;

$$\frac{\partial E[\hat{V}_{\mathrm{Hx}}^{\sigma,p}]}{\partial \hat{V}_{\mathrm{Hx}}^{\sigma,p}(\mathbf{r})} = 2\sum_{i,\mathbf{k}} \tilde{\phi}_{i,\mathbf{k}}^{\sigma,p\dagger}(\mathbf{r})\phi_{i,\mathbf{k}}^{\sigma,p}(\mathbf{r}), \tag{4.8}$$

from equation 3.44 and the Sternheimer equation at iteration p is;

$$(\hat{H}^{\sigma,p} - \varepsilon_{i,\mathbf{k}}^{\sigma,p})|\tilde{\phi}_{i,\mathbf{k}}^{\sigma,p}\rangle + \left(\hat{I} - \sum_{j=1} |\phi_{j,\mathbf{k}}^{\sigma,p}\rangle\langle\phi_{j,\mathbf{k}}^{\sigma,p}|\right)(\hat{V}_{\mathrm{H}}^{p} + \hat{u}_{\mathrm{x},i,\mathbf{k}}^{\sigma,p\dagger} - \hat{V}_{\mathrm{Hx}}^{\sigma,p})|\phi_{i,\mathbf{k}}^{\sigma,p}\rangle = 0, \tag{4.9}$$

from equation 3.52.[110]

Having found the functional derivative the potential is then varied to minimise the HF total energy by addition of the functional derivative convoluted by the electrostatic potential;

$$\hat{V}_{\mathrm{Hx}}^{\sigma,p+1}(\mathbf{r}) = \hat{V}_{\mathrm{Hx}}^{\sigma,p}(\mathbf{r}) + \lambda_{\min}\int d\mathbf{r}' \frac{1}{|\mathbf{r}-\mathbf{r}'|}\frac{\partial E[\hat{V}_{\mathrm{Hx}}^{\sigma,p}]}{\partial \hat{V}_{\mathrm{Hx}}^{\sigma,p}(\mathbf{r}')}, \tag{4.10}$$

where $\lambda_{\min}$ is a real number that minimises the HF total energy for the potential and gradient and is determined by a line search. The new potential then generates a new set of orbitals, $\phi_{i,\mathbf{k}}^{\sigma,p+1}(\mathbf{r})$, and energy, $E^{p+1}[\hat{V}_{\mathrm{Hx}}^{\sigma,p+1}]$. This process is repeated until the change in energy between iterations is below a threshold value, typically 10^{-6} eV.[111]

4.1.4 Solving the Sternheimer Equation

The main minimisation procedure for the EXX potential as outlined above also requires an additional optimisation at each iteration. This is to solve the Sternheimer equation, unlike the main minimising scheme for the EXX potential which is calculated in real space this minimisation is most conveniently performed in reciprocal space, considering each band, spin and k-point individually. The procedure for solving the Sternheimer equation is shown in figure 4.2 and uses a conjugate residual method to find the first order orbital.[125, 126, 128]

This method attempts to minimise the residual of the Sternheimer equation, as for any approximate $|\tilde{\phi}_{i,\mathbf{k}}^{\sigma,p,r}\rangle$ the right hand side of equation 4.9 will be non-zero and will be the residual at Sternheimer equation solver iteration r. The procedure starts with an initial guess of the first order orbital being zero, $|\tilde{\phi}_{i,\mathbf{k}}^{\sigma,p,r=1}\rangle = 0$, the initial residual is then just the second term in equation 4.9.[1]

As long as the change in the first order orbital is small, $\alpha^r \to 0$ between iterations the gradient of the Sternheimer equation with respect to $\tilde{\phi}_{i,\mathbf{k}}^{\sigma}(\mathbf{r})$ can be approximated as the residual. The minimising step α^r is derived from the conjugate gradient condition that all gradient directions $|g^r\rangle$ are orthogonal and the first order orbital is composed of

[1] This is a good guess if the perturbation has no effect on $\phi_{i,\mathbf{k}}^{\sigma}(\mathbf{r})$.

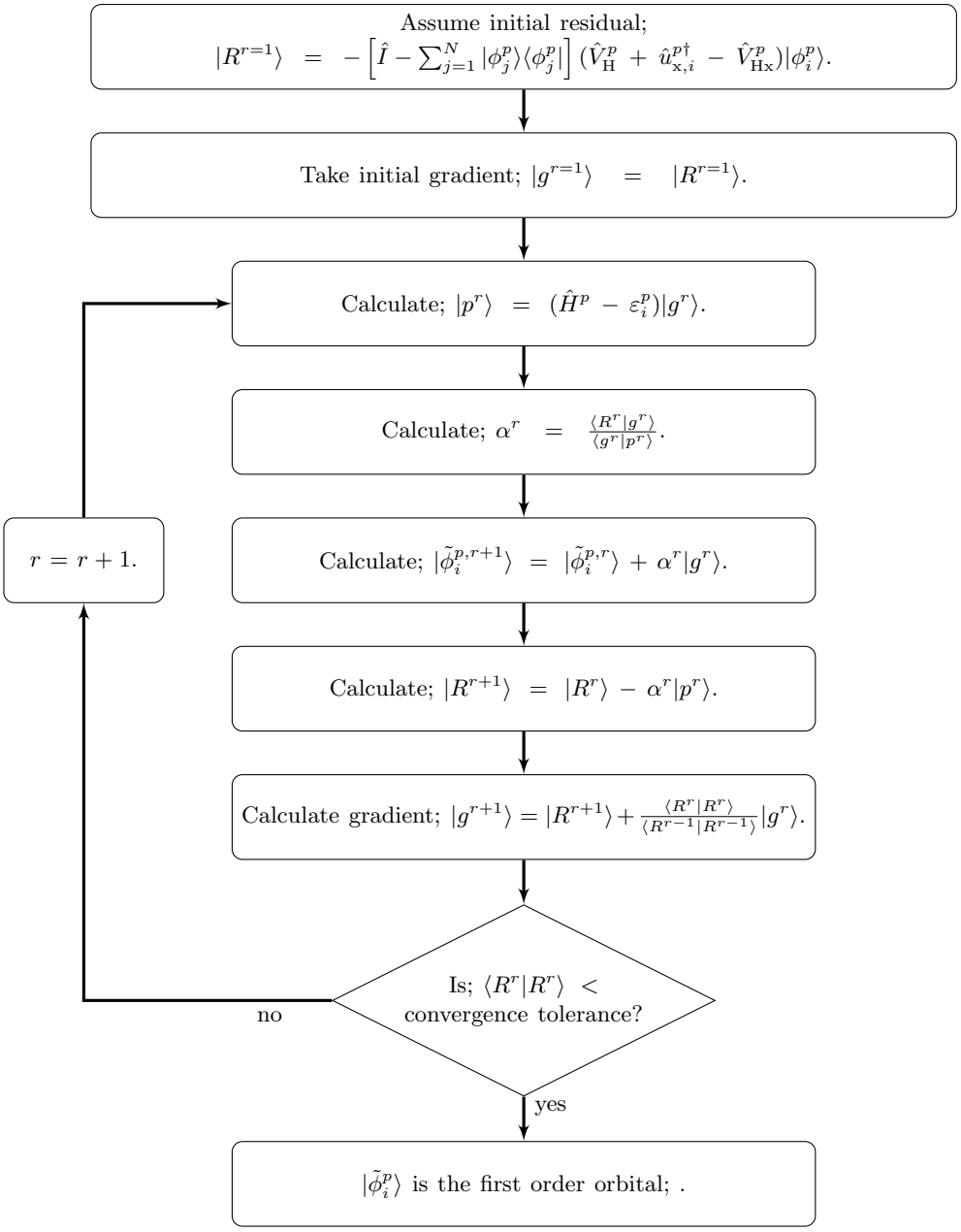

Figure 4.2: The procedure for the calculation of the first order orbital using a Sternheimer equation via a conjugate residual method. Spin and k-point indexes are omitted for clarity.

a sum of these directions;

$$|\tilde{\phi}^{\sigma,p,r}_{i,\mathbf{k}}\rangle = \sum_{k=1}^{r} \alpha^k |g^k\rangle, \tag{4.11}$$

for a given $\langle g^r|$ applied to the Sternheimer equation;

$$\begin{aligned}
\langle g^r|(\hat{H}^{\sigma,p} - \varepsilon^{\sigma,p}_{i,\mathbf{k}})|\tilde{\phi}^{\sigma,p,r}_{i,\mathbf{k}}\rangle &= -\langle g^r|\hat{P}_{\mathrm{c},\mathbf{k}}(\hat{V}^p_{\mathrm{H}} + \hat{u}^{\sigma,p\dagger}_{\mathrm{x},i,\mathbf{k}} - \hat{V}^{\sigma,p}_{\mathrm{Hx}})|\phi^{\sigma,p}_{i,\mathbf{k}}\rangle \\
\langle g^r|(\hat{H}^{\sigma,p} - \varepsilon^{\sigma,p}_{i,\mathbf{k}})\sum_{k=1}^{r}\alpha^k|g^k\rangle &= -\langle g^r|\hat{P}_{\mathrm{c},\mathbf{k}}(\hat{V}^p_{\mathrm{H}} + \hat{u}^{\sigma,p\dagger}_{\mathrm{x},i,\mathbf{k}} - \hat{V}^{\sigma,p}_{\mathrm{Hx}})|\phi^{\sigma,p}_{i,\mathbf{k}}\rangle \\
\langle g^r|(\hat{H}^{\sigma,p} - \varepsilon^{\sigma,p}_{i,\mathbf{k}})\alpha^r|g^r\rangle &= -\langle g^r|\hat{P}_{\mathrm{c},\mathbf{k}}(\hat{V}^p_{\mathrm{H}} + \hat{u}^{\sigma,p\dagger}_{\mathrm{x},i,\mathbf{k}} - \hat{V}^{\sigma,p}_{\mathrm{Hx}})|\phi^{\sigma,p}_{i,\mathbf{k}}\rangle \\
&\quad - \langle g^r|(\hat{H}^{\sigma,p} - \varepsilon^{\sigma,p}_{i,\mathbf{k}})\sum_{k=1}^{r-1}\alpha^k|g^k\rangle \\
\alpha^r\langle g^r|(\hat{H}^{\sigma,p} - \varepsilon^{\sigma,p}_{i,\mathbf{k}})|g^r\rangle &= \langle g^r|R^r\rangle.
\end{aligned} \tag{4.12}$$

Which rearranges to give:

$$\alpha^r = \frac{\langle g^r|R^r\rangle}{\langle g^r|p^r\rangle}, \tag{4.13}$$

where $|p^r\rangle$ was defined in figure 4.2.

The first order orbital and residual are varied by α^r multiplied by $|g^r\rangle$ or $(\hat{H}^{\sigma,p} - \varepsilon^{\sigma,p}_{i,\mathbf{k}})|g^r\rangle$ respectively. This procedure continues until the magnitude of the residual is below a threshold value, typically 10^{-12} eV. The rate of convergence of the Sternheimer equation can be increased by using the TPA preconditioner, this is applied when calculating the gradient.[72]

4.1.5 Determining the Optimal Step Size

A robust method for determining the optimal step size, λ when optimising a function is to use a line search. A line search assumes that the total energy (or any quantity being optimised) is continuously differentiable and approximates to a parabolic function of λ. This assumption is valid as long as the change in the total energy is small and the minimising λ is a small number, as we can then expand the total energy in a Taylor series around $\lambda_{\min}$ is powers of λ giving the total energy as a function of λ;

$$E = a\lambda^2 + b\lambda + c, \tag{4.14}$$

to find a, b and c we need to find the total energy for at least three potentials.[2] One of these potentials can be the current potential and the other two can be the current

[2] Higher order polynomials could be used if required.

potential with a fixed amount of λ times the gradient added on, such that;

$$\begin{aligned}
\lambda_0 =&0, \qquad \hat{V}^{\sigma,p}_{\mathrm{Hx},0}(\mathbf{r}) =\hat{V}^{\sigma,p}_{\mathrm{Hx}}(\mathbf{r}), && E_0[\hat{V}^{\sigma,p}_{\mathrm{Hx},0}],\\
\lambda_1 =&\lambda_1, \qquad \hat{V}^{\sigma,p}_{\mathrm{Hx},1}(\mathbf{r}) =\hat{V}^{\sigma,p}_{\mathrm{Hx}}(\mathbf{r}) + \lambda_1 \int d\mathbf{r}' \frac{1}{|\mathbf{r}-\mathbf{r}'|} \frac{\partial E[\hat{V}^{\sigma,p}_{\mathrm{Hx}}]}{\partial \hat{V}^{\sigma,p}_{\mathrm{Hx}}(\mathbf{r}')}, && E_1[\hat{V}^{\sigma,p}_{\mathrm{Hx},1}],\\
\lambda_2 =&2\lambda_1, \qquad \hat{V}^{\sigma,p}_{\mathrm{Hx},2}(\mathbf{r}) =\hat{V}^{\sigma,p}_{\mathrm{Hx}}(\mathbf{r}) + 2\lambda_1 \int d\mathbf{r}' \frac{1}{|\mathbf{r}-\mathbf{r}'|} \frac{\partial E[\hat{V}^{\sigma,p}_{\mathrm{Hx}}]}{\partial \hat{V}^{\sigma,p}_{\mathrm{Hx}}(\mathbf{r}')}, && E_2[\hat{V}^{\sigma,p}_{\mathrm{Hx},2}],
\end{aligned} \tag{4.15}$$

where the HF total energies, $E_1[\hat{V}^{\sigma,p}_{\mathrm{Hx},1}]$ and $E_2[\hat{V}^{\sigma,p}_{\mathrm{Hx},2}]$ for the potentials, $\hat{V}^{\sigma,p}_{\mathrm{Hx},1}(\mathbf{r})$ and $\hat{V}^{\sigma,p}_{\mathrm{Hx},2}(\mathbf{r})$ are determined by calculating the sets of orbitals ($\phi^{\sigma,p}_{i,\mathbf{k},1}(\mathbf{r})$ and $\phi^{\sigma,p}_{i,\mathbf{k},2}(\mathbf{r})$ respectively) that correspond to the Kohn-Sham equation for each potential.

The terms a, b and c are then determined by taking three linear equations;

$$\begin{aligned}
E_0 =&c,\\
E_1 =&a\lambda_1^2 + b\lambda_1 + c,\\
E_2 =&4a\lambda_1^2 + 2b\lambda_1 + c,
\end{aligned} \tag{4.16}$$

and rearrange to give;

$$a = \frac{E_2 - 2E_1 + E_0}{2\lambda_1^2},$$

$$b = -\frac{E_2 - 4E_1 + 3E_0}{2\lambda_1}, \tag{4.17}$$

$$c = E_0, \tag{4.18}$$

and the minimising $\lambda_{\min}$ is then the minimum of the parabolic function;

$$\left.\frac{\partial E}{\partial \lambda}\right|_{\lambda=\lambda_{\min}} = 2a\lambda_{\min} + b = 0, \qquad \lambda_{\min} = \frac{-b}{2a}, \tag{4.19}$$

if $a > 0$.

A two point minimiser using just two potentials is also possible. By using a line search and taking the magnitude of the gradient at two points $\lambda_{\min}$ can be found. However using this method the minimisation was found to be less robust than using the three energies and prone to finding a $\lambda_{\min}$ that increases the energy.

4.1.6 Iterative Procedure for the Calculation of the CEDA Potential

The procedure for finding the CEDA potential uses the same procedure as the one used to find the EXX potential, see figure 4.1, except we replace the HF total energy with S^{CEDA} (equation 3.90), the functional derivative uses the CEDA form (equation 3.88) and no calculation of the Sternheimer equation is required. An initial calculation using the local density approximation (LDA) exchange correlation potential obtains an initial set of orbitals, $\phi^{\sigma}_i(\mathbf{r})$ from which the density can be calculated; $\rho^{\mathrm{LDA}}(\mathbf{r})$. This density

then allows the initial effective electron interaction potential (Hartree and exchange potentials) to be;

$$\hat{V}^{\sigma,p=1}_{\mathrm{Hx,CEDA}}(\mathbf{r}) = \hat{V}_{\mathrm{H}}[\rho^{\sigma,\mathrm{LDA}}](\mathbf{r}) + \hat{V}^{\mathrm{LDA}}_{\mathrm{xc}}[\rho^{\mathrm{LDA}}](\mathbf{r}), \tag{4.20}$$

where p is the iteration number. The Kohn-Sham Hamiltonian at iteration p is then given by;

$$\hat{H}^{\sigma,p} = -\frac{\nabla^2}{2} + \hat{V}_{\mathrm{ext}}(\mathbf{r}) + V^{\sigma,p}_{\mathrm{Hx}}(\mathbf{r}), \tag{4.21}$$

and the CEDA minimising function at iteration p;

$$\begin{aligned} S^{\mathrm{CEDA},p}[\hat{V}^{\sigma,p}_{\mathrm{Hx}}] = \sum_{\sigma} \Bigg[& \sum_{i,\mathbf{k}} \langle \phi^{\sigma,p}_{i,\mathbf{k}} | (\hat{V}^{p}_{\mathrm{H}} + \hat{u}^{\sigma,p}_{\mathrm{x},i,\mathbf{k}} - \hat{V}^{\sigma,p}_{\mathrm{Hx}})^2 | \phi^{\sigma,p}_{i,\mathbf{k}} \rangle \\ & - \sum_{i,j,\mathbf{k}} | \langle \phi^{\sigma,p}_{i,\mathbf{k}} | \hat{V}^{p}_{\mathrm{H}} + \hat{u}^{\sigma,p}_{\mathrm{x},i,\mathbf{k}} - \hat{V}^{\sigma,p}_{\mathrm{Hx}} | \phi^{\sigma,p}_{j,\mathbf{k}} \rangle |^2 \Bigg], \end{aligned} \tag{4.22}$$

using the orbitals generated by the Kohn-Sham Hamiltonian. The functional derivative at iteration p is given by;

$$\begin{aligned} \frac{\partial S[\hat{V}^{\sigma,p}_{\mathrm{Hx}}]}{\partial \hat{V}^{\sigma,p}_{\mathrm{Hx}}(\mathbf{r})} = & -\sum_{i,\mathbf{k}} \phi^{\sigma\dagger,p}_{i,\mathbf{k}}(\mathbf{r}) \left(\hat{V}^{p}_{\mathrm{H}}(\mathbf{r}) + \hat{u}^{\sigma,p}_{\mathrm{x},i,\mathbf{k}}(\mathbf{r}) - \hat{V}^{\sigma,p}_{\mathrm{Hx}}(\mathbf{r}) \right) \phi^{\sigma,p}_{i,\mathbf{k}}(\mathbf{r}) \\ & + \sum_{i,j,\mathbf{k}} \phi^{\sigma\dagger,p}_{j,\mathbf{k}}(\mathbf{r}) \phi^{\sigma,p}_{i,\mathbf{k}}(\mathbf{r}) \int d\mathbf{r}' \phi^{\sigma\dagger,p}_{i,\mathbf{k}}(\mathbf{r}') \left(\hat{V}^{p}_{\mathrm{H}}(\mathbf{r}') + \hat{u}^{\sigma,p}_{\mathrm{x},i,\mathbf{k}}(\mathbf{r}') - \hat{V}^{\sigma,p}_{\mathrm{Hx}}(\mathbf{r}') \right) \phi^{\sigma,p}_{j,\mathbf{k}}(\mathbf{r}'). \end{aligned} \tag{4.23}$$

Having found the CEDA functional derivative the potential is then varied to minimise S^p by addition of the functional derivative;

$$\hat{V}^{\sigma,p+1}_{\mathrm{Hx}}(\mathbf{r}) = \hat{V}^{\sigma,p}_{\mathrm{Hx}}(\mathbf{r}) + \lambda_{\mathrm{min}} \int d\mathbf{r}' \frac{1}{|\mathbf{r}-\mathbf{r}'|} \frac{\partial S[\hat{V}^{\sigma,p}_{\mathrm{Hx}}]}{\partial \hat{V}^{\sigma,p}_{\mathrm{Hx}}(\mathbf{r}')}, \tag{4.24}$$

where λ_{min} is a real number that minimises $S^p[\hat{V}^{\sigma,p}_{\mathrm{Hx}}]$ for the potential and gradient and is determined by a line search.

The new potential then generates a new set of orbitals, $\phi^{\sigma,p+1}_{i,\mathbf{k}}(\mathbf{r})$, and $S^{\mathrm{CEDA},p+1}[\hat{V}^{\sigma,p+1}_{\mathrm{Hx}}]$. This process is repeated until the change in S^p between iterations is below a threshold value, typically 10^{-6} eV.

4.1.7 Iterative Procedure for the Calculation of the LFX Potential

The procedure for calculating the LFX potential, as outlined in figure 4.3, is via a direct minimisation. Before the optimisation of the potential a HF calculation must be performed to obtain the HF Slater determinant Ψ_{HF} and HF spin-density, $\rho^{\sigma,\mathrm{HF}}(\mathbf{r})$. The initial trial LFX potential is then the sum of the Hartree and LDA exchange-correlation

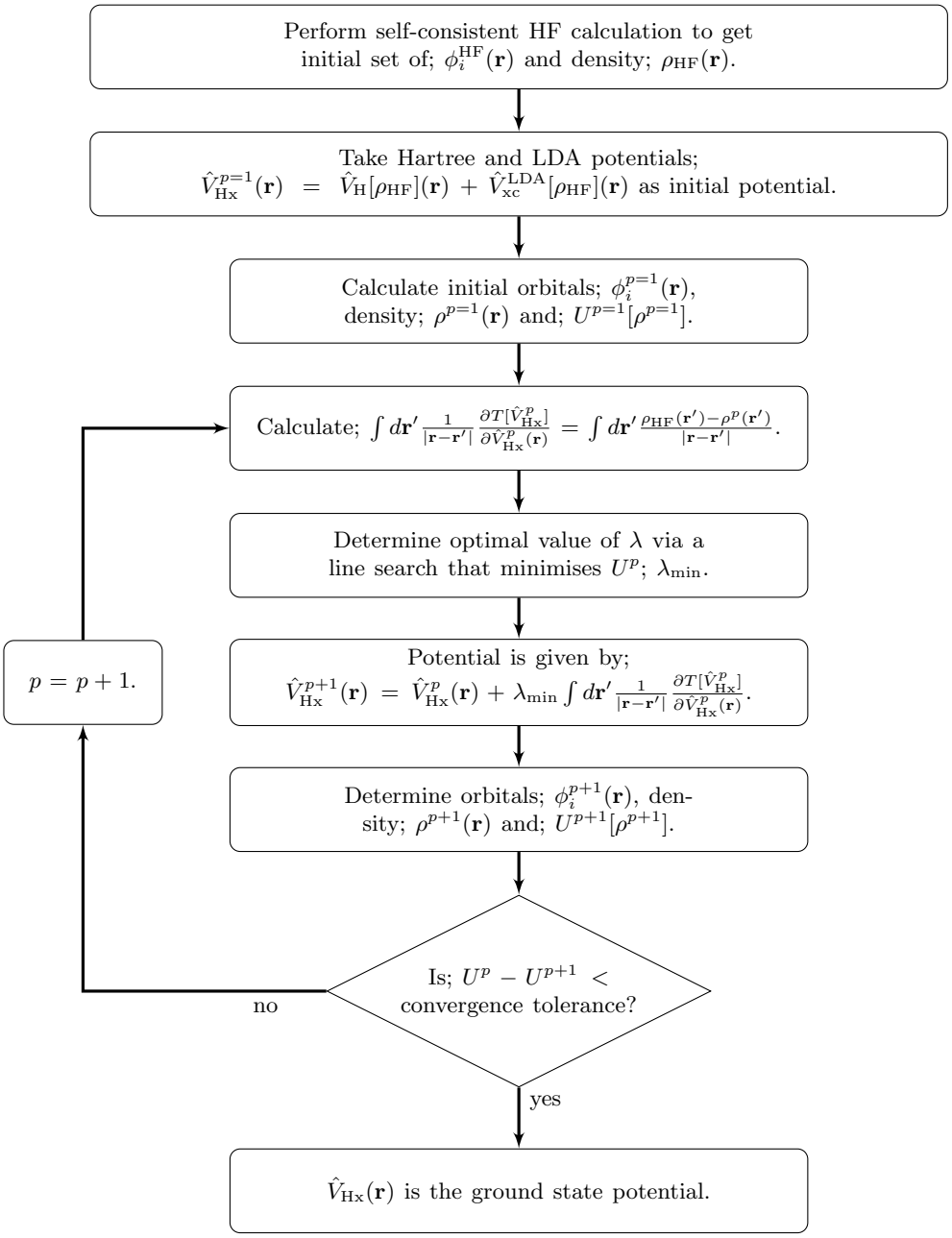

Figure 4.3: The procedure for the calculation of the LFX potential. Spin and k-point indexes are omitted for clarity.

potentials for the HF density;

$$\hat{V}^{\sigma,p=1}_{\mathrm{Hx,LFX}}(\mathbf{r}) = \hat{V}_{\mathrm{H}}[\rho^{\sigma}_{\mathrm{HF}}](\mathbf{r}) + \hat{V}^{\mathrm{LDA}}_{\mathrm{xc}}[\rho^{\sigma}_{\mathrm{HF}}](\mathbf{r}), \tag{4.25}$$

with p the iteration number. Again the effective potential is a combination of Hartree and exchange potentials. The Kohn-Sham Hamiltonian at iteration p is;

$$\hat{H}^{\sigma,p} = -\frac{\nabla^2}{2} + \hat{V}_{\mathrm{ext}}(\mathbf{r}) + V^{\sigma,p}_{\mathrm{Hx}}(\mathbf{r}), \tag{4.26}$$

which generates a set of orbitals, $\phi^{\sigma,p}_{i,\mathbf{k}}(\mathbf{r})$ and a density $\rho^{\sigma,p}_{\mathrm{v}}(\mathbf{r})$. The objective function at p, $U^p[\hat{V}^{\sigma,p}_{\mathrm{Hx}}]$ is given by;

$$U^p[\hat{V}^{\sigma,p}_{\mathrm{Hx}}] = \sum_{\sigma} \iint d\mathbf{r} d\mathbf{r}' \frac{(\rho^{\sigma}_{\mathrm{HF}}(\mathbf{r}) - \rho^{\sigma,p}_{\mathrm{v}}(\mathbf{r}))(\rho^{\sigma}_{\mathrm{HF}}(\mathbf{r}') - \rho^{\sigma,p}_{\mathrm{v}}(\mathbf{r}'))}{|\mathbf{r} - \mathbf{r}'|}, \tag{4.27}$$

and the functional derivative at p is written as;

$$\int d\mathbf{r}' \frac{1}{|\mathbf{r} - \mathbf{r}'|} \frac{\partial T^p[\hat{V}^{\sigma}_{\mathrm{x}}]}{\partial \hat{V}^{\sigma}_{\mathrm{x}}(\mathbf{r}')} = \int d\mathbf{r}' \frac{\rho^{\sigma}_{\mathrm{HF}}(\mathbf{r}) - \rho^{\sigma}_{\mathrm{v}}(\mathbf{r})}{|\mathbf{r} - \mathbf{r}'|}. \tag{4.28}$$

Having found the functional derivative the potential is then varied to minimise $U^p[\hat{V}^{\sigma,p}_{\mathrm{Hx}}]$ by addition of the functional derivative convoluted by the electrostatic potential;

$$\hat{V}^{\sigma,p+1}_{\mathrm{Hx}}(\mathbf{r}) = \hat{V}^{\sigma,p}_{\mathrm{Hx}}(\mathbf{r}) + \lambda_{\mathrm{min}} \int d\mathbf{r}' \frac{1}{|\mathbf{r} - \mathbf{r}'|} \frac{\partial T[\hat{V}^{\sigma,p}_{\mathrm{Hx}}]}{\partial \hat{V}^{\sigma,p}_{\mathrm{Hx}}(\mathbf{r}')}, \tag{4.29}$$

where λ_{min} is a real number that minimises $U^p[\hat{V}^{\sigma,p}_{\mathrm{Hx}}]$ for the potential and gradient and is determined by a line search. The new potential then generates a new set of orbitals, $\phi^{\sigma,p+1}_{i,\mathbf{k}}(\mathbf{r})$, density, $\rho^{\sigma,p+1}_{v}(\mathbf{r})$ and $U^{p+1}[\hat{V}^{\sigma,p+1}_{\mathrm{Hx}}]$. This process is repeated until the change in energy between iterations is below a threshold value, typically 10^{-9} eV.[3][118]

4.2 Minimisation Schemes for the Potential

4.2.1 Conjugate Gradients

So far the minimisation schemes that have been discussed use a steepest-descent minimisation. The search direction, $\mathbf{d}^p$ for iteration p is just the functional derivative with respect to the potential, $\mathbf{g}^p$ at iteration p;

$$\mathbf{d}^p = \mathbf{g}^p. \tag{4.30}$$

The convergence of the minimisation procedure can be improved by using the conjugate-gradient scheme, this ensures that each search direction is conjugate to previous search

[3]This value is most likely too small and a threshold value of 10^{-6} eV is most likely sufficient.

directions.[52] The search direction for iteration p is then;

$$\mathbf{d}^p = \mathbf{g}^p - \gamma^p \mathbf{d}^{p-1}, \tag{4.31}$$

where γ^p is the conjugate gradient update parameter and can be chosen with several forms;

$$\gamma^p_{HS} = \frac{\langle \mathbf{g}^p | (\mathbf{g}^p - \mathbf{g}^{p-1}) \rangle}{\langle \mathbf{d}^{p-1} | (\mathbf{g}^p - \mathbf{g}^{p-1}) \rangle}, \qquad \text{Proposed by Hestenes and Stiefel.[129]} \tag{4.32}$$

$$\gamma^p_{FR} = \frac{\langle \mathbf{g}^p | \mathbf{g}^p \rangle}{\langle \mathbf{g}^{p-1} | \mathbf{g}^{p-1} \rangle}, \qquad \text{Proposed by Fletcher and Reeves.[130]} \tag{4.33}$$

with the caveat that $\gamma^{p=1} = 0$.

4.2.2 Quasi-Newton's Method

Newton's method is an iterative method for finding the minimum (or maximum) of a function, $f(x)$. Where the function, $f(x)$ is twice differentiable. The first and second derivatives are then $\frac{\partial f}{\partial x}$ and $\frac{\partial^2 f}{\partial x^2}$ respectively and the change in x for each iteration, p is;

$$x_{p+1} = x_p + \Delta x_p = x_p - \left(\frac{\partial^2 f}{\partial x^2} \right)^{-1} \Bigg|_{x=x_p} \frac{\partial f}{\partial x} \Bigg|_{x=x_p}, \tag{4.34}$$

which will converge to a minimum so that $\frac{\partial f}{\partial x} = 0$.

Unfortunately the second derivatives of the total energy; E, CEDA objective functional; S or the LFX objective functional; U are difficult to determine and calculate. However the second derivative does not need to be evaluated directly and can be found in approximate form just from the knowledge of the previous values of x_p and $\frac{\partial f}{\partial x}$ using a quasi-Newton's method. The search direction $\mathbf{d}^p$ is given by;

$$\mathbf{d}^p = \left(\hat{B}^p \right)^{-1} \mathbf{g}^p, \tag{4.35}$$

and the vector $\mathbf{x}^p$ is updated;

$$\mathbf{x}^{p+1} = \mathbf{x}^p + \alpha^p \left(\hat{B}^p \right)^{-1} \mathbf{g}^p = \mathbf{x}^p + \alpha^p \hat{H}^p \mathbf{g}^p, \tag{4.36}$$

with α^p is determined via a line search. The matrix $\hat{B}$ is the approximation to the second order derivative, $\hat{H}^p$ its inverse and both can be determined iteratively by the approximation of Broyden-Fletcher-Goldfarb-Shanno (BFGS) [131], $\hat{H}^p$ is updated by;

$$\begin{aligned} \hat{H}^p = \hat{H}^{p-1} &- \hat{H}^{p-1} \frac{|\mathbf{y}^p\rangle\langle\mathbf{s}^p|}{\langle\mathbf{s}^p|\mathbf{y}^p\rangle} - \frac{|\mathbf{s}^p\rangle\langle\mathbf{y}^p|}{\langle\mathbf{s}^p|\mathbf{y}^p\rangle} \hat{H}^{p-1} \\ &+ \frac{|\mathbf{y}^p\rangle\langle\mathbf{y}^p|}{\langle\mathbf{s}^p|\mathbf{y}^p\rangle} \hat{H}^{p-1} \frac{|\mathbf{s}^p\rangle\langle\mathbf{s}^p|}{\langle\mathbf{s}^p|\mathbf{y}^p\rangle} + \frac{|\mathbf{s}^p\rangle\langle\mathbf{s}^p|}{\langle\mathbf{s}^p|\mathbf{y}^p\rangle}, \end{aligned} \tag{4.37}$$

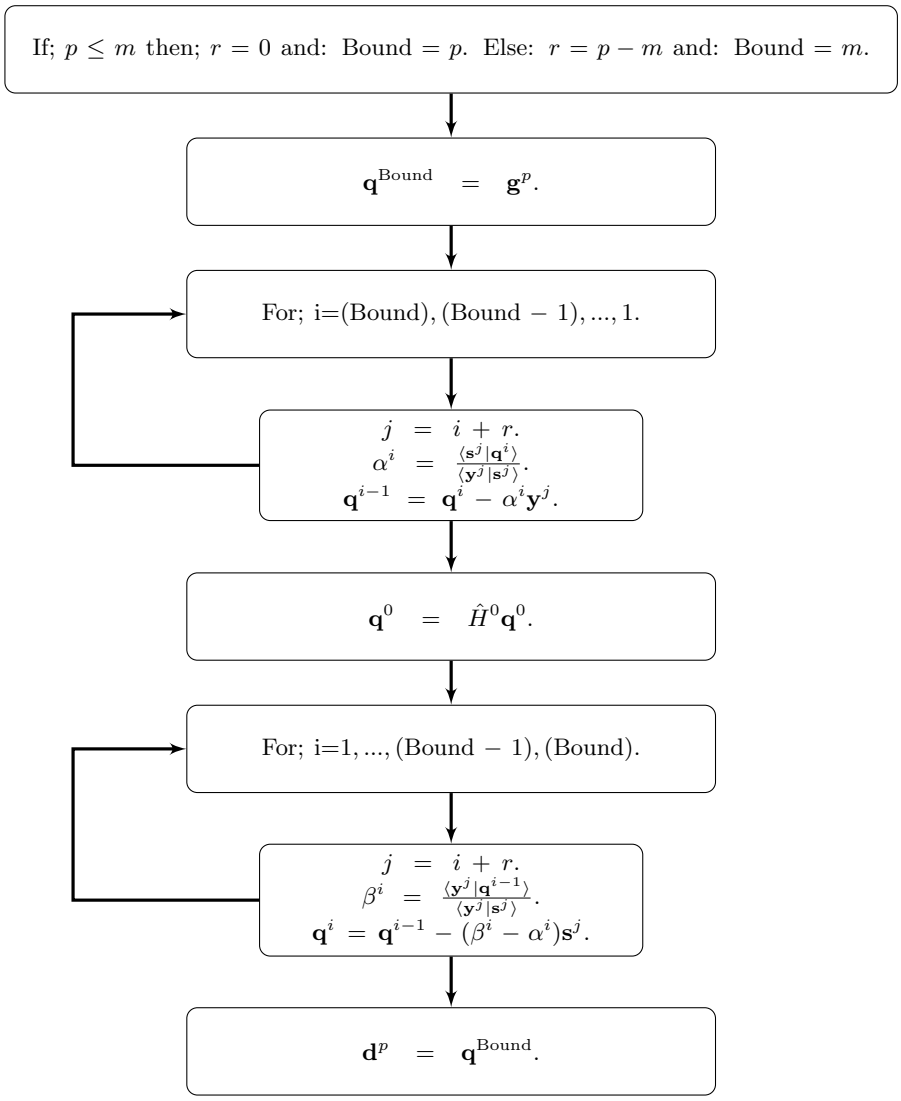

Figure 4.4: The recursive procedure to apply the BFGS matrix with limited memory to the gradient.

where;

$$\mathbf{y}^p = \mathbf{g}^p - \mathbf{g}^{p-1}, \qquad \mathbf{s}^p = \mathbf{x}^p - \mathbf{x}^{p-1}. \tag{4.38}$$

The problem with using this form of the BFGS matrix is that while the full history of the minimisation is known, this requires a matrix of dimensions, maximumsize($\mathbf{x}$) $\times$ maximumsize($\mathbf{x}$) which, as $\mathbf{x}^p$ is the potential (in our scheme) this matrix will be dimension $N_\mathbf{G} \times N_\mathbf{G}$ (which can have 10^{10} elements).

However by using a limited memory form of the BFGS quasi-Newton's method, which only uses the knowledge of the previous m iterations, it then only requires $2 \times m \times N_\mathbf{G}$ memory elements, as the limited memory BFGS matrix $\hat{H}^p$ can be applied recursively.[132] Figure 4.4 shows the recursive update for the BFGS algorithm. Once p becomes greater than the memory length, m for each iteration the oldest set of $\mathbf{y}^{p-m-1}$ and $\mathbf{s}^{p-m-1}$ are discarded and the newest set $\mathbf{y}^p$ and $\mathbf{s}^p$ are included. The matrix $\hat{H}^0$ can be an additional preconditioning matrix but in this implementation is just the identity matrix. This method could also be used to calculate the full BFGS matrix at each iteration. The only constraint is then how many iterations the BFGS method should remember.

The minimisation of EXX for silicon using a cut off energy of 800 eV and a $5 \times 5 \times 5$ MP k-point grid, with different BFGS memory lengths is shown in figure 4.5. The minimisations using steepest-descent (equivalent to a memory of zero), the previous 1, 2, 3, 4, 5, 10, 15 and 20 steps are plotted. The minimisation using the BFGS method does not depend greatly on the chosen memory length, with the BFGS method saturating at a memory length of 4 or 5. Hence a BFGS memory of 10 was chosen, however the rate of convergence should not depend on the memory length beyond the chosen value.

4.2.3 Comparison of Minimisation Schemes

Figure 4.6 compares the performance of the different minimisation schemes discussed in the previous section when applied to the EXX functional derivative in the case of silicon, using a cut off energy of 800 eV and a $5 \times 5 \times 5$ MP k-point grid. While the BFGS method outperforms the steepest descents method, it offers no improvement over the conjugate-gradient methods, for while it outperforms HS, FR is the best quickest converging method to find the EXX ground state energy. Also the BFGS method takes twice as much time per iteration as the FR calculation used for these convergence tests.

The Fletcher-Reeves conjugate gradients method converges the fastest and after approximately 40 iterations the change in energy per iteration is $< 1 \times 10^{-6}$ eVatom^{-1}. The other schemes slowly converge towards the FR minimum value. Hence for the EXX the FR conjugate gradients scheme will be used and the minimisation run until the change in energy per iteration is $< 1 \times 10^{-6}$ eVatom^{-1}.

Figure 4.7 compares the performance of the different minimisation schemes discussed in the previous section when applied to the CEDA functional derivative in the case of sili-

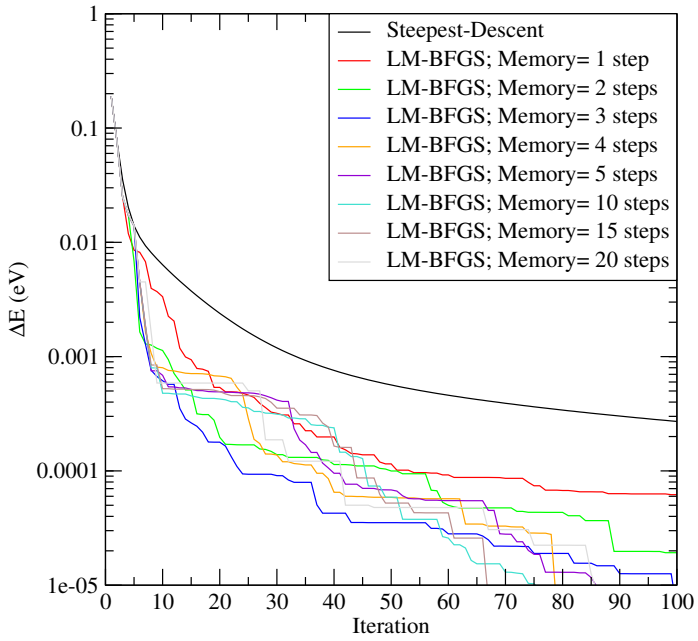

Figure 4.5: Comparison of limited memory BFGS for EXX applied to silicon for different memory lengths. Logarithmic plot of the difference in total energy at each iteration from the converged value for the BFGS scheme with memory of previous 10 iterations.

con, using the same input parameters as for EXX. The HS conjugate-gradient scheme performs very poorly converging much more slowly than even the steepest-descent method. The FR conjugate-gradient and BFGS schemes out-perform the steepest-descent method again, the FR conjugate-gradient method once again is the best method.

FR conjugate-gradient and BFGS quasi-Newton's method converge very fast and after approximately 15-20 iterations the change in energy per iteration is $< 1 \times 10^{-7}$ eVatom^{-1}. The HS conjugate-gradient and steepest-descent converge extremely slowly, towards the FR conjugate-gradient minimum value. Hence for the CEDA the FR scheme will be used and the minimisation run until the change in energy per iteration is $< 1 \times 10^{-6}$ eVatom^{-1}.

Figure 4.8 compares the performance of the different minimisation schemes discussed in the previous section when applied to the LFX functional derivative in the case of silicon, using the same input parameters as for EXX and CEDA. For this calculation the FR and HS conjugate-gradient schemes are almost identical and outperform steepest-descent, converging below the threshold of 1×10^{-7} eVatom^{-1} in approximately 45 iterations. The BFGS scheme converges below this threshold in approximately 40 iterations. The BFGS method is twice as slow per iteration when compared to the FR conjugate gradients method, hence for LFX calculations the FR scheme will be used.

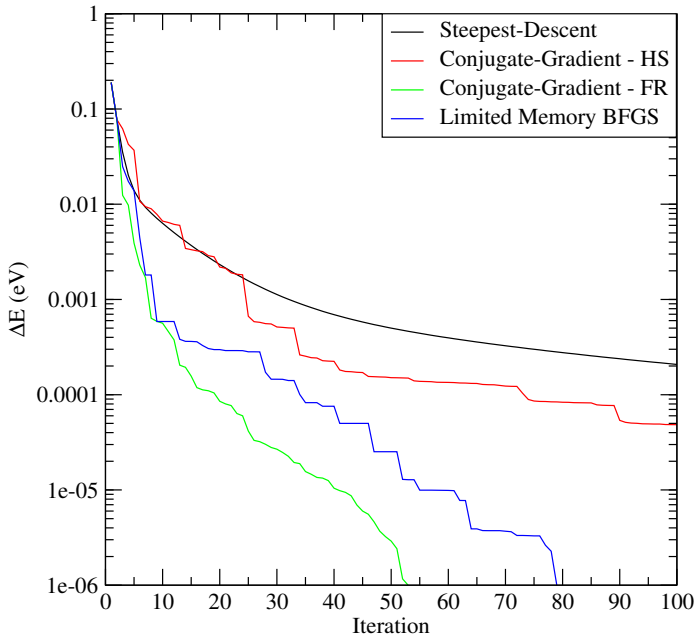

Figure 4.6: Comparison of steepest descents, conjugate gradients and limited memory BFGS for EXX applied to silicon. Logarithmic plot of the difference in total energy at each iteration from the converged value for the conjugate gradients scheme using Fletcher-Reeves.

4.3 Performance and Convergence

4.3.1 Convergence of Calculation Parameters

The numerical factors that determine the accuracy of our calculation are the size of the plane wave basis set, determined by the plane wave cut off energy and the size of the Monkhorst-Pack (MP) k-point grid. In figure 4.9 the total energies for Hartree-Fock, EXX, CEDA and LFX are calculated for a range of cut off energies applied to silicon, using the primitive unit cell, an MP grid of $5 \times 5 \times 5$ and the experimental lattice constants. All four methods converge at the same rate and a cut off energy of 600 eV gives an accuracy on the total energy of less than 0.005 eV, which is our chosen minimal accuracy level. This is determined by the change in the total energies when the cut off energy is increased, as the cut off energy will converge to a singular value, for each method.

Figure 4.10 shows the total energies of silicon for HF, EXX, CEDA and LFX, again using the primitive unit cell, experimental lattice constants and a cut off energy of 800 eV. As silicon is a cubic material the MP grid is cubic also. Again the four methods converge at the same rate and a grid of $6 \times 6 \times 6$ gives the required level of convergence. For non-cubic unit cells each dimension of the MP must be converged individually.

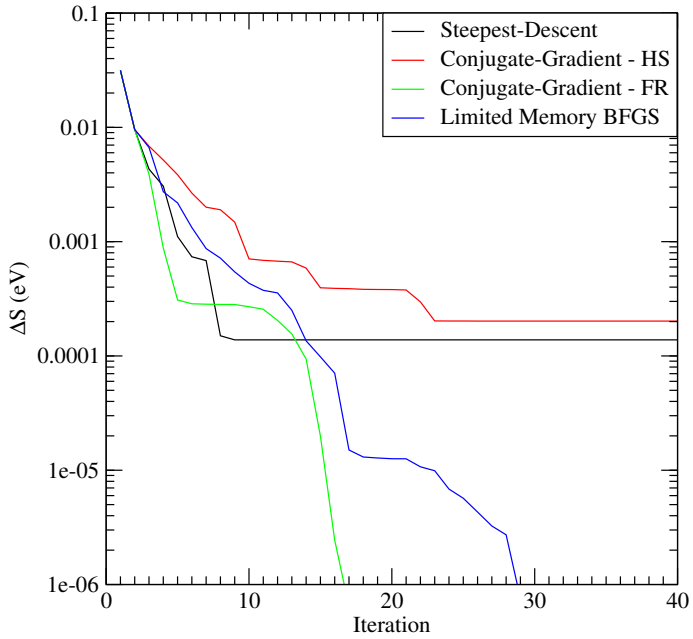

Figure 4.7: Comparison of steepest descents, conjugate gradients and limited memory BFGS for CEDA applied to silicon. Logarithmic plot of the difference in S at each iteration from the value at iteration 200 for the BFGS scheme.

4.3.2 Scaling With Calculation Parameters

The scaling of the methods with respect to the calculation parameters has also been tested, to ensure that the implemented methods scale as expected. Figure 4.11 shows the average time per iteration with varying cut off energy for EXX, CEDA and LFX. Also shown are fitted curves for the expected behaviour. The Fock exchange integral scales as N_{pw}^2 which in terms of the cut off energy scales as E_{cutoff}^4. Through the use of the fast Fourier transforms (FFTs) this becomes $E_{\text{cutoff}}^{\frac{3}{2}} \ln(E_{\text{cutoff}})$. Both the EXX and CEDA potentials scale with the expected form, at the same rate which, is unsurprising given the similarity in the form of the equations used to find the functional derivative. The LFX potential is much faster per iteration and scales more favourably. Which is most likely due to the much simpler form of the LFX functional derivative.

The average time per iteration with varying size of the MP grid is shown in figure 4.12 for EXX, CEDA and LFX. The calculations are parallelised so that there is one k-point per node. The expected behaviour for the methods is to scale as N_k^2 and quadratic fits for the three methods are shown in figure 4.12. The EXX and CEDA potentials indeed scale quadratically, as the calculation of the functional derivatives requires the application of the Fock exchange integral, which requires a double sum over the k-points. However the LFX potential does not require a double sum over k-points, using only a single sum to construct the density to find the functional derivative. Hence it scales linearly with respect to the changing size of the MP grid. However the LFX potential requires an initial HF calculation which scales with the same behaviour as the EXX and

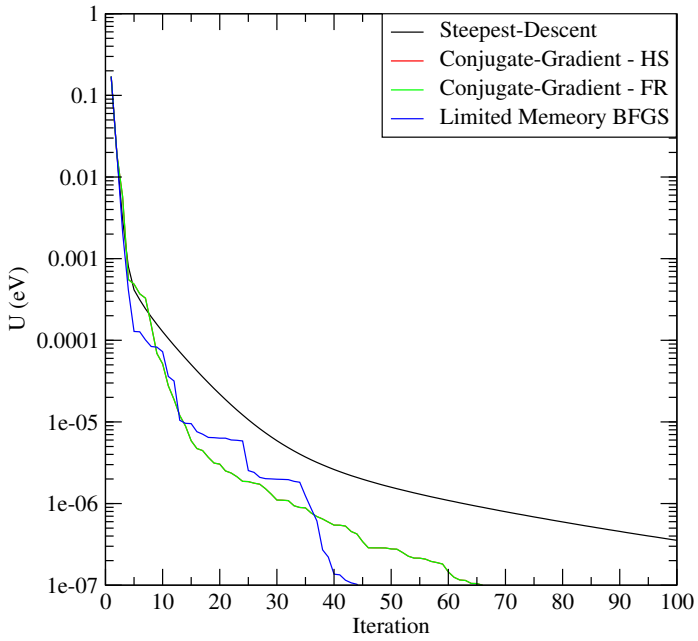

Figure 4.8: Comparison of steepest descents, conjugate gradients and limited memory BFGS for LFX applied to silicon. Logarithmic plot of the value of U at each iteration. HS (red line) and FR (green line) plots overlap.

CEDA calculations which limits the advantages of this linear scaling.

4.3.3 Parallelisation

As mentioned previously the CASTEP code supports parallel processing of the calculation. The set of symmetry reduced k-points are distributed across the processors in groups. Each k-point group can then be subdivided into **G** vector groups, this is shown in figure 4.13. Data is exchanged between the groups of processors, usually when we need to sum a quantity. The code is structured to attempt to minimise the amount of inter-processor communication required in a calculation.

The parallelism with respect to the k-points was tested for primitive cell silicon for EXX using a cut off of 800 eV and a Monkhorst-Pack grid of $5 \times 5 \times 5$ which reduces to 10 k-points. Using 1, 2, 5 and 10 processors, giving 10, 5, 2 and 1 k-point per node the time per iteration is shown in figure 4.14. The calculation scales as the inverse of the number of processors.

The parallelism with respect to G-vectors is shown in figure 4.15, using the same calculation parameters as for the k-point parallelism test, the number of processors per G-vector group is varied between 1-32. The calculation in this case has an optimal number of processors per G-vector group of 10. Further parallelisation increases the calculation time, due to the increased inter-processor communications and associated overheads when using G-vector parallelisation. It should be noted that the degree of G-vector parallelisation is highly computer specific and indeed must be tested on each machine to which the code is ported.

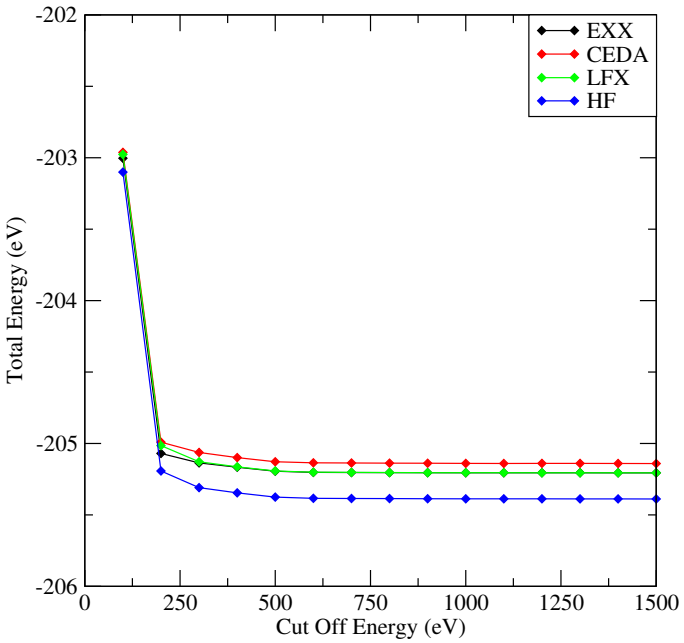

Figure 4.9: Convergence of total energy with respect to the plane wave cut off energy in silicon. EXX (black line) and LFX (green line) plots overlap.

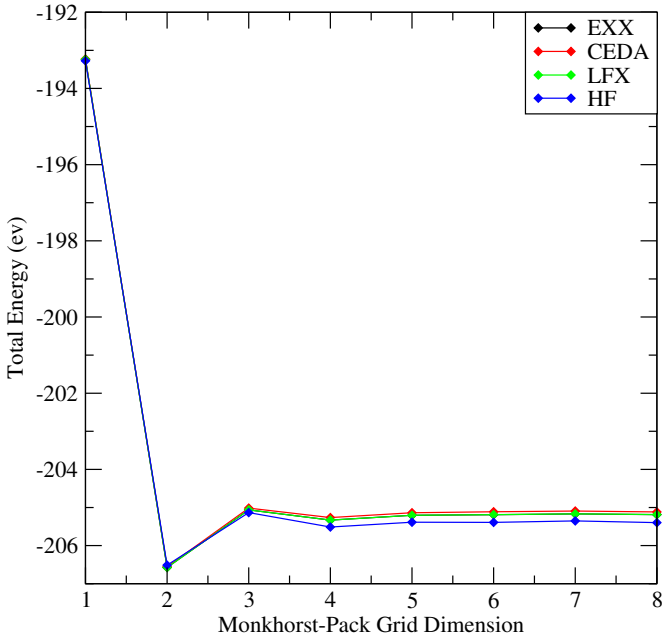

Figure 4.10: Convergence of total energy with respect to the size of the Monkhorst-Pack grid in silicon. The grid is cubic in this case. EXX (black line) and LFX (green line) plots overlap.

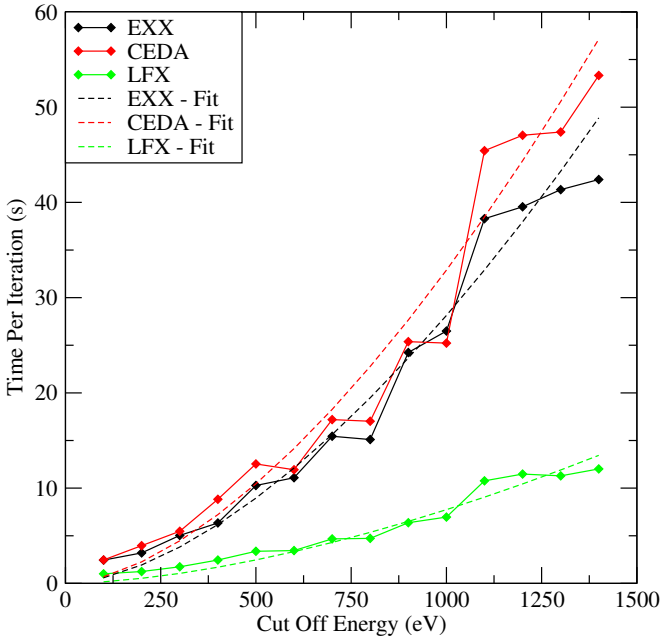

Figure 4.11: Average time per iteration with respect to cut off energy. Fitted curves for $E^{\frac{3}{2}}\log(E)$ are also shown.

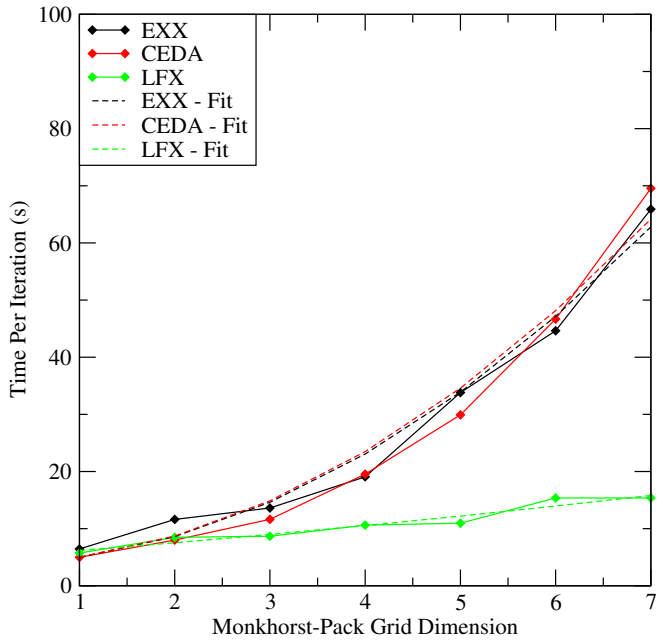

Figure 4.12: Average time per iteration with respect to the Monkhorst-Pack grid. Fitted curves for a quadratic function are also shown.

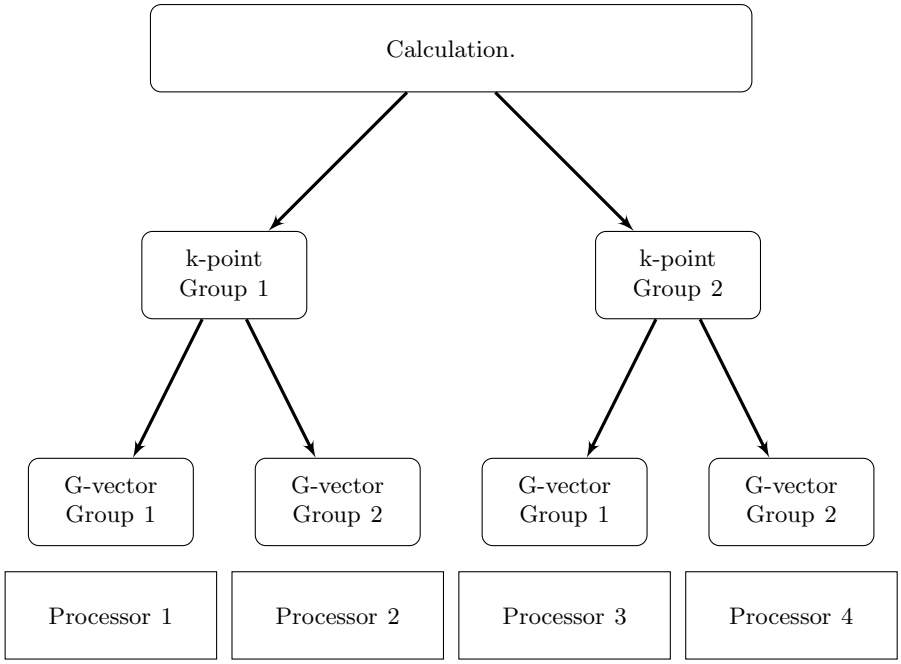

Figure 4.13: Hierarchy of parallelisation in a CASTEP calculation, using four processors in two k-point groups and two G-vector groups.

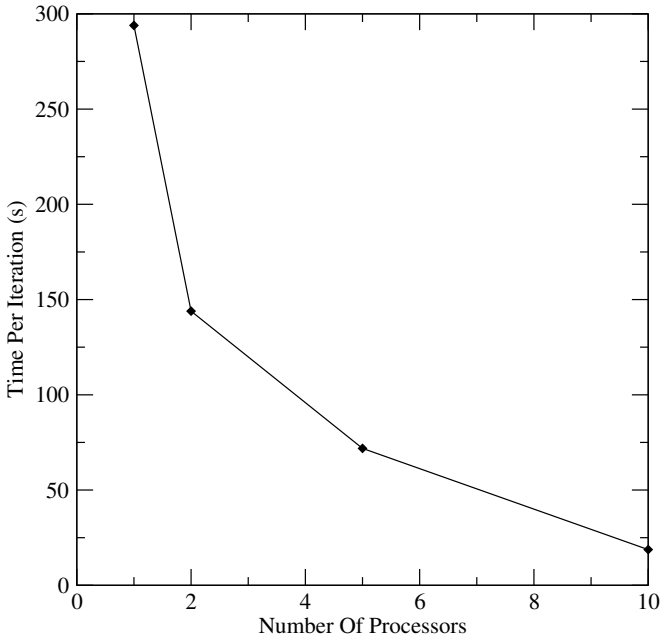

Figure 4.14: Average time per iteration with increasing processor number using parallelism over k-points for EXX applied to silicon.

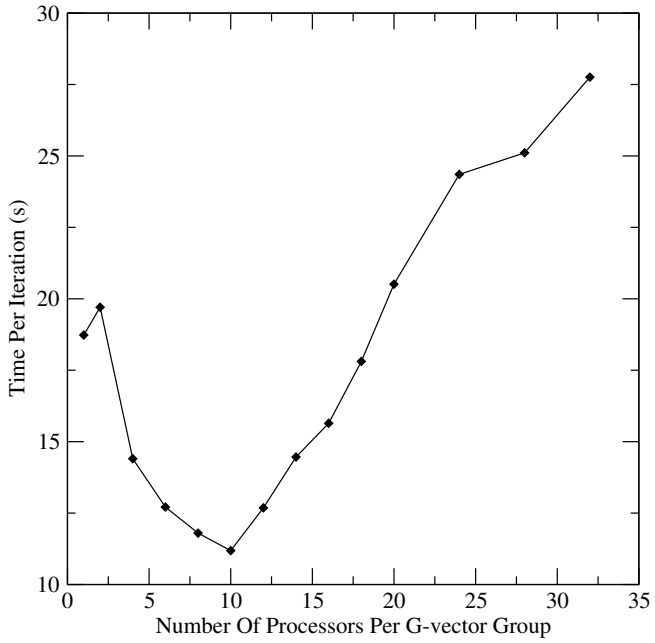

Figure 4.15: Average time per iteration with increasing number of processors in the G-vector groups for EXX applied to silicon.

An additional complication arises from the non-local nature of the Fock exchange integral. The exchange energy in reciprocal space is given by;

$$E_{\mathrm{x}} = \frac{2\pi}{\Omega} \sum_{\sigma} \sum_{i,\mathbf{k}} \sum_{j,\mathbf{q}} \sum_{\mathbf{G},\mathbf{G}',\mathbf{G}''} c_{i\mathbf{k}}^{\sigma\dagger}(\mathbf{G}) \frac{c_{j\mathbf{q}}^{\sigma\dagger}(\mathbf{G}'+\mathbf{G}'')c_{j\mathbf{q}}^{\sigma}(\mathbf{G}+\mathbf{G}'')}{|\mathbf{q}-\mathbf{k}+\mathbf{G}''|^2} c_{i\mathbf{k}}^{\sigma\dagger}(\mathbf{G}'). \tag{4.39}$$

The denominator contains terms that cannot be symmetry reduced, hence the k-points indexed $\mathbf{k}$ can be symmetry reduced but the k-points indexed $\mathbf{q}$ are the full non-symmetry reduced set. For a non-local calculation the k-points indexed by $\mathbf{k}$ are symmetry reduced and distributed across the processors, however a copy of the orbitals indexed by $\mathbf{q}$ must be stored on each processor. This considerably increases the memory overheads associated with the calculation.

4.4 Summary

In this chapter we have described the algorithms and computational implementation of the EXX, CEDA and LFX potentials using the equations derived in chapter 3. Several minimisation techniques for the optimisation of the three potentials were introduced and tested, the optimal minimisation method for all three potentials is to use a Fletcher-Reeves conjugate gradients method. The convergence of these three potentials was tested with varying cut off energy and k-points, as well as the scaling of the calculations with respect to these parameters. Performance of the implementation with parallelisation over k-points is almost linear with distribution of the k-points over the number of processors.

Distribution over **G**-vectors is found to give some speed up but the scaling is less optimal than that found for the parallelisation by k-points.

Chapter 5

Calculated Electronic Structures

5.1 Electronic Structures for Semiconductors and Insulators

5.1.1 Introduction

The band structure and density of states of a semiconductor determines most of the electronic and optical properties that makes them technologically useful for semiconductor devices. Accurate modelling and prediction of the properties of technologically relevant materials is an area of considerable research. Here we present calculated electronic structures for the basic approximations: LDA and PBE, the local exchange potentials; EXX, LFX and CEDA presented in the previous chapter as well as HF applied to group IV, group III-V, group II-VI semiconductors and a selection of insulators. The implications of these results are then discussed.

5.1.2 Definition of the Band gap

It is necessary to define the quantity known as the band gap of a material, there are several experimentally measured band gaps (fundamental band gap, optical band gap). Here we use the fundamental band gap, which is defined as the difference between the ionisation energy, $I(N)$ and the electron affinity, $A(N)$ of an N electron system.

The predicted Kohn-Sham band gap, $E_{\mathrm{g}}^{\mathrm{KS}}$ does not fully model the fundamental band gap, E_{g}. The Kohn-Sham band gap for an N electron system is given by the difference in eigenvalues;

$$E_{\mathrm{g}}^{\mathrm{KS}} = \varepsilon_{N+1} - \varepsilon_N, \tag{5.1}$$

where ε_i is the eigenvalue of the i-th state. Whereas the fundamental band gap is given by;

$$E_{\mathrm{g}} = A(N) - I(N) = E(N+1) + E(N-1) - 2E(N), \tag{5.2}$$

where A is the electron affinity, I is the ionisation potential and $E(M)$ is the total energy

of an M electron system.[133] Using Koopmans' theorem extended to DFT;[134, 135]

$$I(N) = E(N) - E(N-1) = \varepsilon_N^N, \tag{5.3}$$

where ε_N^N is the N-th eigenvalue (subscript) of an N electron system (superscript) and is applicable to the N and $N+1$ electron systems (as $A(N) = I(N+1)$).[133, 136] The fundamental gap is then;

$$E_{\mathrm{g}} = E_{\mathrm{g}}^{\mathrm{KS}} + \varepsilon_{N+1}^{N+1} - \varepsilon_{N+1}^{N} = E_g^{KS} + \Delta_{\mathrm{xc}}, \tag{5.4}$$

the difference between the fundamental and Kohn-Sham band gaps is then Δ_{xc}, known as the derivative discontinuity. This term is also required to be calculated to give the predicted fundamental band gap of a system. A formalism to calculate Δ_{xc} is presented in chapter 6.

It should be noted that a deviation of the predicted Kohn-Sham band gap from the experimental band gap does not indicate a failure of the approximation, since at present Δ_{xc} is ignored. In chapter 6, we complete this study by estimating Δ_{xc} for the LDA and GGA, we also calculate the exchange-only component of the derivative discontinuity, Δ_{x} for EXX and LFX. We also give a formalism to find Δ_{c} for EXX and LFX, the calculation of which is beyond the scope of this thesis.

5.1.3 Group IV Elemental Semiconductors

The band structures for the group IV semiconductors; diamond, silicon and germanium were calculated using the LDA, PBE, EXX, CEDA, LFX potentials and HF. The same calculation parameters were used in all six exchange/exchange-correlation calculations on each material and are shown in table 5.1. The lattice parameters used are the experimental lattice constants, to give the closest like for like comparison between the six methods. Each method will have its own optimal ground state lattice parameter which can be found by performing a geometry optimisation as outlined in section 2.6.5.

Material	E_{cutoff} (eV)	Valence electron configuration	MP k-point grid	Lattice parameter (Å)
C	1100	$2s^2 2p^2$	$8 \times 8 \times 8$	3.56
Si	800	$3s^2 3p^2$	$6 \times 6 \times 6$	5.39
Ge	1000	$4s^2 3d^{10} 4p^2$	$6 \times 6 \times 6$	5.66

Table 5.1: Parameters for calculations on group IV semiconductors. Lattice parameters from [137] and [138].

Silicon

The calculated band structures for silicon are shown in figure 5.1. For all methods the material has an indirect band gap, with conduction band minimum along the $\Gamma \rightarrow$ X

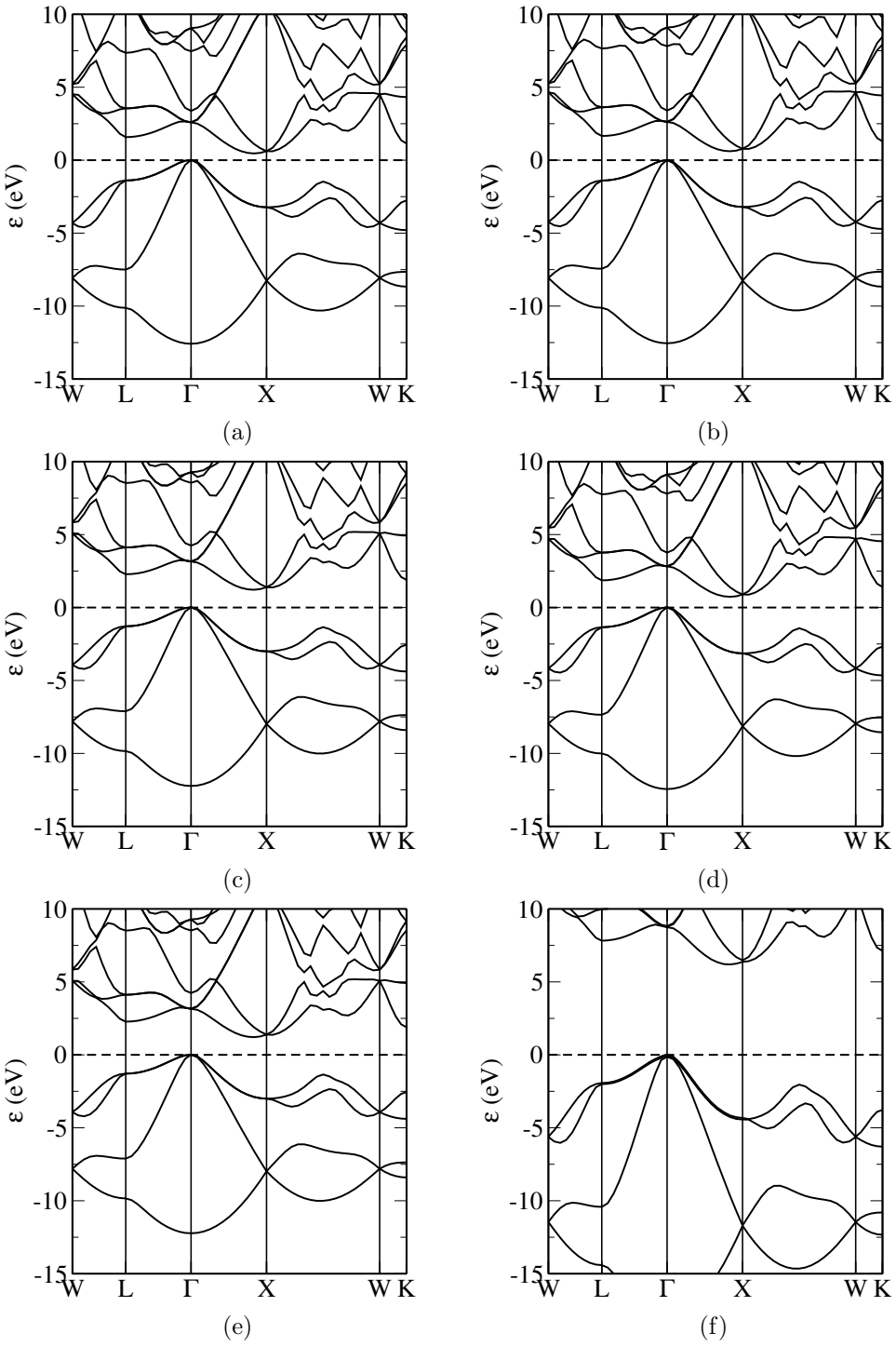

Figure 5.1: Band structures for silicon using the following potentials; (a) LDA, (b) PBE, (c) EXX, (d) CEDA, (e) LFX and (f) HF. The Fermi level has been set to 0 eV for all band structures. Brillouin zone special points are indexed in appendix C.

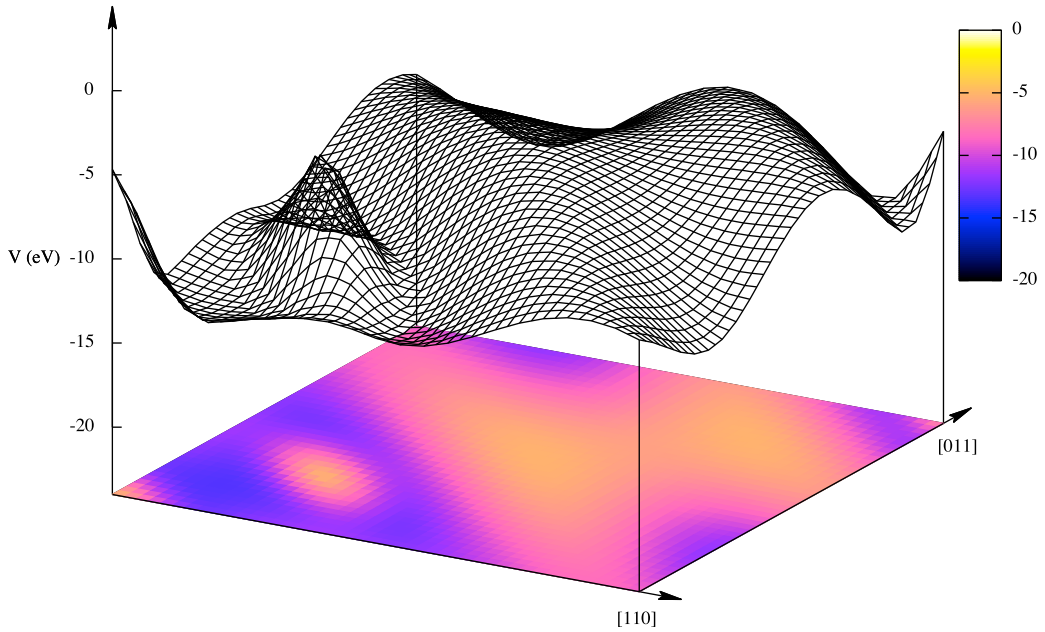

(a)

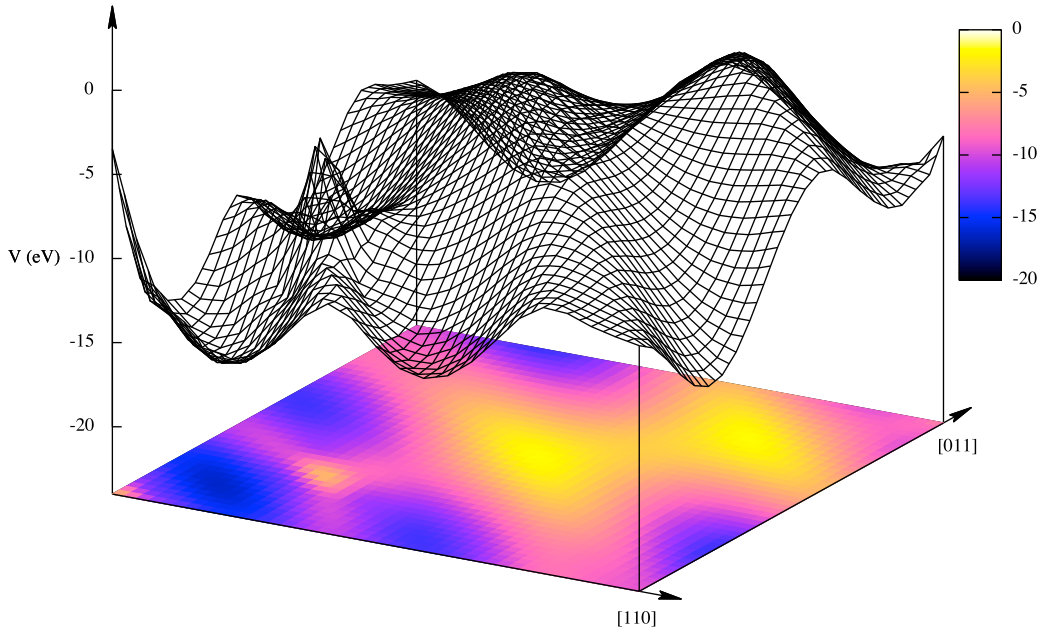

(b)

Figure 5.2: (a) LDA exchange-correlation potential for silicon and (b) EXX exchange potential for silicon.

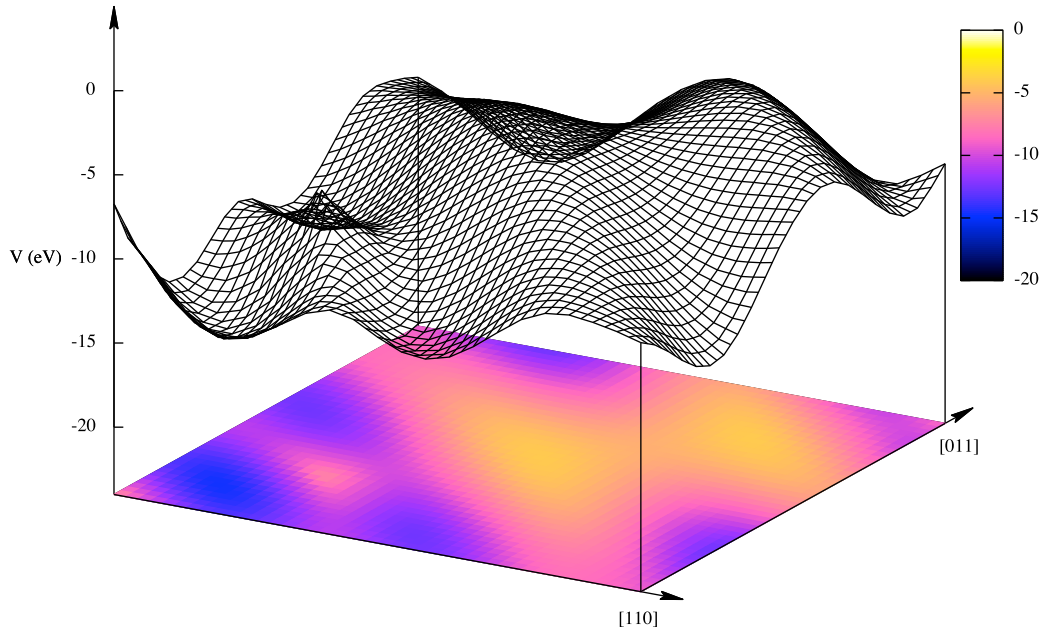

(c)

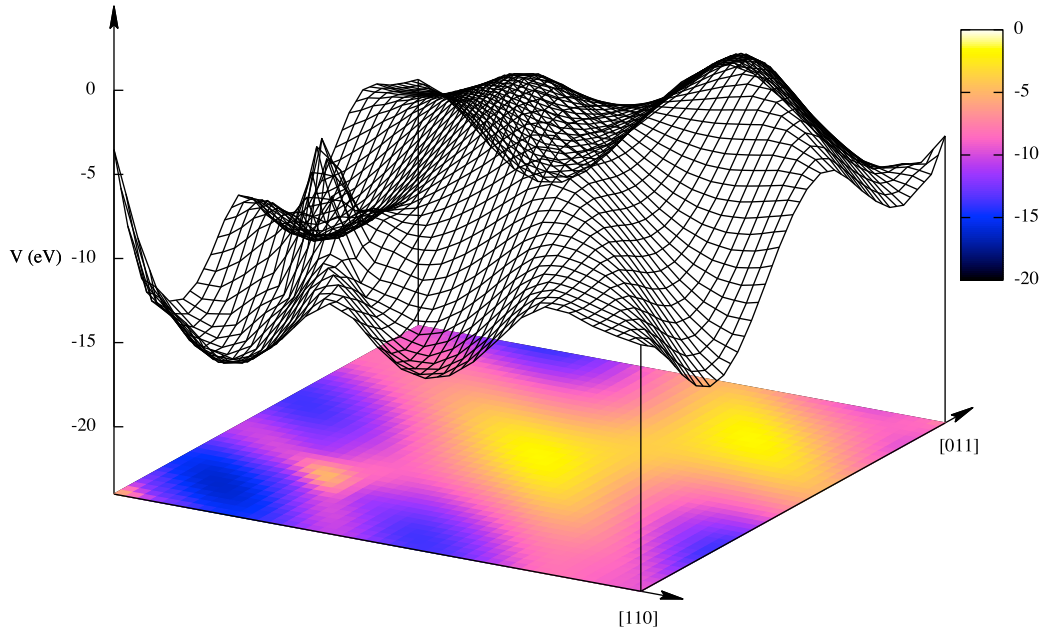

(d)

Figure 5.2: (c) CEDA exchange potential for silicon and (d) LFX exchange potential for silicon.

direction and the band structures are all largely similar in features, expect for the valence bandwidth and band gap. The valence bandwidths are largely the same for LDA, PBE, EXX, CEDA and LFX. The LDA valence bandwidth is 12.60 eV, the EXX and LFX valence bandwidth is 12.24 eV. For HF the valence bandwidth is much wider with a value of 17.87 eV. The experimentally measured valence bandwidth by photo-emission is 12.4 eV. The LDA band gap is 0.44 eV, the PBE value 0.60 eV, the EXX band gap is 1.20 eV, the CEDA band gap is 0.72 eV, the LFX value is 1.20 eV and HF gives 6.16 eV. The experimentally measured band gap by optical transmission is 1.17 eV.[137, 138] Hence the LDA, PBE and CEDA underestimate the band gap, while the EXX and LFX potentials give a value very close to the experimental one and HF hugely overestimates the value. This finding is consistent with previously published results of EXX for silicon. The LDA, PBE and HF results are expected and well known.

The LDA exchange-correlation potential, EXX, CEDA and LFX exchange potentials as a slice along the [111] direction of the silicon primitive unit cell are shown in figure 5.2. Silicon pseudopotentials are located at (000) and $(\frac{1}{4}\frac{1}{4}\frac{1}{4})$ in the unit cells. The EXX and LFX potentials are nearly identical, which is why the two methods give the same band structures, while the CEDA potential has a very similar form but is smoother. The LDA potential has a different form, is smoother than the other three potentials and is largely spherical around the ion cores whereas the tetragonal bonding structure of silicon can be seen in the potentials for EXX, CEDA and LFX. The different shapes of the potentials is most likely due to the LDA potential being explicitly density dependent and the local exchange-only potentials being only implicitly dependent on the density.

Material	ΔE (eV)			E_g (eV)		
	EXX	CEDA	LFX	EXX	CEDA	LFX
C	0.161	0.206	0.162	4.81	4.35	4.81
Si	0.213	0.291	0.214	1.20	0.72	1.20
Ge	0.441	0.542	0.442	0.93	0.40	0.93

Table 5.2: Total energy differences from the HF value for EXX, CEDA and LFX and Kohn-Sham band gaps for EXX, CEDA and LFX calculated for diamond, silicon and germanium.

For the exchange only local potentials (EXX, CEDA and LFX) the total energy difference from the HF value is shown in table 5.2. Total energies are calculated using the HF total energy functional in terms of the occupied orbitals of the corresponding scheme. The HF total energy is always the lowest of the four methods, due to the greater variational freedom of the orbitals when using a non-local potential compared to the local potentials. For silicon the EXX and LFX total energies differ by 8×10^{-5} eV, the similarity in the total energies, band structures and potentials imply the EXX and LFX methods model equally well the physics of the exchange term for the Kohn-Sham system, confirming the theoretical justifications to explain the similarity of EXX and LFX as given in section 3.7. CEDA as an approximation to the EXX gives a total

energy 0.077 eV greater than the EXX total energy. This is to be expected as EXX is defined as the local exchange-only potential that minimises the HF total energy, hence CEDA can only have a total energy greater than the EXX total energy.

Diamond

The calculated band structures using LDA, PBE, EXX, CEDA, LFX and HF for diamond are shown in figure 5.3. For all methods the material has an indirect band gap, with conduction band minimum along the $\Gamma \rightarrow$ X direction and except for the valence bandwidth and band gap the band structures are all largely similar. For HF the valence bands extend over 29.62 eV, which is a much larger range than any other method (between 21.67 eV for LDA to 21.47 eV for LFX). The LDA band gap is 4.02 eV, the PBE value 4.26 eV, the EXX band gap is 4.81 eV, the CEDA band gap is 4.35 eV, the LFX value is 4.81 eV and HF gives 12.51 eV. The experimentally measured band gap is 5.47 eV.[137, 138] Hence the LDA, PBE and CEDA significantly underestimate the band gap, while the EXX and LFX potentials give a value closer to the experimental one but one that is still underestimated and HF hugely overestimates the band gap.

The LDA exchange-correlation potential, EXX, CEDA and LFX exchange potentials are shown in figure 5.4 as a slice along the [111] direction of the diamond primitive unit cell. Carbon pseudopotentials are located at (000) and $(\frac{1}{4}\frac{1}{4}\frac{1}{4})$ in the unit cells. The EXX and LFX potentials are nearly identical, except for near the centre of the ion cores, which is why the two methods give very similar band structures, while the CEDA potential has a very similar form but is smoother. The LDA potential has again a different form, being smoother than the other three potentials and is largely spherical around the ion cores whereas the tetragonal bonding structure of diamond can be seen in the potentials for EXX, CEDA and LFX.

For the exchange-only local potentials (EXX, CEDA and LFX) the total energy difference from the HF value is shown in table 5.2. For diamond the EXX and LFX total energies are different by 3.2×10^{-4} eV, the similarity in the total energies band structures, and potentials imply the EXX and LFX methods are modelling the same exchange physics, (see section 3.7 for theoretical discussion of the physical equivalence of the two potentials). CEDA as an approximation to the EXX gives a total energy 0.045 eV greater than EXX.

Germanium

Calculated band structures for germanium using LDA, PBE, EXX, CEDA, LFX and HF are shown in figure 5.5. The material has an indirect band gap, with conduction band minimum at L. For LDA, PBE and CEDA the conduction band gap minima is along the $\Gamma \rightarrow X$ direction, EXX and LFX give the minimum at L, but the minimum value along $\Gamma \rightarrow X$ is almost the same as the minima at L. The LDA band gap is 0.11 eV, the PBE value 0.14 eV, the EXX band gap is 0.93 eV, the CEDA band gap is 0.40 eV, the

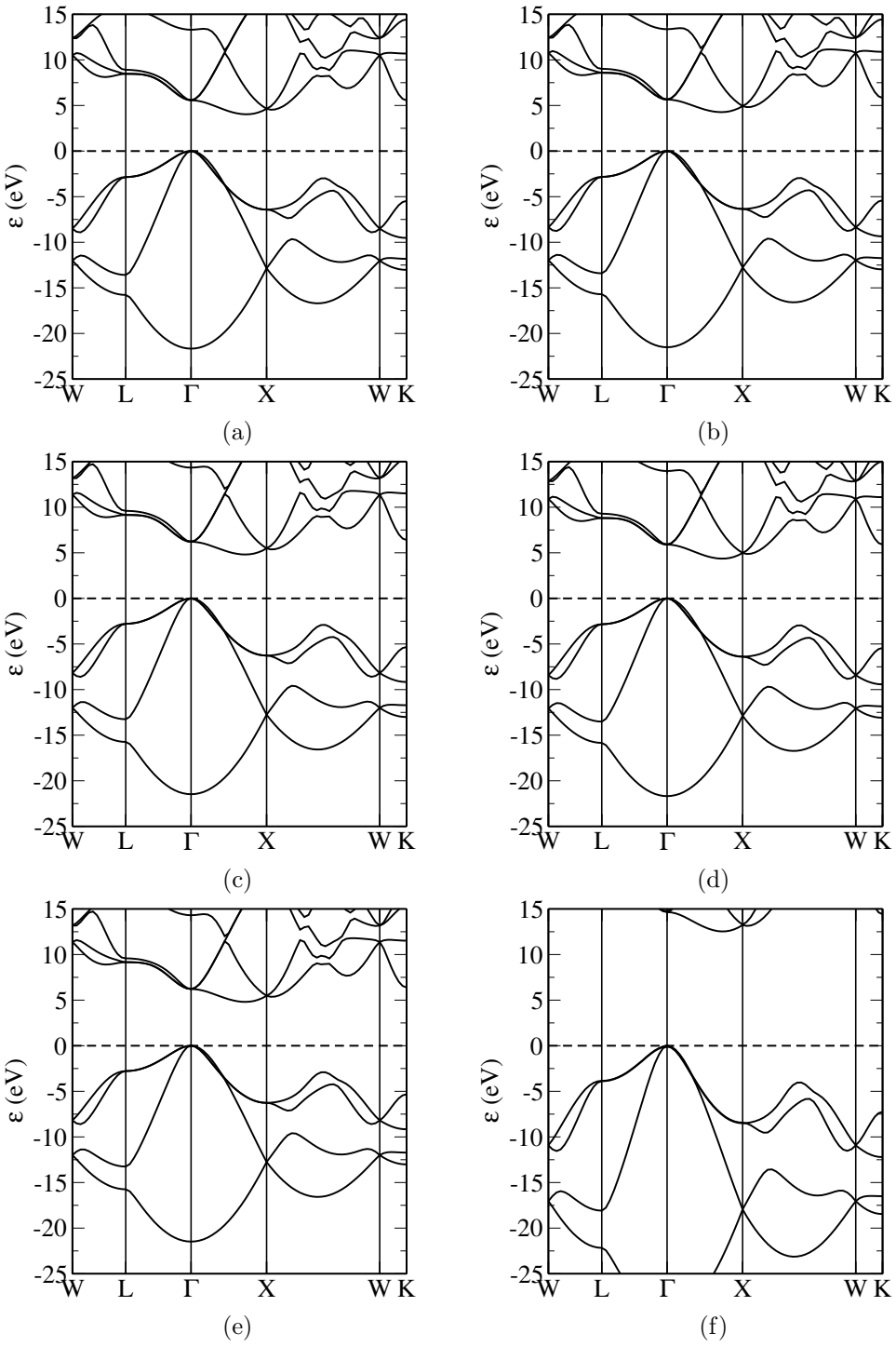

Figure 5.3: Band structures for diamond using the following potentials; (a) LDA, (b) PBE, (c) EXX, (d) CEDA, (e) LFX and (f) HF. The Fermi level has been set to 0 eV for all band structures. Brillouin zone special points are indexed in appendix C.

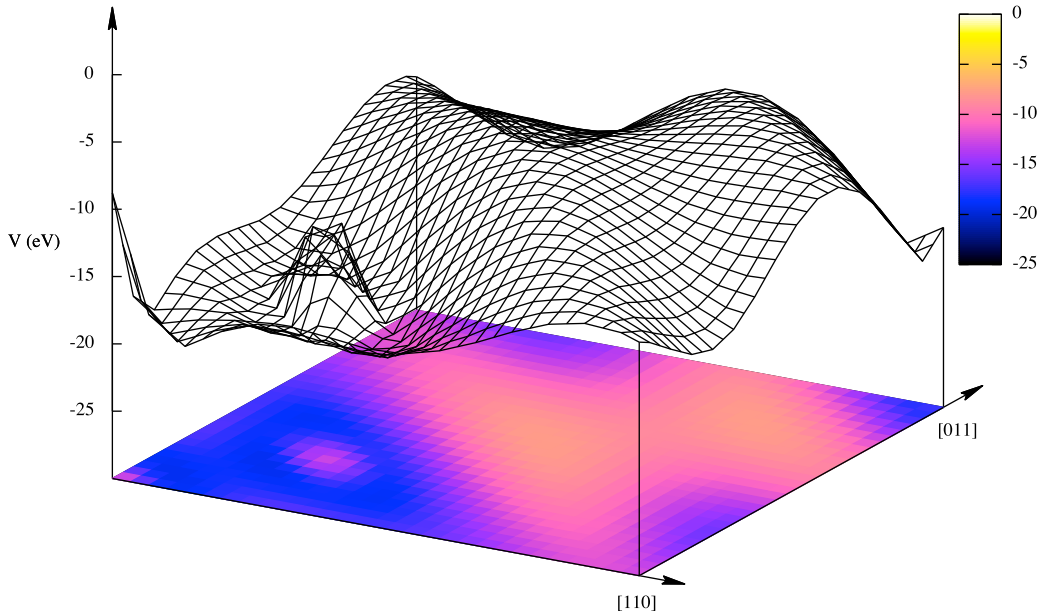

(a)

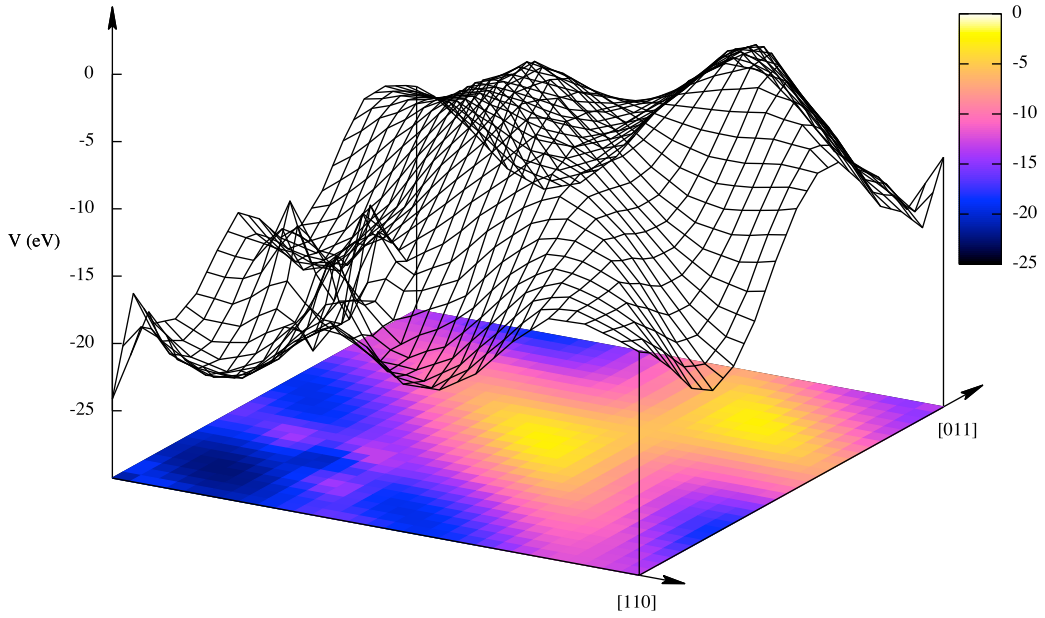

(b)

Figure 5.4: (a) LDA exchange-correlation potential for diamond and (b) EXX exchange potential for diamond.

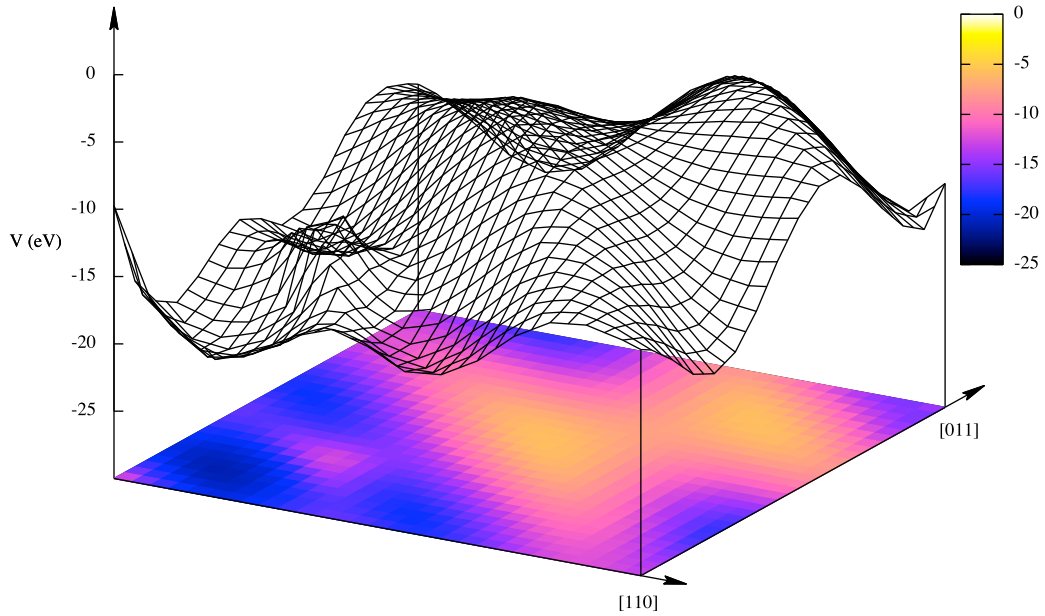

(c)

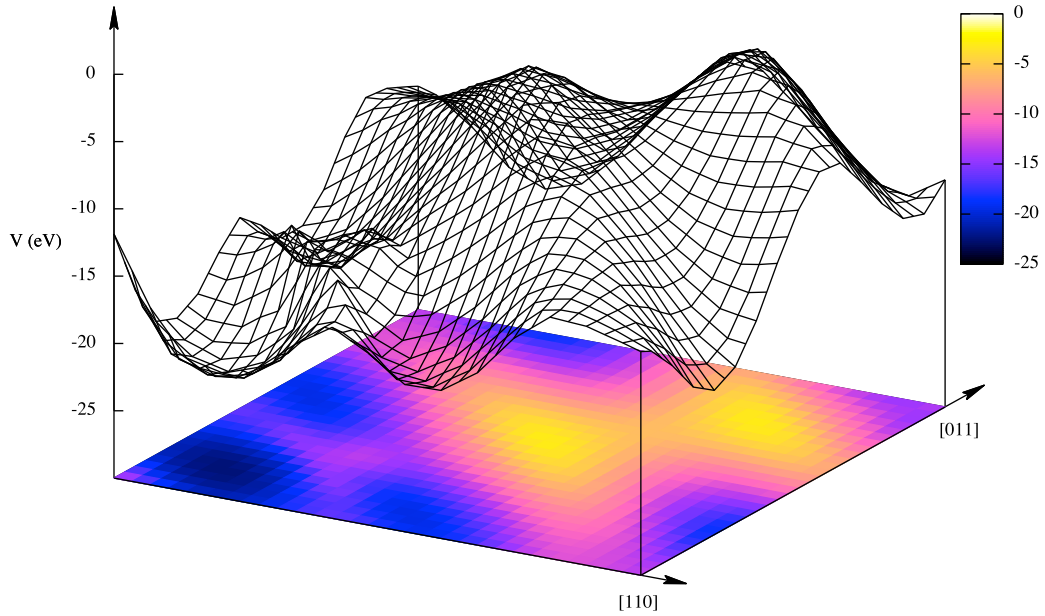

(d)

Figure 5.4: (c) CEDA exchange potential for diamond and (d) LFX exchange potential for diamond.

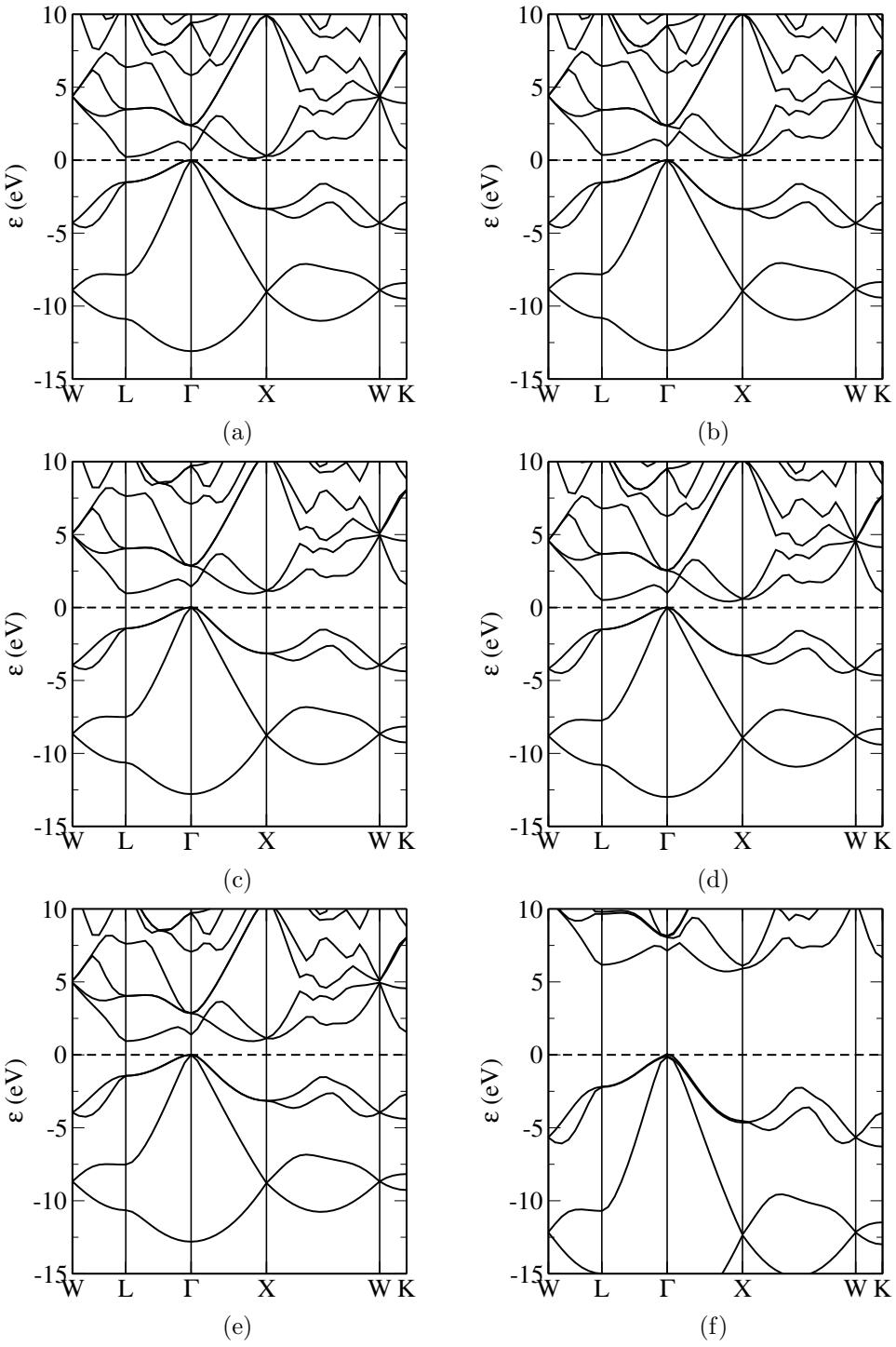

Figure 5.5: Band structures for germanium using the following potentials; (a) LDA, (b) PBE, (c) EXX, (d) CEDA, (e) LFX and (f) HF. The Fermi level has been set to 0 eV for all band structures. Brillouin zone special points are indexed in appendix C.

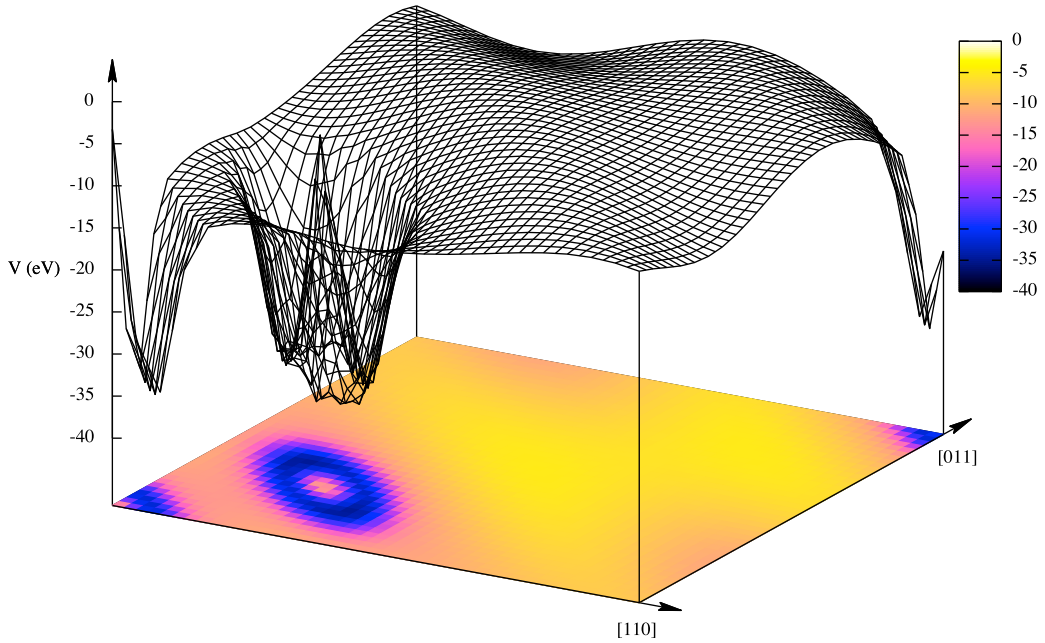

(a)

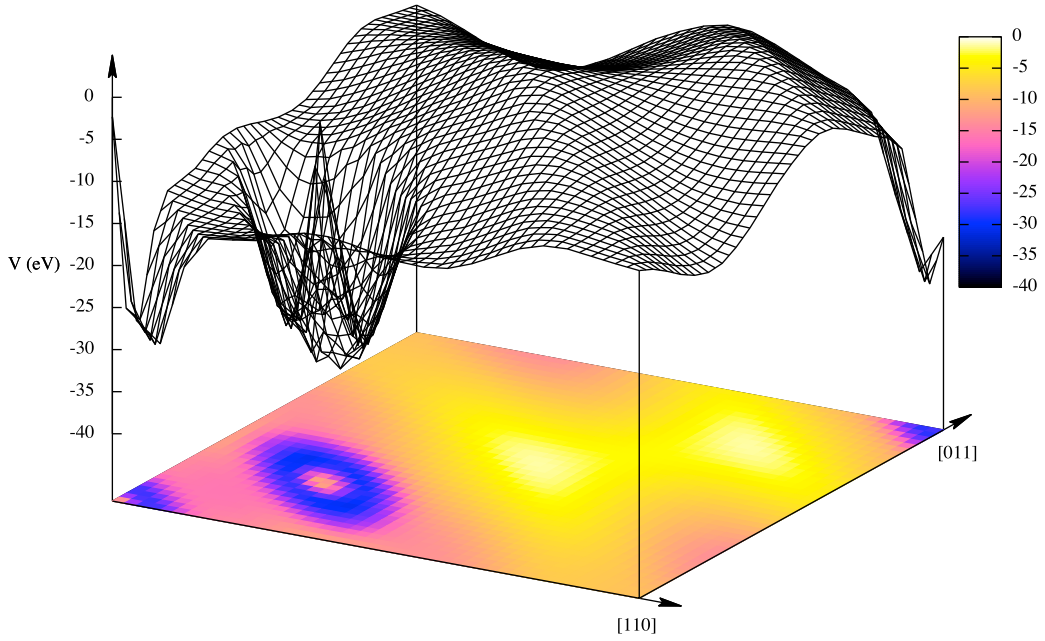

(b)

Figure 5.6: (a) LDA exchange-correlation potential for germanium and (b) EXX exchange potential for germanium.

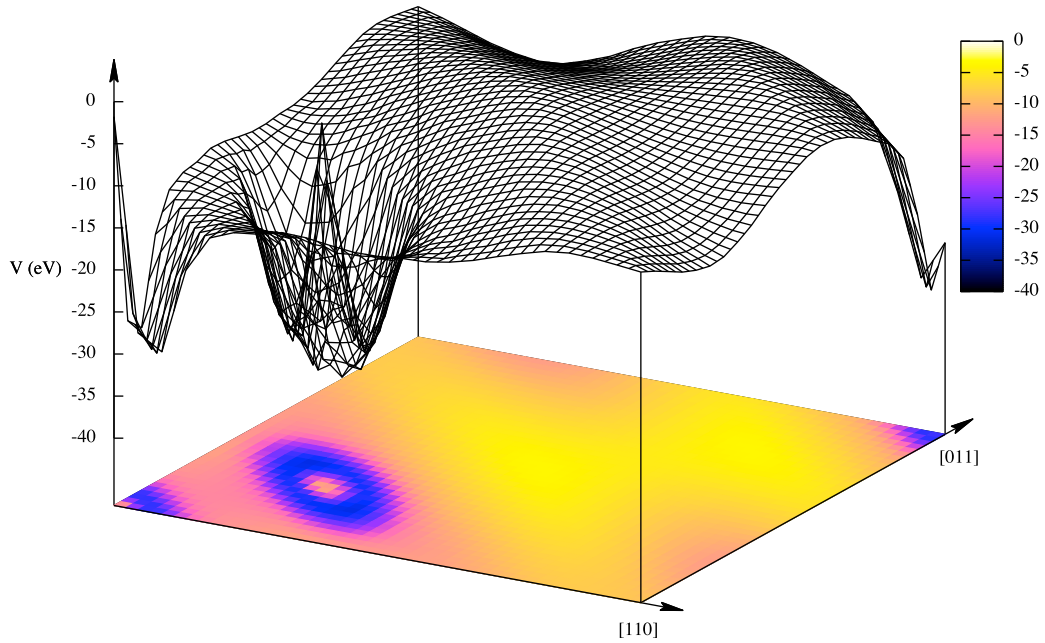

(c)

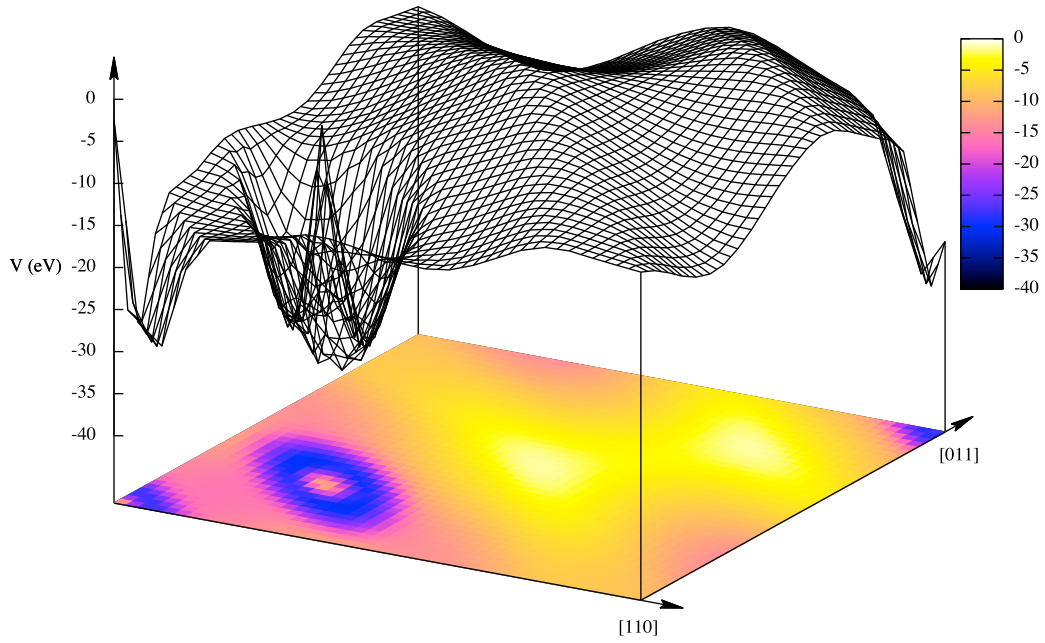

(d)

Figure 5.6: (c) CEDA exchange potential for germanium and (d) LFX exchange potential for germanium.

LFX value is 0.93 eV and HF gives 5.66 eV. The experimentally measured band gap is 0.74 eV.[137, 138] Hence the LDA, PBE and CEDA underestimate the band gap, while the EXX and LFX potentials give a value close to but greater than the experimental value and HF hugely overestimates the band gap. However germanium has a significant experimentally observed spin-orbit splitting of 0.20 eV,[137, 138] which is not included in these calculations. This effect might account for the overestimated gaps predicted by EXX and LFX. It is known that inclusion of relativistic effects from which the spin-orbit interaction arises tend to reduce the predicted band gap.[139, 140]

The LDA exchange-correlation potential, EXX, CEDA and LFX exchange potentials are shown in figure 5.6 as a slice along the [111] direction of the germanium primitive unit cell. Germanium pseudopotentials are located at (000) and $(\frac{1}{4}\frac{1}{4}\frac{1}{4})$ in the unit cells. Inclusion of the $3d$ electrons results in a deep potential around the ions which dominates the features present. The EXX and LFX potentials are nearly identical and the two methods give very similar band structures. The CEDA potential has a very similar form but is slightly smoother than the EXX and LFX potentials. The LDA potential has again a different form, smoother than the other three potentials and deeper in the ion core regions.

For the exchange only local potentials (EXX, CEDA and LFX) the total energy difference from the HF value is shown in table 5.2. For germanium the EXX and LFX total energies are different by 6.3×10^{-4} eV, The similarity in the total energies, band structures, and potentials, coupled with the theoretical justifications in section 3.7 imply the EXX and LFX methods are modelling the same exchange physics. CEDA as an approximation to the EXX gives a total energy 0.101 eV greater than the EXX total energy.

5.1.4 Group II-VI and III-V Semiconductors and Insulators

The band structures for group III-V and group II-VI semiconductors and selected insulators have been calculated, using the LDA, PBE, EXX, CEDA, LFX potentials and HF. The valence electron configurations for the elements used in these calculations are shown in table 5.3 and the calculation parameters for each material are shown in table 5.4 for the cubic zincblende materials and in table 5.5 for the non-cubic materials.

The energy differences from the HF total energy for EXX, CEDA and LFX are shown in table 5.6, the Kohn-Sham band gaps for LDA, PBE, EXX, CEDA, LFX and HF are shown in table 5.7, the valence bandwidths for LDA, PBE, EXX, CEDA, LFX and HF are shown in table 5.8 and semicore state binding energies for LDA, PBE, EXX, CEDA, LFX and HF are shown in table 5.9. The predicted band gaps are compared to experiment in figure 5.7 and average predicted semicore binding energies are also compared to experiment in figure 5.8.

The total energies follow the trend observed for the group IV semiconductors. The HF total energy is the lower bound on the exchange-only total energy, as the orbitals

Element	Valence electron configuration
Al	$3s^2 3p^1$
As	$4s^2 3d^{10} 4p^3$
C	$2s^2 2p^2$
Ca	$3s^2 3p^6 4s^2$
Cd	$5s^2 4^{10}$
Cl	$3s^2 3p^5$
Ga	$4s^2 3d^{10} 4p^1$
Hf	$5s^2 5p^6 6s^2 5d^2$
In	$5s^2 4^{10} 5p^1$
Mg	$2p^6 3s^2$
N	$2s^2 2p^3$
Na	$2p^6 3s^1$
O	$2s^2 2p^4$
P	$3s^2 3p^3$
S	$3s^2 3p^4$
Sb	$5s^2 4^{10} 5p^3$
Se	$4s^2 3d^{10} 4p^4$
Si	$3s^2 3p^2$
Te	$5s^2 4^{10} 5p^4$
Zn	$4s^2 3d^{10}$

Table 5.3: Valence electron configurations used in the calculation of the group II-VI and III-V semiconductors. Semicore states are included to improve the transferability of the pseudopotential.[141]

Material	E_{cutoff} (eV)	MP k-point grid	Lattice parameter (Å)
AlAs	1000	$6 \times 6 \times 6$	5.66
AlP	900	$6 \times 6 \times 6$	5.46
AlSb	1100	$6 \times 6 \times 6$	6.14
CaO	1400	$6 \times 6 \times 6$	4.81
CdO	1000	$6 \times 6 \times 6$	4.69
CdS	900	$6 \times 6 \times 6$	5.82
CdSe	900	$6 \times 6 \times 6$	6.07
CdTe	1100	$6 \times 6 \times 6$	6.46
GaAs	1000	$6 \times 6 \times 6$	6.65
GaP	1000	$6 \times 6 \times 6$	5.45
GaSb	1100	$6 \times 6 \times 6$	6.09
HfO_2	1000	$6 \times 6 \times 6$	5.30
InAs	1100	$6 \times 6 \times 6$	6.05
InP	1100	$6 \times 6 \times 6$	5.86
InSb	1100	$6 \times 6 \times 6$	6.47
MgO	1000	$6 \times 6 \times 6$	4.21
MgS	900	$6 \times 6 \times 6$	5.20
MgSe	1000	$6 \times 6 \times 6$	5.46
MgTe	1100	$6 \times 6 \times 6$	6.02
NaCl	1000	$6 \times 6 \times 6$	5.62
SiC	1100	$8 \times 8 \times 8$	4.35
ZnS	900	$6 \times 6 \times 6$	5.41
ZnSe	1000	$6 \times 6 \times 6$	5.67
ZnTe	1100	$6 \times 6 \times 6$	6.08

Table 5.4: Parameters for calculations on cubic group IV, group III-V and group II-VI materials. Lattice parameters from [137] and [138],except for NaCl.[142]

Material	E_{cutoff} (eV)	MP k-point grid	Lattice parameter a (Å)	Lattice parameter c (Å)
AlN	1000	$6 \times 6 \times 4$	3.11	4.98
GaN	1000	$6 \times 6 \times 4$	3.18	5.18
InN	1100	$6 \times 6 \times 4$	3.54	5.70
SiO_2	1000	$6 \times 6 \times 6$	5.01	5.47
ZnO	1000	$7 \times 7 \times 4$	3.25	5.21

Table 5.5: Parameters for calculations on non-cubic group III-V and group II-VI materials. Lattice parameters from [137] and [138].

Material	ΔE (eV)		
	EXX	LFX	CEDA
AlAs	0.363	0.365	0.449
AlN	0.229	0.229	0.302
AlP	0.150	0.150	0.212
AlSb	0.322	0.323	0.416
C	0.161	0.162	0.206
CaO	0.264	0.268	0.331
CdO	0.231	0.232	0.302
CdS	0.214	0.215	0.268
CdSe	0.509	0.510	0.608
CdTe	0.396	0.397	0.480
GaAs	0.445	0.446	0.537
GaN	0.416	0.418	0.509
GaP	0.247	0.248	0.308
GaSb	0.407	0.408	0.506
Ge	0.441	0.442	0.542
HfO_2	0.412	0.414	0.561
InAs	0.450	0.451	0.541
InN	0.478	0.480	0.611
InP	0.258	0.259	0.323
InSb	0.411	0.412	0.501
MgO	0.107	0.107	0.133
MgS	0.093	0.093	0.123
MgSe	0.417	0.418	0.495
MgTe	0.271	0.272	0.331
NaCl	0.050	0.050	0.062
Si	0.213	0.214	0.291
SiC	0.131	0.131	0.179
SiO_2	0.588	0.590	0.730
ZnO	0.369	0.371	0.467
ZnS	0.186	0.187	0.236
ZnSe	0.487	0.488	0.584
ZnTe	0.374	0.375	0.463

Table 5.6: Total energy differences from the HF total energy for EXX, CEDA and LFX.

Material	E_g (eV)						
	LDA	PBE	EXX	LFX	CEDA	HF	Expt.
AlAs	1.13	1.19	2.25	2.23	1.68	7.54	2.23
AlN	4.25	4.43	5.77	5.72	5.22	13.55	6.28
AlP	1.55	1.75	2.50	2.47	1.99	7.99	2.45
AlSb	0.83	0.90	1.67	1.65	1.17	6.56	1.60
C	4.02	4.26	4.81	4.81	4.35	12.51	5.47
CaO	3.88	4.05	6.13	5.96	5.47	14.62	7.09
CdO	0.34	0.66	1.93	1.84	1.27	9.00	1.12
CdS	1.31	1.65	2.25	2.18	1.76	8.37	2.42
CdSe	0.86	1.12	1.84	1.79	1.30	7.80	1.74
CdTe	1.46	1.80	2.24	2.18	1.73	8.06	1.61
GaAs	1.00	1.10	1.91	1.87	1.43	7.09	1.52
GaN	2.13	2.35	3.36	3.31	2.85	10.38	3.39
GaP	1.52	1.72	2.31	2.28	1.86	7.56	2.35
GaSb	0.45	0.55	1.20	1.19	0.71	5.88	0.81
Ge	0.11	0.14	0.93	0.93	0.40	5.66	0.74
HfO_2	3.12	3.23	5.62	5.56	4.89	13.37	5.90
InAs	0.44	0.67	1.35	1.30	0.85	6.79	0.42
InN	0.21	0.38	1.42	1.35	0.87	7.46	0.93
InP	1.07	1.27	1.92	1.87	1.44	7.29	1.44
InSb	0.91	1.02	1.63	1.60	1.20	6.28	0.24
MgO	4.63	4.97	6.66	6.59	6.14	15.27	7.80
MgS	3.63	3.89	4.82	4.77	4.37	11.41	4.50
MgSe	2.76	2.82	4.16	4.14	3.61	10.39	4.10
MgTe	2.07	2.19	3.12	3.09	2.63	8.71	3.47
NaCl	4.89	5.37	6.30	6.25	5.89	13.79	8.97
Si	0.44	0.60	1.20	1.20	0.72	6.16	1.17
SiC	1.26	1.42	2.42	2.40	1.88	8.44	2.42
SiO_2	5.25	5.71	7.30	7.23	6.78	15.90	9.00
ZnO	1.93	2.28	3.51	3.44	2.95	11.37	3.43
ZnS	2.58	2.94	3.56	3.52	3.05	10.29	3.80
ZnSe	1.85	2.16	2.91	2.87	2.38	9.46	2.80
ZnTe	2.02	2.19	2.84	2.82	2.36	8.25	2.39

Table 5.7: Kohn-Sham band gaps for LDA, PBE, EXX, CEDA, LFX, HF and experimental results for group IV, III-V and II-VI semiconductors and insulators. Experimental results from [137] and [138], except for InN,[143] NaCl,[144] SiO_2 and HfO_2.[145]

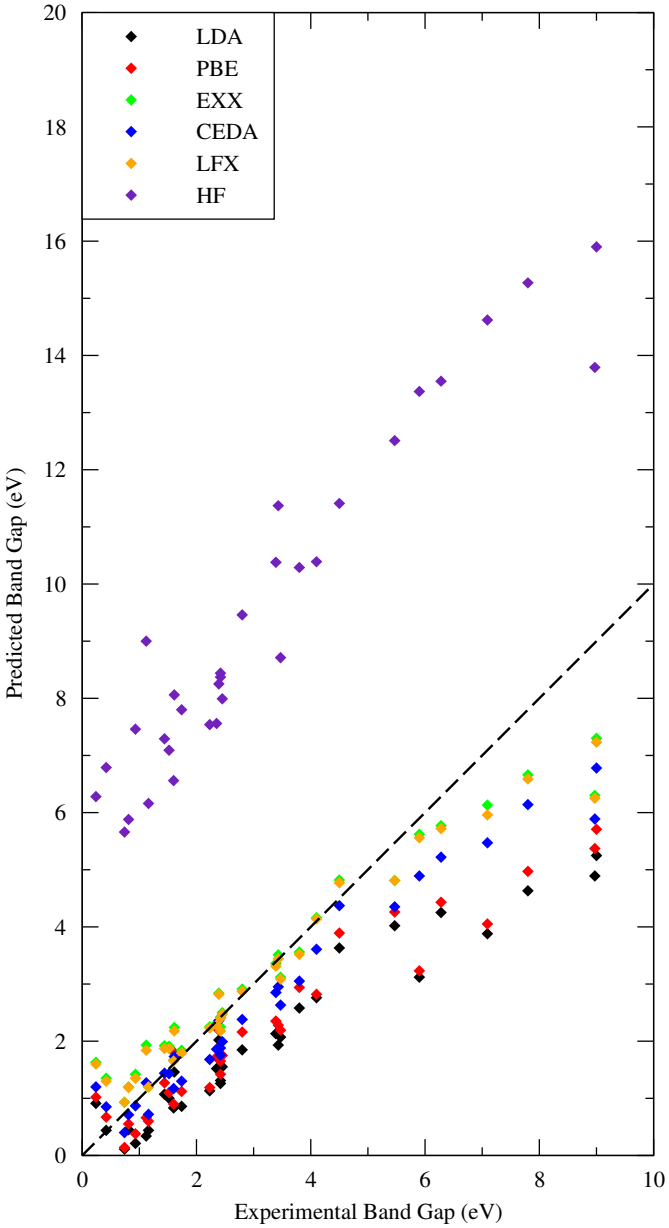

Figure 5.7: Comparison of predicted band gaps against experiment for materials presented in table 5.7.

Material	Valence Bandwidth (eV)						
	LDA	PBE	EXX	LFX	CEDA	HF	Expt.
AlAs	11.99	11.95	11.68	11.69	11.83	17.34	
AlN	6.14	6.04	5.56	5.58	5.76	7.79	
AlP	11.71	11.67	11.41	11.42	11.57	17.53	
AlSb	10.62	10.57	10.32	10.33	10.51	15.01	10.6
C	21.67	21.52	21.48	21.47	21.69	29.62	21
CaO	14.87	14.82	14.86	14.87	14.84	21.07	
CdO	9.84	10.11	7.70	7.76	8.05	11.81	
CdS	10.86	11.05	9.15	9.20	9.52	13.36	
CdSe	11.45	11.74	9.57	9.60	10.02	13.19	
CdTe	10.56	10.44	10.20	10.21	10.57	13.89	10.8
GaAs	12.90	12.83	12.63	12.64	12.78	17.76	12.9
GaN	7.09	6.89	6.66	6.68	6.84	9.32	
GaP	12.66	12.56	12.45	12.46	12.58	18.55	12.0
GaSb	11.51	11.43	11.27	11.28	11.44	16.26	11.6
Ge	13.10	13.04	12.81	12.82	13.00	18.19	12.8
HfO_2	5.36	5.17	4.81	4.82	4.95	6.64	
InAs	11.78	11.70	11.57	11.58	11.69	16.51	12.3
InN	5.54	5.39	5.15	5.17	5.33	7.43	
InP	11.50	11.42	11.32	11.33	11.44	17.24	11.0
InSb	10.46	10.38	10.26	10.28	10.41	14.72	10.9
MgO	16.96	16.84	16.78	16.79	16.79	24.06	
MgS	12.45	12.41	12.26	12.27	12.34	17.15	
MgSe	12.68	12.62	12.54	12.56	12.60	16.81	
MgTe	10.68	10.59	10.50	10.51	10.59	14.43	
NaCl	12.72	12.72	12.61	12.62	12.65	17.33	
Si	12.60	12.56	12.24	12.24	12.46	17.87	12.4
SiC	16.09	16.02	15.80	15.80	15.95	22.49	
SiO_2	9.85	9.77	9.11	9.13	9.34	11.31	9
ZnO	4.56	4.35	4.28	4.29	4.42	5.89	5.0
ZnS	12.82	12.73	12.73	12.74	12.83	18.41	13.5
ZnSe	12.97	12.87	12.88	12.89	12.96	17.52	14.5
ZnTe	12.40	12.77	11.01	11.03	11.14	16.11	13.0

Table 5.8: Valence bandwidths for LDA, PBE, EXX, CEDA, LFX, HF and experimental results for group IV, III-V and II-VI semiconductors and insulators. Experimental results from [34], [137], [146], [147], [148], [149] and [150].

Material		Semicore Binding Energy (eV)						
		LDA	PBE	EXX	LFX	CEDA	HF	Expt.
AlAs	As 3*d*	46.74-46.75	47.74-47.75	43.66-43.67	43.71-43.73	44.40-44.41	48.55 50.22	
AlSb	Sb 4*d*	36.00-36.02	36.42-36.43	33.70-33.73	33.73-33.76	34.26-34.29	38.97 39.19	
CdO	Cd 4*d*	8.79-10.33	9.07-10.59	6.94-8.41	6.97-8.45	7.12-8.65	9.54 12.72	
CdS	Cd 4*d*	10.81-11.13	11.00-11.30	9.08-9.59	9.14-9.63	9.46-9.88	11.76 13.94	9.64
CdSe	Cd 4*d*	11.41-11.68	11.71-11.95	9.53-9.95	9.55-9.96	9.98-10.31	13.00 13.65	9.9
CdSe	Se 3*d*	60.92-60.93	61.87-61.87	58.39-58.40	58.45-58.46	59.28-59.29	62.78 63.03	
CdTe	Cd 4*d*	11.88-12.30	12.11-12.49	10.13-11.01	10.18-11.04	10.59-11.29	13.79 14.92	10.49
CdTe	Te 4*d*	44.59-44.58	44.99-44.98	42.14-42.15	42.19-42.20	42.70-42.71	47.33 47.38	40.94
GaAs	Ga 3*d*	22.92-22.98	23.62-23.68	20.01-20.16	20.03-20.16	20.38-20.47	26.41 26.56	18.82
GaAs	As 3*d*	47.48-47.49	48.43-48.42	44.42-44.44	44.48-44.50	45.19-45.20	50.22 50.28	40.76
GaN	Ga 3*d*	21.22-21.55	21.87-22.16	18.28-18.88	18.32-18.91	18.49-19.04	23.27 24.23	17.94
GaP	Ga 3*d*	22.43-22.52	23.04-23.13	19.65-19.83	19.68-19.86	19.95-20.08	25.04 26.87	18.55
GaSb	Ga 3*d*	23.11-23.15	23.78-23.82	20.29-20.38	20.30-20.39	20.70-20.75	27.20 27.43	19
GaSb	Sb 4*d*	36.61-36.63	36.99-37.01	34.35-34.39	34.38-34.42	34.90-34.92	40.00 40.22	32.79
Ge	Ge 3*d*	35.10-35.23	35.96-36.08	31.83-32.10	31.80-31.97	32.50-32.75	38.82 39.08	29.6
InAs	In 4*d*	20.00-20.13	20.30-20.42	18.03-18.30	18.07-18.32	18.57-18.74	22.90 23.34	17.09
InAs	As 3*d*	47.09-47.10	48.02-48.03	44.03-44.05	44.10-44.12	44.78-44.80	50.07 50.28	40.3
InN	In 4*d*	18.35-18.94	18.63-19.16	16.35-17.30	16.41-17.35	16.76-17.59	19.83 21.71	17.4
InP	In 4*d*	19.58-19.73	19.79-19.93	17.75-18.04	17.82-18.09	18.18-18.38	21.58 23.53	16.8
InSb	In 4*d*	20.28-20.37	20.55-20.62	18.40-18.58	18.45-18.62	18.90-19.02	23.45 23.66	17.29
InSb	Sb 4*d*	36.23-36.25	36.60-36.62	33.97-34.01	34.02-34.05	34.53-34.56	39.53 39.62	32.67
MgSe	Se 3*d*	59.98-59.99	60.96-60.98	57.56-57.57	57.59-57.61	58.30-58.31	61.03 61.16	
MgTe	Te 4*d*	43.90-43.92	44.33-44.35	41.47-41.49	41.50-41.52	41.92-41.94	46.10 46.18	
ZnO	Zn 3*d*	8.68-9.69	9.12-10.08	6.43-7.60	6.44-7.60	6.57-7.74	9.36 10.70	7.6
ZnS	Zn 3*d*	9.93-11.18	10.14-11.51	8.45-9.31	8.44-9.30	8.55-9.42	12.71 14.35	9.2
ZnSe	Zn 3*d*	10.54-11.80	10.70-12.25	9.02-9.72	8.99-9.69	9.14-9.87	14.21 17.30	9.20
ZnSe	Se 3*d*	61.04-61.05	61.99-62.00	58.48-58.49	58.54-58.55	59.27-59.29	62.60 62.71	53.5
ZnTe	Zn 3*d*	12.14-12.40	12.77-12.55	10.07-11.01	10.07-11.03	10.33-11.14	15.44 16.11	9.84
ZnTe	Te 4*d*	44.76-44.77	45.17-45.18	42.30-42.31	42.34-42.35	42.86-42.87	47.59 47.80	41.7

Table 5.9: Semicore binding energies calculated LDA, PBE, EXX, CEDA, LFX, HF and experimental results for group IV, III-V and II-VI semiconductors and insulators. Experimental results from [150] and [151].

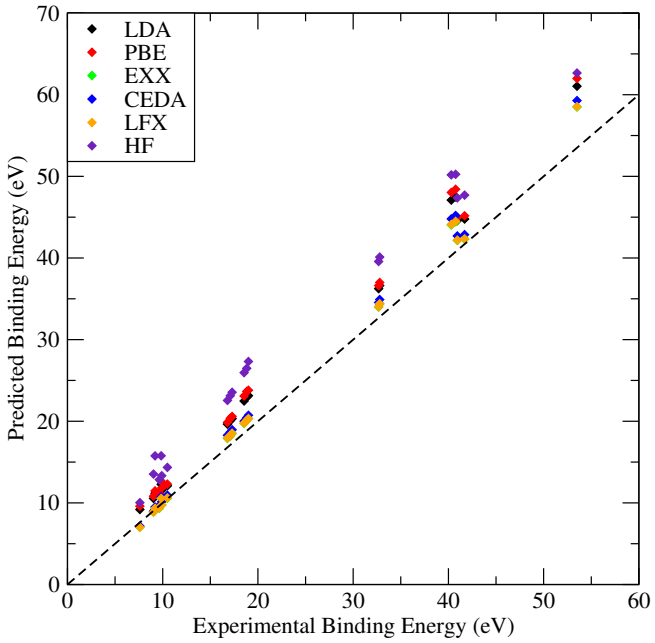

Figure 5.8: Comparison of average predicted semicore binding energies against experiment for materials presented in table 5.9. EXX points (green) are covered by the LFX points (orange).

have greater variational freedom when having a non-local exchange potential. The EXX and LFX total energy values are very close with EXX always lower as it minimises the HF total energy using a local functional, while the LFX has the same density as HF. The EXX and LFX total energies differ at most by 0.0041 eV for CaO, with the CEDA total energy being the highest (for SiO_2 0.142 eV greater than EXX), as approximating the eigenvalue differences with a constant in the EXX functional derivative restricts the variational freedom in the potential.

In figure 5.7 we observe the same trend for the Kohn-Sham band gaps as for the Group IV semiconductors. Overall the LDA and PBE largely underestimate the band gap, HF grossly overestimates the gap, CEDA slightly underestimates and EXX and LFX are very close to the experimental results. As noted for Ge, Si and C the EXX and LFX band gaps overestimate for small gap materials and underestimate the gap for large gap materials.

The small gap materials for which EXX and LFX overestimate the band gap are typically composed of heavy elements where the spin-orbit splitting can be very large. Figure 5.9 shows the band structures for LDA, PBE, EXX, CEDA, LFX and HF for InSb, for which even LDA overestimates the band gap (LDA Kohn-Sham band gap 0.91 eV, experimental gap of 0.23 eV). EXX, CEDA and LFX all hugely overestimate the gap. However the spin orbit splitting at the Γ point in InSb is 0.81 eV which is much larger than the band gap.[137, 138] Similarly for CdTe (the band structures of which are plotted in figure 5.10), where the EXX and LFX band gaps are overestimated relative to experiment, the spin-orbit splitting is 0.950 eV.

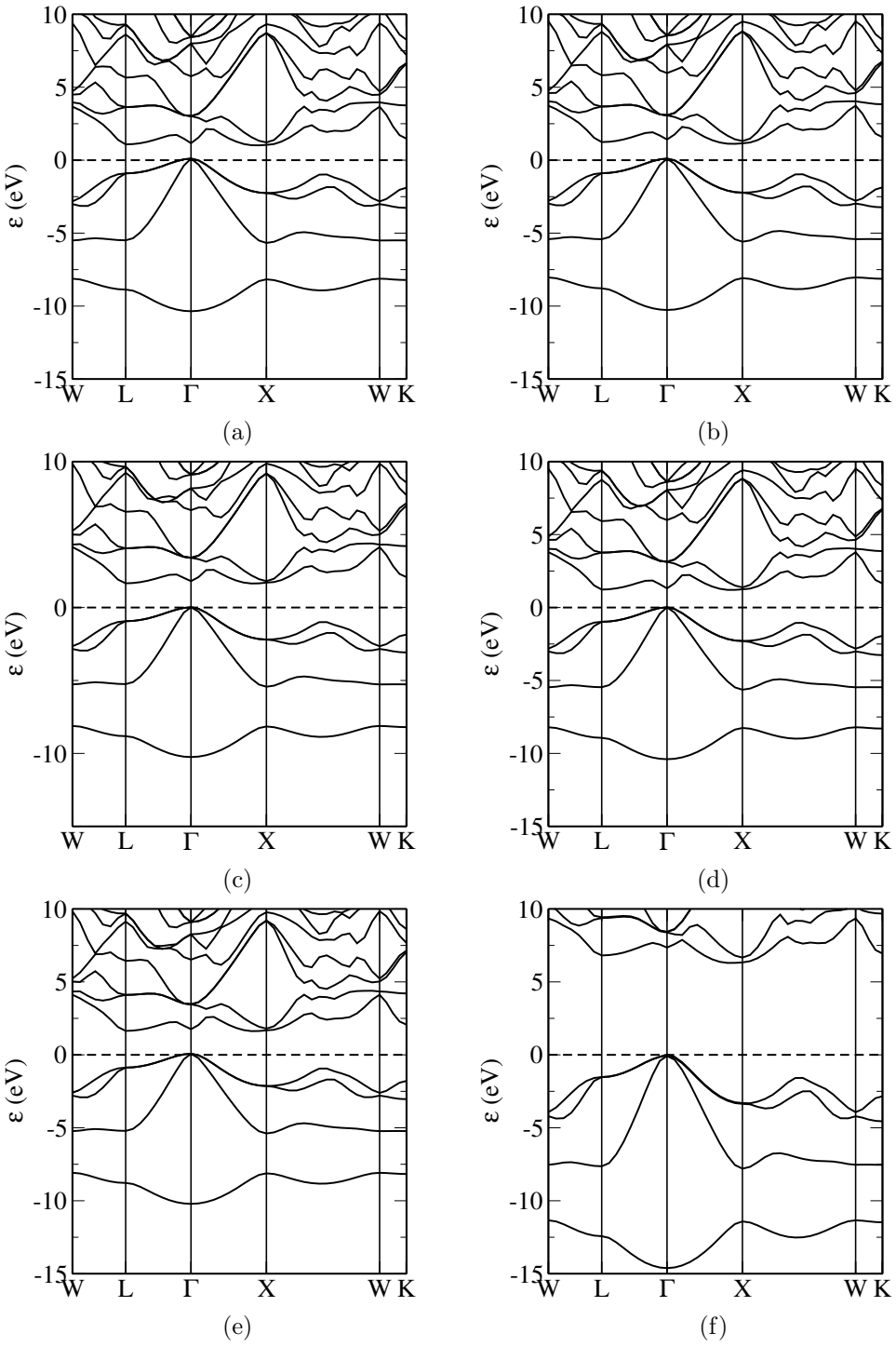

Figure 5.9: Band structures for InSb using the following potentials; (a) LDA, (b) PBE, (c) EXX, (d) CEDA, (e) LFX and (f) HF. The Fermi level has been set to 0 eV for all band structures. Brillouin zone special points are indexed in appendix C.

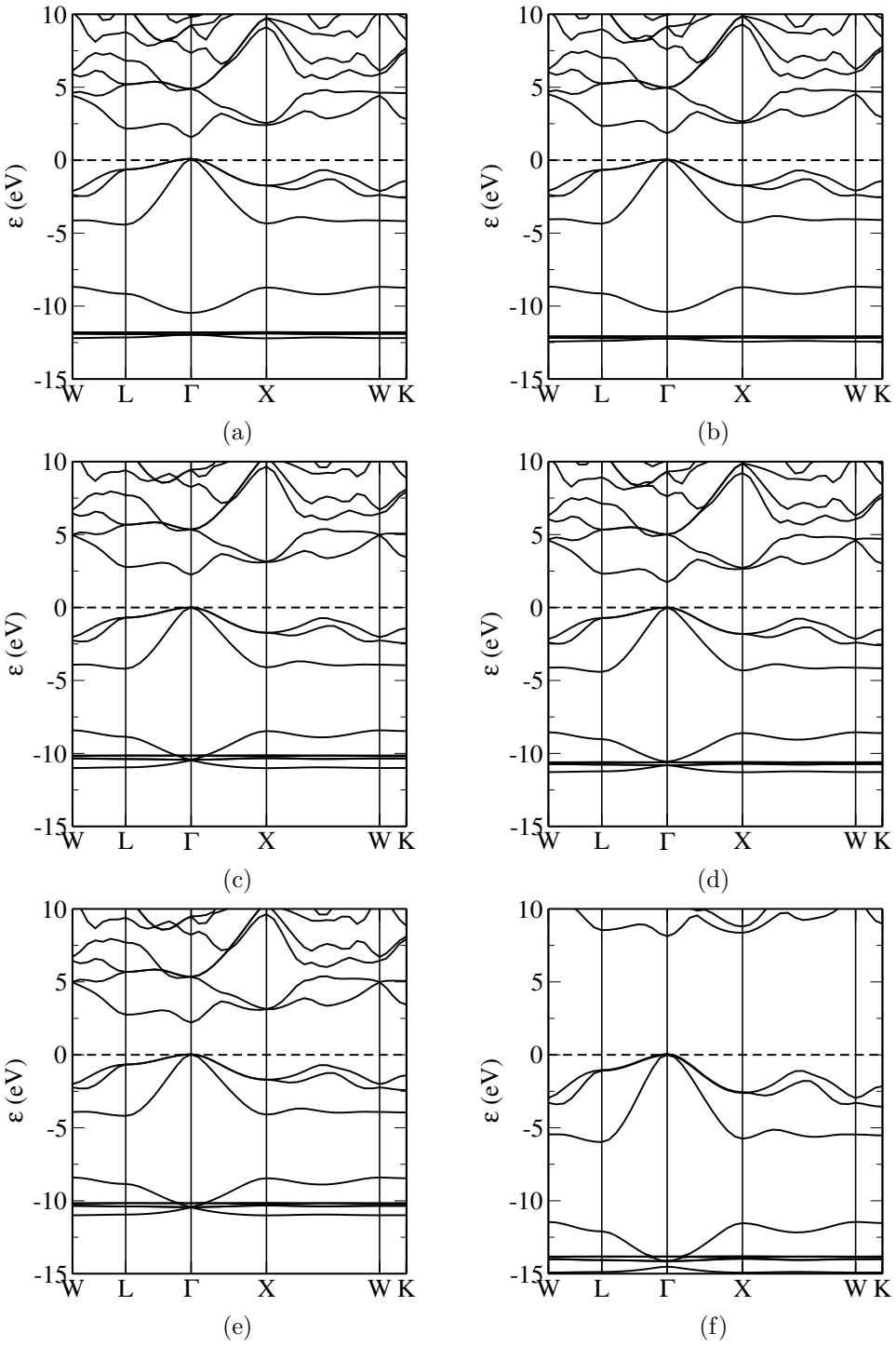

Figure 5.10: Band structures for CdTe using the following potentials; (a) LDA, (b) PBE, (c) EXX, (d) CEDA, (e) LFX and (f) HF. The Fermi level has been set to 0 eV for all band structures. Brillouin zone special points are indexed in appendix C.

While the relativistic effects of spin-orbit coupling were not included at all in these calculations just the inclusion of the spin-orbit splitting does not fully correct for the overestimated gaps. However inclusion of full relativistic effects can decrease the band gap by more than just the observed spin-orbit coupling.[139, 140] Hence we do not feel it is instructive to "correct" measured band gaps by adding the spin-orbit splitting to the experimentally measured band gaps. In addition no relativistic corrections were applied in the generation of the pseudopotentials used in these calculations. Inclusion of both of these effects could improve the band structures for small gap materials.

The EXX, CEDA and LFX give good predictions of the band gap for material composed of lighter elements as evidenced by figures 5.11 and 5.12 which show the band structures for GaN and ZnO respectively. For wider gap materials (figures 5.13 and 5.14 show the band structures for HfO_2 and SiO_2 respectively) EXX, CEDA, LFX all underestimate the band gap. The mean absolute error of the predicted band gaps compared to experiment is; 1.31 eV for LDA, 1.13 eV for PBE, 6.24 eV for HF, 0.49 eV for EXX, 0.49 eV for LFX and 0.67 eV for CEDA. Hence the EXX and LFX results are in good with experiment and CEDA results gives a value reasonably close to experiment.

The numerical results for EXX and the trend of overestimating small band gap materials composed of heavy elements, giving good results for materials composed of lighter elements and underestimating the predicted gap for wide gap materials are consistent with those found in references; [95, 97, 98, 152, 153, 154, 155, 156].

The valence bandwidths for all the materials presented here are largely the same regardless of the exchange-correlation potential chosen except for HF, as shown in table 5.8. The LDA bandwidths are the widest of the local potentials and EXX/LFX have the narrowest width. Compared to experiment all the predicted valence bandwidths for the local potentials are in good agreement, with the differences between the theoretical methods smaller than the error on the experimental measurements (typical experimental errors are of the order of 0.5 eV).

In the calculations presented here some semicore states are included as valence, see table 5.3 for valence electron configurations. The binding energies of localised d-electrons (the bands associated with the d-electrons can be seen in figures 5.10 and 5.12) are shown in table 5.9 and the average value calculated binding energy compared to the experimentally observed values are shown in figure 5.8. Hartree-Fock hugely over-binds the d-electrons, as does the LDA and PBE. EXX and LFX give binding energies closest to the experimental values. For semicore states with low binding energy (Zn ions and Cd ions for example), EXX and LFX give good agreement to the experimental values, but this agreement worsens with an increasing binding energy. However relativistic effects will have increased effect on the states with large energies, hence the increasing error between the calculated and experimental results is indicative that relativity needs to be included (both in the pseudopotential and in the actual calculation) to accurately model these tightly bound states.

The success of EXX and LFX over LDA/GGA may suggest that the accurate treat-

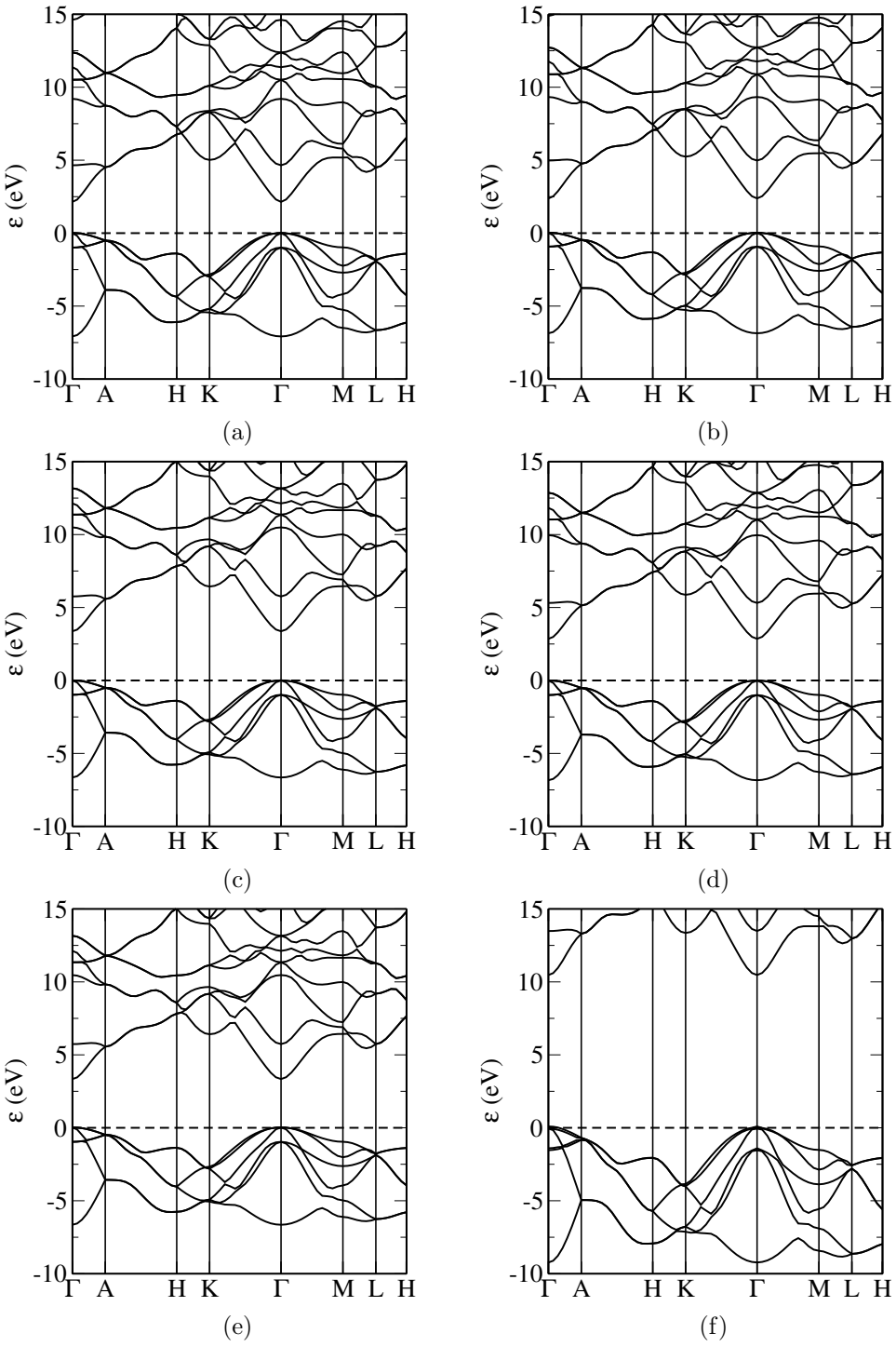

Figure 5.11: Band structures for GaN using the following potentials; (a) LDA, (b) PBE, (c) EXX, (d) CEDA, (e) LFX and (f) HF. The Fermi level has been set to 0 eV for all band structures. Brillouin zone special points are indexed in appendix C.

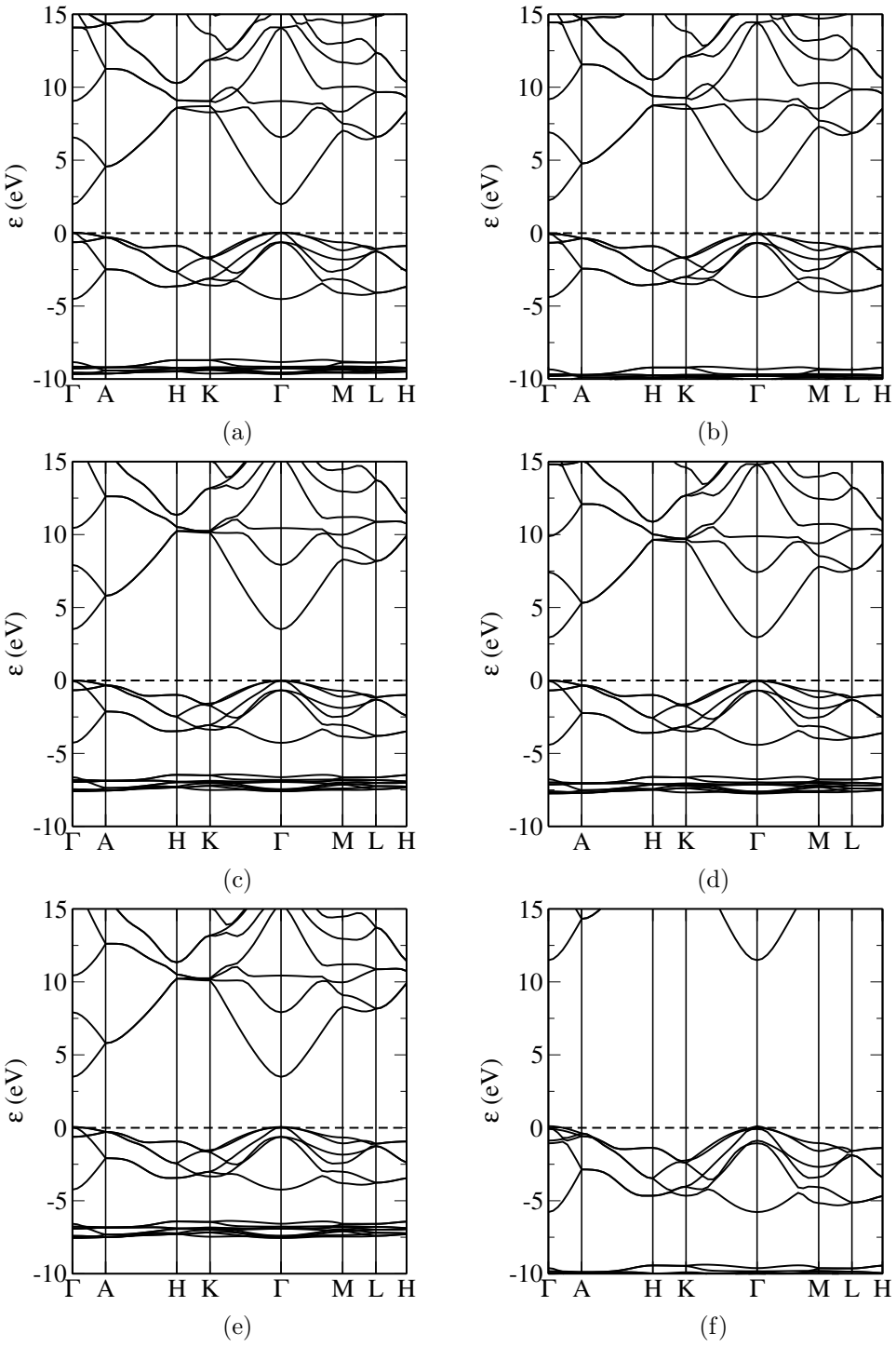

Figure 5.12: Band structures for ZnO using the following potentials; (a) LDA, (b) PBE, (c) EXX, (d) CEDA, (e) LFX and (f) HF. The Fermi level has been set to 0 eV for all band structures. Brillouin zone special points are indexed in appendix C.

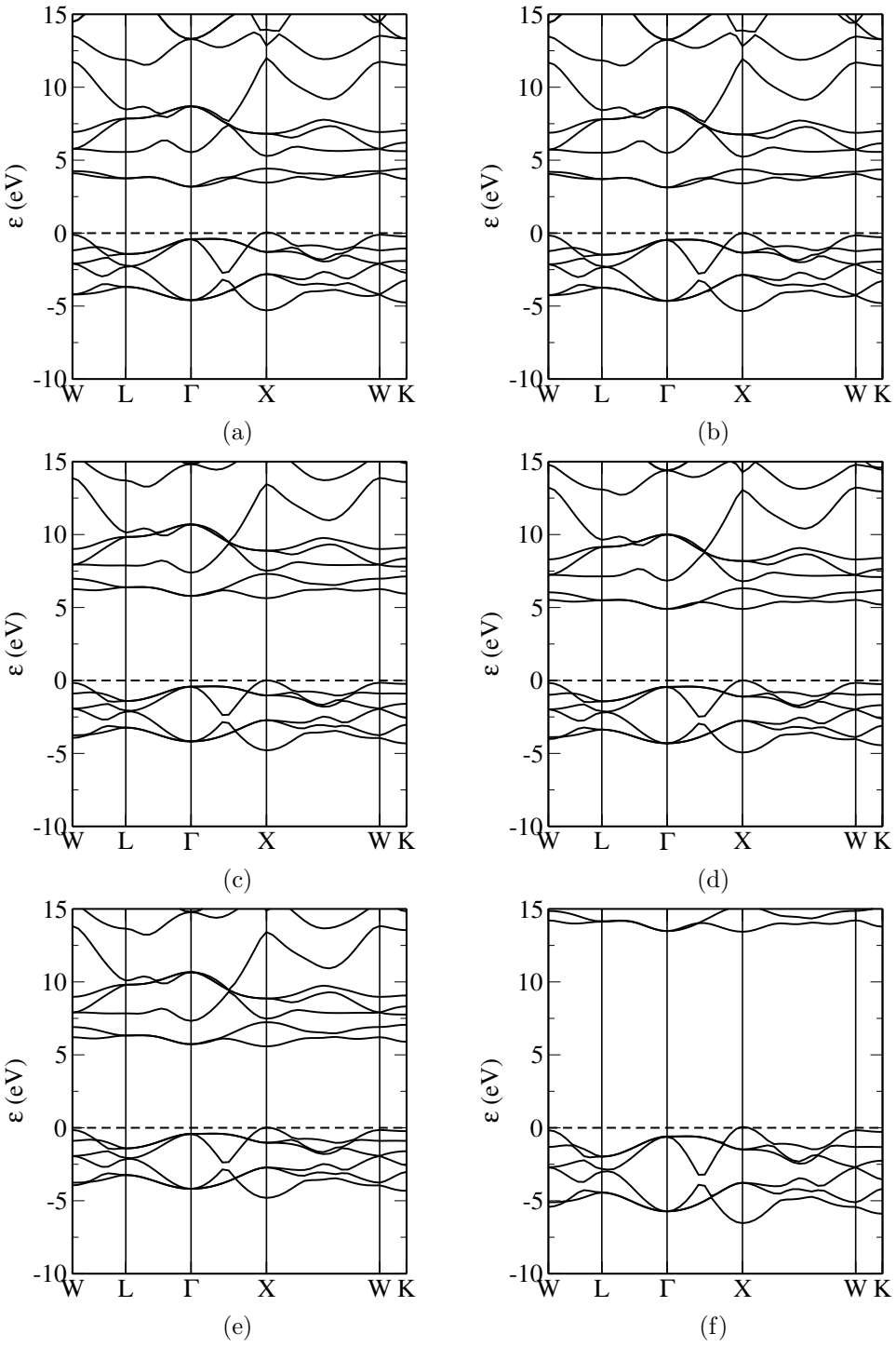

Figure 5.13: Band structures for HfO_2 using the following potentials; (a) LDA, (b) PBE, (c) EXX, (d) CEDA, (e) LFX and (f) HF. The Fermi level has been set to 0 eV for all band structures. Brillouin zone special points are indexed in appendix C.

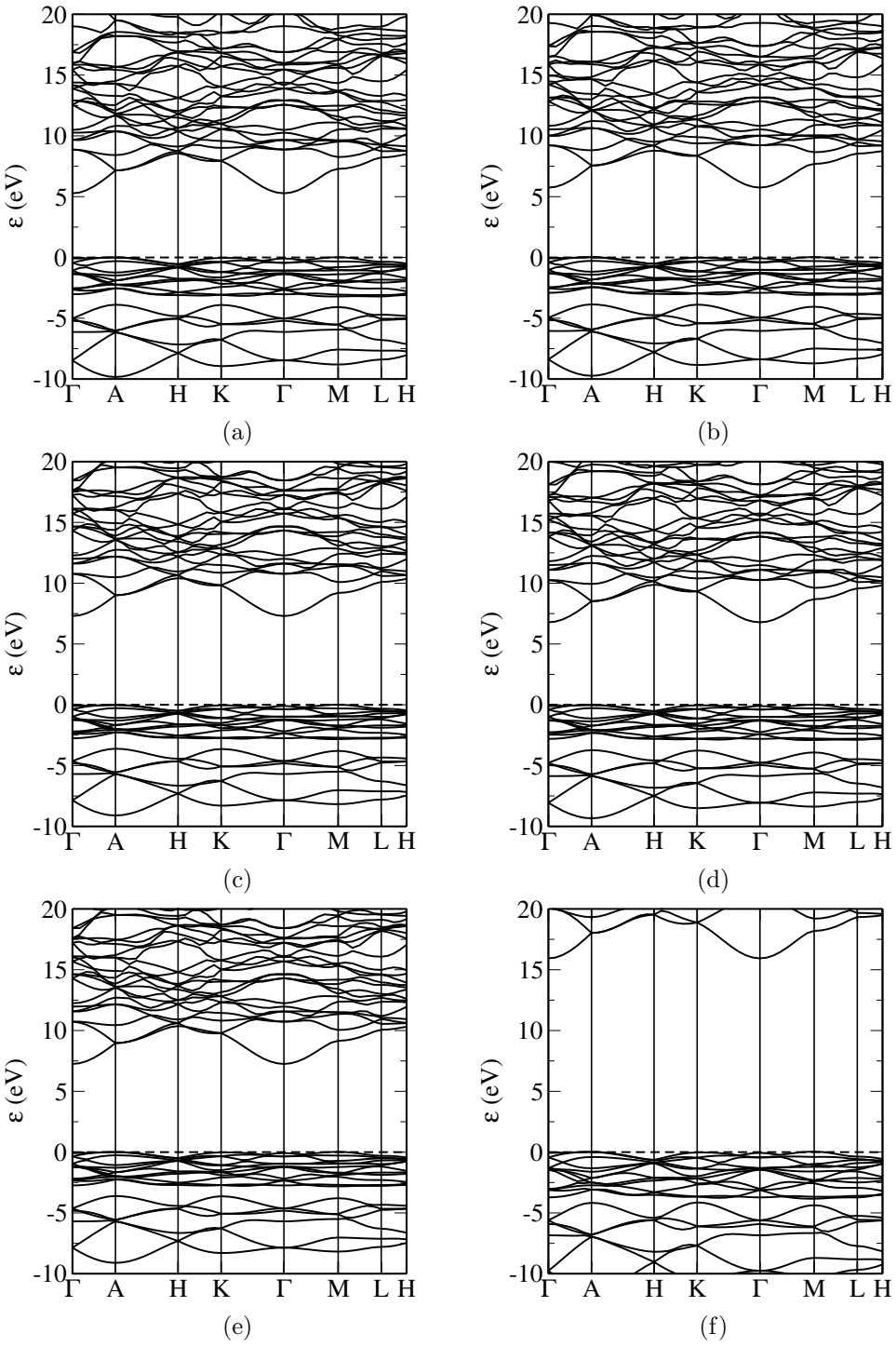

Figure 5.14: Band structures for SiO_2 using the following potentials; (a) LDA, (b) PBE, (c) EXX, (d) CEDA, (e) LFX and (f) HF. The Fermi level has been set to 0 eV for all band structures. Brillouin zone special points are indexed in appendix C.

ment of self interactions is as least as important as inclusion of correlation for the accurate modelling of electronic structures.

5.2 Electronic Structures for Transition Metal Oxides

5.2.1 Introduction

One of the great challenges for density functional theory is the correct description of so called "strongly correlated" materials. The prototypes of these are the transition metal monoxides; MnO, FeO, CoO and NiO. All four of these materials adopt an anti-ferromagnetic insulating ground state. The LDA and GGA to do not correctly reproduce the electronic structure of these materials, giving marginal band gaps in the case of MnO and NiO and metallic behaviour for CoO and FeO. The application of the self-interaction free exchange-only potentials (EXX and LFX) to these materials and the accuracy of the resulting band structures, can be used to determine whether the poor description of the transition metal monoxides by conventional exchange-correlation functionals e.g. LDA, GGA, is due to self-interaction error or an insufficiently nuanced description of correlation.

5.2.2 Calculation Parameters and Unit Cell

The transition metal monoxides adopt a rock salt structure with an antiferromagnetic ground state with the magnetic moments arranged along the [111] direction in the material. The rock salt unit cell is used for all four materials, the rhombohedral distortion for MnO, FeO and NiO and the tetragonal distortion for CoO are ignored, as the distortions are small.[157, 158, 159, 160] The calculation parameters are shown in table 5.10. All

Material	Valence electron configuration	E_{cutoff} (eV)	MP k-point grid	Lattice parameter (Å)
MnO	$3s^2 3p^6 4s^2 3d^5$	2100	$4 \times 4 \times 4$	4.44
FeO	$3s^2 3p^6 4s^2 3d^6$	2100	$4 \times 4 \times 4$	4.33
CoO	$3s^2 3p^6 4s^2 3d^7$	2100	$4 \times 4 \times 4$	4.25
NiO	$3s^2 3p^6 4s^2 3d^8$	2100	$4 \times 4 \times 4$	4.17

Table 5.10: Parameters for calculations on transition metal monoxides. Lattice parameters from [161]. Valence electron configurations are for the transition metal ion, oxygen valence electron configuration is from table 5.3.

calculations on these materials use a rhombohedral unit cell orientated along the [111] direction, to allow magnetic structure to be commensurate with the periodic unit cell. The unit cell for MnO is shown in figure 5.15.

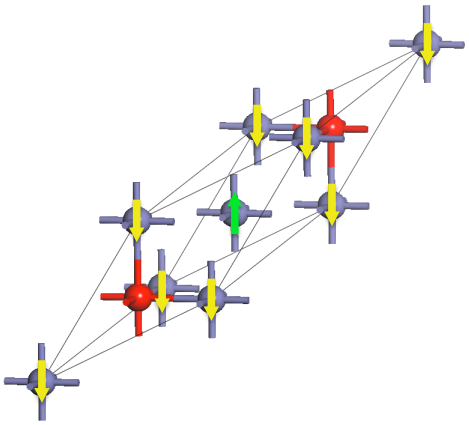

Figure 5.15: Unit cell for MnO, red spheres are O ions and violet spheres are Mn ions. Arrows indicate possible spin moment directions.

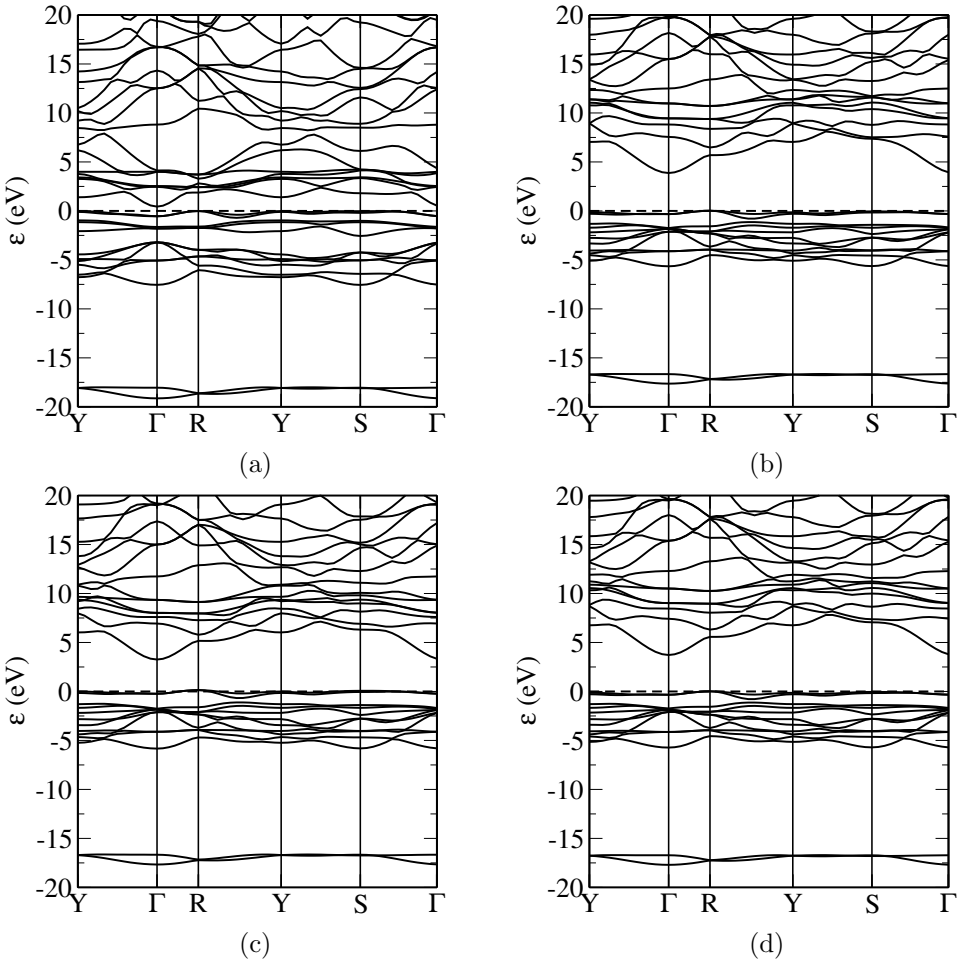

Figure 5.16: Band structures for MnO using the following potentials; (a) LDA, (b) EXX, (c) CEDA and (d) LFX. The Fermi level has been set to 0 eV for all band structures. Brillouin zone special points are indexed in appendix C.

5.2.3 Electronic Structure of MnO

The calculated band structures for MnO for LDA, EXX, CEDA and LFX are shown in figure 5.16. The LDA gives a small band gap with the conduction band minima along the $R \rightarrow Y$ direction and the valence band maxima at the Y point. The EXX, CEDA and LFX band structures are very different from the LDA, because the LDA (and PBE) adopt a different magnetic ground state to that adopted by EXX, CEDA and LFX. This can be seen in the calculated magnetic moments, table 5.11) where the EXX, CEDA, LFX and HF moments are largely the same with the LDA and PBE moments smaller. EXX, CEDA and LFX give conduction band minima at the Γ point.

The EXX and LFX results are also slightly different, in contrast to the results obtained for the semiconductors. The differences from the HF total energy for EXX, CEDA and LFX (table 5.12), show that the trend observed for the semiconductors continues. The EXX and LFX total energies are very close (0.008 eV different) and the CEDA total energy difference from the EXX total energy is an order of magnitude greater at 0.236 eV, which is very similar to the semiconductor results. The calculated Kohn-Sham and experimental band gaps are shown in table 5.13. The EXX and LFX band gap differ by 0.14 eV which is more than was observed for the semiconductors, however both are close to the experimental value. The CEDA result is much better than the LDA and PBE band gaps but is underestimated relative to experiment.

Material	μ (μ_B)						
	LDA	PBE	EXX	CEDA	LFX	HF	Expt.
MnO	4.66	4.76	5.06	5.10	5.04	4.98	4.58, 4.79
FeO	3.68	3.72	4.00	4.06	3.98	3.94	3.32, 4.2
CoO	2.68	2.66	2.98	2.96	2.94	2.90	3.35, 3.98
NiO	1.44	1.58	1.94	1.88	1.90	1.88	1.64, 1.90

Table 5.11: Calculated magnetic moments the transition metal ions for LDA, PBE, EXX, CEDA, LFX and experimental band gaps for transition metal monoxides. A range of experimental values from refs [161].

Material	ΔE (eV)		
	EXX	CEDA	LFX
MnO	0.840	1.076	0.848
FeO	1.487	4.874	1.623
CoO	1.658	2.854	1.748
NiO	1.723	2.724	1.783

Table 5.12: Total energy differences from HF for EXX, CEDA and LFX for transition metal monoxides.

Material	E_g (eV)					
	LDA	PBE	EXX	CEDA	LFX	Expt.
MnO	0.45	0.89	3.85	3.12	3.71	3.9
FeO	0.00	0.00	1.18	0.00	0.70	2.4
CoO	0.00	0.04	2.19	0.27	1.91	2.5
NiO	0.56	1.43	3.84	2.17	3.68	4.0, 4.3

Table 5.13: Calculated Kohn-Sham band gaps for LDA, PBE, EXX, CEDA, LFX and experimental band gaps for transition metal monoxides. Experimental values from refs [161].

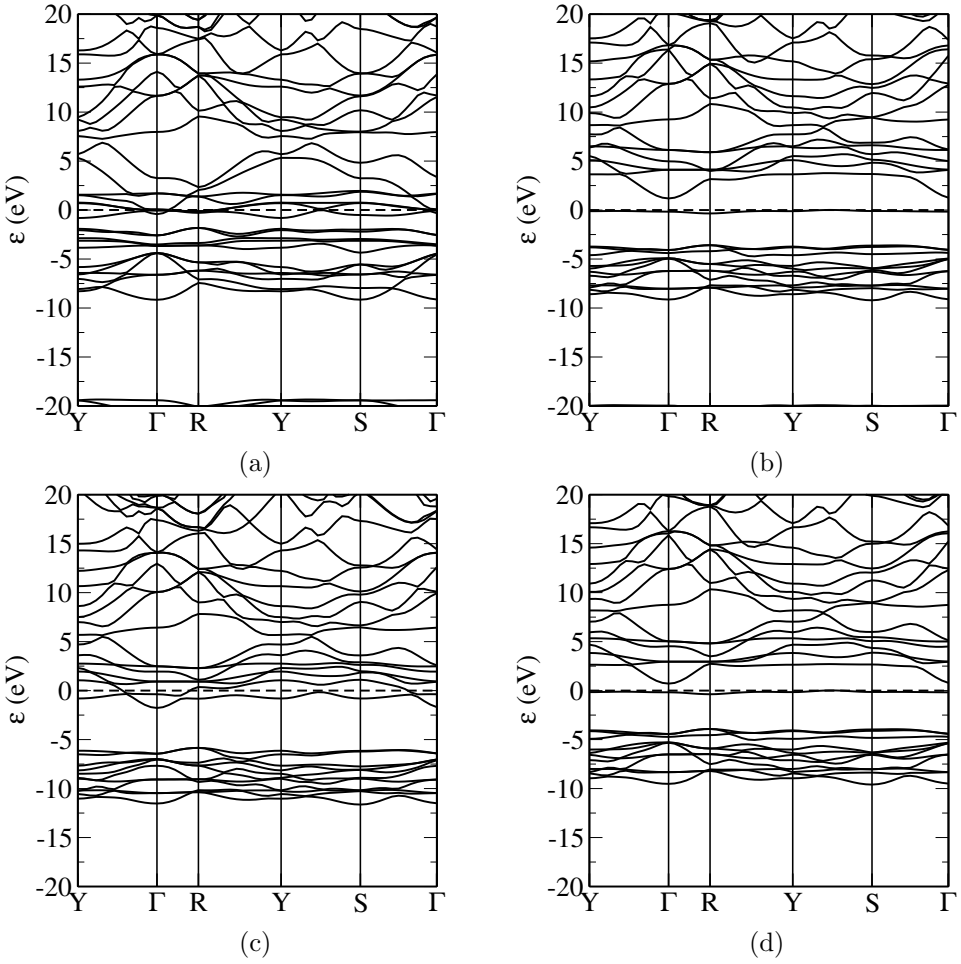

Figure 5.17: Band structures for FeO using the following potentials; (a) LDA, (b) EXX, (c) CEDA and (d) LFX. The Fermi level has been set to 0 eV for all band structures. Brillouin zone special points are indexed in appendix C.

5.2.4 Electronic Structure of FeO

For FeO the LDA, EXX, CEDA and LFX band structures are shown in figure 5.17. Both the LDA and CEDA band structures are qualitatively incorrect giving metallic band structures. Only the EXX and LFX give the correct insulating behaviour with the valence band maxima half way along the $Y \rightarrow S$ direction and the conduction band minima at the Γ point, however the difference in band gap between the two methods is large. The calculated magnetic moments suggest that EXX, CEDA and LFX are adopting the same magnetic state and are in good agreement with experiment. However the EXX and LFX band gaps are not in good agreement with experiment, which suggests that the missing correlation potential in the material has a strong influence on the band structure. The total energy differences also vary much more than for MnO, with a difference of 0.14 eV between EXX and LFX. The CEDA total energy is much higher due to the metallic ground state it adopts.

5.2.5 Electronic Structure of CoO

The band structures for LDA, EXX, CEDA and LFX applied to CoO are shown in figure 5.18. The LDA gives a qualitatively incorrect band structure, with metallic behaviour, CEDA gives a very small gap and EXX and LFX give gaps slightly smaller than the experimental value. The conduction band minimum is again at the Γ point and the valence band maxima are at both the Y and S points. The EXX and LFX again show a significant difference in band gap of 0.28 eV however this is smaller than the difference seen for FeO. The total energy difference between EXX and LFX is also noticeable although again not as large as the difference for FeO. The calculated magnetic moments are also slightly underestimated relative to the experimental values.

5.2.6 Electronic Structure of NiO

Finally the band structures for NiO are shown in figure 5.19. The LDA gives a small gap and EXX, CEDA and LFX give much wider gaps with the EXX and LFX band gaps being quite close to the experimental value. The LDA result is different to the EXX, CEDA and LFX band structures with the conduction band minima in the $R \rightarrow Y$ direction and the valence band maxima at the Y point. The EXX, CEDA and LFX band structures give the conduction band minimum at the Γ point. The LDA (and PBE) adopts a different magnetic ground state from EXX, CEDA and LFX, as can be seen in the calculated magnetic moments. The LDA and PBE moments are smaller than the EXX, CEDA, LFX and HF, which are very close to the experimental values. The energy difference between the EXX and LFX is smaller than FeO and CoO but larger than MnO and the semiconductors. The Kohn-Sham band gap difference between EXX and LFX is similar to that found for MnO, while CEDA underestimates the band gap value significantly.

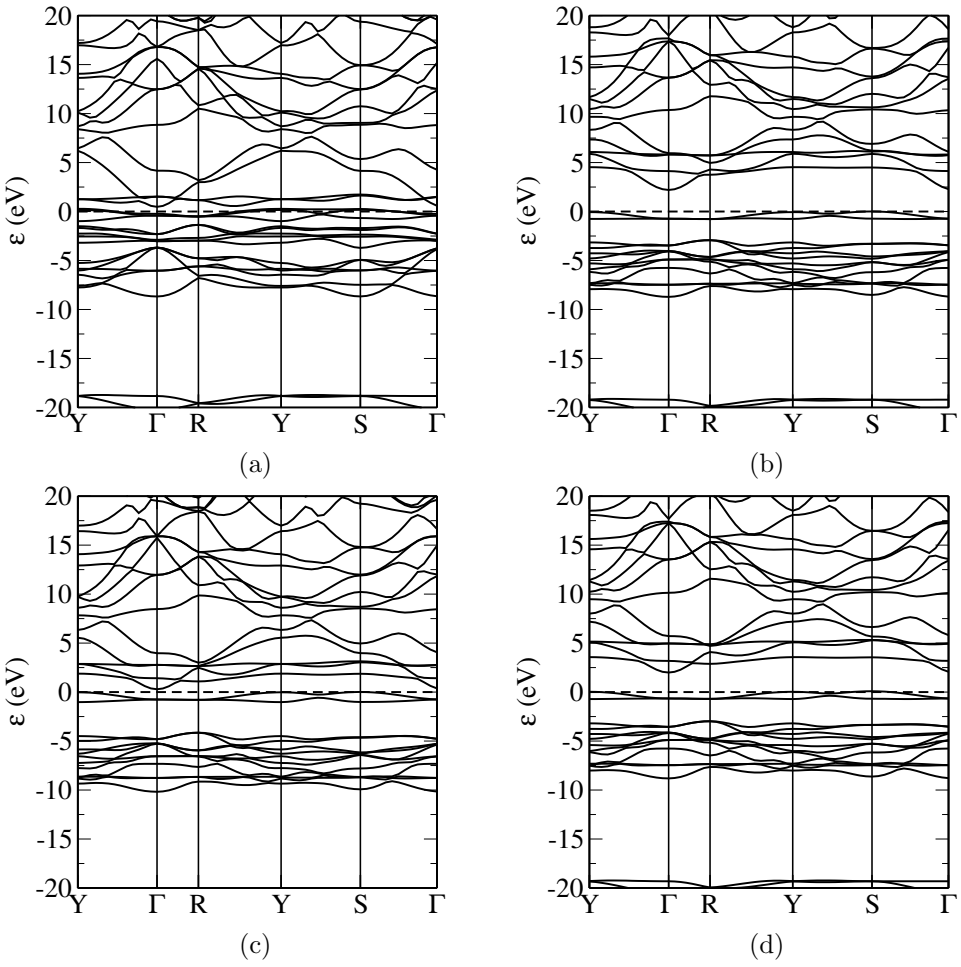

Figure 5.18: Band structures for CoO using the following potentials; (a) LDA, (b) EXX, (c) CEDA and (d) LFX. The Fermi level has been set to 0 eV for all band structures. Brillouin zone special points are indexed in appendix C.

5.2.7 Conclusions for the Transition Metal Monoxides

EXX and LFX give an improved description of the antiferromagnetic transition metal monoxides relative to the LDA and PBE, due to the cancellation of the self interactions in the local exchange-only potentials. However the description is not as close to experiment as that found for the semiconductors. This is not surprising as these materials are strongly correlated and our calculations up to this point neglect this significant contribution. Also unlike for the semiconductors the EXX and LFX results are not nearly identical to each other, as was found previously, but are highly material dependent. The differences between EXX and LFX can probably be explained using the theoretical arguments presented in section 3.7. The band structures, band gaps and magnetic moments for the transition metal monoxides for EXX and CEDA are very similar to those found by Engel *et al.*[103]

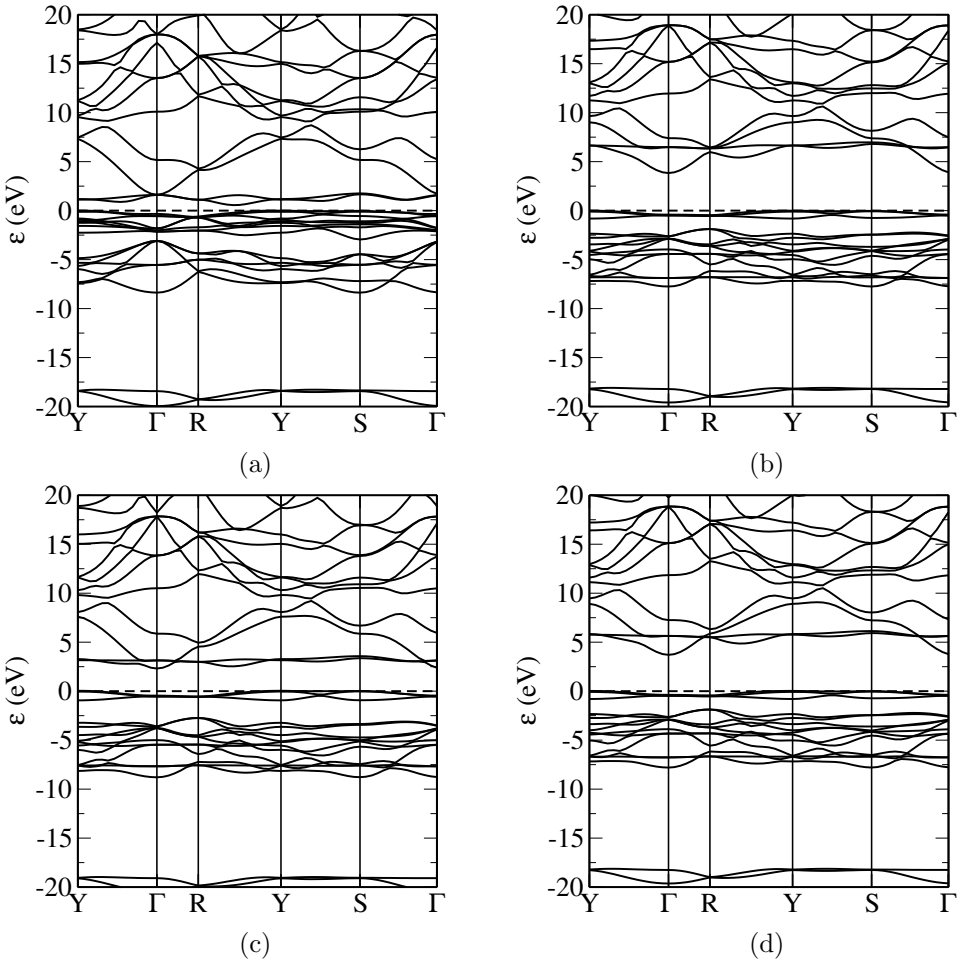

Figure 5.19: Band structures for NiO using the following potentials; (a) LDA, (b) EXX, (c) CEDA and (d) LFX. The Fermi level has been set to 0 eV for all band structures. Brillouin zone special points are indexed in appendix C.

5.3 Band Structures for Metals

5.3.1 Hartree-Fock Treatment of Metals

The different treatment of occupied and unoccupied bands in Hartree-Fock leads to a poor description of the band structure when using HF, see section 3.1.2 in chapter 3. By contrast the LDA gives a good treatment of simple metals. By construction the LDA is exact for the homogeneous electron gas and the closer the metal is to the homogeneous electron gas the more accurate the calculated LDA band structure.

For metals the incorrect behaviour in HF can be best illustrated by using the homogeneous electron gas.[1] If we consider the homogeneous electron gas as a periodic system, it is the simplest possible metal, known as jellium. Jellium is a solid composed of a set of electrons moving in a uniform positive background charge.[41] As the electron gas is homogeneous the density is a constant;

$$\rho(\mathbf{r}) = \frac{N}{\Omega}, \tag{5.5}$$

and the external potential is also uniform and equal and opposite to the homogeneous density, hence the Hartree and external potentials exactly cancel. The solutions to the Schrödinger equation are plane waves;

$$\phi_{\mathbf{k}}(\mathbf{r}) = \frac{1}{\sqrt{\Omega}} e^{i\mathbf{k}.\mathbf{r}}, \tag{5.6}$$

and the Schrödinger equation for jellium is then just composed of the kinetic and exchange terms which assuming a spin degenerate system is given by;

$$-\frac{\nabla^2}{2}\phi_i(\mathbf{r}) - \sum_j^{\frac{N}{2}} \int d\mathbf{r}' \frac{\phi_j^\dagger(\mathbf{r}')\phi_i(\mathbf{r}')}{|\mathbf{r}-\mathbf{r}'|}\phi_j(\mathbf{r}) = \varepsilon_i \phi_i(\mathbf{r}). \tag{5.7}$$

Using the reciprocal form of the Coulomb potential;

$$\frac{1}{|\mathbf{r}-\mathbf{r}'|} = \int \frac{d\mathbf{q}}{(2\pi)^3} \frac{4\pi}{|\mathbf{q}|^2} e^{i\mathbf{q}.(\mathbf{r}-\mathbf{r}')}. \tag{5.8}$$

Substitution of the above into equation 5.7 along with the plane wave form of the wave functions gives the HF dispersion for jellium;

$$\begin{aligned} \varepsilon(\mathbf{k}) &= \frac{|\mathbf{k}|^2}{2} - \int_{|\mathbf{k}'|<|\mathbf{k}_\mathrm{F}|} \frac{d\mathbf{k}'}{(2\pi)^3} \frac{4\pi}{|\mathbf{k}-\mathbf{k}'|^2}, \\ &= \frac{k^2}{2} - \frac{k_\mathrm{F}}{\pi} - \left(\frac{k_\mathrm{F}^2 - k^2}{2\pi k}\right) \ln\left|\frac{k_\mathrm{F}+k}{k_\mathrm{F}-k}\right|. \end{aligned} \tag{5.9}$$

The dispersion for HF diverges logarithmically (has infinite gradient) at the Fermi

[1] These effects are well known for HF, for completeness a brief summary is given below.

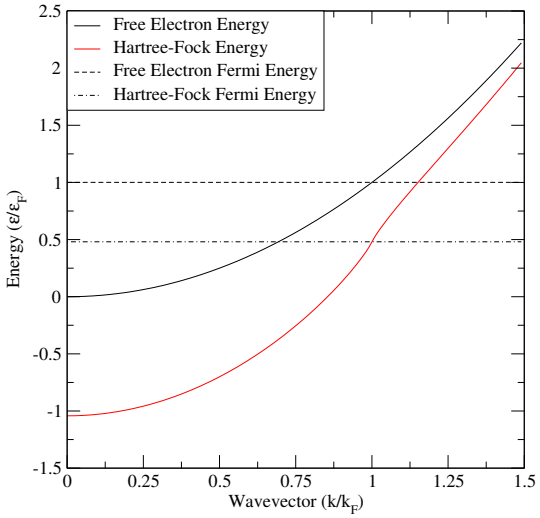

Figure 5.20: Free electron dispersion compared with Hartree-Fock dispersion calculated from equation 5.9.

level. This is plotted compared to the free electron dispersion in figure 5.20. This divergence results in a zero density of states at the Fermi level even for free electrons, as the density of states is proportional to the inverse of the gradient, $\frac{\delta\varepsilon}{\delta\mathbf{k}}$.[41] The valence bandwidth is increased relative to the free electron case, a result that has also been noted in the calculations for semiconductors.

While HF gives a qualitatively incorrect band structure for a free electron the LDA will give the correct (exact) form as it is parameterised by construction to be exact for the case of the homogeneous electron gas. The behaviour of the EXX and LFX potentials when applied to metals remains to be determined.

5.3.2 Application of EXX and LFX to Metals

For a set of metals; jellium, sodium, magnesium, aluminium, calcium and graphene, the band structures were calculated using LDA, EXX, LFX and HF. The calculation parameters for these elemental metals are listed in table 5.14, using the same valence electron configurations for the pseudopotentials listed in table 5.3. Occupancies are smeared with a width of 0.025 eV using Gaussian smearing.

The calculated jellium band structures with 2 electrons per unit cell using LDA, EXX, LFX and HF are shown in figure 5.21. The LDA band structure is the free electron dispersion and the HF band structure shows the expected increased bandwidth and logarithmic dispersion. However the LFX and EXX results show a band structure that is free electron like and identical to the LDA band structure.

The difference in the HF band structure and the EXX/LFX results is likely due to the difference in treatment of the unoccupied bands, in HF the unoccupied bands have self-interaction errors while the occupied bands are self-interaction free. The self-interaction of the HF unoccupied states immediately above the Fermi level pushes the unoccupied

Material	E_{cutoff} (eV)	MP k-point grid	Lattice parameter (Å)	Crystal structure
Jellium	400	$12 \times 12 \times 12$	3.00	simple cubic
Na	1000	$8 \times 8 \times 8$	4.29	body centred cubic
Mg	900	$10 \times 10 \times 7$	3.21/5.21	hexagonal
Al	900	$12 \times 12 \times 12$	4.05	face centred cubic
Ca	1400	$8 \times 8 \times 8$	5.58	face centred cubic
Graphene	1100	$16 \times 16 \times 1$	2.47/20.0	hexagonal

Table 5.14: Parameters for calculations on simple metals. Lattice parameters from [138] except for graphene.[162]

states to higher energies, diminishing the density of states at the Fermi level. For the EXX and LFX all bands are treated identically and are self-interaction free, hence the band structure is that of a free electron.

The EXX and LFX for jellium give the same total energy as shown in table 5.15 which is slightly higher than the HF total energy.

Material	ΔE (eV)	
	EXX	LFX
Jellium	0.003	0.003
Na	0.009	0.009
Mg	0.057	0.058
Al	0.036	0.036
Ca	0.298	0.314
Graphene	0.110	0.110

Table 5.15: Total energy differences from the HF total energy for EXX and LFX.

The band structures for sodium, magnesium and aluminium are shown in figures 5.22, 5.23 and 5.24 respectively. The LDA, EXX and LFX band structures are remarkably similar and the HF band structures show the increased bandwidths and steep slope (possibly logarithmically divergent) at the Fermi level as observed for jellium.

The total energy differences for these three metals, have the same trend seen for semiconductors with the HF total energy bounding the minimal value of the total energy and the EXX total energy lower than the LFX value but within the numerical uncertainty (less than 0.005 eV). They are shown in table 5.15.

The band structures for calcium are shown in figure 5.25, the HF band structure is insulating which is a qualitative failure of the method and most likely due to the energetic preference for fully occupied bands over partially occupied, due to the $n_i^\sigma n_j^\sigma$ term in the (partially occupied) Fock exchange integral. However the EXX and LFX band structures are correctly metallic, which is why the energy difference from the HF total energy is so large as the bands that cross the Fermi level have partial occupancy.

For calcium the LDA, EXX and LFX band structures are similar but not identical as we had found for the band structures of the previous calculations (Jellium, Na, Mg and

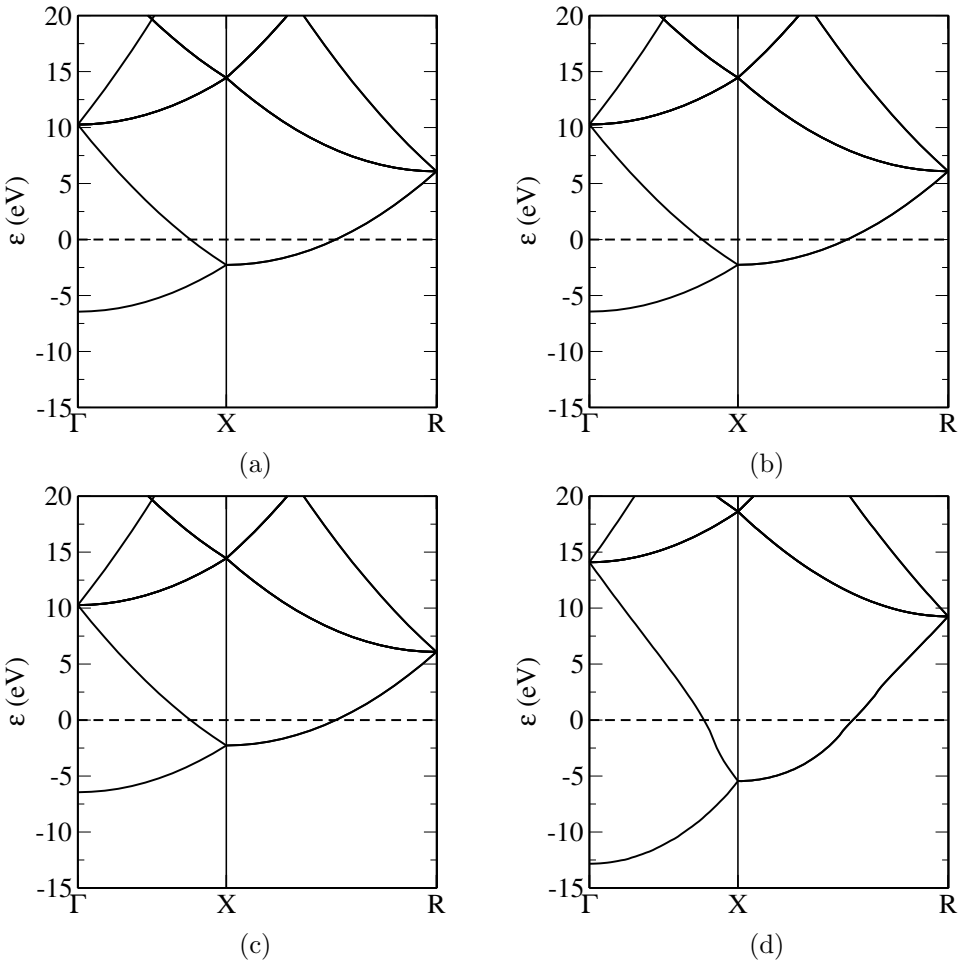

Figure 5.21: Band structures for Jellium using the following potentials; (a) LDA, (b) EXX, (c) LFX and (d) HF. The Fermi level has been set to 0 eV for all band structures. Brillouin zone special points are indexed in appendix C.

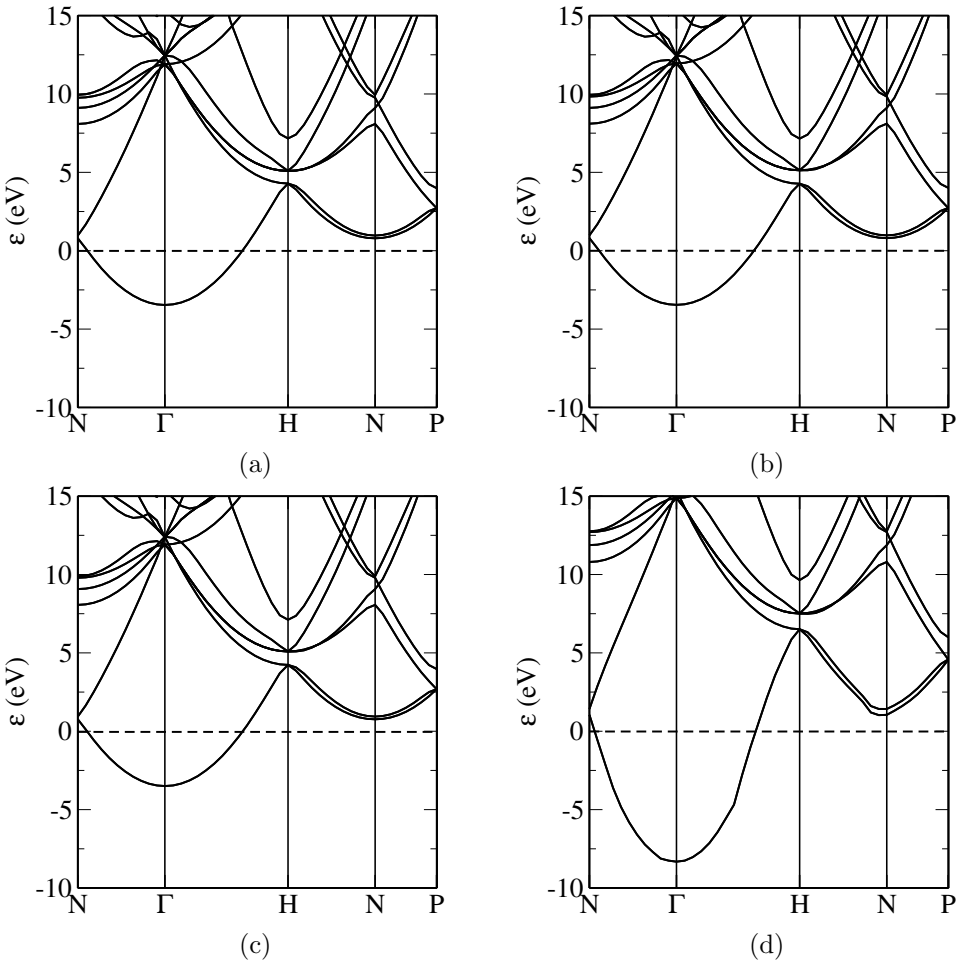

Figure 5.22: Band structures for Na using the following potentials; (a) LDA, (b) EXX, (c) LFX and (d) HF. The Fermi level has been set to 0 eV for all band structures. Brillouin zone special points are indexed in appendix C.

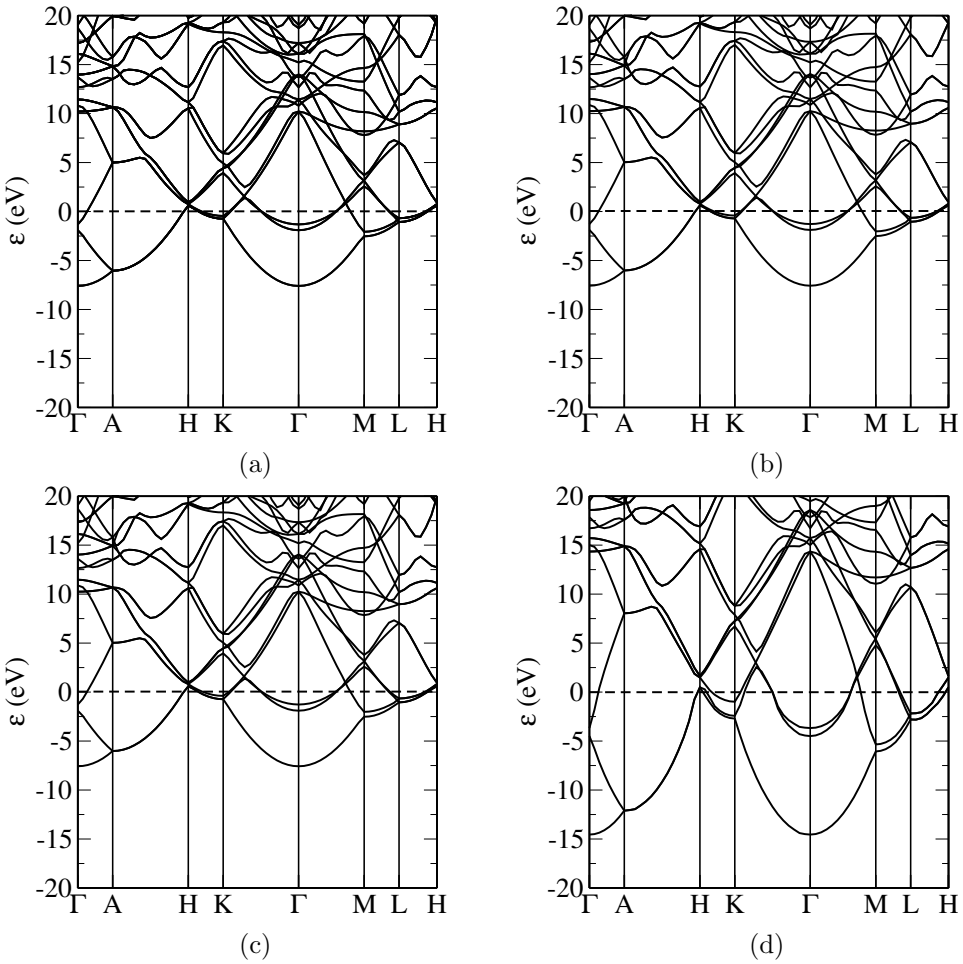

Figure 5.23: Band structures for Mg using the following potentials; (a) LDA, (b) EXX, (c) LFX and (d) HF. The Fermi level has been set to 0 eV for all band structures. Brillouin zone special points are indexed in appendix C.

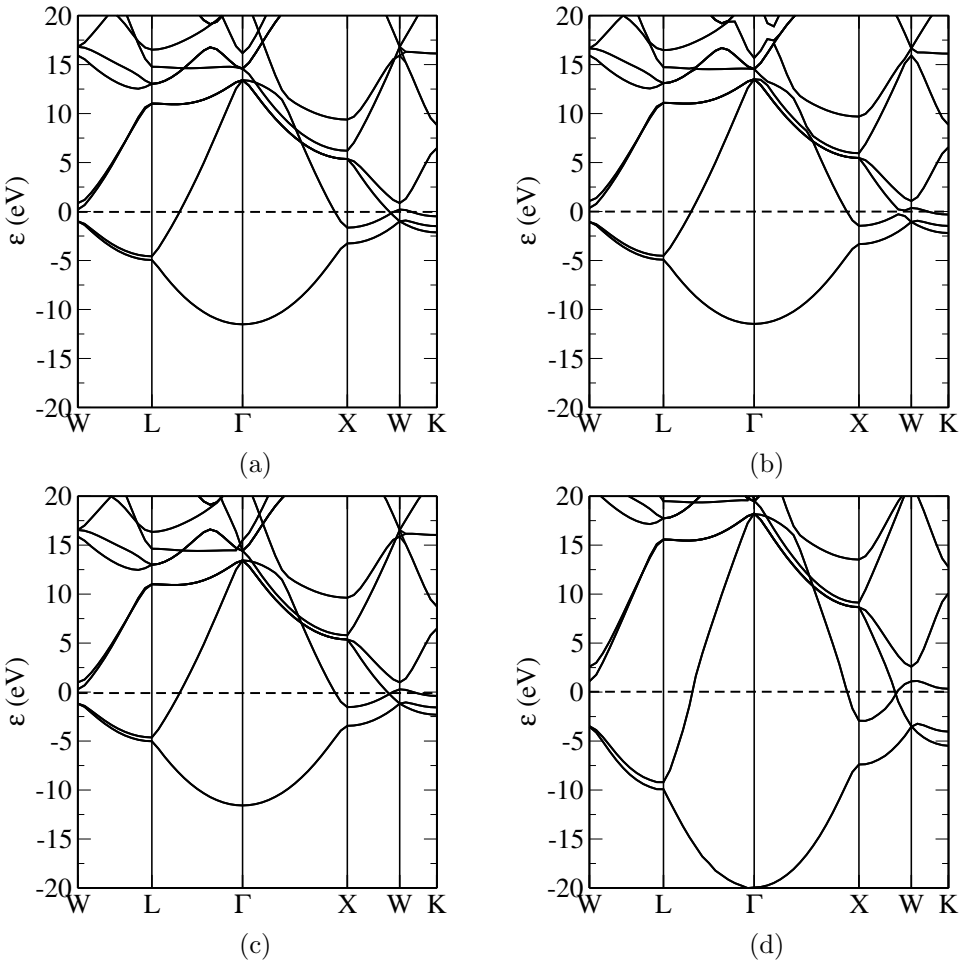

Figure 5.24: Band structures for Al using the following potentials; (a) LDA, (b) EXX, (c) LFX and (d) HF. The Fermi level has been set to 0 eV for all band structures. Brillouin zone special points are indexed in appendix C.

Al). The shape of the bands are almost the same but the most significant difference is at the Fermi level where the band crossings around the W point are different. For EXX and LFX the two bands that cross along the $W \rightarrow L$ direction are split with one crossing close to the W point and one halfway along the direction, whereas for LDA these two bands are nearly degenerate and cross one third of the way along the direction. For the crossing along the $X \rightarrow W$ and $W \rightarrow K$ for EXX and LFX the band crosses much closer to the W point than with LDA. These differences reduce the density states at the Fermi level for EXX and LFX relative to LDA. This was a result noted for calcium in reference [96].

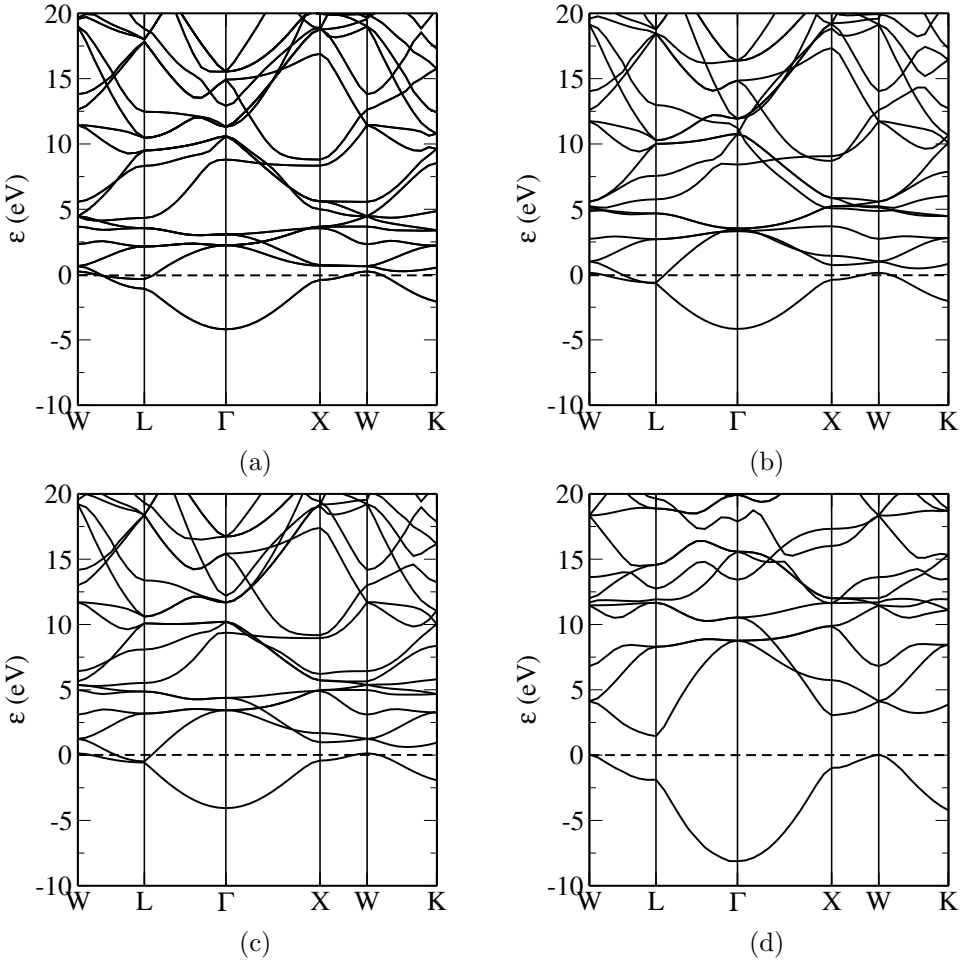

Figure 5.25: Band structures for Ca using the following potentials; (a) LDA, (b) EXX, (c) LFX and (d) HF. The Fermi level has been set to 0 eV for all band structures. Brillouin zone special points are indexed in appendix C.

Graphene band structures for LDA, EXX, LFX and HF are shown in figure 5.26. For LDA, EXX and LFX the characteristic crossing at the K point is reproduced and the EXX and LFX band structures have a slightly increased valence bandwidth relative to LDA. However yet again HF gives a metallic material as insulating. This is for the same reasons as found for calcium, due to the incorrect treatment of the HF unoccupied bands, which is corrected by using a local potential that does not distinguish between

occupied and unoccupied bands.

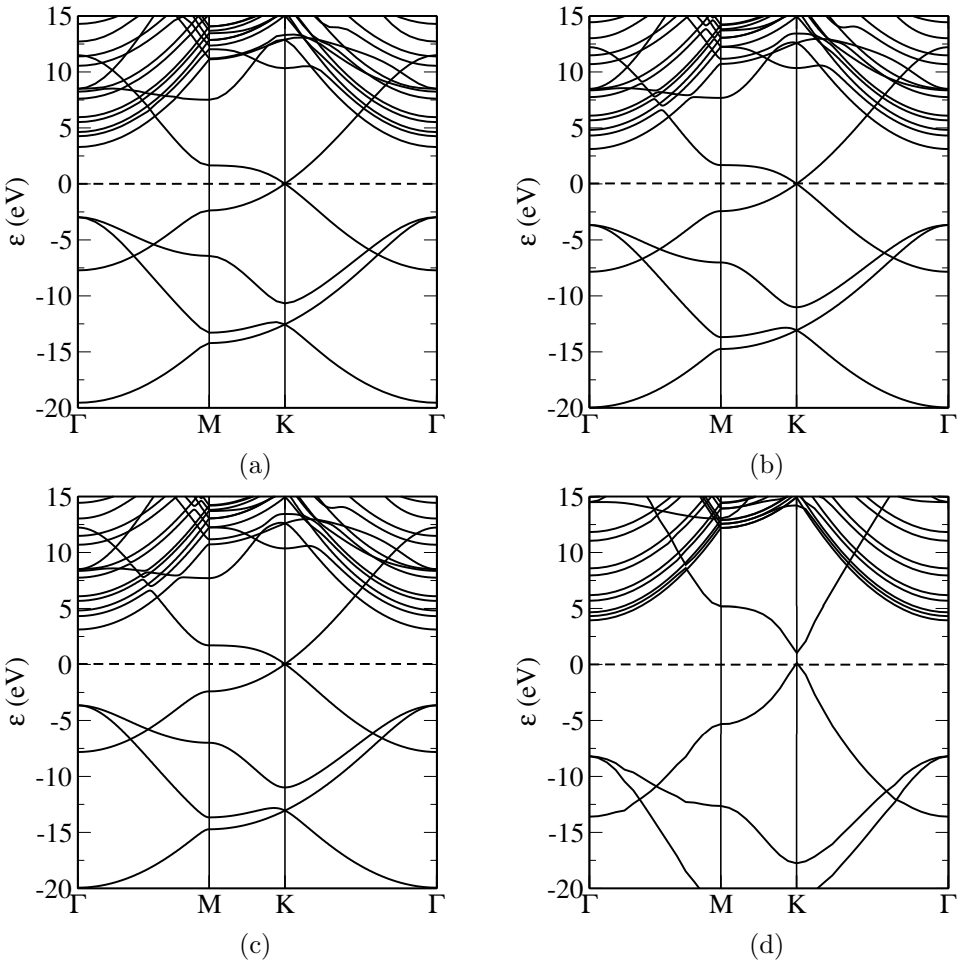

Figure 5.26: Band structures for graphene using the following potentials; (a) LDA, (b) EXX, (c) LFX and (d) HF. The Fermi level has been set to 0 eV for all band structures. Brillouin zone special points are indexed in appendix C.

5.4 Summary

In this chapter the calculated band structures for semiconductors, insulators, transition metal oxides and metals for the LDA, PBE, EXX, LFX, CEDA and HF functionals were presented. The local exchange potentials EXX, CEDA and LFX give a much improved description of the band structures of all the materials presented, relative to the LDA, PBE and HF. As the resulting band structures and potentials are largely identical for EXX and LFX, this confirms the expectation (from section 3.7) that the two potentials capture the same exchange physics. CEDA being an approximation does not give results of the same quality as EXX and LFX but still improves upon the LDA and PBE. For semiconductors and insulators EXX and LFX give band gaps close to experiment, with this agreement becoming less evident the wider the band gap of the material under

investigation. Inclusion of relativity and spin-orbit coupling could improve the accuracy of the calculated band structures for small gap heavy element semiconductors.

EXX, CEDA and LFX perform slightly worse for the transition metal oxides. Although they all give correctly an antiferromagnetic ground state for the materials, the band structures agreement with experiment is poor. For CEDA FeO is metallic and CoO is nearly metallic also. The band structures for EXX and LFX also slightly disagree from each other especially for FeO and CoO.

As was shown, section 3.7 the EXX and LFX are the zeroth order terms of two similar interacting perturbative expansions. It is expected that for weakly correlated systems EXX and LFX will agree, while for strongly correlated systems the two potentials will give different results.

EXX and LFX also give a good description of metals, in contrast to the poor description that results from using HF. This is particularly striking for LFX, which is based on the same HF calculation that gives qualitatively the wrong result, predicting for example semimetallic behaviour for the jellium model.[41, 163] Neither EXX or LFX display the divergence, or steep slope of the dispersion relation, $\varepsilon^{\sigma}_{i,\mathbf{k}}$ vs $\mathbf{k}$, at the Fermi level seen in some HF band structures and both correctly give metallic states when HF would give insulating (calcium and graphene). In the literature (and textbooks)[41, 163, 164], the failure of HF to correctly describe jellium as a metal is attributed is attributed to the lack of correlation in the treatment of the electron-electron interaction and it is argued that by including correlation, the qualitatively incorrect description of metals by HF is rectified. In this case, the main effect of correlation is the screening of the Coulomb repulsion between two electrons at $\mathbf{r}$ and $\mathbf{r}'$, caused by the rearrangement of the other electrons, so as to shield the bare Coulomb field of the exchange potential. By introducing a term that exponentially screens the Hartree-Fock exchange term (see equation 2.56 for the screened exchange (sX) exchange-correlation term) the denominator in the first line of equation 5.9 acquires a constant term that eliminates the divergence.[34, 165] However from the EXX and LFX calculations it is evident that the divergence (or steep slope of the dispersion curve) vanishes when using a local exchange only potential. Hence in the context of density functional theory with a non-interacting system of electrons, the divergence is most likely an artefact of the non-local exchange potential used in HF. While the EXX/LFX band structures for simple metals coincide (almost) with the LDA band structures, the EXX/LFX total energies neglect correlation and differ substantially from the LDA total energies.

Chapter 6

The Derivative Discontinuity

6.1 The Fundamental Band Gap

As discussed in section 5.1.4 there is a difference between the fundamental band gap of a system, E_g, and the Kohn-Sham band gap, E_g^{KS}. The calculated band gaps so far discussed are calculated by;

$$E_{\mathrm{g}}^{\mathrm{KS}} = \varepsilon_{N+1} - \varepsilon_N. \tag{6.1}$$

where ε_{N+1} and ε_N are the $N+1$th and Nth eigenvalues of an N electron system. Whereas the fundamental band gap for an N electron system is defined as the difference between the ionisation energy, $I(N)$ and the electron affinity, $A(N)$ of an N electron system;

$$\begin{aligned} E_{\mathrm{g}} =& I(N) - A(N) \\ =& E(N+1) + E(N-1) - 2E(N), \end{aligned} \tag{6.2}$$

where $E(M)$ is the ground state energy of an m electron system.

From the extension of Koopmans' theorem to density functional theory, the ionisation energy is; $I(N) = -\varepsilon_N^N$ where the superscript is the number of electrons in the system and the subscript is the eigenvalue number.[133] Also the electron affinity of the N system is equal to the ionisation energy of the $N+1$ system. Hence the fundamental band gap can be written;

$$E_{\mathrm{g}} = \varepsilon_{N+1}^{N+1} - \varepsilon_N^N = E_{\mathrm{g}}^{\mathrm{KS}} + \Delta_{\mathrm{xc}}. \tag{6.3}$$

where $\Delta_{\mathrm{xc}} = \varepsilon_{N+1}^{N+1} - \varepsilon_{N+1}^N > 0$ because the $N+1$-th orbital of the $N+1$ system is repelled by N other electrons, while the $N+1$-th orbital of the N system is repelled by $N-1$ other electrons.

To consider the fundamental band gap of an N electron system we must consider the $N+1$ and $N-1$ electron systems as well. For an isolated system (atom or molecule) this is a tractable problem to solve. For a periodic system the number of electrons is infinite,

hence the addition or subtraction of an electron is not a meaningful thing to consider.

However for the exact exchange correlation functional the total energy varies between the $N+1$, N and $N-1$ electron states linearly.[166] Hence the total energies for these three states determine the gradients of the total energy between these three points.

6.2 Fractional Charges

To determine the behaviour of an exchange correlation functional as the number of particles varies between the $N+1$, N and $N-1$ states, we must consider a system with a fractional number of electrons, $N+\omega$, where $0 \leq \omega \leq 1$. Considering such a system there will be $N+1$ orbitals, with occupancies of 1 for all orbitals between 1 and N and occupancy ω for the $N+1$ orbital.[1] The density is given by;

$$\rho^{N+\omega}(\mathbf{r}) = \sum_{i=1}^{N} |\phi_i(\mathbf{r})|^2 + \omega|\phi_{N+1}(\mathbf{r})|^2 = \rho^N(\mathbf{r}) + \omega\rho_{N+1}(\mathbf{r}), \tag{6.4}$$

where a subscript indicates a single particle state index and a superscript the number of electrons in the system. So $\rho_{N+1}(\mathbf{r})$ is a single orbital density for the $N+1$-th state. Directly inputting the density of $N+\omega$ electrons, the ground state total energy is;

$$\begin{aligned}
E^{N+\omega} =& -\frac{1}{2}\sum_{i=1}^{N}\int d\mathbf{r}\phi_i^\dagger(\mathbf{r})\nabla^2\phi_i(\mathbf{r}) - \omega\frac{1}{2}\int d\mathbf{r}\phi_{N+1}^\dagger(\mathbf{r})\nabla^2\phi_{N+1}(\mathbf{r}) \\
&+ \int d\mathbf{r}\hat{V}_{\text{ext}}(\mathbf{r})\rho^{N+\omega}(\mathbf{r}) + \frac{1}{2}\iint d\mathbf{r}d\mathbf{r}'\frac{\rho^{N+\omega}(\mathbf{r})\rho^{N+\omega}(\mathbf{r}')}{|\mathbf{r}-\mathbf{r}'|} + E_{\text{xc}}[\rho^{N+\omega}] \\
=& -\frac{1}{2}\sum_{i=1}^{N}\int d\mathbf{r}\phi_i^\dagger(\mathbf{r})\nabla^2\phi_i(\mathbf{r}) - \omega\frac{1}{2}\int d\mathbf{r}\phi_{N+1}^\dagger(\mathbf{r})\nabla^2\phi_{N+1}(\mathbf{r}) \\
&+ \int d\mathbf{r}\hat{V}_{\text{ext}}(\mathbf{r})\rho^{N+\omega}(\mathbf{r}) + E_{\text{xc}}[\rho^{N+\omega}] + \frac{1}{2}\iint d\mathbf{r}d\mathbf{r}'\frac{\rho^{N}(\mathbf{r})\rho^{N}(\mathbf{r}')}{|\mathbf{r}-\mathbf{r}'|} \\
&+ \omega\iint d\mathbf{r}d\mathbf{r}'\frac{\rho^{N}(\mathbf{r})\rho_{N+1}(\mathbf{r}')}{|\mathbf{r}-\mathbf{r}'|} + \frac{\omega^2}{2}\iint d\mathbf{r}d\mathbf{r}'\frac{\rho_{N+1}(\mathbf{r})\rho_{N+1}(\mathbf{r}')}{|\mathbf{r}-\mathbf{r}'|},
\end{aligned} \tag{6.5}$$

where, the total energy behaves quadratically with changing ω, unless the exchange-correlation term cancels the ω^2 self interaction term for the $N+1$ orbital. Also note the exchange-correlation energy will possibly include higher and/or fractional powers in ω as well.

[1] Assuming the system is spin restricted and there are no degenerate states. The assumption of restricted spin is valid, as we treat the electrons with spin 'up' and spin 'down' as two separate systems coupled by the density. Hence we can add an electron to one spin channel and keep the number of electrons in the other channel fixed.

However in the case of Hartree-Fock, EXX or LFX the total energy is given by;

$$\begin{aligned}
E^{N+\omega} =& -\frac{1}{2}\sum_{i=1}^{N}\int d\mathbf{r}\phi_i^\dagger(\mathbf{r})\nabla^2\phi_i(\mathbf{r}) - \omega\frac{1}{2}\int d\mathbf{r}\phi_{N+1}^\dagger(\mathbf{r})\nabla^2\phi_{N+1}(\mathbf{r}) \\
&+ \int d\mathbf{r}\hat{V}_{\text{ext}}(\mathbf{r})\rho^{N+\omega}(\mathbf{r}) + \frac{1}{2}\iint d\mathbf{r}d\mathbf{r}'\frac{\rho^N(\mathbf{r})\rho^N(\mathbf{r}')}{|\mathbf{r}-\mathbf{r}'|} \\
&+ \frac{2\omega}{2}\iint d\mathbf{r}d\mathbf{r}'\frac{\rho^N(\mathbf{r})\rho_{N+1}(\mathbf{r}')}{|\mathbf{r}-\mathbf{r}'|} + \frac{\omega^2}{2}\iint d\mathbf{r}d\mathbf{r}'\frac{\rho_{N+1}(\mathbf{r})\rho_{N+1}(\mathbf{r}')}{|\mathbf{r}-\mathbf{r}'|} \\
&- \frac{1}{2}\iint d\mathbf{r}d\mathbf{r}'\frac{|\rho^N(\mathbf{r},\mathbf{r}')|^2}{|\mathbf{r}-\mathbf{r}'|} - \omega\iint d\mathbf{r}d\mathbf{r}'\frac{\rho^N(\mathbf{r},\mathbf{r}')\rho_{N+1}(\mathbf{r}',\mathbf{r})}{|\mathbf{r}-\mathbf{r}'|} \\
&- \frac{\omega^2}{2}\iint d\mathbf{r}d\mathbf{r}'\frac{\rho_{N+1}(\mathbf{r})\rho_{N+1}(\mathbf{r}')}{|\mathbf{r}-\mathbf{r}'|} \qquad (6.6) \\
=& -\frac{1}{2}\sum_{i=1}^{N}\int d\mathbf{r}\phi_i^\dagger(\mathbf{r})\nabla^2\phi_i(\mathbf{r}) - \omega\frac{1}{2}\int d\mathbf{r}\phi_{N+1}^\dagger(\mathbf{r})\nabla^2\phi_{N+1}(\mathbf{r}) \\
&+ \int d\mathbf{r}\hat{V}_{\text{ext}}(\mathbf{r})\rho^{N+\omega}(\mathbf{r}) + \frac{1}{2}\iint d\mathbf{r}d\mathbf{r}'\frac{\rho^N(\mathbf{r})\rho^N(\mathbf{r}')}{|\mathbf{r}-\mathbf{r}'|} \\
&+ \omega\iint d\mathbf{r}d\mathbf{r}'\frac{\rho^N(\mathbf{r})\rho_{N+1}(\mathbf{r}')}{|\mathbf{r}-\mathbf{r}'|} - \frac{1}{2}\iint d\mathbf{r}d\mathbf{r}'\frac{|\rho^N(\mathbf{r},\mathbf{r}')|^2}{|\mathbf{r}-\mathbf{r}'|} \\
&- \omega\iint d\mathbf{r}d\mathbf{r}'\frac{\rho^N(\mathbf{r},\mathbf{r}')\rho_{N+1}(\mathbf{r}',\mathbf{r})}{|\mathbf{r}-\mathbf{r}'|},
\end{aligned}$$

which is linear in ω, as the exchange term cancels the self-interaction.

Note the HF total energy is linear under the assumption the orbitals are frozen during the change in occupation, but the behaviour of the total energy will also be strongly influenced by the relaxation of the orbitals during the energy minimisation. The behaviour of the HF total energy with changing occupancy will be demonstrated in the next section.

6.3 Total Energy of Fluorine for Fractional Charges

The energy dependence of fluorine for the LDA, EXX, LFX and HF was calculated for the F atom, F^+ and F^- ions as well as for fractional charges in-between. Fluorine was chosen as it is the most electronegative atom in the periodic table and hence most likely to strongly bind a negative ion. The neutral fluorine atom has 9 electrons, hence one spin channel has 5 electrons and the other has 4 electrons. To respect Hund's rules the F^+ ion has 5 and 3 electrons respectively in each spin channel and the F^- ion has 5 electrons in each spin channel.

Calculations were carried out using an isolated atom/ion in a cubic box for which no symmetry operations were applied. Addition or removal of charge leads to a divergence in the total energy as the unit cell is non-charge neutral and we have an infinite periodic lattice of such non-charge neutral cells. To account for this a uniform background charge is added to create a neutral unit cell, as was done to overcome the divergences in the

electrostatic potential energy as was shown in section 2.4.6.

Calculations were performed using a cut off of 1000 eV and a single k-point at the Γ point, hence these calculations were converged to an accuracy of 0.001 eV. To account for the electrostatic effects of having ions and uniform background charges, calculations were performed using three cubic unit cells, with lattice parameters of 10Å, 12Å and 15Å. Using the three calculated total energy values the total energy is found in the limit of an infinite unit cell size, which would have no interaction of the ions between the unit cells and vanishing uniform background charge.[2] This is shown in figure 6.1, for the neutral atom the total energies are largely invariant to the changing unit cell size, however the two charged cells have significant electrostatic interactions, which are eliminated by projecting the total energies to the infinite cell size limit.

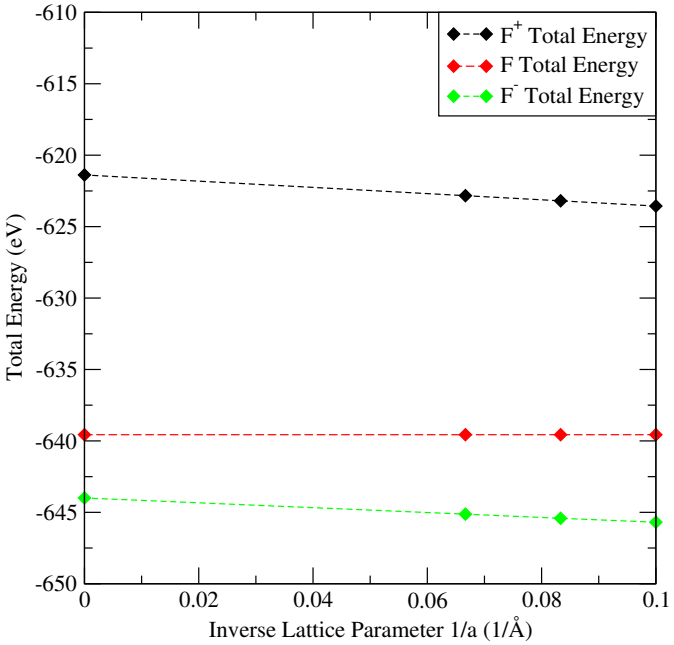

Figure 6.1: LDA total energies for fluorine for the F atom, F^+ and F^- ions, using the 10Å, 12Å and 15Å lattice parameters with projected total energy for an infinite lattice parameter.

The total energies for fluorine are shown in figure 6.2, as can be seen for all four functionals none display the linear behaviour of the exact exchange correlation functional. The LDA is quadratic with changing fractional charge, as the self-interaction term in ω^2 is not cancelled. The HF, EXX and LFX are much closer to the desired linear behaviour as the self interactions are cancelled, but as the orbitals are minimised for the given occupation and change as ω is varied the total energy is not perfectly linear.[167, 168, 169] Despite fluorine's electronegativity for the a fractional charge of 0.1 the ion is unbound for HF. The unbound state for a fractional charge of 0.1 is unexpected as fractional charges greater than 0.1 are bound. The cause of the unbound state is not currently

[2]The uniform background charge density should integrate to the excess fractional charge in the non-charge neutral cell. Hence for an infinite cell the background charge density tends to zero.

understood.

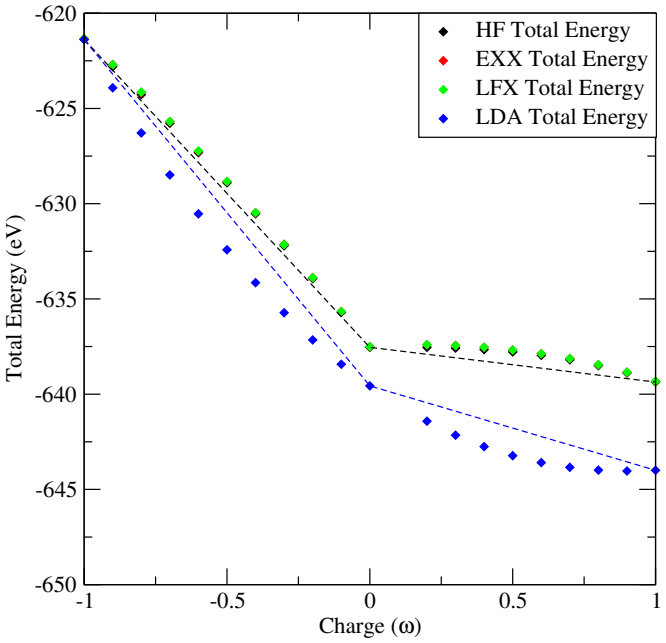

Figure 6.2: Total energies for fluorine for LDA, EXX, LFX and HF projected to the infinite lattice parameter limit. Dashed lines are the linear behaviour for; black HF and blue LDA. The HF, EXX and LFX points overlap.

6.4 Ensembles

The physically correct description of a system of fractional charges is to consider an ensemble of integer electron states.[3] The ensemble total energy is;

$$E^{N+\omega} = (1-\omega)E^{N}[\rho^{N}] + \omega E^{N+1}[\rho^{N+1}], \tag{6.7}$$

the ensemble density retains its definition from equation 6.4 and the orbitals satisfy the ensemble Kohn-Sham equations;

$$\left[-\frac{\nabla^2}{2} + \hat{V}_{\text{ext}}(\mathbf{r}) + \int d\mathbf{r}' \frac{\rho^{N+\omega}(\mathbf{r})}{|\mathbf{r}-\mathbf{r}'|} + \frac{\partial E_{\text{xc}}^{N+\omega}}{\partial \rho(\mathbf{r})}\right] \phi_i(\mathbf{r}) = \varepsilon_i \phi_i(\mathbf{r}). \tag{6.8}$$

[3]This is a correct description as a system with non-integer electron number is unphysical.

The ensemble energy functional is then;

$$\begin{aligned}E^{N+\omega} =& -\frac{1}{2}\sum_{i=1}^{N}\int d\mathbf{r}\phi_i^\dagger(\mathbf{r})\nabla^2\phi_i(\mathbf{r}) - \omega\frac{1}{2}\int d\mathbf{r}\phi_{N+1}^\dagger(\mathbf{r})\nabla^2\phi_{N+1}(\mathbf{r})\\ &+\int d\mathbf{r}\hat{V}_{\text{ext}}(\mathbf{r})\rho^{N+\omega}(\mathbf{r}) + \frac{1}{2}\iint d\mathbf{r}d\mathbf{r}'\frac{\rho^N(\mathbf{r})\rho^N(\mathbf{r}')}{|\mathbf{r}-\mathbf{r}'|}\\ &+\frac{2\omega}{2}\iint d\mathbf{r}d\mathbf{r}'\frac{\rho^N(\mathbf{r})\rho_{N+1}(\mathbf{r}')}{|\mathbf{r}-\mathbf{r}'|} + \frac{\omega}{2}\iint d\mathbf{r}d\mathbf{r}'\frac{\rho^N(\mathbf{r})\rho^N(\mathbf{r}')}{|\mathbf{r}-\mathbf{r}'|},\\ &+(1-\omega)E_{\text{xc}}^N[\rho^N] + \omega E_{\text{xc}}^{N+1}[\rho^{N+1}].\end{aligned} \tag{6.9}$$

This function is linear in ω.[4] This allows us to consider the fundamental band gap in terms of the derivatives of the energy with respect to the occupancy;

$$E_{\text{g}} = \left.\frac{\partial E^{N+\omega}}{\partial N}\right|_{N+\omega} - \left.\frac{\partial E^{N-\omega}}{\partial N}\right|_{N-\omega}, \tag{6.10}$$

the gradient is given by;

$$\begin{aligned}\frac{\partial E^{N+\omega}}{\partial N} =& E(N+1) - E(N)\\ =& -\frac{1}{2}\int d\mathbf{r}\phi_{N+1}^\dagger(\mathbf{r})\nabla^2\phi_{N+1}(\mathbf{r}) + \int d\mathbf{r}\hat{V}_{\text{ext}}(\mathbf{r})\rho_{N+1}(\mathbf{r})\\ &+\iint d\mathbf{r}d\mathbf{r}'\frac{\rho^N(\mathbf{r})\rho_{N+1}(\mathbf{r}')}{|\mathbf{r}-\mathbf{r}'|} + \frac{1}{2}\iint d\mathbf{r}d\mathbf{r}'\frac{\rho_{N+1}(\mathbf{r})\rho_{N+1}(\mathbf{r}')}{|\mathbf{r}-\mathbf{r}'|}\\ &+E_{\text{xc}}^{N+1}[\rho^{N+1}] - E_{\text{xc}}^N[\rho^N]\\ =& \left[-\frac{1}{2}\int d\mathbf{r}\phi_{N+1}^\dagger(\mathbf{r})\nabla^2\phi_{N+1}(\mathbf{r}) + \int d\mathbf{r}\hat{V}_{\text{ext}}(\mathbf{r})\rho_{N+1}(\mathbf{r})\right.\\ &\left.+\iint d\mathbf{r}d\mathbf{r}'\frac{\rho^N(\mathbf{r})\rho_{N+1}(\mathbf{r}')}{|\mathbf{r}-\mathbf{r}'|} + \int d\mathbf{r}\frac{\partial E_{\text{xc}}^N}{\partial\rho(\mathbf{r})}\rho_{N+1}(\mathbf{r})\right]\\ &+\frac{1}{2}\iint d\mathbf{r}d\mathbf{r}'\frac{\rho_{N+1}(\mathbf{r})\rho_{N+1}(\mathbf{r}')}{|\mathbf{r}-\mathbf{r}'|} - \int d\mathbf{r}\frac{\partial E_{\text{xc}}^N}{\partial\rho(\mathbf{r})}\rho_{N+1}(\mathbf{r})\\ &+E_{\text{xc}}^{N+1}[\rho^{N+1}] - E_{\text{xc}}^N[\rho^N],\end{aligned} \tag{6.11}$$

the term in the square brackets is the $N+1$ eigenvalue of an N electron system;

$$\begin{aligned}\frac{\partial E^{N+\omega}}{\partial N} =& \varepsilon_{N+1}^N + \frac{1}{2}\iint d\mathbf{r}d\mathbf{r}'\frac{\rho_{N+1}(\mathbf{r})\rho_{N+1}(\mathbf{r}')}{|\mathbf{r}-\mathbf{r}'|} - \int d\mathbf{r}\frac{\partial E_{\text{xc}}^N}{\partial\rho(\mathbf{r})}\rho_{N+1}(\mathbf{r})\\ &+E_{\text{xc}}^{N+1}[\rho^{N+1}] - E_{\text{xc}}^N[\rho^N],\end{aligned} \tag{6.12}$$

alternatively the gradient can be arranged to give the $N+1$ eigenvalue of an $N+1$

[4] We continue to consider a spin restricted system.

electron system, which becomes;

$$\frac{\partial E^{N+\omega}}{\partial N} = \varepsilon_{N+1}^{N+1} - \frac{1}{2}\iint d\mathbf{r}d\mathbf{r}' \frac{\rho_{N+1}(\mathbf{r})\rho_{N+1}(\mathbf{r}')}{|\mathbf{r}-\mathbf{r}'|} - \int d\mathbf{r} \frac{\partial E_{\mathrm{xc}}^{N+1}}{\partial \rho(\mathbf{r})}\rho_{N+1}(\mathbf{r}) + E_{\mathrm{xc}}^{N+1}[\rho^{N+1}] - E_{\mathrm{xc}}^{N}[\rho^{N}]. \tag{6.13}$$

6.5 The Derivative Discontinuity

6.5.1 The Exact Derivative Discontinuity

From equation 6.10 we have a definition of the fundamental band gap in terms of the gradients. Hence the exact fundamental band gap is;

$$\begin{aligned} E_{\mathrm{g}} &= \left.\frac{\partial E^{N+\omega}}{\partial N}\right|_{N+\omega} - \left.\frac{\partial E^{N-\omega}}{\partial N}\right|_{N-\omega} \\ &= \varepsilon_{N+1}^{N} - \varepsilon_{N}^{N} + \frac{1}{2}\iint d\mathbf{r}d\mathbf{r}' \frac{\rho_{N+1}(\mathbf{r})\rho_{N+1}(\mathbf{r}')}{|\mathbf{r}-\mathbf{r}'|} + \frac{1}{2}\iint d\mathbf{r}d\mathbf{r}' \frac{\rho_{N}(\mathbf{r})\rho_{N}(\mathbf{r}')}{|\mathbf{r}-\mathbf{r}'|} \\ &\quad - \int d\mathbf{r} \frac{\partial E_{\mathrm{xc}}^{N}}{\partial \rho(\mathbf{r})}[\rho_{N+1}(\mathbf{r}) - \rho_{N}(\mathbf{r})] + E_{\mathrm{xc}}^{N+1}[\rho^{N+1}] - 2E_{\mathrm{xc}}^{N}[\rho^{N}] + E_{\mathrm{xc}}^{N-1}[\rho^{N-1}]. \end{aligned} \tag{6.14}$$

Returning to the definition of the fundamental band gap and Kohn-Sham band gap;

$$E_{\mathrm{g}} = E_{\mathrm{g}}^{\mathrm{KS}} + \varepsilon_{N+1}^{N+1} - \varepsilon_{N+1}^{N} = E_{\mathrm{g}}^{\mathrm{KS}} + \Delta_{\mathrm{xc}}, \tag{6.15}$$

and the exact derivative discontinuity is then;

$$\begin{aligned} \Delta_{\mathrm{xc}} &= \frac{1}{2}\iint d\mathbf{r}d\mathbf{r}' \frac{\rho_{N+1}(\mathbf{r})\rho_{N+1}(\mathbf{r}')}{|\mathbf{r}-\mathbf{r}'|} + \frac{1}{2}\iint d\mathbf{r}d\mathbf{r}' \frac{\rho_{N}(\mathbf{r})\rho_{N}(\mathbf{r}')}{|\mathbf{r}-\mathbf{r}'|} \\ &\quad - \int d\mathbf{r} \frac{\partial E_{\mathrm{xc}}^{N}}{\partial \rho(\mathbf{r})}[\rho_{N+1}(\mathbf{r}) - \rho_{N}(\mathbf{r})] + E_{\mathrm{xc}}^{N+1}[\rho^{N+1}] - 2E_{\mathrm{xc}}^{N}[\rho^{N}] + E_{\mathrm{xc}}^{N-1}[\rho^{N-1}]. \end{aligned} \tag{6.16}$$

6.5.2 Derivative Discontinuity for Local Density Functionals

For any density dependent functional (LDA and GGAs) the first term in the second line of equation 6.16 is the Taylor expansion of the last term in the second line;

$$\int d\mathbf{r} \frac{\partial E_{\mathrm{xc}}^{N}}{\partial \rho(\mathbf{r})}[\rho_{N+1}(\mathbf{r}) - \rho_{N}(\mathbf{r})] \simeq E_{\mathrm{xc}}^{N+1}[\rho^{N+1}] - 2E_{\mathrm{xc}}^{N}[\rho^{N}] + E_{\mathrm{xc}}^{N-1}[\rho^{N-1}], \tag{6.17}$$

and the derivative discontinuity simplifies to;

$$\Delta_{\mathrm{xc}}^{\mathrm{LDA,GGA}} = \frac{1}{2}\iint d\mathbf{r}d\mathbf{r}' \frac{\rho_{N+1}(\mathbf{r})\rho_{N+1}(\mathbf{r}')}{|\mathbf{r}-\mathbf{r}'|} + \frac{1}{2}\iint d\mathbf{r}d\mathbf{r}' \frac{\rho_{N}(\mathbf{r})\rho_{N}(\mathbf{r}')}{|\mathbf{r}-\mathbf{r}'|}. \tag{6.18}$$

This is an unexpected result as the LDA and GGA are presumed to have no derivative discontinuity.[167, 168] This assumption is based on the LDA total energy in figure 6.2 being continuous around $\omega = 0$, when directly considering fractional charges.

6.5.3 Derivative Discontinuity for Orbital Dependent Local Functionals

For EXX and LFX, if the correlation energy terms are neglected we obtain;

$$\begin{aligned}\Delta_{\mathrm{x}} = &\frac{1}{2}\iint d\mathbf{r}d\mathbf{r}'\frac{\rho_{N+1}(\mathbf{r})\rho_{N+1}(\mathbf{r}')}{|\mathbf{r}-\mathbf{r}'|} + \frac{1}{2}\iint d\mathbf{r}d\mathbf{r}'\frac{\rho_{N}(\mathbf{r})\rho_{N}(\mathbf{r}')}{|\mathbf{r}-\mathbf{r}'|} \\ &- \int d\mathbf{r}\frac{\partial E_{\mathrm{x}}^{N}}{\partial\rho(\mathbf{r})}[\rho_{N+1}(\mathbf{r})-\rho_{N}(\mathbf{r})] + E_{\mathrm{x}}^{N+1}[\rho^{N+1}] - 2E_{\mathrm{x}}^{N}[\rho^{N}] + E_{\mathrm{x}}^{N-1}[\rho^{N-1}],\end{aligned} \tag{6.19}$$

the difference in the exchange energies between $N+1$ and N is;

$$\begin{aligned}E_{\mathrm{x}}^{N+1} - E_{\mathrm{x}}^{N} =& -\frac{1}{2}\iint d\mathbf{r}d\mathbf{r}'\frac{\rho^{N+1}(\mathbf{r},\mathbf{r}')\rho^{N+1}(\mathbf{r}',\mathbf{r})}{|\mathbf{r}-\mathbf{r}'|} \\ &+\frac{1}{2}\iint d\mathbf{r}d\mathbf{r}'\frac{\rho^{N}(\mathbf{r},\mathbf{r}')\rho^{N}(\mathbf{r}',\mathbf{r})}{|\mathbf{r}-\mathbf{r}'|} \\ =& -\frac{1}{2}\iint d\mathbf{r}d\mathbf{r}'\frac{[\rho^{N}(\mathbf{r},\mathbf{r}')+\rho_{N+1}(\mathbf{r},\mathbf{r}')][\rho^{N}(\mathbf{r}',\mathbf{r})+\rho_{N+1}(\mathbf{r}',\mathbf{r})]}{|\mathbf{r}-\mathbf{r}'|} \\ &+\frac{1}{2}\iint d\mathbf{r}d\mathbf{r}'\frac{\rho^{N}(\mathbf{r},\mathbf{r}')\rho^{N}(\mathbf{r}',\mathbf{r})}{|\mathbf{r}-\mathbf{r}'|} \\ =& -\frac{1}{2}\iint d\mathbf{r}d\mathbf{r}'\frac{\rho^{N}(\mathbf{r},\mathbf{r}')\rho^{N}(\mathbf{r}',\mathbf{r})}{|\mathbf{r}-\mathbf{r}'|} - \iint d\mathbf{r}d\mathbf{r}'\frac{\rho_{N+1}(\mathbf{r},\mathbf{r}')\rho^{N}(\mathbf{r}',\mathbf{r})}{|\mathbf{r}-\mathbf{r}'|} \\ &-\frac{1}{2}\iint d\mathbf{r}d\mathbf{r}'\frac{\rho_{N+1}(\mathbf{r})\rho_{N+1}(\mathbf{r}')}{|\mathbf{r}-\mathbf{r}'|} + \frac{1}{2}\iint d\mathbf{r}d\mathbf{r}'\frac{\rho^{N}(\mathbf{r},\mathbf{r}')\rho^{N}(\mathbf{r}',\mathbf{r})}{|\mathbf{r}-\mathbf{r}'|} \\ =& -\iint d\mathbf{r}d\mathbf{r}'\frac{\rho_{N+1}(\mathbf{r},\mathbf{r}')\rho^{N}(\mathbf{r}',\mathbf{r})}{|\mathbf{r}-\mathbf{r}'|} - \frac{1}{2}\iint d\mathbf{r}d\mathbf{r}'\frac{\rho_{N+1}(\mathbf{r})\rho_{N+1}(\mathbf{r}')}{|\mathbf{r}-\mathbf{r}'|},\end{aligned} \tag{6.20}$$

and the difference in the exchange energies between $N-1$ and N is;

$$\begin{aligned}E_{\mathrm{x}}^{N-1} - E_{\mathrm{x}}^{N} =& -\frac{1}{2}\iint d\mathbf{r}d\mathbf{r}'\frac{\rho^{N-1}(\mathbf{r},\mathbf{r}')\rho^{N-1}(\mathbf{r}',\mathbf{r})}{|\mathbf{r}-\mathbf{r}'|} \\ &+\frac{1}{2}\iint d\mathbf{r}d\mathbf{r}'\frac{\rho^{N}(\mathbf{r},\mathbf{r}')\rho^{N}(\mathbf{r}',\mathbf{r})}{|\mathbf{r}-\mathbf{r}'|} \\ =& -\frac{1}{2}\iint d\mathbf{r}d\mathbf{r}'\frac{[\rho^{N}(\mathbf{r},\mathbf{r}')-\rho_{N}(\mathbf{r},\mathbf{r}')][\rho^{N}(\mathbf{r}',\mathbf{r})-\rho_{N}(\mathbf{r}',\mathbf{r})]}{|\mathbf{r}-\mathbf{r}'|} \\ &+\frac{1}{2}\iint d\mathbf{r}d\mathbf{r}'\frac{\rho^{N}(\mathbf{r},\mathbf{r}')\rho^{N}(\mathbf{r}',\mathbf{r})}{|\mathbf{r}-\mathbf{r}'|} \\ =& \iint d\mathbf{r}d\mathbf{r}'\frac{\rho_{N}(\mathbf{r},\mathbf{r}')\rho^{N}(\mathbf{r}',\mathbf{r})}{|\mathbf{r}-\mathbf{r}'|} - \frac{1}{2}\iint d\mathbf{r}d\mathbf{r}'\frac{\rho_{N}(\mathbf{r})\rho_{N}(\mathbf{r}')}{|\mathbf{r}-\mathbf{r}'|}.\end{aligned} \tag{6.21}$$

Hence the Hartree self-interaction terms are cancelled and the exchange only deriva-

tive discontinuity is given by;

$$\Delta_{\mathrm{x}}^{\mathrm{EXX,LFX}} = -\int d\mathbf{r}\hat{V}_{\mathrm{x}}^{\mathrm{EXX,LFX}}(\mathbf{r})[\rho_{N+1}(\mathbf{r}) - \rho_N(\mathbf{r})] - \iint d\mathbf{r}d\mathbf{r}' \frac{\rho_{N+1}(\mathbf{r},\mathbf{r}')\rho^N(\mathbf{r}',\mathbf{r})}{|\mathbf{r}-\mathbf{r}'|} + \iint d\mathbf{r}d\mathbf{r}' \frac{\rho_N(\mathbf{r},\mathbf{r}')\rho^N(\mathbf{r}',\mathbf{r})}{|\mathbf{r}-\mathbf{r}'|}. \quad (6.22)$$

Adding this term to the EXX or LFX Kohn-Sham band gap is expected to reproduce the HF fundamental band gap (but calculated using the EXX or LFX orbitals). From Koopmans' theorem the HF fundamental band gap is equal to the HF eigenvalue difference between the highest occupied orbital and the lowest unoccupied orbital (the HF equivalent of the Kohn-Sham band gap), under the assumption of frozen orbitals. Hence the exchange-only EXX and LFX fundamental band gap is expected to have similar value to the HF Kohn-Sham band gap. This is a good test for our formalism.

6.6 Convergence of Calculated Derivative Discontinuities

Tests for the convergence of Δ_{xc} for the LDA and Δ_{x} for EXX where performed by varying the size of the plane wave basis set as determined by the cut off energy and the size of the Monkhorst-Pack grid. Using same sets of input parameters as the convergence tests detailed in section 4.3.1, the convergence with respect to cut off energy is shown in figure 6.3, the convergence is much faster than that shown by the total energy, the required level of convergence is achieved by using a cut off energy of 200 eV for LDA and 400 eV for EXX, rather than 600 eV (for both) as seen for the total energy.

In figure 6.4 the convergence of the derivative discontinuity for EXX and LDA with respect to changing Monkhorst-Pack grid is shown. A $6 \times 6 \times 6$ grid for EXX gives the required level of convergence, which is the same as that of the grid used for the total energy, whereas for the LDA the grid is converged using a $4 \times 4 \times 4$ grid.

6.7 Results

6.7.1 Fundamental Band Gaps for LDA and PBE

The calculated semiconductor Kohn-Sham band gaps and derivative discontinuities for group IV, III-V and II-VI semiconductors and insulators, are shown in table 6.1, for the LDA and PBE the calculated Kohn-Sham band gaps and fundamental band gaps (Kohn-Sham plus derivative discontinuity) are shown in figure 6.5, the fundamental band gaps for LDA and PBE are much closer to the experimental band gaps than the Kohn-Sham band gaps, (the exception appears to be CdO, which is greatly overestimated). The mean absolute error for LDA Kohn-Sham band gaps is 1.31 eV, for the fundamental band gap is 0.57 eV, for PBE the mean absolute error on the Kohn-Sham band gaps is 1.13 eV and for the fundamental band gap is 0.51 eV. The mean absolute error of the Kohn-Sham band gaps for EXX is 0.49 eV and for LFX 0.49 eV. Hence, compared with

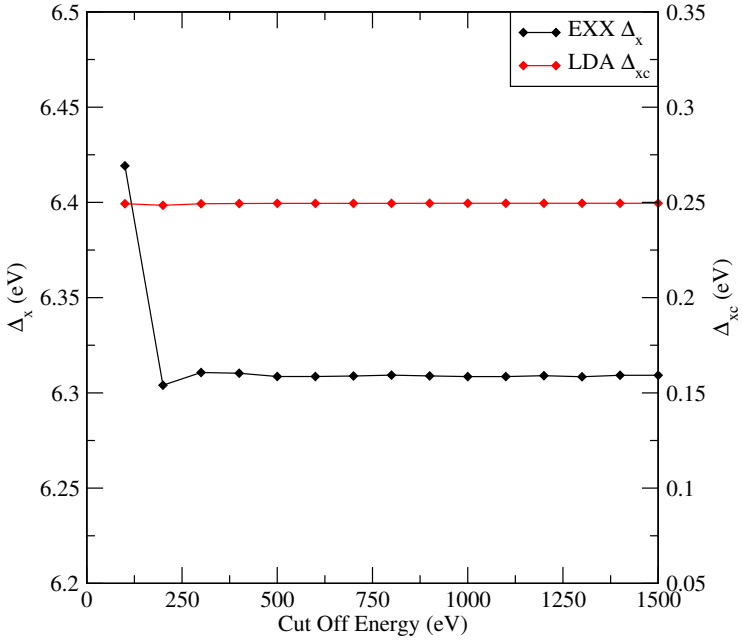

Figure 6.3: Convergence of the derivative discontinuity with respect to cut off energy in silicon for EXX and LDA.

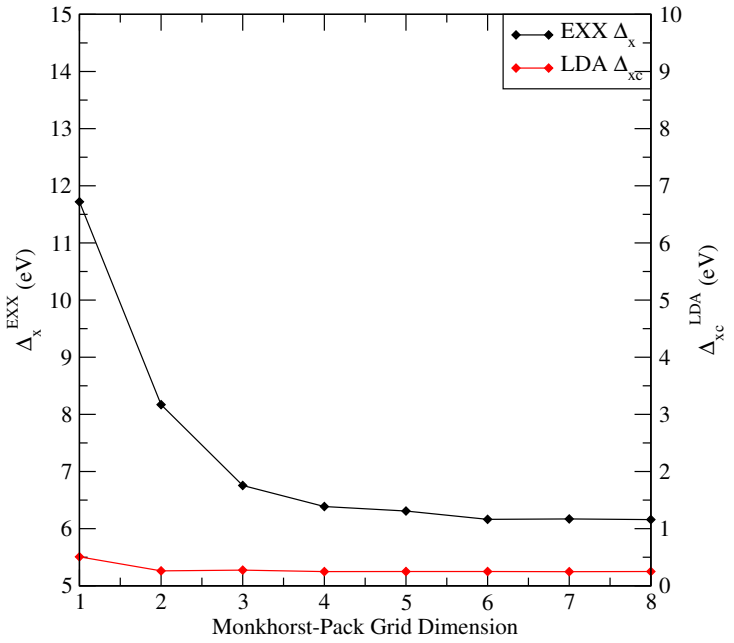

Figure 6.4: Convergence of the derivative discontinuity with respect to the Monkhorst-Pack grid in silicon for EXX and LDA. The grid in this case is cubic.

	E_g^{KS} (eV)		Δ_{xc} (eV)		$E_g^{KS} + \Delta_{xc}$		
	LDA	PBE	LDA	PBE	LDA	PBE	Expt.
AlAs	1.13	1.19	0.35	0.34	1.47	1.53	2.23
AlN	4.25	4.43	1.04	1.05	5.29	5.48	6.28
AlP	1.55	1.75	0.46	0.48	2.01	2.23	2.45
AlSb	0.83	0.90	0.24	0.24	1.07	1.14	1.60
C	4.02	4.26	0.70	0.72	4.72	4.98	5.47
CaO	3.88	4.05	2.92	3.14	6.80	7.19	7.09
CdO	0.34	0.66	3.11	3.18	3.45	3.84	1.12
CdS	1.31	1.65	1.01	1.04	2.32	2.68	2.42
CdSe	0.86	1.12	0.68	0.68	1.54	1.80	1.74
CdTe	1.46	1.80	0.44	0.45	1.91	2.25	1.61
GaAs	1.00	1.10	0.33	0.32	1.32	1.42	1.52
GaN	2.13	2.35	1.09	1.11	3.22	3.46	3.39
GaP	1.52	1.72	0.45	0.47	1.97	2.19	2.35
GaSb	0.45	0.55	0.22	0.22	0.67	0.76	0.81
Ge	0.11	0.14	0.22	0.21	0.33	0.35	0.74
HfO_2	3.12	3.23	2.02	2.11	5.13	5.34	5.90
InAs	0.44	0.67	0.40	0.39	0.84	1.06	0.42
InN	0.21	0.38	1.23	1.24	1.44	1.63	0.93
InP	1.07	1.27	0.55	0.57	1.62	1.85	1.44
InSb	0.91	1.02	0.25	0.25	1.16	1.27	0.24
MgO	4.63	4.97	2.84	2.89	7.47	7.86	7.80
MgS	3.63	3.89	0.98	1.01	4.61	4.90	4.50
MgSe	2.76	2.82	0.66	0.66	3.43	3.47	4.10
MgTe	2.07	2.19	0.41	0.41	2.49	2.61	3.47
NaCl	4.89	5.37	1.56	1.59	6.45	6.97	8.97
Si	0.44	0.60	0.25	0.26	0.69	0.87	1.17
SiC	1.26	1.42	0.81	0.82	2.07	2.24	2.42
SiO_2	5.25	5.71	0.71	0.73	5.97	6.44	9.00
ZnO	1.93	2.28	1.57	1.61	3.50	3.89	3.43
ZnS	2.58	2.94	0.84	0.87	3.41	3.80	3.80
ZnSe	1.85	2.16	0.55	0.55	2.40	2.71	2.80
ZnTe	2.02	2.19	0.35	0.35	2.37	2.54	2.39

Table 6.1: Kohn-Sham band gaps for LDA, PBE, derivative discontinuities for LDA, PBE, fundamental band gaps for LDA, PBE and experimental results for group IV, III-V and II-VI semiconductors and insulators. Experimental results from [137] and [138], except for InN,[143] NaCl,[144] SiO_2 and HfO_2.[145]

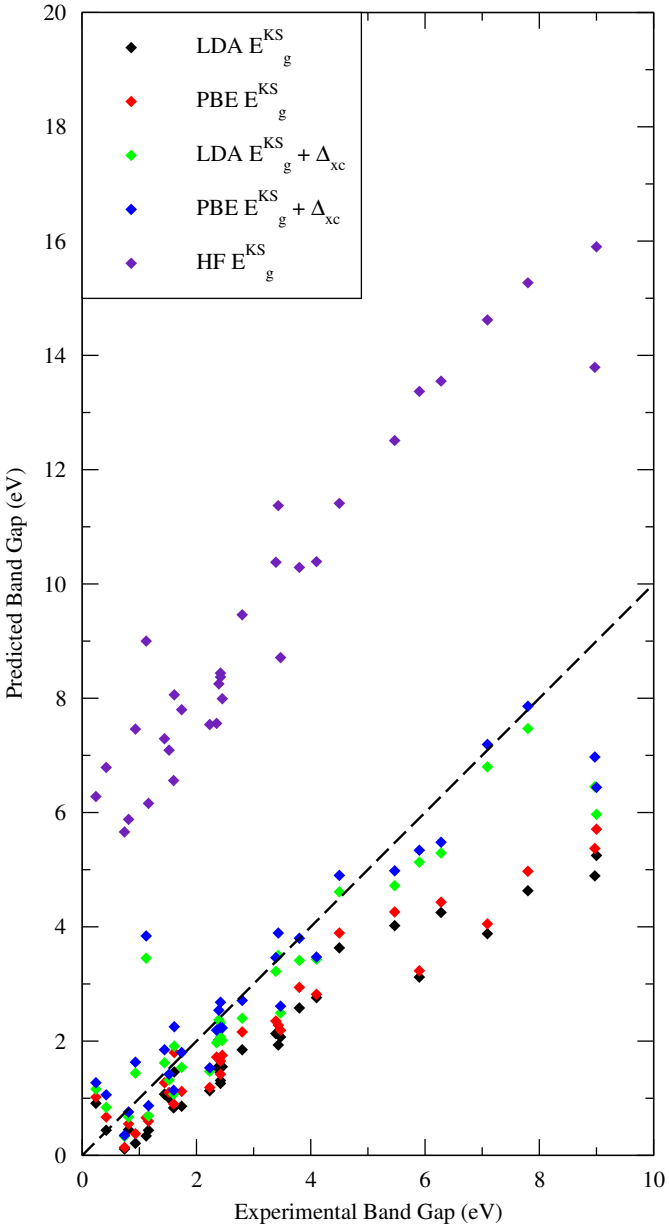

Figure 6.5: Comparison of predicted Kohn-Sham band gaps for LDA and PBE, the LDA and PBE fundamental band gaps and HF band gaps against experiment for materials presented in table 6.1.

experiment the LDA and PBE the fundamental band gaps are greatly improved relative to the Kohn-Sham band gaps. They have almost the same accuracy as the EXX and LFX Kohn-Sham band gaps (without the derivative discontinuity correction).

The formulation of the LDA derivative discontinuity from ensemble considerations was independently demonstrated in refs; [169, 170]. The authors of those references find a vanishing derivative discontinuity for LDA, in the thermodynamic limit. Work is in progress to employ ensemble DFT for degenerate states,[171, 172, 173] for the set of local exchange-correlation potentials like the LDA and GGA, to derive an expression for Δ_{xc} that remains finite in the thermodynamic limit. Preliminary results from symmetry arguments, indicate that the Δ_{xc} (per particle) will be the same as the one we have employed in our calculations.

6.7.2 Fundamental Band Gaps for EXX and LFX

For EXX and LFX the calculated Kohn-Sham band gaps and fundamental band gaps are shown in figure 6.6. The fundamental band gaps are larger than even the HF Kohn-Sham band gaps, but of similar magnitude which is the expected behaviour. The mean absolute error for the EXX Kohn-Sham band gaps is 0.49 eV, for EXX the mean absolute error for the fundamental band gaps is 4.04 eV. For the LFX Kohn-Sham band gaps the mean absolute error is 0.49 eV and for the LFX fundamental band gaps the mean absolute error is 4.05 eV. Considering the exchange derivative discontinuity without the correlation component leads to highly overestimated fundamental band gaps. The calculated exchange only derivative discontinuities for Si, C, GaN and InN are of comparable magnitude to those found in reference [97]. The expectation for the correlation derivative discontinuities is that they have opposite sign and similar magnitude to the exchange derivative discontinuity. The accurate reproduction of the (too large) HF band gaps confirms the validity of our formulation.

6.8 Correlation Energy Derivative Discontinuity

From equation 6.16 the exact derivative discontinuity for an orbital dependent local functional can be written;

$$\begin{aligned}
\Delta_{\mathrm{xc}} &= \frac{1}{2}\iint d\mathbf{r}d\mathbf{r}'\frac{\rho_{N+1}(\mathbf{r})\rho_{N+1}(\mathbf{r}')}{|\mathbf{r}-\mathbf{r}'|} + \frac{1}{2}\iint d\mathbf{r}d\mathbf{r}'\frac{\rho_{N}(\mathbf{r})\rho_{N}(\mathbf{r}')}{|\mathbf{r}-\mathbf{r}'|} \\
&- \int d\mathbf{r}\frac{\partial E_{\mathrm{xc}}^{N}}{\partial\rho(\mathbf{r})}[\rho_{N+1}(\mathbf{r})-\rho_{N}(\mathbf{r})] + E_{\mathrm{x}}^{N+1}[\rho^{N+1}] - 2E_{\mathrm{x}}^{N}[\rho^{N}] + E_{\mathrm{x}}^{N-1}[\rho^{N-1}] \\
&+ E_{\mathrm{c}}^{N+1}[\rho^{N+1}] - 2E_{\mathrm{c}}^{N}[\rho^{N}] + E_{\mathrm{c}}^{N-1}[\rho^{N-1}] \\
&= -\int d\mathbf{r}\hat{V}_{\mathrm{x}}(\mathbf{r})[\rho_{N+1}(\mathbf{r})-\rho_{N}(\mathbf{r})] - \iint d\mathbf{r}d\mathbf{r}'\frac{\rho_{N+1}(\mathbf{r},\mathbf{r}')\rho^{N}(\mathbf{r}',\mathbf{r})}{|\mathbf{r}-\mathbf{r}'|} \\
&\quad + \iint d\mathbf{r}d\mathbf{r}'\frac{\rho_{N}(\mathbf{r},\mathbf{r}')\rho^{N}(\mathbf{r}',\mathbf{r})}{|\mathbf{r}-\mathbf{r}'|} + \Delta_{\mathrm{c}}.
\end{aligned} \tag{6.23}$$

	E_g^{KS} (eV)			Δ_{xc} (eV)		$E_g^{KS} + \Delta_{xc}$		
	EXX	LFX	HF	EXX	LFX	EXX	LFX	Expt.
AlAs	2.25	2.23	7.54	6.20	6.21	8.45	8.44	2.23
AlN	5.77	5.72	13.55	8.17	8.22	13.95	13.94	6.28
AlP	2.50	2.47	7.99	6.53	6.55	9.04	9.02	2.45
AlSb	1.67	1.65	6.56	5.69	5.70	7.36	7.35	1.60
C	4.81	4.81	12.51	9.97	9.97	14.77	14.78	5.47
CaO	6.13	5.96	14.62	9.99	10.28	16.12	16.24	7.09
CdO	1.93	1.84	9.00	8.50	8.56	10.42	10.40	1.12
CdS	2.25	2.18	8.37	6.92	6.96	9.17	9.14	2.42
CdSe	1.84	1.79	7.80	6.51	6.52	8.34	8.31	1.74
CdTe	2.24	2.18	8.06	6.05	6.07	8.29	8.25	1.61
GaAs	1.91	1.87	7.09	6.12	6.12	8.03	7.99	1.52
GaN	3.36	3.31	10.38	7.92	7.96	11.28	11.27	3.39
GaP	2.31	2.28	7.56	6.47	6.49	8.78	8.77	2.35
GaSb	1.20	1.19	5.88	5.62	5.62	6.82	6.81	0.81
Ge	0.93	0.93	5.66	5.81	5.81	6.74	6.75	0.74
HfO_2	5.62	5.56	13.37	7.97	8.05	13.60	13.61	5.90
InAs	1.35	1.30	6.79	5.87	5.88	7.22	7.18	0.42
InN	1.42	1.35	7.46	7.15	7.19	8.57	8.54	0.93
InP	1.92	1.87	7.29	6.15	6.17	8.07	8.04	1.44
InSb	1.63	1.60	6.28	5.52	5.52	7.15	7.12	0.24
MgO	6.66	6.59	15.27	9.97	10.03	16.63	16.62	7.80
MgS	4.82	4.77	11.41	7.41	7.45	12.23	12.22	4.50
MgSe	4.16	4.14	10.39	6.96	6.97	11.12	11.11	4.10
MgTe	3.12	3.09	8.71	6.29	6.31	9.41	9.39	3.47
NaCl	6.30	6.25	13.79	8.08	8.12	14.38	14.37	8.97
Si	1.20	1.20	6.16	6.16	6.16	7.36	7.36	1.17
SiC	2.42	2.40	8.44	7.81	7.82	10.23	10.22	2.42
SiO_2	7.30	7.23	15.90	9.32	9.37	16.61	16.60	9.00
ZnO	3.51	3.44	11.37	8.95	9.00	12.45	12.44	3.43
ZnS	3.56	3.52	10.29	7.33	7.36	10.89	10.87	3.80
ZnSe	2.91	2.87	9.46	6.87	6.88	9.78	9.75	2.80
ZnTe	2.84	2.82	8.25	6.29	6.31	9.14	9.12	2.39

Table 6.2: Kohn-Sham band gaps for EXX, LFX, HF, derivative discontinuities for EXX, LFX, fundamental band gaps for EXX, LFX and experimental results for group IV, III-V and II-VI semiconductors and insulators. Experimental results from [137] and [138], except for InN,[143] NaCl,[144] SiO_2 and HfO_2.[145]

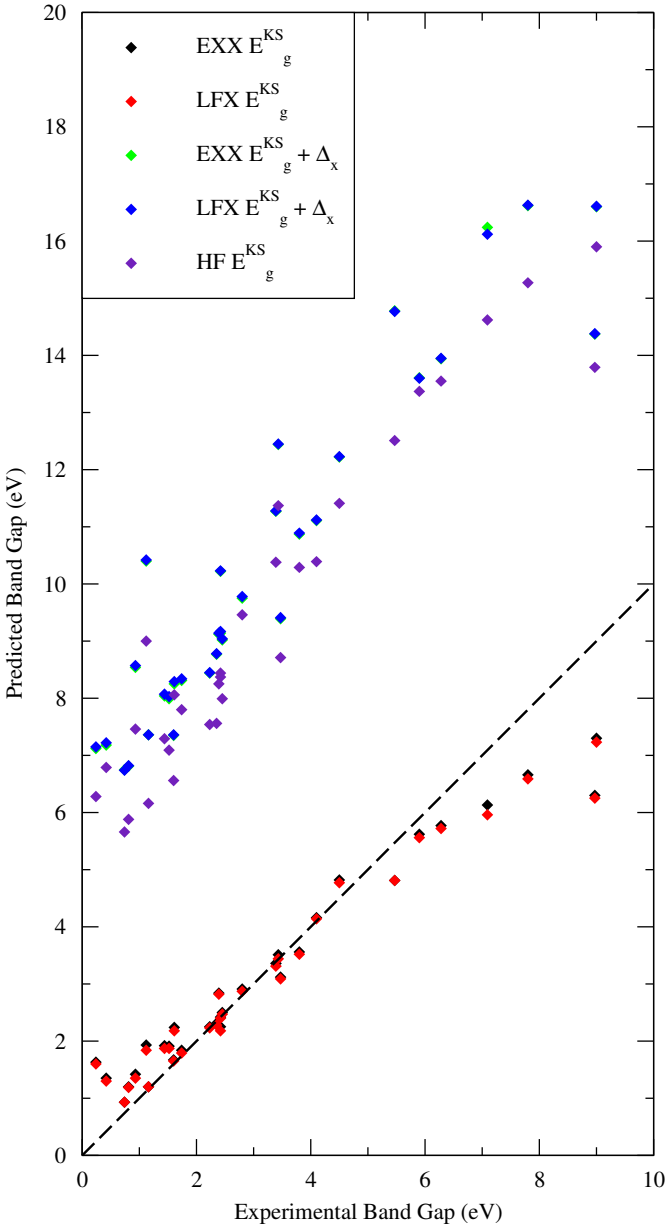

Figure 6.6: Comparison of predicted Kohn-Sham band gaps for EXX, LFX, the EXX and LFX fundamental exchange only band gaps and HF band gaps against experiment for materials presented in table 6.2.

Rather than using the exact correlation energy we can approximate it. From appendix B, equation B.11;

$$T_{\mathrm{u}}'' = \sum_{n}^{\infty} \frac{|\langle \Phi_0 | \hat{U}_{\mathrm{ee}} - \hat{V}_{\mathrm{H}} - \hat{V}_{\mathrm{x}} | \Phi_n \rangle|^2}{E_n - E_0}, \tag{6.24}$$

T_{u}'' is the second order energy of a perturbative expansion. Φ_0 is the ground state Slater determinant and Φ_n is an excited Slater determinant. The negative of T_{u}'' is approximately equal to the correlation energy (expanded to second order when treating interactions as a perturbation).[112, 133] Hence we take the correlation energy of an N electron system to be;

$$E_{\mathrm{c}}^N[\rho^N] = -T_{\mathrm{u}}''. \tag{6.25}$$

In section 3.3.5, equation 3.73 was found by decomposing equation B.11 using the Slater-Condon rules and considering only single excitations. If we also include double excitations, equation 6.24 in terms of the Kohn-Sham orbitals becomes;[4]

$$\begin{aligned} E_{\mathrm{c}}^N[\rho^N] =& -\frac{1}{4} \sum_{i,j=1}^{N} \sum_{a,b=N+1}^{\infty} \frac{|\langle \phi_a \phi_b | \hat{U}_{\mathrm{ee}} | \phi_i \phi_j \rangle|^2}{\varepsilon_a + \varepsilon_b - \varepsilon_i - \varepsilon_j} - \sum_{i}^{N} \sum_{a}^{\infty} \frac{|\langle \phi_a | \hat{V}_{\mathrm{x}} - \hat{V}_{\mathrm{x}}^{\mathrm{NL}} | \phi_i \rangle|^2}{\varepsilon_a - \varepsilon_i} \\ =& \sum_{i,j=1}^{N} \sum_{a,b=N+1}^{\infty} f^{\mathrm{d}}(i,j:a,b) + \sum_{i}^{N} \sum_{a}^{\infty} f^{\mathrm{s}}(i:a) \\ =& E_{\mathrm{c}}^{\mathrm{d}}[\rho^N] + E_{\mathrm{c}}^{\mathrm{s}}[\rho^N]. \end{aligned} \tag{6.26}$$

The first term is a sum over double excitations and the second is a sum over single excitations, where $\hat{U}_{\mathrm{ee}}$ is a two particle Coulomb operator, $\hat{V}_{\mathrm{x}}$ is the local exchange potential and $\hat{V}_{\mathrm{x}}^{\mathrm{NL}}$ is the non-local Fock exchange operator. For simplicity $f^{\mathrm{d}}(i,j:a,b)$ is the matrix element of the double excitations and $f^{\mathrm{s}}(i:a)$ is the matrix element of the single excitations. The matrix element of $\hat{U}_{\mathrm{ee}}$ is given by;

$$\langle \phi_a \phi_b | \hat{U}_{\mathrm{ee}} | \phi_i \phi_j \rangle = f^{\mathrm{d}}(i,j:a,b) = \iint d\mathbf{r} d\mathbf{r}' \frac{\phi_a^\dagger(\mathbf{r}) \phi_b(\mathbf{r}') [\phi_i(\mathbf{r}) \phi_j^\dagger(\mathbf{r}') - \phi_i^\dagger(\mathbf{r}') \phi_j(\mathbf{r})]}{|\mathbf{r} - \mathbf{r}'|}, \tag{6.27}$$

hence if $i = j$ or $a = b$ this matrix element is zero and $f^{\mathrm{d}}(i,j:a,b) = f^{\mathrm{d}}(j,i:a,b) = f^{\mathrm{d}}(i,j:b,a)$.

For the correlation energy due to the double excitations, partitioning the sums gives;

$$\begin{aligned}
E_{\mathrm{c}}^{\mathrm{d}}[\rho^N] &= \left[\sum_{i=1}^{N-1}\delta_{l,i}+\delta_{l,N}\right]\left[\sum_{j=1}^{N-1}\delta_{m,j}+\delta_{m,N}\right]\left[\delta_{c,N+1}+\sum_{a=N+2}^{\infty}\delta_{c,a}\right] \\
&\quad\times\left[\delta_{d,N+1}+\sum_{b=N+2}^{\infty}\delta_{d,b}\right]f^{\mathrm{d}}(l,m:c,d) \\
&= \sum_{i,j=1}^{N-1}\sum_{a,b=N+2}^{\infty}f^{\mathrm{d}}(i,j:a,b)+2\sum_{i,j=1}^{N-1}\sum_{a=N+2}^{\infty}f^{\mathrm{d}}(i,j:a,N+1) \\
&\quad+2\sum_{i=1}^{N-1}\sum_{a,b=N+2}^{\infty}f^{\mathrm{d}}(i,N:a,b)+4\sum_{i=1}^{N-1}\sum_{a=N+2}^{\infty}f^{\mathrm{d}}(i,N:a,N+1),
\end{aligned}$$

$$\begin{aligned}
E_{\mathrm{c}}^{\mathrm{d}}[\rho^{N+1}] &= \left[\sum_{i=1}^{N-1}\delta_{l,i}+\delta_{l,N}+\delta_{l,N+1}\right]\left[\sum_{j=1}^{N-1}\delta_{m,j}+\delta_{m,N}+\delta_{m,N+1}\right]\sum_{a,b=N+2}^{\infty}f^{\mathrm{d}}(l,m:a,b) \\
&= \sum_{i,j=1}^{N-1}\sum_{a,b=N+2}^{\infty}f^{\mathrm{d}}(i,j:a,b)+2\sum_{i=1}^{N-1}\sum_{a,b=N+2}^{\infty}f^{\mathrm{d}}(i,N:a,b) \\
&\quad+2\sum_{i=1}^{N-1}\sum_{a,b=N+2}^{\infty}f^{\mathrm{d}}(i,N+1:a,b)+2\sum_{a,b=N+2}^{\infty}f^{\mathrm{d}}(N,N+1:a,b),
\end{aligned}$$

$$\begin{aligned}
E_{\mathrm{c}}^{\mathrm{d}}[\rho^{N-1}] &= \left[\delta_{c,N}+\delta_{c,N+1}+\sum_{a=N+2}^{\infty}\delta_{c,a}\right]\left[\delta_{d,N}+\delta_{d,N+1}+\sum_{b=N+2}^{\infty}\delta_{d,b}\right]\sum_{i,j=1}^{N-1}f^{\mathrm{d}}(i,j:c,d) \\
&= \sum_{i,j=1}^{N-1}\sum_{a,b=N+2}^{\infty}f^{\mathrm{d}}(i,j:a,b)+2\sum_{i,j=1}^{N-1}\sum_{a=N+2}^{\infty}f^{\mathrm{d}}(i,j:a,N+1) \\
&\quad+2\sum_{i,j=1}^{N-1}\sum_{a=N+2}^{\infty}f^{\mathrm{d}}(i,j:a,N)+2\sum_{i,j=1}^{N-1}f^{\mathrm{d}}(i,j:N,N+1).
\end{aligned}$$

Summing the three terms to get the double excitation contribution to the derivative

discontinuity gives;

$$\begin{aligned}\Delta_{\rm c}^{\rm d} =& E_{\rm c}^{\rm d}[\rho^{N+1}] + E_{\rm c}^{\rm d}[\rho^{N-1}] - 2E_{\rm c}^{\rm d}[\rho^{N}] \\ =& 2\sum_{i,j=1}^{N-1}\sum_{a=N+2}^{\infty} f^{\rm d}(i,j:a,N) - 2\sum_{i,j=1}^{N-1}\sum_{a=N+2}^{\infty} f^{\rm d}(i,j:a,N+1) \\ &+ 2\sum_{i=1}^{N-1}\sum_{a,b=N+2}^{\infty} f^{\rm d}(i,N+1:a,b) - 2\sum_{i=1}^{N-1}\sum_{a,b=N+2}^{\infty} f^{\rm d}(i,N:a,b) \\ &+ 2\sum_{i,j=1}^{N-1} f^{\rm d}(i,j:N,N+1) + 2\sum_{a,b=N+2}^{\infty} f^{\rm d}(N,N+1:a,b) \\ &- 8\sum_{i=1}^{N-1}\sum_{a=N+2}^{\infty} f^{\rm d}(i,N:a,N+1).\end{aligned}$$

For the correlation energy due to the single excitations;

$$\begin{aligned}E_{\rm c}^{\rm s}[\rho^{N}] &= \left[\sum_{i=1}^{N-1}\delta_{l,i} + \delta_{l,N}\right]\left[\delta_{c,N+1} + \sum_{a=N+2}^{\infty}\delta_{c,a}\right] f^{\rm s}(l:c) \\ &= \sum_{i=1}^{N-1}\sum_{a=N+2}^{\infty} f^{\rm s}(i:a) + \sum_{i=1}^{N-1} f^{\rm s}(i:N+1) + f^{\rm s}(N:N+1) \\ &\quad + \sum_{a=N+2}^{\infty} f^{\rm s}(N:a),\end{aligned} \tag{6.28}$$

$$\begin{aligned}E_{\rm c}^{\rm s}[\rho^{N+1}] &= \left[\sum_{i=1}^{N-1}\delta_{l,i} + \delta_{l,N} + \delta_{l,N+1}\right]\sum_{a=N+2}^{\infty}\delta_{c,a} f^{\rm s}(l:c) \\ &= \sum_{i=1}^{N-1}\sum_{a=N+2}^{\infty} f^{\rm s}(i:a) + \sum_{a=N+2}^{\infty} f^{\rm s}(N:a) + \sum_{a=N+2}^{\infty} f^{\rm s}(N+1:a),\end{aligned} \tag{6.29}$$

$$\begin{aligned}E_{\rm c}^{\rm s}[\rho^{N-1}] &= \sum_{i=1}^{N-1}\delta_{l,i}\left[\delta_{c,N} + \delta_{c,N+1} + \sum_{a=N+2}^{\infty}\delta_{c,a}\right] f^{\rm s}(l:c) \\ &= \sum_{i=1}^{N-1}\sum_{a=N+2}^{\infty} f^{\rm s}(i:a) + \sum_{i=1}^{N-1} f^{\rm s}(i:N+1) + \sum_{i=1}^{N-1} f^{\rm s}(i:N),\end{aligned} \tag{6.30}$$

Summing the three terms to get the single excitations contributions gives;

$$\begin{aligned}
\Delta_{\mathrm{c}}^{\mathrm{s}} =& E_{\mathrm{c}}^{\mathrm{s}}[\rho^{N+1}] + E_{\mathrm{c}}^{\mathrm{s}}[\rho^{N-1}] - 2E_{\mathrm{c}}^{\mathrm{s}}[\rho^{N}] \\
&= \sum_{i=1}^{N-1}\sum_{a=N+2}^{\infty} f^{\mathrm{s}}(i:a) + \sum_{a=N+2}^{\infty} f^{\mathrm{s}}(N:a) + \sum_{a=N+2}^{\infty} f^{\mathrm{s}}(N+1:a), \\
&\quad + \sum_{i=1}^{N-1}\sum_{a=N+2}^{\infty} f^{\mathrm{s}}(i:a) + \sum_{i=1}^{N-1} f^{\mathrm{s}}(i:N+1) + \sum_{i=1}^{N-1} f^{\mathrm{s}}(i:N), \\
&\quad - 2\left(\sum_{i=1}^{N-1}\sum_{a=N+2}^{\infty} f^{\mathrm{s}}(i:a) + \sum_{i=1}^{N-1} f^{\mathrm{s}}(i:N+1) + f^{\mathrm{s}}(N:N+1)\right. \\
&\quad \left. + \sum_{a=N+2}^{\infty} f^{\mathrm{s}}(N:a)\right), \\
&= \sum_{a=N+2}^{\infty} f^{\mathrm{s}}(N+1:a) - \sum_{a=N+2}^{\infty} f^{\mathrm{s}}(N:a) - \sum_{i=1}^{N-1} f^{\mathrm{s}}(i:N+1) \\
&\quad + \sum_{i=1}^{N-1} f^{\mathrm{s}}(i:N) - 2f^{\mathrm{s}}(N:N+1).
\end{aligned}$$

In a plane-wave code to calculate this correlation derivative discontinuity is prohibitively expensive due to the double sum over all virtual orbitals. This would require using a very high cut off energy and truncating the infinite sums, whilst using a large amount of memory as every set of orbitals needs to be stored. Due to the non-local terms in E_c we must use two sets of k-points, one that can be symmetrised and parallelised ($\mathbf{k}$) and ($\mathbf{q}$) which cannot be symmetrised or parallelised. Alternately a modified version of the Hylleraas variational method can be used but the resulting Sternheimer equation is dependent on $\mathbf{r}$ and $\mathbf{r}'$, similarly to the way the screened Coulomb interaction, W in the GW approximation is calculated.[174] However the calculation of this correlation component of the derivative discontinuity in second order perturbation theory is beyond the scope of this work.

6.9 Summary

The treatment of a system with fractional charge in density functional theory was demonstrated and the non-linear behaviour of the LDA, EXX, LFX and HF total energies with varying fractional charge was calculated. The proper treatment of fractional charge using an ensemble description that is linear in energy when the fractional charge is varied was shown.

The fundamental band gap for a system was derived using the derivatives in terms of the gradient in the total energy with respect to the fractional charge. Hence the exact derivative discontinuity was derived, the approximate derivative discontinuities were also derived for local density exchange-correlation functionals (LDA/GGAs) and for the

exchange-only local potentials (EXX/LFX). We also derived the correlation derivative discontinuity, Δ_c for EXX and LFX, using a approximate (2nd order) orbital dependent correlation energy. With the exception of a very recent independent publication, the discovery of finite Δ_{xc} for LDA/GGA is surprising and contrary to the established opinion in the literature.

The derivative discontinuities for the LDA, PBE, EXX and LFX were implemented and tested with respect to the input parameters of cut off energy and Monkhorst Pack grids, demonstrating equal convergence to the total energy. The derivative discontinuities were then calculated for group IV, III-V and II-VI semiconductors and insulators. The LDA and PBE fundamental gaps give a much improved value relative to experimental values for the band gap compared to the Kohn-Sham band gaps. As expected the EXX and LFX exchange-only fundamental gaps are comparable in magnitude to the HF band gaps and are greatly overestimated relative to the experimental values. The EXX and LFX Kohn-Sham band gaps remain the closest to experimental values.

It remains to be seen whether the (2nd order) derivative discontinuity for the correlation energy, Δ_c will effectively cancel Δ_x and yield an improvement over the EXX/LFX Kohn-Sham band gaps.

Chapter 7

Conclusions and Future Work

7.1 Conclusions

The work presented in this thesis was centred on developing new methods to accurately treat the exchange potential in density functional theory calculations, to yield improved electronic structures. In the second chapter the many-electron problem was introduced and the Hartree and Hartree-Fock approximations outlined. The Kohn-Sham (KS) DFT was also outlined and the Hohenberg-Kohn theorems that underpin the theory proven. The exchange-correlation potential and common approximations were discussed. The implementation of DFT into a crystalline system using a plane wave basis set and pseudopotentials was also described.

In chapter 3 some desirable properties of the exchange-correlation potential were discussed. The derivation of the local exact exchange potential (EXX) was undertaken using the optimised effective potential method. An alternative method for finding the EXX potential by exact minimisation of the HF total energy using perturbation theory and the Hylleraas variational method was proposed, avoiding the infinite sum over states needed in the optimised effective potential method. A simple algorithm for minimising this potential was also proposed. Three common approximations to the EXX potential, the approximations of Krieger, Li and Iafrate (KLI) and Slater were derived, the common energy denominator approximation (CEDA) was rigorously derived and an algorithm for finding the CEDA potential that is very similar to the one used to find the EXX potential proposed. A new local exact exchange potential that reproduces the HF density was proposed; the local Fock exchange potential (LFX), the functional derivative and minimising function for this potential were also derived. The extension of DFT to metallic system was discussed and the extension of the EXX and LFX potentials to metallic systems were shown. A modified scheme for finding the EXX potential for a metal was proposed that retains the structure of the originally proposed method.

Chapter 4 proceeds by describing the implementation of EXX, CEDA and LFX potentials in a plane wave pseudopotential code. The choice of norm-conserving pseudopotentials was explained. The exact iterative procedures for finding each potential was

discussed. Various minimisation schemes were presented and compared for EXX, CEDA and LFX and the chosen method of Fletcher-Reeves conjugate gradients explained. The convergence of the total energy with respect to plane wave cut off energy and Monkhorst-Pack grid size was tested for EXX, CEDA and LFX and compared to the HF convergence. The parallelisation of the problem was discussed and performance tests were performed to demonstrate the scaling with changing number of processors. Distribution over k-points was found to scale almost linearly, whereas the distribution by reciprocal lattice vector was found to offer some performance increase but is limited by interprocessor communication limitations.

In chapter 5 the application was presented of the EXX, CEDA and LFX potentials to semiconductors, insulators, antiferromagnetic insulators and metals for the calculation of the band structures of these materials. A selection of technologically-relevant material band structures were presented for the LDA, PBE, EXX, CEDA, LFX and HF exchange-correlation functionals. Additionally the calculated exchange-correlation potentials for the LDA, EXX, LFX and CEDA were plotted for Si, C and Ge. For semiconductors EXX and LFX give near identical results; both giving accurate band structures with KS band gaps close the experimental values, LDA and PBE KS band gaps grossly underestimate the band gaps of the materials, CEDA slightly underestimates and HF grossly overestimates the band gap. For insulators the wider the experimental band gap the poorer the agreement with experiment for the EXX and LFX potentials. The requirement to include relativistic effects in the calculation was highlighted to explain the overestimation of the band gap for small gap heavy element semiconductors. The need to complete the calculation of the fundamental band gap by including the derivative discontinuity is also discussed.

The application to the band structures of four transition metal monoxides is also presented. The LDA and PBE give poor (metallic) results for these materials. EXX, CEDA and LFX give all four as antiferromagnetic insulators and whilst the description of their band structures is greatly improved relative to LDA and GGA, the agreement with experiment is not as good as that found for the semiconductors, with CEDA giving FeO as a metal. These materials also show differences between the calculated band structures for EXX and LFX.

The calculated band structures for a selection of elemental metals were also presented. The poor description of metals by HF was discussed and explained (contrary to current belief in the literature). The band structures for EXX and LFX both give much improved descriptions relative to HF, being very similar to those found by the LDA. EXX and LFX band structures were free of logarithmic divergence at the Fermi level and gave metallic band structures when HF gave semi-metallic behaviour.

The physical equivalence of EXX and LFX was also shown by considering the quantities that EXX and LFX minimise. The EXX and LFX exchange potentials (plus the Hartree potential) are the zeroth order potentials of two similar perturbative expansions of the exact Kohn-Sham potential, where switching on interactions between electrons

is considered the perturbation. These arguments also explain why EXX and LFX give very similar results for weakly correlated systems and differing results for systems where correlation plays a more important role.

Chapter 6 presents the fundamental band gap and its difference from the Kohn-Sham band gap. The behaviour of LDA, EXX, LFX and HF for a fractional charged fluorine atom were presented. The LDA shows a quadratic behaviour in the total energy, whereas EXX, LFX and HF show an almost linear behaviour. Using a quantum mechanical ensemble of states with different numbers of particles the exact derivative discontinuity is found. The approximate forms it takes when using a density dependent functional (LDA or GGA) or exact exchange potentials are also found, and a form using an approximate orbital dependent correlation energy was also derived. Calculated fundamental band gaps for the LDA, PBE, EXX and LFX were presented. The calculated fundamental band gaps for the LDA and PBE are in good agreement with experiment, the EXX and LFX fundamental band gaps are in much worse agreement with experiment than the Kohn-Sham band gaps, highlighting the need to include correlation when calculating the derivative discontinuity. Nevertheless the exchange-only results are expected as they are close to the corresponding HF eigenvalue differences and confirms the validity of our formulation.

7.2 Future Work

7.2.1 Including Correlation

Correlation Energy Functionals

To extend the exact exchange only theories presented in this thesis to higher levels of accuracy, the correlation energy of system needs to be evaluated, especially to give an accurate representation of strongly correlated materials. Using density dependent correlation functionals will be insufficient to describe correlation accurately (as seen for the transition metal oxides where the LDA and PBE give very poor results). An orbital dependent correlation energy, (as detailed in section 6.8) will be very computationally involved and hence would be limited in its possible applications. An orbital dependent correlation energy that retains similar scaling behaviour as HF would be ideal. One way to accomplish this is to extend DFT using reduced density matrix functional theory (RDMFT) expressions. RDMFT introduces static correlation by extending the many-body wave function beyond a single Slater determinant.

Reduced Density Matrix Functional Theory

Returning to the many-electron problem, any system of N electrons can be described by the N-body density matrix as well as by its many-electron wave function.[175] This

N-body density matrix is written;

$$\Gamma^{(N)}(\mathbf{r_1}...\mathbf{r_N} : \mathbf{r'_1}...\mathbf{r'_N}) = \Psi^{\dagger}(\mathbf{r'_1}...\mathbf{r'_N})\Psi(\mathbf{r_1}...\mathbf{r_N}). \tag{7.1}$$

The pth body reduced density matrix can be defined;

$$\Gamma^{(p)}(\mathbf{r_1}...\mathbf{r_p} : \mathbf{r'_1}...\mathbf{r'_p}) = \binom{N}{p} \int d\mathbf{r}_{p+1}.. \int d\mathbf{r}_N \Psi^{\dagger}(\mathbf{r'_1}...\mathbf{r'_p}, \mathbf{r_{p+1}}...\mathbf{r_N})\Psi(\mathbf{r_1}...\mathbf{r_N}). \tag{7.2}$$

For a Hamiltonian with an external potential the many-body system can be fully determined in terms of the one-body and two-body reduced density matrices;

$$\begin{aligned}\hat{H}\Psi =& E\Psi \\ =& \iint d\mathbf{r}d\mathbf{r}'\delta(\mathbf{r}-\mathbf{r}')\left[\left(-\frac{\nabla^2}{2}\right)\Gamma^{(1)}(\mathbf{r}:\mathbf{r}')\right] + \iint d\mathbf{r}d\mathbf{r}'\frac{\Gamma^{(2)}(\mathbf{r},\mathbf{r}':\mathbf{r},\mathbf{r}')}{|\mathbf{r}-\mathbf{r}'|} \\ &+ \iint d\mathbf{r}d\mathbf{r}'\delta(\mathbf{r}-\mathbf{r}')\hat{V}_{ext}(\mathbf{r})\Gamma^{(1)}(\mathbf{r}:\mathbf{r}').\end{aligned} \tag{7.3}$$

However the form of $\Gamma^{(2)}$ is not known, while the form of $\Gamma^{(1)}$ is known. The two quantities are related by equation 7.2. Hence using $\Gamma^{(1)}$ as the basic variable for the problem analogous to the density in DFT is potentially a good idea, with $\Gamma^{(2)}$ being a functional of $\Gamma^{(1)}$. The use of $\Gamma^{(1)}$ as the basic variable satisfies a Hohenberg-Kohn like theorem known as Gilbert's theorem.[176]

The one-body reduced matrix can be expanded in a basis of its eigenfunctions, ϕ_i referred to as natural orbitals. The reduced density matrix can then by written;

$$\Gamma^{(1)}(\mathbf{r}:\mathbf{r}') = \sum_{i=1}^{\infty} n_i \phi_i^{\dagger}(\mathbf{r}')\phi_i(\mathbf{r}), \tag{7.4}$$

where n_i is the occupancy of state i, with values bound to the conditions that; $0 \leq n_i \leq 1$ and $\sum_{i=1}^{\infty} n_i = N$. These are the N-representability conditions for $\Gamma^{(1)}$ (for an N-fermion wave function). Both the occupancies and natural orbitals are functionals of the one-body reduced density matrix, hence we can write the energy as a functional of the occupancies and orbitals and use orbital dependent functionals from DFT for the operators. Here the partial occupancies are not determined from a smearing scheme as was done in DFT, but must be determined as the occupancies that minimise the energy functional for a given set of natural orbitals.

Approximations to the Two-Body Reduced Density Matrix

The term $\Gamma^{(2)}$ is unknown and it can be determined as the approximate functional of $\Gamma^{(1)}$. The simplest functional form is the Hartree-Fock approximation, the two-body

reduced density matrix is then given by;

$$\Gamma^{(2)}(\mathbf{r_1}, \mathbf{r_2} : \mathbf{r'_1}, \mathbf{r'_2}) = \frac{1}{2}\Gamma^{(1)}(\mathbf{r_1}, \mathbf{r'_1})\Gamma^{(1)}(\mathbf{r_2}, \mathbf{r'_2}) - \frac{1}{2}\Gamma^{(1)}(\mathbf{r_1}, \mathbf{r'_2})\Gamma^{(1)}(\mathbf{r_2}, \mathbf{r'_1}). \tag{7.5}$$

The total energy functional is then the HF total energy for a partially occupied system;

$$\begin{aligned} E[n_i, \phi_i] = &- \sum_{i=1}^{\infty} n_i \int d\mathbf{r} \phi_i^\dagger(\mathbf{r}) \frac{\nabla^2}{2} \phi_i(\mathbf{r}) + \sum_{i=1}^{\infty} n_i \int d\mathbf{r} \phi_i^\dagger(\mathbf{r}) \hat{V}_{ext}(\mathbf{r}) \phi_i(\mathbf{r}) \\ &+ \frac{1}{2} \sum_{i=1}^{\infty} \sum_{j=1}^{\infty} n_i n_j \iint d\mathbf{r} d\mathbf{r}' \frac{\phi_i^\dagger(\mathbf{r}) \phi_i(\mathbf{r}) \phi_j^\dagger(\mathbf{r}') \phi_j(\mathbf{r}')}{|\mathbf{r} - \mathbf{r}'|} \\ &- \frac{1}{2} \sum_{i=1}^{\infty} \sum_{j=1}^{\infty} n_i n_j \iint d\mathbf{r} d\mathbf{r}' \frac{\phi_i^\dagger(\mathbf{r}) \phi_j(\mathbf{r}) \phi_j^\dagger(\mathbf{r}') \phi_i(\mathbf{r}')}{|\mathbf{r} - \mathbf{r}'|}, \end{aligned} \tag{7.6}$$

which is non-interacting and the optimal occupancies turn out to be either 0 or 1. To introduce correlation reduced density functionals can be constructed by changing the functional form of the occupancies for the Fock exchange integral. The functional of Müller gives the exchange correlation functional as;[177]

$$E_{xc}[n_i, \phi_i] = -\frac{1}{2} \sum_{i=1}^{\infty} \sum_{j=1}^{\infty} \sqrt{n_i n_j} \iint d\mathbf{r} d\mathbf{r}' \frac{\phi_i^\dagger(\mathbf{r}) \phi_j(\mathbf{r}) \phi_j^\dagger(\mathbf{r}') \phi_i(\mathbf{r}')}{|\mathbf{r} - \mathbf{r}'|}. \tag{7.7}$$

Other functionals for example are the self interaction corrected Müller functional[178] and the BBC functionals; BBC1, BBC2, BBC3.[179] Hence implementation of RDMFT can use a partially occupied HF formalism with a modified Fock term. Minimisation of the energy requires a minimisation of occupancies which is easy to accomplish, however the determination of the natural orbitals cannot be reduced to an iterative eigenvalue problem like HF or DFT and is computationally expensive to carry out. Additionally RDMFT has no directly associated single particle eigenvalue spectrum, so calculations are limited to properties that involve absolute energies or projections of the density matrix to find out spectral information, which is again computationally expensive.[175]

Static Correlation Effects in DFT

Rather than solving a full RDMFT calculation the RDMFT energy functional could instead be used in a Kohn-Sham calculation. Using the methodology of the optimised effective potential following the method for variationally minimising the EXX potential as detailed in previous chapters. The approximate natural orbitals for this system are determined from a KS equation using a local exchange-correlation potential, allowing an iterative eigenvalue scheme to determine the orbitals. The total energy functional would be the RDMFT energy functional, occupancies would be determined by fixing the orbitals and minimising total energy relative to the occupancies. The local potential could then be varied using the partially occupied EXX functional derivative with the non-local

Fock exchange term replaced with the non-local RMDFT exchange-correlation term. As we use a Kohn-Sham equation to determine the eigenfunctions and eigenvalues of the system, band structures and other spectral properties would be trivially accessible and derivative discontinuities could potentially be calculated by generalising the ensemble method detailed in the previous chapter to the RDMFT energy functional. Potential drawbacks would be the increased number of orbitals with small partial occupancy needed relative to a EXX or HF calculation (up to 50 extra orbitals[175]) which would increase the memory overheads and computational effort required, as HF and hence RDMFT scale as N^2 with respect to the number of orbitals.

7.3 Final Remarks

In this work we have derived and implemented accurate local exchange potentials in DFT. The accuracy of these potentials was demonstrated by calculating the electronic structures of a selection of materials. The correct treatment of excitation energies was discussed in relation to the derivative discontinuity. We have demonstrated that exchange and correlation contributions to the discontinuity must be treated together. A second order correlation energy was proposed to allow the treatment of the correlation contribution. Based on the calculated electronic structures the local exact exchange potentials give accurate structures for systems where the exchange energy is dominant relative to the correlation energy. For systems where this is not the case, we discussed, in this final chapter, one possible method beyond DFT to improve the treatment of strongly correlated materials, while retaining a local exchange-correlation potential. With the proposed extensions to the local potentials, derivative discontinuity and increases in computational capability, the implementations shown here could become an invaluable tool in the first principles calculation of the electronic structure of any material.

Appendix A

Symbols and Abbreviations

In this appendix we list some of symbols and abbreviations that are frequently used throughout this thesis.

A.1 Variables

A.1.1 Integers

N	Number of electrons
M	Number of nuclei
Z	Atomic number
$N_{\mathbf{k},\mathbf{q}}$	Number of $\mathbf{k}, \mathbf{q}$-points
N_b	Number of bands
N_pw	Number of plane waves
n	Electron index
i, k	Occupied orbital index
k	Orbital index
a, b	Unoccupied orbital index

A.1.2 Real variables

E	Total energy
T	Kinetic energy
T_s	Non-interacting kinetic energy
E_ext	External potential energy
E_ee	Electron-electron interaction energy
E_H	Hartree energy
E_x	Exchange energy
E_xc	Exchange-correlation energy
E_c	Correlation energy
ε_i^σ	Eigenvalue for the i-th orbital of spin σ
E_g	Fundamental band gap
E_g^KS	Kohn-Sham band gap
Δ_xc	Derivative Discontinuity
n_i^σ	Occupancy of the i-th orbital of spin σ
Ω	Unit cell volume
λ	Step size
θ	Smearing width
E_cutoff	Plane wave cut off energy

A.1.3 Vectors

$\mathbf{r}$	Position vector
$\mathbf{R}_I$	Position vector for a nuclei
$\mathbf{R}$	Lattice vector
$\mathbf{G}$	Reciprocal lattice vector
$\mathbf{a}, \mathbf{b}, \mathbf{c}$	Unit cell vector
$\mathbf{a}^*, \mathbf{b}^*, \mathbf{c}^*$	Reciprocal unit cell vector
$\mathbf{k}, \mathbf{q}$	Bloch wave vector

A.1.4 Real Fields

$\rho(\mathbf{r})$	Electron density

A.1.5 Complex Fields

$\psi_i(\mathbf{r})$	Single particle orbital
$\phi_i^\sigma(\mathbf{r})$	Kohn-Sham single particle orbital
$\tilde{\phi}_i^\sigma(\mathbf{r})$	First order Kohn-Sham single particle orbital
$c_i^\sigma(\mathbf{G})$	Reciprocal space plane wave component

A.1.6 Operators

$\hat{H}$	Hamiltonian
$\hat{T}$	Kinetic energy operator
$\hat{T}_\mathrm{s}$	Non-interacting kinetic energy operator
$\hat{V}_\mathrm{ext}(\mathbf{r})$	External potential
$\hat{V}_\mathrm{H}(\mathbf{r})$	Hartree potential
$\hat{V}_\mathrm{x}(\mathbf{r})$	Exchange potential
$\hat{V}_\mathrm{xc}(\mathbf{r})$	Exchange-correlation potential
$\hat{P}_\mathrm{c}$	Conduction band projector operator

A.1.7 Two-Particle Objects

$\rho(\mathbf{r},\mathbf{r}')$	One body reduced density matrix
$\Gamma(\mathbf{r},\mathbf{r}')$	Pair density

A.1.8 Many-Particle Objects

Ψ	Many-electron wave function
Φ	Kohn-Sham Slater determinant

A.1.9 Other variables

σ	Spin coordinate

A.2 Abbreviations

DFT	Density functional theory
HF	Hartree-Fock
LDA	Local density approximation
GGA	Generalised gradient approximation
PBE	The generalised gradient approximation of Perdew, Burke and Ernzerhof.[23]
EXX	Exact exchange
KLI	Approximation of Kriger, Li and Iafrate
CEDA	Common energy denominator approximation
LFX	Local Fock exchange
MP	Monkhorst-Pack

Appendix B

Derivation of the 2nd Order Energy Difference

In section 3.3.5, we consider the energy difference T_Ψ;

$$T_\Psi[\hat{V}] = \langle\Psi|\hat{H}_\mathrm{v}|\Psi\rangle - E_\mathrm{v} > 0, \tag{B.1}$$

where Ψ is the ground state many-body wave function of a system of N interacting electrons. The interacting wave function, Ψ is expanded in a perturbative expansion.[112] We start with a non-interacting Hamiltonian as our zeroth-order approximation, where $\hat{U}(\mathbf{r})$ is an undetermined potential that mimics the electron interaction potential. The non-interacting zeroth-order Hamiltonian is;

$$\hat{H}_{\hat{V}_\mathrm{ext}+\hat{U}} = \hat{T} + \hat{V}_\mathrm{ext} + \hat{U}, \qquad\qquad \hat{U} = \sum_i \hat{U}(\mathbf{r}_i), \tag{B.2}$$

the eigenstates and eigenvalues of which are $\Phi_{\mathrm{u},n}$ and $E_{\mathrm{u},n}$ respectively. It is worth noting that $\Phi_{\mathrm{u},n}$ is an excited Slater determinant of the zeroth-order Hamiltonian, the index n sums all possible excited Slater determinants. The ground state Slater determinant is Φ_u.

Considering the interaction as a perturbation to the non-interacting zeroth order Hamiltonian, we can define a tunable Hamiltonian that switches on interactions as a perturbation;

$$\hat{H}(\alpha) = \hat{H}_{\hat{V}_\mathrm{ext}+\hat{U}} + \alpha(V_\mathrm{ee} - \sum_{i=1}^{N} \hat{U}(\mathbf{r}_i)), \qquad\qquad 0 \leq \alpha \leq 1. \tag{B.3}$$

The interaction is linear in α and for $\alpha = 1$ the Hamiltonian is fully interacting and for $\alpha = 0$ the Hamiltonian is fully non-interacting. For small α the properly normalised interacting ground state wave function of $\hat{H}(\alpha)$, $\Psi(\alpha)$ is to first order;

$$\Psi(\alpha) = \Phi_\mathrm{u} + \alpha\Phi'_\mathrm{u} - \frac{\alpha^2}{2}\Phi_\mathrm{u}\langle\Phi'_\mathrm{u}|\Phi'_\mathrm{u}\rangle, \tag{B.4}$$

The first order correction Φ'_{u} is then given by;

$$\Phi'_{\mathrm{u}} = -\sum_n \frac{\langle \Phi_{\mathrm{u},n}|\hat{V}_{\mathrm{ee}} - \hat{U}|\Phi_{\mathrm{u}}\rangle}{E_{\mathrm{u},n} - E_{\mathrm{u}}}\Phi_{\mathrm{u},n}. \tag{B.5}$$

Turning to the effective non-interacting Hamiltonian, $\hat{H}_{\mathrm{v}}$ with the interacting wave function $\Psi(\alpha)$ as its approximate ground state, the effective potential $\hat{V}$ will be close to $\hat{V}_{\mathrm{ext}} + \hat{U}$ since at $\alpha = 0$, $\hat{V} = \hat{V}_{\mathrm{ext}} + \hat{U}$. Hence for small α, $\hat{V} = \hat{V}_{\mathrm{ext}} + \hat{U} + \alpha\hat{V}'$ where $\hat{V}'$ is a perturbing potential. We then consider the perturbed non-interacting Hamiltonian;

$$\hat{H}_{\mathrm{v}} = \hat{H}_{\hat{V}_{\mathrm{ext}}+\hat{U}} + \alpha\sum_{i=1}^{N}\hat{V}'(\mathbf{r}_i), \tag{B.6}$$

with a ground state Slater determinant given by, $\Phi_{\hat{\mathrm{u}}+\alpha\hat{\mathrm{v}}'}$. This ground state too can be expanded up to order α;

$$\Phi_{\hat{\mathrm{u}}+\hat{\mathrm{v}}'} = \Phi_{\mathrm{u}} + \alpha\tilde{\Phi}'_{\mathrm{u}} - \frac{\alpha^2}{2}\Phi_{\mathrm{u}}\langle\tilde{\Phi}'_{\mathrm{u}}|\tilde{\Phi}'_{\mathrm{u}}\rangle. \tag{B.7}$$

The first order correction $\tilde{\Phi}'_{\mathrm{u}}$ is then given by;

$$\tilde{\Phi}'_{\mathrm{u}} = -\sum_n \frac{\langle \Phi_{\mathrm{u},n}|\hat{V}'|\Phi_{\mathrm{u}}\rangle}{E_{\mathrm{u},n} - E_{\mathrm{u}}}\Phi_{\mathrm{u},n}. \tag{B.8}$$

The total energy for the non-interacting system is to order α^2;

$$\begin{aligned}
E_{\mathrm{v}} =& E_{\mathrm{u}} + \alpha\langle\Phi_{\mathrm{u}}|\hat{V}'|\Phi_{\mathrm{u}}\rangle + \alpha^2\Big(\langle\tilde{\Phi}'_{\mathrm{u}}|\hat{V}'|\Phi_{\mathrm{u}}\rangle + \langle\Phi_{\mathrm{u}}|\hat{V}'|\tilde{\Phi}'_{\mathrm{u}}\rangle + \langle\tilde{\Phi}'_{\mathrm{u}}|\hat{H}_{\hat{V}_{\mathrm{ext}}+\hat{U}}|\tilde{\Phi}'_{\mathrm{u}}\rangle \\
&- \frac{1}{2}\langle\tilde{\Phi}'_{\mathrm{u}}|\tilde{\Phi}'_{\mathrm{u}}\rangle\langle\Phi_{\mathrm{u}}|\hat{H}_{\hat{V}_{\mathrm{ext}}+\hat{U}}|\Phi_{\mathrm{u}}\rangle - \frac{1}{2}\langle\Phi_{\mathrm{u}}|\hat{H}_{\hat{V}_{\mathrm{ext}}+\hat{U}}|\Phi_{\mathrm{u}}\rangle\langle\tilde{\Phi}'_{\mathrm{u}}|\tilde{\Phi}'_{\mathrm{u}}\rangle\Big) \\
=& E_{\mathrm{u}} + \alpha\langle\Phi_{\mathrm{u}}|\hat{V}'|\Phi_{\mathrm{u}}\rangle + \alpha^2\left[\sum_n\sum_m \frac{\langle\Phi_{\mathrm{u}}|\hat{V}'|\Phi_{\mathrm{u},n}\rangle\langle\Phi_{\mathrm{u},n}|\hat{H}_{\hat{V}_{\mathrm{ext}}+\hat{U}}|\Phi_{\mathrm{u},m}\rangle\langle\Phi_{\mathrm{u},m}|\hat{V}'|\Phi_{\mathrm{u}}\rangle}{(E_{\mathrm{u},n} - E_{\mathrm{u}})(E_{\mathrm{u},m} - E_{\mathrm{u}})}\right. \\
&- \sum_n \frac{\langle\Phi_{\mathrm{u}}|\hat{V}'|\Phi_{\mathrm{u},n}\rangle\langle\Phi_{\mathrm{u},n}|\hat{V}'|\Phi_{\mathrm{u}}\rangle}{E_{\mathrm{u},n} - E_{\mathrm{u}}} - \sum_n \frac{\langle\Phi_{\mathrm{u}}|\hat{V}'|\Phi_{\mathrm{u},n}\rangle\langle\Phi_{\mathrm{u},n}|\hat{V}'|\Phi_{\mathrm{u}}\rangle}{E_{\mathrm{u},n} - E_{\mathrm{u}}} \\
&\left.- \sum_n\sum_m \langle\Phi_{\mathrm{u}}|\hat{H}_{\hat{V}_{\mathrm{ext}}+\hat{U}}|\Phi_{\mathrm{u}}\rangle \frac{\langle\Phi_{\mathrm{u}}|\hat{V}'|\Phi_{\mathrm{u},n}\rangle\langle\Phi_{\mathrm{u},n}|\Phi_{\mathrm{u},m}\rangle\langle\Phi_{\mathrm{u},m}|\hat{V}'|\Phi_{\mathrm{u}}\rangle}{(E_{\mathrm{u},n} - E_{\mathrm{u}})(E_{\mathrm{u},m} - E_{\mathrm{u}})}\right] \\
=& E_{\mathrm{u}} + \alpha\langle\Phi_{\mathrm{u}}|\hat{V}'|\Phi_{\mathrm{u}}\rangle - \alpha^2\sum_n \frac{\langle\Phi_{\mathrm{u}}|\hat{V}'|\Phi_{\mathrm{u},n}\rangle\langle\Phi_{\mathrm{u},n}|\hat{V}'|\Phi_{\mathrm{u}}\rangle}{E_{\mathrm{u},n} - E_{\mathrm{u}}}.
\end{aligned} \tag{B.9}$$

The expectation of the non-interacting Hamiltonian, $\hat{H}_{\hat{V}_{\mathrm{ext}}+\hat{U}}$ applied to the interacting

state, $\Psi(\alpha)$ is;

$$
\begin{aligned}
&\langle\Psi(\alpha)|\hat{H}_{\mathrm{v}}|\Psi(\alpha)\rangle \\
=&\langle\Phi_{\mathrm{u}}+\alpha\Phi'_{\mathrm{u}}-\frac{\alpha^2}{2}\Phi_{\mathrm{u}}\langle\Phi'_{\mathrm{u}}|\Phi'_{\mathrm{u}}\rangle|\hat{H}_{\hat{V}_{\mathrm{ext}}+\hat{U}}+\alpha\hat{V}'|\Phi_{\mathrm{u}}+\alpha\Phi'_{\mathrm{u}}-\frac{\alpha^2}{2}\Phi_{\mathrm{u}}\langle\Phi'_{\mathrm{u}}|\Phi'_{\mathrm{u}}\rangle\rangle \\
=&\langle\Phi_{\mathrm{u}}|\hat{H}_{\hat{V}_{\mathrm{ext}}+\hat{U}}|\Phi_{\mathrm{u}}\rangle+\alpha\langle\Phi'_{\mathrm{u}}|\hat{V}'|\Phi'_{\mathrm{u}}\rangle+\alpha^2\Big(\langle\Phi'_{\mathrm{u}}|\hat{H}_{\hat{V}_{\mathrm{ext}}+\hat{U}}|\Phi'_{\mathrm{u}}\rangle \\
&+\langle\Phi'_{\mathrm{u}}|\hat{V}'|\Phi_{\mathrm{u}}\rangle+\langle\Phi_{\mathrm{u}}|\hat{V}'|\Phi'_{\mathrm{u}}\rangle-\frac{1}{2}\langle\Phi'_{\mathrm{u}}|\Phi'_{\mathrm{u}}\rangle\langle\Phi_{\mathrm{u}}|\hat{V}'|\Phi_{\mathrm{u}}\rangle \\
&-\frac{1}{2}\langle\Phi_{\mathrm{u}}|\hat{V}'|\Phi_{\mathrm{u}}\rangle\langle\Phi'_{\mathrm{u}}|\Phi'_{\mathrm{u}}\rangle\Big) \\
=&E_{\mathrm{u}}+\alpha\langle\Phi'_{\mathrm{u}}|\hat{V}'|\Phi'_{\mathrm{u}}\rangle \\
&+\alpha^2\left[\sum_n\sum_m\frac{\langle\Phi_{\mathrm{u}}|\hat{V}_{\mathrm{ee}}-\hat{U}|\Phi_{\mathrm{u},n}\rangle\langle\Phi_{\mathrm{u},n}|\hat{H}_{\hat{V}_{\mathrm{ext}}+\hat{U}}|\Phi_{\mathrm{u},m}\rangle\langle\Phi_{\mathrm{u},m}|\hat{V}_{\mathrm{ee}}-\hat{U}|\Phi_{\mathrm{u}}\rangle}{(E_{\mathrm{u},n}-E_{\mathrm{u}})(E_{\mathrm{u},m}-E_{\mathrm{u}})}\right. \\
&-\sum_n\frac{\langle\Phi_{\mathrm{u}}|\hat{V}_{\mathrm{ee}}-\hat{U}|\Phi_{\mathrm{u},n}\rangle\langle\Phi_{\mathrm{u},n}|\hat{V}'|\Phi_{\mathrm{u}}\rangle}{E_{\mathrm{u},n}-E_{\mathrm{u}}}-\sum_n\frac{\langle\Phi_{\mathrm{u}}|\hat{V}'|\Phi_{\mathrm{u},n}\rangle\langle\Phi_{\mathrm{u},n}|\hat{V}_{\mathrm{ee}}-\hat{U}|\Phi_{\mathrm{u}}\rangle}{E_{\mathrm{u},n}-E_{\mathrm{u}}} \\
&\left.-\sum_n\sum_m\langle\Phi_{\mathrm{u}}|\hat{H}_{\hat{V}_{\mathrm{ext}}+\hat{U}}|\Phi_{\mathrm{u}}\rangle\frac{\langle\Phi_{\mathrm{u}}|\hat{V}_{\mathrm{ee}}-\hat{U}|\Phi_{\mathrm{u},n}\rangle\langle\Phi_{\mathrm{u},n}|\Phi_{\mathrm{u},m}\rangle\langle\Phi_{\mathrm{u},m}|\hat{V}_{\mathrm{ee}}-\hat{U}|\Phi_{\mathrm{u}}\rangle}{(E_{\mathrm{u},n}-E_{\mathrm{u}})(E_{\mathrm{u},m}-E_{\mathrm{u}})}\right] \\
=&E_{\mathrm{u}}+\alpha\langle\Phi'_{\mathrm{u}}|\hat{V}'|\Phi'_{\mathrm{u}}\rangle+\alpha^2\left[\sum_n\frac{\langle\Phi_{\mathrm{u}}|\hat{V}_{\mathrm{ee}}-\hat{U}|\Phi_{\mathrm{u},n}\rangle\langle\Phi_{\mathrm{u},n}|\hat{V}_{\mathrm{ee}}-\hat{U}|\Phi_{\mathrm{u}}\rangle}{(E_{\mathrm{u},n}-E_{\mathrm{u}})}\right. \\
&\left.-\sum_n\frac{\langle\Phi_{\mathrm{u}}|\hat{V}_{\mathrm{ee}}-\hat{U}|\Phi_{\mathrm{u},n}\rangle\langle\Phi_{\mathrm{u},n}|\hat{V}'|\Phi_{\mathrm{u}}\rangle}{E_{\mathrm{u},n}-E_{\mathrm{u}}}-\sum_n\frac{\langle\Phi_{\mathrm{u}}|\hat{V}'|\Phi_{\mathrm{u},n}\rangle\langle\Phi_{\mathrm{u},n}|\hat{V}_{\mathrm{ee}}-\hat{U}|\Phi_{\mathrm{u}}\rangle}{E_{\mathrm{u},n}-E_{\mathrm{u}}}\right].
\end{aligned}
\tag{B.10}
$$

Substituting equations B.9 and B.10 into T_Ψ gives;

$$
\begin{aligned}
&T_\Psi[\hat{V}_{\mathrm{ext}}+\hat{U}+\alpha\hat{V}'] \\
=&E_{\mathrm{u}}+\alpha\langle\Phi'_{\mathrm{u}}|\hat{V}'|\Phi'_{\mathrm{u}}\rangle+\alpha^2\left[\sum_n\frac{\langle\Phi_{\mathrm{u}}|\hat{V}_{\mathrm{ee}}-\hat{U}|\Phi_{\mathrm{u},n}\rangle\langle\Phi_{\mathrm{u},n}|\hat{V}_{\mathrm{ee}}-\hat{U}|\Phi_{\mathrm{u}}\rangle}{(E_{\mathrm{u},n}-E_{\mathrm{u}})}\right. \\
&\left.-\sum_n\frac{\langle\Phi_{\mathrm{u}}|\hat{V}_{\mathrm{ee}}-\hat{U}|\Phi_{\mathrm{u},n}\rangle\langle\Phi_{\mathrm{u},n}|\hat{V}'|\Phi_{\mathrm{u}}\rangle}{E_{\mathrm{u},n}-E_{\mathrm{u}}}-\sum_n\frac{\langle\Phi_{\mathrm{u}}|\hat{V}'|\Phi_{\mathrm{u},n}\rangle\langle\Phi_{\mathrm{u},n}|\hat{V}_{\mathrm{ee}}-\hat{U}|\Phi_{\mathrm{u}}\rangle}{E_{\mathrm{u},n}-E_{\mathrm{u}}}\right] \\
&-E_{\mathrm{u}}-\alpha\langle\Phi_{\mathrm{u}}|\hat{V}'|\Phi_{\mathrm{u}}\rangle+\alpha^2\sum_n\frac{\langle\Phi_{\mathrm{u}}|\hat{V}'|\Phi_{\mathrm{u},n}\rangle\langle\Phi_{\mathrm{u},n}|\hat{V}'|\Phi_{\mathrm{u}}\rangle}{E_{\mathrm{u},n}-E_{\mathrm{u}}}. \\
=&\alpha^2T''_{\mathrm{u}}[\hat{V}]=\alpha^2\sum_n\frac{\langle\Phi_{\mathrm{u}}|\hat{V}_{\mathrm{ee}}-\hat{V}|\Phi_{\mathrm{u},n}\rangle\langle\Phi_{\mathrm{u},n}|\hat{V}_{\mathrm{ee}}-\hat{V}|\Phi_{\mathrm{u}}\rangle}{(E_{\mathrm{u},n}-E_{\mathrm{u}})},
\end{aligned}
\tag{B.11}
$$

where $\hat{V}=\hat{U}+\hat{V}'$. T_Ψ also contains terms in higher orders of α. T''_{u} is a functional of the unknown potential $\hat{U}$, which is kept fixed.

Considering only single excitations, decomposing the Slater determinants, Φ_{u} and

$\Phi_{\mathrm{u},n}$ into single particle orbitals, using the Slater-Condon rules gives;[10, 11]

$$T''_{\mathrm{u}} = \sum_{\sigma} \sum_{i=1}^{N^\sigma} \sum_{a=N^\sigma+1}^{\infty} \frac{|\langle \phi^\sigma_{\mathrm{u},i} | \hat{V}_{H,\mathbf{u}}(\mathbf{r}) + \hat{\mathrm{u}}^\sigma_{x,\mathbf{u},i}(\mathbf{r}) - \hat{V}^\sigma(\mathbf{r}) | \phi^\sigma_{\mathrm{u},a} \rangle|^2}{\varepsilon^\sigma_{\mathrm{u},a} - \varepsilon^\sigma_{\mathrm{u},i}} > 0. \tag{B.12}$$

T''_{u} should also contain a term including double excitations, but that term is only dependent on $\hat{U}$ which is kept fixed. As we are only interested in the behaviour of T''_{u} as $\hat{V}$ changes, the double excitation term is a constant and is hence neglected.

Appendix C

Brillouin Zones and Special Points

In this appendix we show the Brillouin zones and special points used in the calculation of band structures.

Point	Coordinates
Face centred cubic	
Γ	(0,0,0)
K	$(\frac{3}{8},\frac{3}{8},\frac{3}{4})$
L	$(\frac{1}{2},\frac{1}{2},\frac{1}{2})$
W	$(\frac{1}{2},\frac{1}{4},\frac{3}{4})$
X	$(\frac{1}{2},\frac{1}{2},0)$

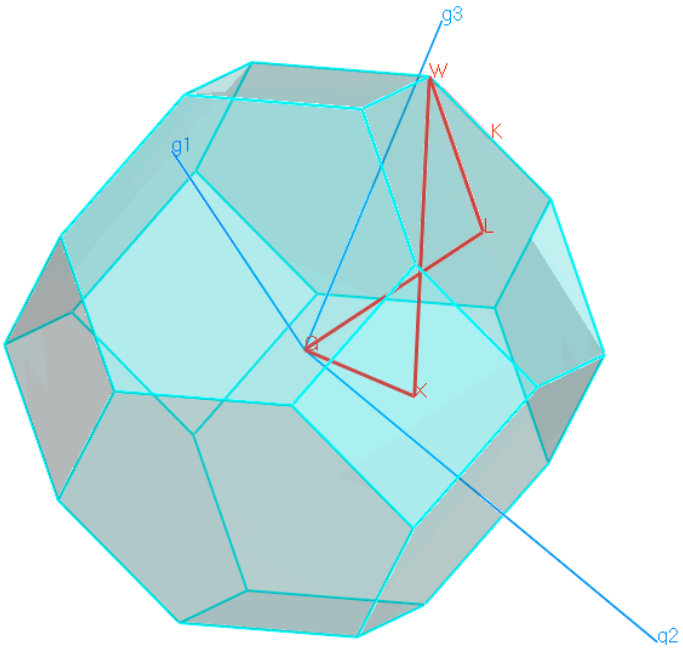

Figure C.1: Brillouin zone and special points for a face centred cubic lattice.

Point	Coordinates
Hexagonal	
A	$(0,0,\frac{1}{2})$
Γ	$(0,0,0)$
H	$(\frac{2}{3},\frac{2}{3},\frac{1}{2})$
K	$(\frac{2}{3},\frac{2}{3},0)$
L	$(0,\frac{1}{2},\frac{1}{2})$
M	$(0,\frac{1}{2},0)$

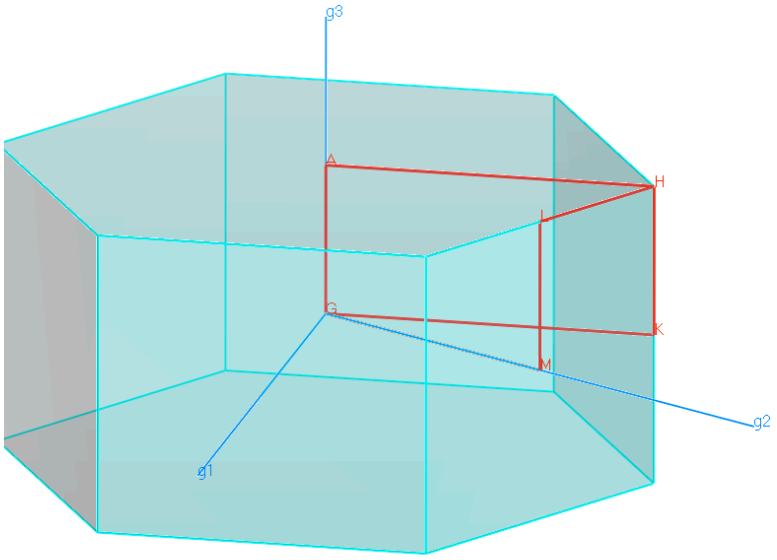

Figure C.2: Brillouin zone and special points for a hexagonal lattice.

Point	Coordinates
Orthorhombic	
Γ	$(0,0,0)$
R	$(\frac{1}{2},\frac{1}{2},\frac{1}{2})$
S	$(\frac{1}{2},\frac{1}{2},0)$
Y	$(0,\frac{1}{2},0)$

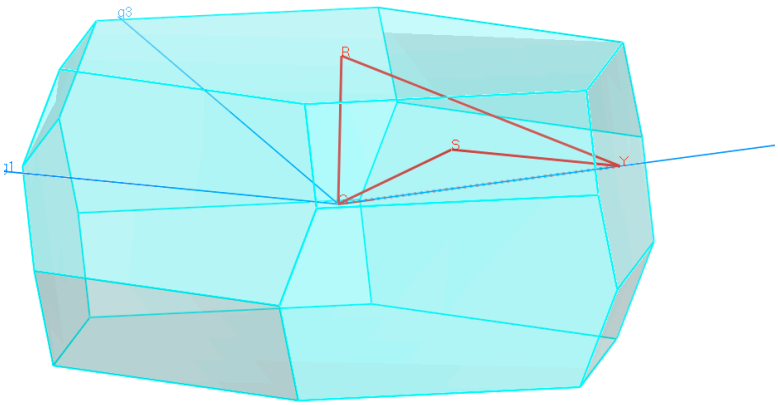

Figure C.3: Brillouin zone and special points for a orthorhombic lattice.

Point	Coordinates
Simple cubic cubic	
Γ	(0,0,0)
R	$(\frac{1}{2},\frac{1}{2},\frac{1}{2})$
X	$(0,\frac{1}{2},0)$

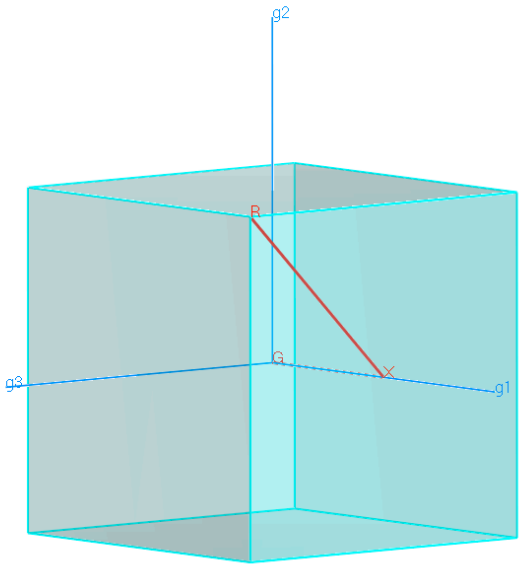

Figure C.4: Brillouin zone and special points for a simple cubic lattice.

Point	Coordinates
Body centred cubic	
Γ	(0,0,0)
H	$(\frac{1}{2},\frac{1}{2},\frac{1}{2})$
N	$(0,0,\frac{1}{2})$
P	$(\frac{1}{4},\frac{1}{4},\frac{1}{4})$

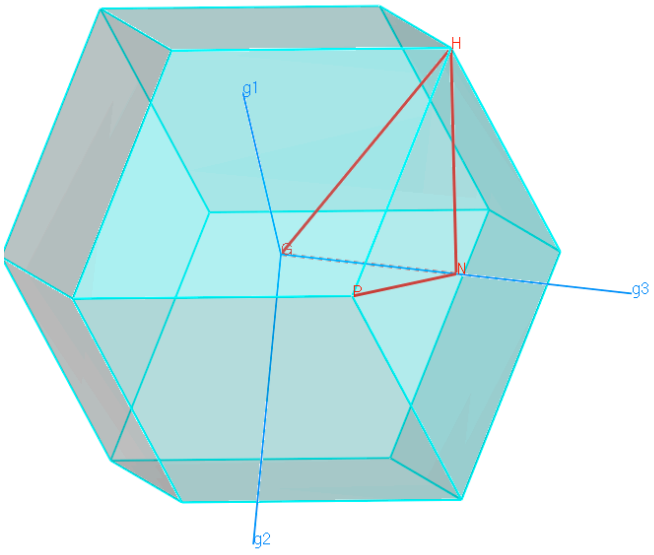

Figure C.5: Brillouin zone and special points for a body centred cubic lattice.

Bibliography

[1] R. M. Martin. *Electronic Structure: Basic Theory And Practical Methods*. Cambridge University Press, 2008.

[2] J. Kohanoff. *Electronic Structure Calculations for Solids and Molecules*. Cambridge University Press, 2006.

[3] C. A. Ullrich. *Time-dependent density-functional theory. Concepts and applications.* Oxford Graduate Texts. Oxford: Oxford University Press., 2012.

[4] J. Kohanoff and N. Gidopoulos. Density Functional Theory: Basics, New Trends and Applications. In S. Wilson, editor, *Handbook of Molecular Physics and Quantum Chemistry*, pages 532–568. John Wiley & Sons Ltd., 2002.

[5] M. Born and J. M. Oppenheimer. Zur quantentheorie der molekin. *Ann. Physik*, 389:457, 1927.

[6] D. R. Hartree. The wave mechanics of an atom with a non-coulomb central field. part i. theory and methods. *Mathematical Proceedings of the Cambridge Philosophical Society*, 24:89–110, 1928.

[7] D. R. Hartree. The wave mechanics of an atom with a non-coulomb central field. part ii. some results and discussion. *Mathematical Proceedings of the Cambridge Philosophical Society*, 24:111–132, 1928.

[8] D. R. Hartree. The wave mechanics of an atom with a non-coulomb central field. part iii. term values and intensities in series in optical spectra. *Mathematical Proceedings of the Cambridge Philosophical Society*, 24:426–437, 1928.

[9] J. C. Slater. A simplification of the Hartree-Fock method. *Phys. Rev.*, 81:385–390, 1951.

[10] J. C. Slater. The theory of complex spectra. *Phys. Rev.*, 34:1293–1322, 1929.

[11] E. U. Condon. The theory of complex spectra. *Phys. Rev.*, 36:1121–1133, 1930.

[12] V. Fock. Näherungsmethode zur lösung des quantenmechanischen mehrkörperproblems. *Zeitschrift für Physik*, 61(1-2):126–148, 1930.

[13] E. R. Davidson. Properties and uses of natural orbitals. *Rev. Mod. Phys.*, 44:451–464, 1972.

[14] R. O. Jones and O. Gunnarsson. The density functional formalism, its applications and prospects. *Rev. Mod. Phys.*, 61:689–746, 1989.

[15] P. Hohenberg and W. Kohn. Inhomogeneous electron gas. *Phys. Rev.*, 136:B864–B871, 1964.

[16] W. Kohn and L. J. Sham. Self-consistent equations including exchange and correlation effects. *Phys. Rev.*, 140:A1133–A1138, 1965.

[17] D. M. Ceperley and B. J. Alder. Ground state of the electron gas by a stochastic method. *Phys. Rev. Lett.*, 45:566–569, 1980.

[18] J. P. Perdew and A. Zunger. Self-interaction correction to density-functional approximations for many-electron systems. *Phys. Rev. B*, 23:5048–5079, 1981.

[19] J. P. Perdew and Yue Wang. Accurate and simple density functional for the electronic exchange energy: Generalized gradient approximation. *Phys. Rev. B*, 33:8800–8802, 1986.

[20] J. P. Perdew and Yue Wang. Accurate and simple analytic representation of the electron-gas correlation energy. *Phys. Rev. B*, 45:13244–13249, 1992.

[21] J. P. Perdew. Accurate density functional for the energy: Real-space cutoff of the gradient expansion for the exchange hole. *Phys. Rev. Lett.*, 55:1665–1668, 1985.

[22] J. P. Perdew, K. Burke, and Yue Wang. Generalized gradient approximation for the exchange-correlation hole of a many-electron system. *Phys. Rev. B*, 54:16533–16539, 1996.

[23] J. P. Perdew, K. Burke, and M. Ernzerhof. Generalized gradient approximation made simple. *Phys. Rev. Lett.*, 77:3865–3868, 1996.

[24] Zhigang Wu and R. E. Cohen. More accurate generalized gradient approximation for solids. *Phys. Rev. B*, 73:235116, 2006.

[25] J. P. Perdew, S. Kurth, A. Zupan, and P. Blaha. Accurate density functional with correct formal properties: A step beyond the generalized gradient approximation. *Phys. Rev. Lett.*, 82:2544–2547, 1999.

[26] Book of Genesis; 28:10-19.

[27] J. P. Perdew and K. Schmidt. Jacob's ladder of density functional approximations for the exchange-correlation energy. *AIP Conference Proceedings*, 577(1):1–20, 2001.

[28] A. D. Becke. Density-functional thermochemistry. iii. the role of exact exchange. *The Journal of Chemical Physics*, 98(7):5648–5652, 1993.

[29] A. D. Becke. Density-functional thermochemistry. iv. a new dynamical correlation functional and implications for exact-exchange mixing. *The Journal of Chemical Physics*, 104(3):1040–1046, 1996.

[30] A. D. Becke. Density-functional thermochemistry. v. systematic optimization of exchange-correlation functionals. *The Journal of Chemical Physics*, 107(20):8554–8560, 1997.

[31] F. Gygi and A. Baldereschi. Self-consistent Hartree-Fock and screened-exchange calculations in solids: Application to silicon. *Phys. Rev. B*, 34:4405–4408, 1986.

[32] A. Seidl, A. Görling, P. Vogl, J. A. Majewski, and M. Levy. Generalized Kohn-Sham schemes and the band-gap problem. *Phys. Rev. B*, 53:3764–3774, 1996.

[33] S. Chawla and G. A. Voth. Exact exchange in ab initio molecular dynamics: An efficient plane-wave based algorithm. *The Journal of Chemical Physics*, 108(12):4697–4700, 1998.

[34] S. J. Clark and J. Robertson. Screened exchange density functional applied to solids. *Phys. Rev. B*, 82:085208, 2010.

[35] S. Kümmel and L. Kronik. Orbital-dependent density functionals: Theory and applications. *Rev. Mod. Phys.*, 80:3–60, 2008.

[36] U. von Barth and L. Hedin. A local exchange-correlation potential for the spin polarized case. i. *Journal of Physics C: Solid State Physics*, 5(13):1629, 1972.

[37] O. Gunnarsson and B. I. Lundqvist. Exchange and correlation in atoms, molecules, and solids by the spin-density-functional formalism. *Phys. Rev. B*, 13:4274–4298, 1976.

[38] F. L. Pratt, P. J. Baker, S. J. Blundell, T. Lancaster, S. Ohira-Kawamura, C. Baines, Y. Shimizu, K. Kanoda, I. Watanabe, and G. Saito. Magnetic and non-magnetic phases of a quantum spin liquid. *Nature*, 471(7340):612–616, 2011.

[39] Key Yosida. *Theory of Magnetism.* Springer-Verlag, Berlin, 1996.

[40] G. Scalmani and M. J. Frisch. A new approach to noncollinear spin density functional theory beyond the local density approximation. *Journal of Chemical Theory and Computation*, 8(7):2193–2196, 2012.

[41] N.W. Ashcroft and N.D. Mermin. *Solid State Physics.* Saunders College, Philadelphia, 1976.

[42] A. Messiah. *Quantum Mechanics Volume II.* Elsevier Science B.V., 1961.

[43] B. Delley. An all–electron numerical method for solving the local density functional for polyatomic molecules. *The Journal of Chemical Physics*, 92(1):508–517, 1990.

[44] S. F. Boys. Electronic wave functions. i. a general method of calculation for the stationary states of any molecular system. *Proceedings of the Royal Society of London. Series A. Mathematical and Physical Sciences*, 200(1063):542–554, 1950.

[45] T. L. Loucks. Fermi surfaces of Cr, Mo, and W by the augmented-plane-wave method. *Phys. Rev.*, 139:A1181–A1188, 1965.

[46] T. L. Loucks. *Augmented plane wave method: a guide to performing electronic structure calculations.* Frontiers in physics. W.A. Benjamin, 1967.

[47] O. K. Andersen. Linear methods in band theory. *Phys. Rev. B*, 12:3060–3083, 1975.

[48] D. D. Koelling and G. O. Arbman. Use of energy derivative of the radial solution in an augmented plane wave method: application to copper. *Journal of Physics F: Metal Physics*, 5(11):2041, 1975.

[49] P. E. Blöchl. Projector augmented-wave method. *Phys. Rev. B*, 50:17953–17979, 1994.

[50] G. Kresse and D. Joubert. From ultrasoft pseudopotentials to the projector augmented-wave method. *Phys. Rev. B*, 59:1758–1775, 1999.

[51] H. J. Monkhorst and J. D. Pack. Special points for brillouin-zone integrations. *Phys. Rev. B*, 13:5188–5192, 1976.

[52] M. C. Payne, M. P. Teter, D. C. Allan, T. A. Arias, and J. D. Joannopoulos. Iterative minimization techniques for ab-initio total-energy calculations: molecular dynamics and conjugate gradients. *Rev. Mod. Phys.*, 64:1045–1097, 1992.

[53] M. C. Gibson. *Implmentation And Application Of Advanced Density Functionals.* PhD thesis, Department of Physics, University of Durham, 2006.

[54] P. P. Ewald. Die berechnung optischer und elektrostatischer gitterpotentiale. *Annalen der Physik*, 369(3):253–287, 1921.

[55] J. Ihm, A. Zunger, and M. L. Cohen. Momentum-space formalism for the total energy of solids. *Journal of Physics C: Solid State Physics*, 12(21):4409, 1979.

[56] J. C. Phillips. Energy-band interpolation scheme based on a pseudopotential. *Phys. Rev.*, 112:685–695, 1958.

[57] J. C. Phillips and L. Kleinman. New method for calculating wave functions in crystals and molecules. *Phys. Rev.*, 116:287–294, 1959.

[58] M. L. Cohen and V. Heine. The fitting of pseudopotentials to experimental data and their subsequent application. *Solid State Physics*, 24:37 – 248, 1970.

[59] D. R. Hamann, M. Schlüter, and C. Chiang. Norm-conserving pseudopotentials. *Phys. Rev. Lett.*, 43:1494–1497, 1979.

[60] A. M. Rappe, K. M. Rabe, E. Kaxiras, and J. D. Joannopoulos. Optimized pseudopotentials. *Phys. Rev. B*, 41:1227–1230, 1990.

[61] G. P. Kerker. Non-singular atomic pseudopotentials for solid state applications. *Journal of Physics C: Solid State Physics*, 13(9):L189, 1980.

[62] G. B. Bachelet and M. Schlüter. Relativistic norm-conserving pseudopotentials. *Phys. Rev. B*, 25:2103–2108, 1982.

[63] X. Gonze, R. Stumpf, and M. Scheffler. Analysis of separable potentials. *Phys. Rev. B*, 44:8503–8513, 1991.

[64] N. Troullier and J. L. Martins. Efficient pseudopotentials for plane-wave calculations. *Phys. Rev. B*, 43:1993–2006, 1991.

[65] J. S. Lin, A. Qteish, M. C. Payne, and V. Heine. Optimized and transferable nonlocal separable ab initio pseudopotentials. *Phys. Rev. B*, 47:4174–4180, 1993.

[66] W. A. Al-Saidi, E. J. Walter, and A. M. Rappe. Optimized norm-conserving Hartree-Fock pseudopotentials for plane-wave calculations. *Phys. Rev. B*, 77:075112, 2008.

[67] J. R. Trail and R. J. Needs. Norm-conserving Hartree-Fock pseudopotentials and their asymptotic behavior. *The Journal of Chemical Physics*, 122(1):–, 2005.

[68] L. Kleinman and D. M. Bylander. Efficacious form for model pseudopotentials. *Phys. Rev. Lett.*, 48:1425–1428, 1982.

[69] X. Gonze, P. Käckell, and M. Scheffler. Ghost states for separable, norm-conserving, iab initiop pseudopotentials. *Phys. Rev. B*, 41:12264–12267, 1990.

[70] D. Vanderbilt. Soft self-consistent pseudopotentials in a generalized eigenvalue formalism. *Phys. Rev. B*, 41:7892–7895, 1990.

[71] R. Fletcher and C. M. Reeves. Function minimization by conjugate gradients. *The Computer Journal*, 7(2):149–154, 1964.

[72] M. P. Teter, M. C. Payne, and D. C. Allan. Solution of schrödingers equation for large systems. *Phys. Rev. B*, 40:12255–12263, 1989.

[73] M. Jaros, C. O. Rodriguez, and S. Brand. Self-consistent pseudopotential calculation of electronic states associated with a reconstructed silicon vacancy. *Phys. Rev. B*, 19:3137–3151, 1979.

[74] P. Bendt and A. Zunger. New approach for solving the density-functional self-consistent-field problem. *Phys. Rev. B*, 26:3114–3137, 1982.

[75] C. G. Broyden. A class of methods for solving nonlinear simultaneous equations. *Math. Comp.*, 19:577–593, 1965.

[76] P. Pulay. Convergence acceleration of iterative sequences. the case of scf iteration. *Chemical Physics Letters*, 73(2):393 – 398, 1980.

[77] P. Pulay. Improved scf convergence acceleration. *Journal of Computational Chemistry*, 3(4):556–560, 1982.

[78] R. P. Feynman. Forces in molecules. *Phys. Rev.*, 56:340–343, 1939.

[79] C. J. Pickard and R. J. Needs. Ab initio random structure searching. *Journal of Physics: Condensed Matter*, 23(5):053201, 2011.

[80] M. D. Segall, P. J. D. Lindan, M. J. Probert, C. J. Pickard, P. J. Hasnip, S. J. Clark, and M. C. Payne. First-principles simulation: ideas, illustrations and the CASTEP code. *Journal of Physics: Condensed Matter*, 14(11):2717, 2002.

[81] S. J. Clark, M. D. Segall, C. J. Pickard, P. J. Hasnip, M. J. Probert, K. Refson, and M.C. Payne. First principles methods using CASTEP. *Z. Kristall.*, 220:567–570, 2005.

[82] J. P. Perdew and S. Kurth. Density functionals for non-revelativistic Coulomb system in the new century. In C. Fiolhais, F. Nogueira, and M. Marques, editors, *A Primer in density functional theory*. Springer, Berlin [etc.], 2003.

[83] R. T. Sharp and G. K. Horton. A variational approach to the unipotential many-electron problem. *Phys. Rev.*, 90:317–317, 1953.

[84] T. Grabo, T. Kribich, S. Kurth, and E. K. U. Gross. Orbital functionals in density functional theory, the optimized effective potential method. In V. I. Anisimov, editor, *Strong Coulomb Correlations in Electronic Structure: Beyond the Local Density Approximation*, pages 1–97. Gordon and Breach, 1988.

[85] J. D. Talman and W. F. Shadwick. Optimized effective atomic central potential. *Phys. Rev. A*, 14:36–40, 1976.

[86] V. R. Shaginyan. Construction of the exact exchange potential of density-functional theory. *Phys. Rev. A*, 47:1507–1509, 1993.

[87] A. Görling and M. Levy. Exact Kohn-Sham scheme based on perturbation theory. *Phys. Rev. A*, 50:196–204, 1994.

[88] J. P. Perdew and M. R. Norman. Electron removal energies in Kohn-Sham density-functional theory. *Phys. Rev. B*, 26:5445–5450, 1982.

[89] J. B. Krieger, Yan Li, and G. J. Iafrate. Construction and application of an accurate local spin-polarized Kohn-Sham potential with integer discontinuity: Exchange-only theory. *Phys. Rev. A*, 45:101–126, 1992.

[90] M. R. Norman and D. D. Koelling. Towards a Kohn-Sham potential via the optimized effective-potential method. *Phys. Rev. B*, 30:5530–5540, 1984.

[91] T. Grabo and E. K. U. Gross. Density-functional theory using an optimized exchange-correlation potential. *Chemical Physics Letters*, 240(13):141 – 150, 1995.

[92] N. I. Gidopoulos and N. N. Lathiotakis. Nonanalyticity of the optimized effective potential with finite basis sets. *Phys. Rev. A*, 85:052508, 2012.

[93] Takao Kotani. Exact exchange-potential band-structure calculations by the LMTO-ASA method: MgO and CaO. *Phys. Rev. B*, 50:14816–14821, 1994.

[94] Takao Kotani. Erratum: Exact exchange-potential band-structure calculations by the LMTO-ASA method: MgO and CaO. *Phys. Rev. B*, 51:13903–13904, 1995.

[95] Takao Kotani. Exact exchange potential band-structure calculations by the linear muffin-tin orbital-atomic-sphere approximation method for Si, Ge, C, and MnO. *Phys. Rev. Lett.*, 74:2989–2992, 1995.

[96] Takao Kotani and Hisazumi Akai. Exact exchange potential band-structure calculations for simple metals: Li, Na, K, Rb, and Ca. *Phys. Rev. B*, 52:17153–17157, 1995.

[97] M. Städele, J. A. Majewski, P. Vogl, and A. Görling. Exact Kohn-Sham exchange potential in semiconductors. *Phys. Rev. Lett.*, 79:2089–2092, 1997.

[98] M. Städele, M. Moukara, J. A. Majewski, P. Vogl, and A. Görling. Exact exchange Kohn-Sham formalism applied to semiconductors. *Phys. Rev. B*, 59:10031–10043, 1999.

[99] D. M. Bylander and L. Kleinman. Energy gaps and cohesive energy of Ge from the optimized effective potential. *Phys. Rev. Lett.*, 74:3660–3663, 1995.

[100] D. M. Bylander and L. Kleinman. Optimized effective potentials for semiconductors. *Phys. Rev. B*, 52:14566–14570, 1995.

[101] D. M. Bylander and L. Kleinman. Gradient-corrected correlation with nearly exact Kohn-Sham exchange: Calculations for Si and Ge. *Phys. Rev. B*, 55:9432–9438, 1997.

[102] R. J. Magyar, A. Fleszar, and E. K. U. Gross. Exact-exchange density-functional calculations for noble-gas solids. *Phys. Rev. B*, 69:045111, 2004.

[103] E. Engel and R. N. Schmid. Insulating ground states of transition-metal monoxides from exact exchange. *Phys. Rev. Lett.*, 103:036404, 2009.

[104] S. Baroni, S. de Gironcoli, A. Dal Corso, and P. Giannozzi. Phonons and related crystal properties from density-functional perturbation theory. *Rev. Mod. Phys.*, 73:515–562, 2001.

[105] X. Gonze. Perturbation expansion of variational principles at arbitrary order. *Phys. Rev. A*, 52:1086–1095, 1995.

[106] X. Gonze. Adiabatic density-functional perturbation theory. *Phys. Rev. A*, 52:1096–1114, 1995.

[107] S. Kümmel and J. P. Perdew. Simple iterative construction of the optimized effective potential for orbital functionals, including exact exchange. *Phys. Rev. Lett.*, 90:043004, 2003.

[108] S. Kümmel and J. P. Perdew. Optimized effective potential made simple: Orbital functionals, orbital shifts, and the exact Kohn-Sham exchange potential. *Phys. Rev. B*, 68:035103, 2003.

[109] E. A. Hylleraas. Über den grundterm der zweielektronenprobleme von H-, He, Li+, Be++ usw. *Zeitschrift für Physik*, 65(3-4):209–225, 1930.

[110] R. M. Sternheimer. Electronic polarizabilities of ions from the Hartree-Fock wave functions. *Phys. Rev.*, 96:951–968, 1954.

[111] T. W. Hollins, S. J. Clark, K. Refson, and N. I. Gidopoulos. Optimized effective potential using the Hylleraas variational method. *Phys. Rev. B*, 85:235126, 2012.

[112] N. I. Gidopoulos. Progress at the interface of wave-function and density-functional theories. *Phys. Rev. A*, 83:040502, 2011.

[113] A. Unsöld. Quantentheorie des wasserstoffmolekülions und der born-landséchen abstoßungskräfte. *Zeitschrift für Physik*, 43(8):563–574, 1927.

[114] M. Grüning, O. V. Gritsenko, and E. J. Baerends. Exchange potential from the common energy denominator approximation for the Kohn-Sham Green's function: Application to (hyper)polarizabilities of molecular chains. *The Journal of Chemical Physics*, 116(15):6435–6442, 2002.

[115] F. A. Bulat and M. Levy. Formal expressions and corresponding expansions for the exact Kohn-Sham exchange potential. *Phys. Rev. A*, 80:052510, 2009.

[116] V. N. Staroverov, G. E. Scuseria, and E. R. Davidson. Effective local potentials for orbital-dependent density functionals. *The Journal of Chemical Physics*, 125(8), 2006.

[117] F. Della Sala and A. Görling. Efficient localized Hartree-Fock methods as effective exact-exchange Kohn-Sham methods for molecules. *The Journal of Chemical Physics*, 115(13):5718–5732, 2001.

[118] T. W. Hollins, S. J. Clark, K. Refson, and N. I. Gidopoulos. The exchange potential in Kohn-Sham theory. *To be submitted*, 2014.

[119] F. R. Manby, M. Stella, J. D. Goodpaster, and T. F. Miller. A simple, exact density-functional-theory embedding scheme. *Journal of Chemical Theory and Computation*, 8(8):2564–2568, 2012.

[120] T. A. Wesolowski and A. Warshel. Frozen density functional approach for ab initio calculations of solvated molecules. *The Journal of Physical Chemistry*, 97(30):8050–8053, 1993.

[121] S. de Gironcoli. Lattice dynamics of metals from density-functional perturbation theory. *Phys. Rev. B*, 51:6773–6776, 1995.

[122] R. J. Bartlett, V. F. Lotrich, and I. V. Schweigert. Ab initio density functional theory: The best of both worlds? *The Journal of Chemical Physics*, 123(6):062205, 2005.

[123] R. Car and M. Parrinello. Unified approach for molecular dynamics and density-functional theory. *Phys. Rev. Lett.*, 55:2471–2474, 1985.

[124] http://opium.sourceforge.net/index.html. Opium pseduopotential code, 2011. [Last accessed 4-April-2014].

[125] C. J. Pickard and F. Mauri. All-electron magnetic response with pseudopotentials: Nmr chemical shifts. *Phys. Rev. B*, 63:245101, 2001.

[126] J. R. Yates, C. J. Pickard, and F. Mauri. Calculation of NMR chemical shifts for extended systems using ultrasoft pseudopotentials. *Phys. Rev. B*, 76:024401, 2007.

[127] J. Paier, R. Hirschl, M. Marsman, and G. Kresse. The Perdew Burke Ernzerhof exchange-correlation functional applied to the G2-1 test set using a plane-wave basis set. *The Journal of Chemical Physics*, 122(23), 2005.

[128] Y. Saad and M. H. Schultz. GMRES : A generalized minimal residual algorithm for solving nonsymmetric linear systems. *Journal on Scientific Computing*, 7(3):856–869, 1986.

[129] M. R. Hestenes and E. Stiefel. Methods of conjugate gradients for solving linear systems. *Journal of Research of the National Bureau of Standards*, 49(6):409–436, 1952.

[130] R. Fletcher and C. M. Reeves. Function minimization by conjugate gradients. *The Computer Journal*, 7(2):149–154, 1964.

[131] C. G. Broyden. The convergence of a class of double-rank minimization algorithms. I: General considerations. *Journal of the Institute of Mathematics and its Applications*, 6:76–90, 1970.

[132] J. Nocedal. Updating quasi-newton matrices with limited storage. *Math. Comp.*, 35:773–782, 1980.

[133] M. Levy and J. P. Perdew. Hellmann-Feynman, virial, and scaling requisites for the exact universal density functionals. shape of the correlation potential and diamagnetic susceptibility for atoms. *Phys. Rev. A*, 32:2010–2021, 1985.

[134] L. J. Sham and M. Schlüter. Density-functional theory of the band gap. *Phys. Rev. B*, 32:3883–3889, 1985.

[135] L. J. Sham. Theory of the shallow impurity states in semiconductors. *Phys. Rev.*, 150:720–727, 1966.

[136] T. Koopmans. Über die zuordnung von wellenfunktionen und eigenwerten zu den einzelnen elektronen eines atoms. *Physica*, 1(1):104 – 113, 1934.

[137] O. Madelung. *Semiconductors: Data Handbook*. Data in science and technology. Springer Berlin Heidelberg, 2004.

[138] W. Martienssen and H. Warlimont. *Springer Handbook Of Condensed Matter And Materials Data*. Springer Berlin Heidelberg, 2005.

[139] J. E. Peralta, J. Uddin, and G. E. Scuseria. Scalar relativistic all-electron density functional calculations on periodic systems. *The Journal of Chemical Physics*, 122(8), 2005.

[140] J. Heyd, J. E. Peralta, G. E. Scuseria, and R. L. Martin. Energy band gaps and lattice parameters evaluated with the Heyd-Scuseria-Ernzerhof screened hybrid functional. *The Journal of Chemical Physics*, 123(17), 2005.

[141] E. Engel. Relevance of core-valence interaction for electronic structure calculations with exact exchange. *Phys. Rev. B*, 80:161205, 2009.

[142] M. Prencipe, A. Zupan, R. Dovesi, E. Apra, and V. R. Saunders. Ab initio study of the structural properties of LiF, NaF, KF, LiCl, NaCl, and KCl. *Phys. Rev. B*, 51:3391–3396, 1995.

[143] V.Yu. Davydov, A.A. Klochikhin, R.P. Seisyan, V.V. Emtsev, S.V. Ivanov, F. Bechstedt, J. Furthmller, H. Harima, A.V. Mudryi, J. Aderhold, O. Semchinova, and J. Graul. Absorption and emission of hexagonal InN. evidence of narrow fundamental band gap. *Physica Status Solidi (b)*, 229(3):r1–r3, 2002.

[144] R. T. Poole, J. Liesegang, R. C. G. Leckey, and J. G. Jenkin. Electronic band structure of the alkali halides. ii. critical survey of theoretical calculations. *Phys. Rev. B*, 11:5190–5196, 1975.

[145] N. V. Nguyen, Albert V. Davydov, Deane Chandler-Horowitz, and Martin M. Frank. Sub-bandgap defect states in polycrystalline hafnium oxide and their suppression by admixture of silicon. *Applied Physics Letters*, 87(19), 2005.

[146] F. J. Himpsel, J. F. van der Veen, and D. E. Eastman. Experimental bulk energy bands for diamond using hν-dependent photoemission. *Phys. Rev. B*, 22:1967–1971, 1980.

[147] D. E. Eastman, W. D. Grobman, J. L. Freeouf, and M. Erbudak. Photoemission spectroscopy using synchrotron radiation. I. overviews of valence-band structure for Ge, GaAs, GaP, InSb, ZnSe, CdTe, and AgCl. *Phys. Rev. B*, 9:3473–3488, 1974.

[148] L. Ley, R. A. Pollak, F. R. McFeely, S. P. Kowalczyk, and D. A. Shirley. Total valence-band densities of states of iii-v and ii-vi compounds from x-ray photoemission spectroscopy. *Phys. Rev. B*, 9:600–621, 1974.

[149] J. Chelikowsky, D. J. Chadi, and Marvin L. Cohen. Calculated valence-band densities of states and photoemission spectra of diamond and zinc-blende semiconductors. *Phys. Rev. B*, 8:2786–2794, 1973.

[150] R. A. Powell, W. E. Spicer, and J. C. McMenamin. Photoemission studies of wurtzite zinc oxide. *Phys. Rev. B*, 6:3056–3065, 1972.

[151] L. Ley, R. A. Pollak, F. R. McFeely, S. P. Kowalczyk, and D. A. Shirley. Total valence-band densities of states of iii-v and ii-vi compounds from x-ray photoemission spectroscopy. *Phys. Rev. B*, 9:600–621, 1974.

[152] M. Betzinger, C. Friedrich, S. Blügel, and A. Görling. Local exact exchange potentials within the all-electron FLAPW method and a comparison with pseudopotential results. *Phys. Rev. B*, 83:045105, 2011.

[153] P. Rinke, A. Qteish, J. Neugebauer, and M. Scheffler. Exciting prospects for solids: Exact-exchange based functionals meet quasiparticle energy calculations. *Physica Status Solidi (b)*, 245(5):929–945, 2008.

[154] P. Rinke, A. Qteish, J. Neugebauer, C. Freysoldt, and M. Scheffler. Combining GW calculations with exact-exchange density-functional theory: an analysis of valence-band photoemission for compound semiconductors. *New Journal of Physics*, 7(1):126, 2005.

[155] Yan Li, J. B. Krieger, M. R. Norman, and G. J. Iafrate. Band-structure calculations of noble-gas and alkali halide solids using accurate Kohn-Sham potentials with self-interaction correction. *Phys. Rev. B*, 44:10437–10443, 1991.

[156] Takao Kotani and Hisazumi Akai. KKR-ASA method in exact exchange-potential band-structure calculations. *Phys. Rev. B*, 54:16502–16514, 1996.

[157] H. P. Rooksby. A note on the structure of nickel oxide at subnormal and elevated temperatures. *Acta Crystallographica*, 1(4):226, 1948.

[158] H. P. Rooksby. Structure of nickel oxide. *Nature*, 152:304, 1943.

[159] H. P. Rooksby and N. C. Tombs. Structure of Monoxides of some transistion elements at low temperatures. *Nature*, 165:442, 1950.

[160] H. P. Rooksby and N. C. Tombs. Changes of crystal structure of antiferromagnetic compounds. *Nature*, 167:364, 1951.

[161] F. Tran, P. Blaha, K. Schwarz, and P. Novák. Hybrid exchange-correlation energy functionals for strongly correlated electrons: Applications to transition-metal monoxides. *Phys. Rev. B*, 74:155108, 2006.

[162] G. I. Finch and H. Wilman. The diffraction of electrons by graphite. *Proc. R. Soc. Lond. A.*, 155:345–365, 1936.

[163] J. C. Inkson. *Many-body theory of solids: an introduction.* Plenum Press, 1984.

[164] Charles Kittel. *Introduction to Solid State Physics*. John Wiley & Sons, Inc., New York, 6th edition, 1986.

[165] Yuzheng Guo, Stewart J. Clark, and John Robertson. Calculation of metallic and insulating phases of V2O3 by hybrid density functionals. *The Journal of Chemical Physics*, 140(5), 2014.

[166] J. P. Perdew, R. G. Parr, M. Levy, and J. L. Balduz. Density-functional theory for fractional particle number: Derivative discontinuities of the energy. *Phys. Rev. Lett.*, 49:1691–1694, 1982.

[167] A. J. Cohen, P. Mori-Sánchez, and W. Yang. Fractional charge perspective on the band gap in density-functional theory. *Phys. Rev. B*, 77:115123, 2008.

[168] P. Mori-Sánchez, A. J. Cohen, and W. Yang. Localization and delocalization errors in density functional theory and implications for band-gap prediction. *Phys. Rev. Lett.*, 100:146401, 2008.

[169] E. Kraisler and L. Kronik. Piecewise linearity of approximate density functionals revisited: Implications for frontier orbital energies. *Phys. Rev. Lett.*, 110:126403, 2013.

[170] E. Kraisler and L. Kronik. Fundamental gaps with approximate density functionals: The derivative discontinuity revealed from ensemble considerations. *The Journal of Chemical Physics*, 140(18):18A450;1–10, 2014.

[171] A. K. Theophilou. The energy density functional formalism for excited states. *Journal of Physics C: Solid State Physics*, 12(24):5419, 1979.

[172] N. I. Gidopoulos, P. G. Papaconstantinou, and E. K. U. Gross. Spurious interactions, and their correction, in the ensemble-Kohn-Sham scheme for excited sstates. *Phys. Rev. Lett.*, 88:033003, 2002.

[173] E. Pastorczak, N. I. Gidopoulos, and K. Pernal. Calculation of electronic excited states of molecules using the helmholtz free-energy minimum principle. *Phys. Rev. A*, 87:062501, 2013.

[174] H. Lambert and F. Giustino. Ab initio sternheimer-gw method for quasiparticle calculations using plane waves. *Phys. Rev. B*, 88:075117, 2013.

[175] N. Helbig. *Orbital Functionals in Density-Matrix- and Current-Density-Functional Theory*. PhD thesis, Department of Physics, Freien Universität Berlin, 2006.

[176] T. L. Gilbert. Hohenberg-Kohn theorem for nonlocal external potentials. *Phys. Rev. B*, 12:2111–2120, 1975.

[177] A. M. K. Müller. Explicit approximate relation between reduced two- and one-particle density matrices. *Physics Letters A*, 105(9):446 – 452, 1984.

[178] S. Goedecker and C. J. Umrigar. Natural orbital functional for the many-electron problem. *Phys. Rev. Lett.*, 81:866–869, 1998.

[179] O. Gritsenko, K. Pernal, and E. J. Baerends. An improved density matrix functional by physically motivated repulsive corrections. *The Journal of Chemical Physics*, 122(20):–, 2005.